Modeling the Impact of Climate and Land Use/Land Cover Change on Hydrological Responses in Lake Tana Basin, Ethiopia

by

Achenafi Teklay Gebresilassie

A Dissertation Submitted
to
Ethiopian Institute of Water Resources

Presented in Fulfillment of the Requirements for the Degree of Doctor of Philosophy (Ph.D.) in Water Resources Engineering and Management

Addis Ababa University
Addis Ababa, Ethiopia
July 2020

Modeling the Impact of Climate and Land Use/Land Cover Change on Hydrological Responses in Lake Tana Basin, Ethiopia

by

Achenafi Teklay Gebresilassie

A Dissertation Submitted to:

Ethiopian Institute of Water Resources

Presented in Fulfillment of the Requirements for the Degree of Doctor of Philosophy (Ph.D.) in Water Resources Engineering and Management

Supervisors:

Main Advisor:	**Dr. Dereje H. Asfaw** Addis Ababa University (AAU)
Co-Advisor:	**Dr. Yihun T. Dile** Texas A & M University
Co-Advisor:	**Dr. Haimanote K. Bayabil** University of Florida

Addis Ababa University

Addis Ababa, Ethiopia

July 2020

APPROVAL PAGE

I, the undersigned, declare that this thesis is based on my original work and that it has not been presented for a degree in any other university. All sources of materials have been duly acknowledged.

Achenafi Teklay  July 2020

This thesis has been submitted for examination with my approval as supervisor of the dissertation.

Main Advisor 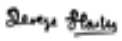

Dr. Dereje H. Asfaw

Co-Advisor 

Dr. Yihun T. Dile

Co-Advisor 

Dr. Haimanote K. Bayabil

Addis Ababa University

School of Graduate Studies

This is to certify that the thesis presented by Achenafi Teklay Gebresilassie entitled: **"Modeling the Impact of Climate and Land Use/Land Cover Change on Hydrological Responses in Lake Tana Basin, Ethiopia"** and submitted in partial fulfillment of the requirements for the degree of Doctor of Philosophy (Water Resources Engineering and Management) complies with the regulations of the University and meets the accepted standards with respect to originality and quality.

Signed by the Examining Committee:

Chair, Examining Committee_____ Signature _____ Date _____

External Examiner _____ Signature _____ Date _____

Internal Examiner _____ Signature _____ Date _____

Internal Examiner _____ Signature _____ Date _____

_____

Chair of Department or Graduate Program Coordinator

Acknowledgements

First of all, I would like to thank God for his never-ending love and care in my life. This research would not have been possible without proper guidance, support, and encouragement from different people and organizations.

I would like first to express my sincere gratitude to my supervisors Dr. Dereje Asfaw, Dr. Yihun T. Dile, and Dr. Haimanote K. Bayabil for their great support, kind guidance, and encouragement throughout my Ph.D. studies. I have been extremely lucky to have supervisors who cared so much about my research work, and who responded to my questions and queries so promptly for the accomplishment of my Ph.D. research work.

My acknowledgments are also extended to the Ministry of Water, Irrigation, and Electricity (MoWIE), the National Meteorological Agency (NMA), and Mapping Agency of Ethiopia for providing me relevant data including hydro-meteorological, soil map and geo-spatial data for the study area. I am indebted to Addis Ababa University, Institute of Geophysics, Space Science and Astronomy (IGSSA) for allowing me to access high-performance computing facility.

I must be thankful to Dr. Kibruyisfa Sisay for his guidance and support during climate model simulation and analysis, for his scholarly contributions, and brotherly understanding of everything. I will never forget your help when I faced a computing facility shortage during climate modeling. Equally, I extend my sincere gratitude to Eyayaw Worku for his unwavering support and encouragement throughout the entire process. I am very grateful to all colleagues at Gondar University. In particular, I want to thank Asrat Ayalw, Amanuel Abate, and Abraham Tegenu. Also, my sincere thanks go to Yaya families including Alemayehu Kassa, Amare Setegn, Birhane Ewnetu, Getachew Dagnaw, and Melak Alemu.

I owe many thanks to my parents Teklay Gebresilassie and Asemu Lakew for their continuous encouragement throughout the research period. Simegnish, Solomon, Addiszemen, Kumlachew, Yemisrach, and Sisay; your significant contributions are highly appreciated and let to the successful completion of my study.

Last but not least, I would like to thank my wife Workalem Sisay for her consistent love, care and encouragement throughout the research period. Workiy, I will never forget your sacrifice for this research.

Abstract

Environmental pressure resulting from interlinked climate and land use land cover (LULC) change is increasingly threatening water resources. Evaluating the effect of climate and LULC change on watershed hydrology has become an important research topic for developing appropriate strategies for the water resources sector. Recently, hydrological impact assessments focused on separate impacts of either LULC or climate change. However, both LULC and climate have been changed significantly since the mid-20th century, and in most parts of the world, including Ethiopia, the change will continue in the future. Hence, the focus of this study was to model the impact of LULC and climate change on hydrologic processes. Additionally, the climate model's sensitivity to land-use data and land surface model (LSM) was investigated. The study was conducted in the Lake Tana basin which located in northern Ethiopia. The Lake Tana basin is the headwater of the Upper Blue Nile basin having a catchment area of 15,140 km^2. This study mainly focused on the major tributaries rivers including Gilgel Abay, Gumara, Ribb, and Megech watershed.

LULC changes are one of the main human-induced factors influencing the hydrological process. The SWAT hydrological model was calibrated and validated using static land-use (SLU) and dynamic land-use (DLU) setup to evaluate the impact of LULC changes on the hydrological processes and parameters in Gumara watershed (case study watershed). The SLU setup used single land-use data (1985), whereas the DLU setup used four land-use data (1985, 1995, 2005, and 2015). Results from the LULC study showed that expansion of agriculture (11.1%) and decrease of forest (2.3%) and shrub-land (8.8%) occurred between 1985 and 2015. SWAT model with DLU setup showed a slightly higher performance than SLU setup, particularly during the calibration period. The LULC data for 2015 showed an overall increase in surface runoff (11.6 mm) and peak flow (2.4 m^3/s) and a decrease in evapotranspiration relative to 1985 LULC data. The incorporation of DLU into the SWAT model results in a more realistic representation of changes in temporal land-use, thus improving the accuracy of estimation of temporal and spatial hydrological processes. Therefore, hydrological modelers should take into account the temporal dynamics of LULC data to improve model simulation performance.

Besides LULC change, climate change could be a threat to the water resource sector. In order to accurately simulate climate data, the Weather Research and Forecasting (WRF) model parameters were chosen on local bases, in particular land-use data and LSM. The result indicated that

simulations of temperature and rainfall were sensitive to the choice of LSM and land-use data. The combination of updated new land-use (NLU) with Rapid Update Cycle (RUC) and Thermal Diffusion (TD) produced very small cold bias (0.27 °C) and warm bias (0.20 °C) for maximum and minimum temperature, respectively, whereas rainfall simulation with NLU and Noah configuration produced the lowest mean bias (2.39 mm/day). The WRF model had limitations in terms of detection ability during the occurrence of heavy rainfall. Overall, results suggested that the application of updated land-use data substantially improved the performance of the WRF model in simulating temperature and rainfall. The study would provide valuable support in identifying suitable LSM and land-use data that can accurately predict the climate variables in the Blue Nile basin.

Lake Tana basin is vulnerable to climate change and variability. Climate data for the baseline (2005-2015) and future period (2045-2055) under two Representative Concentration Pathways (RCP) scenarios (RCP4.5 and RCP8.5) were simulated using the WRF model. The SWAT model was used to investigate the impacts of climate change on the four main tributary watersheds of the Lake Tana basin: Gilgel Abay, Gumara, Ribb, and Megech. The result showed that projected changes in rainfall vary with seasons and watershed under both scenarios. On average, under RCP4.5 and RCP8.5 scenarios, the mean annual rainfall may increase by 7.9% and 21.1%, respectively. Minimum temperature may increase by 1.4 °C and 1.9 °C while maximum temperature may increase by 1.4 °C and 2.4 °C under RCP4.5 and RCP8.5 scenarios, respectively. Climate change under RCP4.5 and RCP8.5 scenarios can increase streamflow by 7.2% and 33% and evapotranspiration by 11.2% and 15.2%, respectively. The findings provide valuable insights to implement appropriate water management strategies to mitigate and adapt the negative impacts of climate change and variability.

The effect of LULC and climate change on Gumara watershed hydrology was assessed using projected LULC and climate data. Three future LULC scenarios (BAU, EFL, and EIC) were developed using Land-use Change Evaluation Module in QGIS, based on hypothetical scenarios. Projected climate data were simulated using the WRF model under the RCP4.5 and RCP8.5. The result showed that BAU scenario can increase surface runoff by 5.1% and decrease base-flow by 6.5% without altering streamflow and evapotranspiration noticeably. On the contrary, EIC and EFL scenarios can decrease streamflow by 12.5% and 5.2%, and surface runoff by 7.9% and 10%,

respectively, and increase evapotranspiration by 4.9% and 8.9%, respectively. Climate change under RCP8.5 can increase streamflow, surface runoff and evapotranspiration significantly by 34.3%, 51.8%, and 12.2%, respectively. The simulated SF, SR and ET may increase significantly under the combination of all three land-use and RCP8.5 scenarios. The findings suggested that climate change may have a greater effect on hydrologic responses than land-use change. The expansion of agriculture (BAU) and the wetter climate (RCP8.5) would exacerbate flooding, while the expansion of irrigation and forest offset SF increase. The findings from this study can be useful to decision-makers and planners in the design of adaptive measures to LULC and climate changes.

Keywords: Dynamic land-use, Static land-use, SWAT, Updated land-use, LSM, WRF, land-use change, climate change, hydrological response, Lake Tana basin

List of Original Papers

This dissertation is based on the following four original papers, which are listed from paper 1 to 4.

Paper 1. Teklay, A., Dile, Y. T., Setegn, S. G., Demissie, S. S., & Asfaw, D. H. (2018). Evaluation of static and dynamic land use data for watershed hydrologic process simulation : A case study in Gummara watershed, Ethiopia. *Catena*, *172*, 65–75. https://doi.org/10.1016/j.catena.2018.08.013 (Puplished).

Paper 2. Teklay, A., Dile, Y. T., Asfaw, D. H., Bayabil, H. K., & Sisay, K. (2019). Impacts of land surface model and land use data on WRF model simulations of rainfall and temperature over Lake Tana Basin, Ethiopia. *Heliyon*, *5*(9), 1–14. https://doi.org/10.1016/j.heliyon.2019.e02469 (Puplished).

Paper 3. Teklay, A., Dile, Y. T., Asfaw, D. H., Bayabil, H. K., & Sisay, K. (2019). Modeling the Impact of Climate Change on Hydrological Responses in the Lake Tana Basin, Ethiopia. *Environmental Research System.* Springer. (Under review).

Paper 4. Teklay, A, Dile, Y. T., Asfaw, D. H., & Bayabil, H. K. (2020). The Impact of Climate and Land Use Land Cover Change on Hydrological Response in Gumara Watershed, Ethiopia. Sciences of the Total Environment. Elsevier (Manuscript in preparation).

Table of Content

List of Figures

List of Tables

List of Acronyms

AR5	Fifth Assessment Report
BAU	Business-as-usual
BS	Bias Score
CDKN	Climate and Development Knowledge Network
CESM	Community Earth System Model
CMIP5	Coupled Model Intercomparison Project Phase 5
CN	Curve Number
CSA	Central Statistical Agency
CSI	Critical Success Index
CUP	Calibration and Uncertainty Program
DEM	Digital Elevation Model
DLU	Dynamic Land Use
EFL	Expansion of Forestland
EIC	Expansion of Irrigation Crop
FAR	False Alarm Ratio
GCM	General Circulation Model
GHG	Greenhouse Gas
GIS	Geographic Information System
GPS	Global Position System
HRU	Hydrologic Response Units
IPCC	Intergovernmental Panel on Climate Change
LSM	Land Surface Model
LULC	Land Use Land Cover
MB	Mean Bias
MOLUSCE	Module for Land-use Change Evaluation
MoWIE	Ministry of Water, Irrigation and Electricity
NCAR	National Center for Atmospheric Research
NCEP	National Centers for Environmental Prediction
NMA	National Meteorology Agency
NSE	Nash-Sutcliffe Efficiency

PBIAS	Percent Bias
POD	Probability of Detection
RCM	Regional Climate Model
RCP	Representative Concentration Pathway
RMSE	Root Mean Square Error
RS	Remote Sensing
RUC	Rapid Update Cycle
SCS	Soil Conservation Service
SLU	Static Land Use
SRES	Special Report on Emissions Scenarios
SRTM	Shuttle Radar Topographic Mission
SWAT	Soil and Water Assessment Tool
TD	Thermal Diffusion
USGS	United States Geological Survey
WRF	Weather Research and Forecasting

DEDICATION

This dissertation is dedicated to my mum Asemu Lakew, dad Teklay Gebressilasie and wife Workalem Sisay for their support and encouragement throughout the study.

1. INTRODUCTION

1.1 Background

Changes in climate and land use land cover (LULC) are the two inseparable linked global environmental challenges the world faces today (Intergovernmental Panel on Climate Change [IPCC], 2019). Since the beginning of the industrial revolution in the mid-eighteenth century, the contribution of human activity to climate change has increased dramatically, by increasing the concentration of greenhouse gases (GHGs) in the atmosphere. The largest known contribution comes from fossil fuel combustion and the change in LULC that releases carbon dioxide gas into the atmosphere (IPCC, 2014). Nevertheless, LULC management plays an important role in the climate system, both as a contributor to GHG emissions and as a potential reducer of negative impacts (Boysen *et al.*, 2014; Quesada *et al.*, 2017). According to the IPCC (2019), agriculture and forestry land-use change account for as much as 22% of human-induced GHG emissions.

Human-induced GHGs have most likely contributed more than half of the global average surface temperature rise from 1951 to 2010 (IPCC, 2014). If human activities continue to emit GHGs at current rates, then the average global temperature can rise by 2.6 – 4.8 °C by the end of the 21st century (Hayhoe *et al.*, 2017). Climate change due to human activity has led to changes in precipitation patterns and increased the frequency of heavy precipitation events which have been significant effects on the ecological system (Thornton *et al.*, 2014; Simane *et al.*, 2017). Although Africa's contributed less than 4% of global GHG emissions (IPCC, 2007), the region significantly affected by climate change and variability. The East African region has experienced a considerable rise in temperature since the early 1980s. Besides, rainfall is very variable in time and space in this area and it is influenced by several physical processes including the El Niño Southern Oscillation (Climate and Development Knowledge Network, 2014). Continued warming in the Indian Ocean has led to more severe spring and droughts over the past 30 years. Studies have shown that Ethiopia is vulnerable to climate change and variability (e.g., Conway, 2005; World Bank, 2006).

Ethiopia's population, which is the second-largest in Africa next to Nigeria's. In the last 50 years, the population of Ethiopia has increased from 22 million to over 100 million as of 2017 (World Bank, 2017). More than 90% of the Ethiopian population lives in the highlands (> 1000 meters above sea level), which covers more than 50% of the country (Hurni *et al.*, 2010). The population pressure has led to agrarian growth. Agriculture land coverage has been increased to 90%, whereas

the forest coverage has been reduced to less than 4% (Hurni *et al.*, 2010). The intensive cultivation on a steep slope and marginal area without soil and water conservation practices resulted in extreme soil erosion.

The agro-ecological belts in Ethiopia have been affected by climate change since about the 1970s, a trend that is evident not only in terms of rainfall variability but also the rise of temperature (World Bank, 2019). Therefore, extreme hydrological variability and seasonality are the main challenges in the water resource management sectors that affect agriculture, hydropower generation, and water infrastructure directly. Study by World Bank (2006) showed that the Ethiopian economy costed more than one-third of its growth potential due to the extreme hydrological variability which occurred in 2005. That is because of the national economy's heavy reliance on natural resources and rain-fed farming. Studies have shown that changes in LULC could further increase the hydrological variability by altering the hydrologic cycle (Gashaw *et al.*, 2018; Gebremicael *et al.*, 2019). However, the interaction effect of climate and LULC change on hydrological processes are still inadequately understood. Changes in LULC could exacerbate climate change impacts in some areas (Mekonnen *et al.*, 2018). On the other hand, enhancing LULC will mitigate the negative effects of climate change (Woldesenbet *et al.*, 2018; Berihun *et al.*, 2019). This suggests that the combined effect of climate and LULC change on hydrological responses requires site-specific investigation.

1.2 State of the Art

1.2.1 Modeling hydrological consequences of climate change

The simulation of the hydrological consequences of climate and land-use change is receiving the last decades increasing attention, both from the hydrology and land-surface modeling communities. According to Baldassarre *et al.* (2011) the framework for the quantification of the effects of climate change on water resource and adaptation mechanism can be summarized as follows: a) choice of one or more scenarios from the IPCC special report on emission scenarios, which depend on the future economy and energy use policies; b) choice of one or General Circulation Models (GCM); c) downscaling of the GCM climate output such as rainfall to the specific river basin scale; d) use of the downscaled GCM outputs as inputs for a hydrological model; and e) analysis of hydrological model results by comparing them to the corresponding results related to the current climate or different possible future climates. Baldassarre *et al.* (2011)

offer in their paper a discussion on the progress and improvements made in the above mentioned framework.

The uncertainty due to the choice of emission scenario is less important for the near term, because most scenarios show very similar levels of emissions through the 2050s and it takes time for the atmosphere to respond (Wilby and Harris, 2006). The four IPCC SRES (Special Report on Emissions Scenarios: Nakićenović and Swart, 2000) storylines, which form the basis for many studies of projected climate change and water resources, consider a range of plausible changes in population and economic activity over the 21st century. Among the scenarios that assume a world economy dominated by global trade and alliances (A1 and B1), global population is expected to increase from today's 6.6 billion and peak at 8.7 billion in 2050, while in the scenarios with less globalization and co-operation (A2 and B2), global population is expected to increase until 2100, reaching 10.4 billion (B2) and 15 billion (A2) by the end of the century. In general, all SRES scenarios depict a society that is more affluent than today, with world gross domestic product (GDP) rising to 10–26 times today's levels by 2100.

The Integrated Assessment Models (IAMs) explored a range of technological, socioeconomic, and policy futures that could lead to particular concentration pathways and magnitudes of climate change, which is represented by the RCPs. The RCPs include four different scenarios (Table 1.1), i.e., one mitigation scenario leading to a very low forcing level (RCP2.6), two medium stabilization scenarios (RCP4.5/RCP6), and one very high baseline emission scenarios (RCP8.5), all of which could be obtained with different combinations of economic, technological, demographic, policy, and institutional futures. The development of the RCPs in the first phase allows climate modelers to proceed with experiments in parallel to the development of emission and socioeconomic scenarios, expediting the overall scenario development process (Moss *et al.*, 2010).

Table 1.1 Description of Representative Concentration Pathways (RCPs).

RCPs	Description
RCP8.5	Rising radiative forcing pathway leading to 8.5 W/m^2 in 2100
RCP6	Stabilization without overshoot pathway to 6 W/m^2 at stabilization
RCP4.5	Stabilization without overshoot pathway 4.5 W/m^2 at stabilization after 2100
RCP2.6	Peak in radiative forcing at 3 W/m^2 before 2100 and decline

Most GCMs, used to generate projections of future climate change, operate on large spatial scales; a common resolution of regional climate models is 50 to 100-km or 0.5 to 1 degree latitude, and are typically run in model time steps on the order of half an hour to one hour. Owing to their coarse horizontal resolution, GCMs are not well-suited to simulate sub-grid, mesoscale hydroclimatologic processes, nor can they provide sufficient detail in the spatial patterns of temperature and precipitation in areas of complex topography and land-use. Although it is possible to run a full GCM at finer resolution, one should be aware that the model would take much longer to complete a simulation, in which case either a very powerful computer (e.g. the Earth Simulator in Japan, Tetsuya, 2004) or a much shorter simulation period (e.g. 5 years) is required. A better alternative, according to Kitoh *et al.* (2015), is dynamic downscaling by means of Regional Climate Models (RCM) nested within a GCM. Doing so has important advantages over GCM-based scenarios as the physical processes are represented at a higher resolution. As mentioned by Wangpimool *et al.* (2013) the horizontal resolution of RCM simulations increased considerably and now approaches a level that allows a realistic simulation of the temperature and precipitation at the scale of river basins and small catchments. Teutschbein and Seibert (2013) used simulations from the ensemble of 11 different RCM-simulated temperature and precipitation series with a horizontal resolution of 25-km as direct input into a catchment-based rainfall-runoff model, resulting in relatively good estimates of the daily stream flow in 5 small catchments across Sweden. Tramblay *et al.* (2013) used the results of ALADIN-RCM for two different Radiative Concentration Pathway scenarios (RCP4.5 and RCP8.5) simulations, with two 12 km and 50 km spatial resolutions, as input into a hydrological model of the catchment of the Makhazine dam in North Morocco. They found better reproduce the seasonal patterns, the seasonal distributions and the extreme events of precipitation in 12 km resolution from ALADIN-RCM. For the climate change signal under scenarios 4.5 and 8.5 indicates a decrease of respectively −30 to −57 % in surface runoff for the future, when for the same period the projections for precipitation are ranging between −15 and −19 % and for temperature between +1.3 and +1.9 °C

Many climate change experiments have been performed with GCMs, also in Africa (Baldassarre *et al.*, 2011). There have been a number of such exercises for Africa using an array of GCM scenarios (CSIRO2, HadCM3, CGCM2, ECHAM, PCM, etc.), usually for SRES emissions scenarios A2, A1B and B2 (Elshamy *et al.*, 2009; Beyene *et al.*, 2010; Dessu and Melesse, 2012; Demisssie *et al.*, 2013). Each of the GCMs has their own strengths and weaknesses in terms of

simulating various features, and different climate models show rather distinct patterns, even with almost opposite projections.

1.2.2 Modeling hydrological consequences of land use change

Land use land cover changes are additionally to climate change one of the main human induced activities altering the quantity and quality of a hydrological system (Homdee *et al.,* 2011; Zhu *et al.,* 2012; Gebremicael *et al.,* 2013; Alexakis *et al.,* 2014; Tekleab *et al.,* 2014; Budiyanto *et al.,* 2015; Huang and Lo, 2015;). Many studies analyzed land-use change impact at catchment scale (e.g., Bewket and Sterk, 2005; Rientjes *et al.,* 2011; Getachew and Melesse, 2012; Huang *et al.,* 2013) or on the hydrological response of changes in vegetation cover (Stehr *et al.,* 2010; McNider *et al.,* 2015; Li *et al.,* 2015). In traditional applications of spatially distributed hydrological models, the land-use input is pre-composed and taken as fixed. It does not change during the simulation period. This means that the vegetation cover (vegetation types, or vegetation development states; represented in the model by, for instance, the leaf area index (LAI) and/or the root depth) does not vary according to the water availability. The common method is to change the land-use maps (land use change scenario) over time to predict the impact on water availability under the assumption that the water demand for vegetation development is satisfied under any condition. Verbeiren *et al.* (2011) used the land-use change modeling in conjunction with a fully distributed, physically based rainfall-runoff model WetSpa for surface runoff prediction. Xu *et al.* (2013) applied the land-use change allocation model (CLUE-s) in combination with the physically based distributed hydrological model (SWAT) for examining the impact of various land-use change scenarios in a region undergoing rapid change in land-use – the Xiangjiang River basin in China. Alexakis *et al.* (2014) quantified the sensitivity the HEC-HMS distributed hydrological model together with Cellular Automata (CA) land-use forecasting model. Gebremicael *et al.* (2013) observed that changing land-uses could alter the hydrology and sedimentation in a watershed; however, this information is unknown to a model that is operating based on a single land-use geospatial dataset. But, a few modelers have been tried to incorporate more the one land use land cover layer. To name a few, Pai and Saraswat (2011) highlighted the opportunities for the integration of land use change module (LUC) and SWAT hydrological model. Koch *et al.* (2012) integrated the Land use Update and Soil Assessment (LUPSA) to the SWAT hydrological model to improve the overall SWAT abilities to handle land-use change.

1.2.3 Modeling the impact of land use and climate change on hydrological response

As climate change and land-cover change, two major drivers of global change, are expected to continue throughout the twenty first century (Olson *et al.,* 2008), there is a growing concern that the sustainability of freshwater resources are threatened in many parts of the world. To assess potential regional impacts of global change and to improve understanding of the interactions of climate change and land-cover change in hydrology and water resources, an increasing number of basin-scale hydrological modeling studies take both changes into account. This line of research is important for water resource management, because the two types of changes may either ameliorate or amplify one another's effects at different spatial and temporal scales (Praskievicz and Chang, 2009). Identifying the sensitivity of changes in runoff and water resources to climate and land-use change is the basic requirement for integrated water resource management and guide climate adaptation strategies at the regional scale (Li *et al.,* 2010).

Due to nonlinear and complicated response of hydrological cycle to combined effects of climate and land-use change (Guo *et al.,* 2008); very few studies have been carried out on the combined effect. Guo *et al.* (2008) used SWAT to examine the climate and land-use and land-cover effects on hydrology and stream flow in the Xinjiang River basin of the Poyang Lake. The results included an increase in basin discharge of 199% as a result of projected climatic and land-use changes. Similarly, Li *et al.* (2010) found an increase of up to 42.1% in basin discharge under simulated land-use and climate change scenarios in the Heihe watershed on the Loess Plateau of China. Mishra *et al.* (2010) examined the separate and combined impacts of climate change, land use land cover change, on water and energy cycle in the upper Midwest United States, finding that climate change decrease or slightly increase mean annual evapotranspiration, depending on the emission scenario used, and increases nutrient annual surface runoff by up to 30.5 mm. Morán-Tejeda *et al.* (2014) simulated runoff for present and future land-use and climate scenario in a coastal basin in a mountain watershed and found that, with an increase in basin pine forest area from 36.5% to 61.3% and with an increase of temperature by 1.86 °C and with a decrease of precipitation by 6.63%, the mean event runoff will decrease by 13% by 2050. Bossa *et al.* (2014) predict land and water degradation based on the combined land-use and climate change scenarios from the meso to regional scale in West Africa, regardless the modeling scale surface runoff, groundwater flow, sediment and organic nitrogen load are found mainly sensitive to land-use change with roughly

−8% to 50% of changes; and water yield and evapotranspiration are found more sensitive to climate change with roughly −31% to +2% of changes as consequence of rainfall reduction over the simulated period 2000 to 2029.

It has been widely accepted that climate variability and land use land cover changes are two critical drivers for influencing watershed hydrological changes. Because of this, it is important to separate their relative contributions to hydrological change so that their individual effects can be quantified. In small watersheds, a paired watersheds approach is usually used to remove the effect of climate variability so that the effects of forest or land-cover changes can be quantitatively assessed. However, this experimental paired watersheds approach is generally not feasible for large watersheds. Thus, alternative methods must be used for studying this subject in large watersheds. In the past 20–30 years, researchers have developed and applied diverse techniques for this research subject. These techniques can be broadly classified into statistical and modeling categories. Hydrological modeling with the one-factor-at-a-time approach (OFAT) commonly used in sensitivity analysis (Mengistu and Sorteberg, 2012) is also used in association with hydrological models to distinguish the impact of climate factors and land-cover change on watershed hydrology (Chawla and Mujumdar, 2015). Trend analysis is a commonly used method to qualitatively assess hydrologic responses (Zhang *et al.*, 2008). The trend analysis uses historic data to fit a curve, which reflects a trend of the interested hydrological variable and can then be used to predict any future values if the trend is statistically significant. When the trend analysis is applied to detect the effects of forest change on hydrology, information on climate change and land-use change is needed. If there is no a significant trend in climate variable (e.g., precipitation), the significant trend in hydrological variable is then judged to be caused by land-use change (Claessens *et al.*, 2006). Clearly, this method is simple and qualitative, but may not be reliable, as the interactions between land-use change and climatic variability are not considered.

1.3 Problem of the Statement

Although the Lake Tana basin is intensively utilized and has vast potential for irrigation, hydropower, and other development activities, there is inadequate information about the effect of LULC and climate change on the hydrological process in the basin. Most of the previous studies focused on the impact of either climate change (Setegn *et al.*, 2011; Dile *et al.*, 2013; Enyew *et al.*, 2014; Ayele *et al.*, 2016; Nigatu *et al.*, 2016; Melke and Abegaz, 2017) or LULC change

(Andualem and Gebremariam, 2015; Gumindoga *et al.*, 2015; Chakilu and Moges, 2017; Woldesenbet *et al.*, 2017; Gashaw *et al.*, 2018) on the hydrological response. There was a clear general lack of modeling on the integrated impact of LULC and climate change on watershed hydrology. Moreover, the previous studies used a hydrological model to evaluate the influence of LULC change or climate change on hydrological response; however, the model was calibrated and validated using static land-use data. This may result in model responses being stationary because the hydrological model prediction performance depends on the temporal resolution of land-use input data (Pai and Saraswat, 2011). Besides, most of the climate change studies used climate variables that estimated from coarse spatial resolution General Circulation Models (GCMs) using empirical-statistical relationships between large-scale predictors (i.e., GCM-derived atmospheric parameters) and local predictands (e.g., rainfall or temperature). However, climate variables have a strong association with local soil conditions, topography, and LULC dynamics (Haile *et al.*, 2009; Collow *et al.*, 2014; Cao *et al.*, 2015), which is not properly incorporated in a statistical relationship. Therefore, climate simulation using a regional climate model (RCM) is important to incorporate local conditions at a high spatial resolution to reduce uncertainties. The current and future impact of climate and LULC change on the seasonal water budget remains uncertain and requires a high level of spatial and temporal investigation through a better understanding of the interaction of the atmospheric and hydrologic systems. Moreover, the likely environmental implications of the irrigation development plan along with the changing climate have not been fully evaluated. Therefore, this study is designed to investigate the combined impact of climate and LULC change on hydrological processes to support the integrated water resources management practices in the headwaters of the Upper Blue Nile basin.

1.4 Research Question

The overall purpose of this hydrological process modeling is to determine the effect of climate and LULC change for integrated water resource management in the Lake Tana basin, northern Ethiopia. The study methodology will help the scientific community and decision-maker by improving the understanding of the interaction effect of land surface and atmosphere on the hydrological response at large scale watersheds. This study can also contribute to regional water resources planning by quantifying the possible hydrological response under the predicted LULC and climate scenarios and assessing the relative impacts of climate and LULC change on

hydrologic responses. Besides, enhancing the capability of hydrologic and climate model using updated land-use information will have scientific merit by improving our understanding of the hydrologic and climate modeling processes through new insight and innovative approaches for water resources and environmental applications. These outputs will achieve by designing this study to answer the following major research questions:

a. How does updated land-use information affect the spatial and temporal prediction performance of a semi-distributed hydrologic model (SWAT)?
b. What are the contributions of updated land-use information on climate simulation using the Weather Research and Forecasting (WRF) model?
c. How does the predicted rainfall and temperature trend of the future period (2045 – 2055) affect hydrological responses compare to the reference period (2005 – 2015)?
d. What are the relative impact of LULC and climate change on future hydrologic processes?

1.5 Research Objective

The general objective of this research is to investigate and model the spatial and temporal variability of water resources under the dynamics of climate and LULC in the Lake Tana basin using land-use change, climate, and hydrological model. Thus, it is to conduct an evaluation and improving the simulation performance of hydrologic and climate models. Towards this framework, this study attempt to target the following specific objectives:

a. To evaluate the effect of updated land-use information on the SWAT model performance and hydrological processes;
b. To investigate the sensitivity of the WRF model to updated land-use information and land surface model (LSM);
c. To investigate the impact of climate change on hydrological responses for the period 2045 – 2055;
d. To study the sensitivity of the hydrological processes on LULC and climate change effect.

1.6 Conceptual Framework

In addition to changes in climate, LULC can be expected to continue to change in a watershed with time. Land-use is determined in part by biophysical and socioeconomic factors. These

determinants significantly alter in the future, land-use will most likely change as well. Changes in land-use affect the hydrologic processes, but the magnitude of these changes is unknown.

Beyond the negative hydrological impacts of a warming climate (e.g., higher precipitation intensities), irrigation activities in the Lake Tana basin will provide several opportunities through double-cropping, cash crop planting, and cultivating new areas of land. Accordingly, the evapotranspiration rate may increase due to double-cropping practices. On the other hand, afforestation activities could reduce agricultural land area but it may increase the dry season flow and decrease surface runoff that causes erosion. The framework to evaluate the impact of climate and LULC change on hydrological response is shown in Figure 1.1.

1.7 Organization of the Dissertation

This dissertation is organized into seven chapters, which consists of four research outputs from chapters 3 to 6. A brief description of the outline of the contents is presented to simplify the understanding of the connection between the chapters.

- Chapter 1 presents an overview of the dissertation: the research background, the problem of the statement, the research questions, the research objectives, and the conceptual framework.
- Chapter 2 presents a literature review of the existing knowledge of the research topic.
- Chapter 3 focuses on the effect of static and dynamic land-use data on hydrological model parameters and hydrological processes.
- Chapter 4 presents the impacts of the land surface models and land-use data on WRF model simulations (rainfall and temperature).
- Chapter 5 investigates the impact of climate change on hydrological responses.
- Chapter 6 predicts the effect of climate and land-use change on hydrological responses.
- Chapter 7 presents a general conclusion and recommendation for further research.

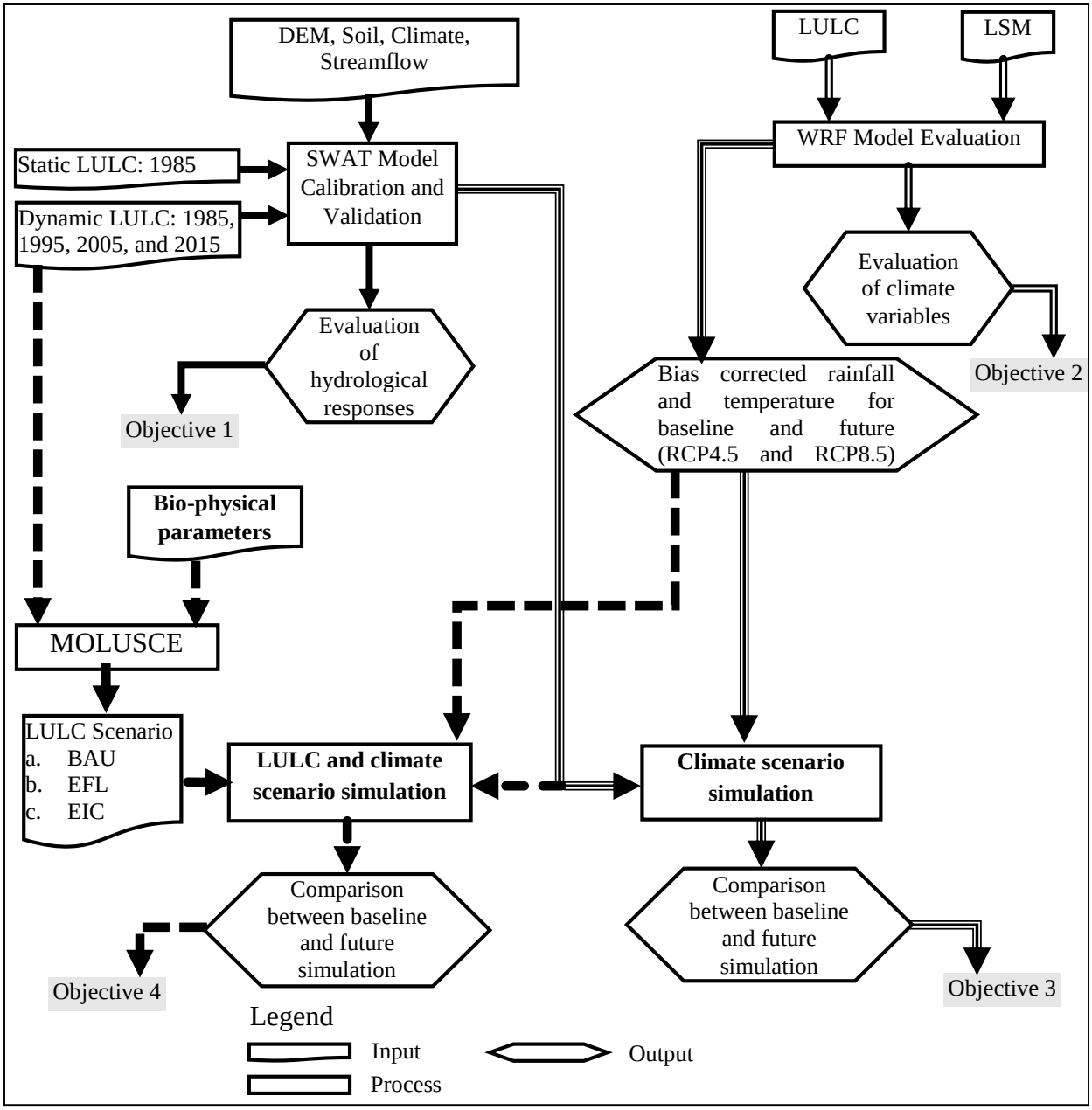

Figure 1.1 The conceptual framework (SWAT = Soil and Water Assessment Tool; WRF = Weather Research and Forecasting; MOLUSCE = Module for Land-use Change Evaluation; LULC = Land Use Land Cover; BAU = Business-as-usual; EFL = Expansion of Forestland; EIC = Expansion of Irrigation Crop; LSM = Land Surface Model).

2. EVALUATION OF STATIC AND DYNAMIC LAND USE FOR WATERSHED HYDROLOGIC PROCESS SIMULATION: A CASE STUDY IN GUMARA WATERSHED, ETHIOPIA

Abstract

Land Use Land Cover (LULC) change significantly affects hydrological process. In this study, the Soil and Water Assessment Tool (SWAT) hydrological model was applied to assess the impacts of land-use change on hydrological responses in Gumara watershed, Ethiopia. Moreover, the effects of static and dynamic land use data applications on the SWAT model performance were evaluated. Two model setups, Static Land Use (SLU) and Dynamic Land Use (DLU), were studied to investigate the effect of accounting dynamic land-use on hydrological responses. The SLU setup used the 1985 land use layer, whereas the DLU setup used 1985, 1995, 2005, and 2015 land-use data. The SWAT model was calibrated (1985-2005) and validated (2006-2015) under both setup. Results showed that the SWAT model satisfactorily predicted observed streamflow with Nash-Sutcliffe Efficiency (NSE) of 0.75 and 0.73 during the calibration period, in the DLU and SLU setups, respectively. Both model setups equally predicted daily streamflow during the validation period with NSE value of 0.71. However, the DLU model setup simulated the detailed biophysical processes better during the calibration period. Better performance was obtained while applying the DLU model setup because of improved representation of the dynamic watershed characteristics such as curve number (CN2), overland Manning's (OV_N), and canopy storage (CANMX). Expansion of agriculture *by 11.1% and reduction of forest cover by 2.3% during the period from 1985 to 2015 increased surface runoff and peak flow by 11.6 mm and 2.4 m^3/s, respectively and decreased evapotranspiration by 5.3 mm. On the other hand, the expansion of shrub-land by 1% decreased surface runoff by 1.2 mm and increased evapotranspiration by 1.1 mm. The results showed that accounting DLU into the SWAT model led to a more realistic representation of temporal land-use changes, thereby improving the accuracy of temporal and spatial hydrological processes estimation.*

Keywords: Dynamic land-use, Static land-use, land-use change, Hydrological model parameters Hydrological response, SWAT

2.1 Introduction

Land Use Land Cover (LULC) change is one of the major global environmental challenges to humanity. It significantly affected hydrological response (Su *et al.*, 2015; Wagner *et al.*, 2016), ecosystem services (Lawler *et al.*, 2014), and climate processes (Malhi *et al.*, 2008). Gebremicael *et al.* (2013) showed that the expansion of agriculture land causes a significant change in runoff and sediment load. A significant variation of evapotranspiration has occurred due to LULC and leaf area index change (Li *et al.*, 2015). Land-use change can lead to a significant change in groundwater recharge and base-flow (Budiyanto *et al.*, 2015), flood frequency and interval (Alexakis *et al.*, 2014), peak flow (Ahn *et al.*, 2014), and total suspended sediment and nutrient concentration (Hwang *et al.*, 2016). Moreover, the land-use change affects local, regional and global climate system (Deng *et al.*, 2013) and degrades the health of a wetland ecosystem (Alam *et al.*, 2011).

Remote Sensing (RS), Geographic Information System (GIS), and hydrological model played a significant role in assessing the impact of LULC change on hydrological processes. LULC information derived from RS data has been used in a variety of hydrological modeling studies, especially in streamflow, water balance, flood event and soil erosion simulations (e.g., Ahn *et al.*, 2014; Du *et al.*, 2012; Dang and Kumar, 2017). The GIS technology provided suitable alternatives for the efficient management of large and complex databases. It also enhanced modeling efficiency and capability (Alexakis *et al.*, 2014). For example, integration of the Soil and Water Assessment Tool (SWAT) with GIS helped to understand the impacts of spatially explicit processes such as land-use change on the hydrological response (Yalew *et al.*, 2013). Such tools have become vital for integrated river basin planning and management.

The SWAT model has a strong track-record of evaluating the impacts of different land management practices on the water budget, nutrient quantity and transport, and soil erosion in complex watersheds with varying soils, land-uses, and management conditions over a long period (Arnold *et al.*, 2012). For example, Briones *et al.* (2016) calibrated and validated the SWAT model to study the impact of LULC change on total water yields, groundwater, and base-flow at sub-basin level in the Palico watershed in Batangas, Philippines. They showed that forest and rangeland expansion by 22% increased base-flow by 1-15%, and reduced streamflow by 1-17% in the rainy seasons. On the other hand, the reduction of forest cover by 54% decreased base-flow between

11% and 17% in the rainy season, and increased surface runoff by 4–24%. Jemberie *et al.* (2016) investigated the effect of land use land cover change on streamflow using SWAT model in Dedissa basin, Ethiopia. Their result showed that cropland land expansion by 12% increased streamflow by 29.4 m^3/s in the wet season. On the contrary, the dry season streamflow decreased by 4.4 m^3/s due to the expansion of cropland. Likewise, Huang and Lo (2015) applied the SWAT model to study the impacts of land-use change on water budget and sediment losses over Yang Ming Shan National Park Watershed in northern Taiwan, and they reported that the conversion of forest land into agricultural land increased sediment loss.

Most SWAT model applications have been exclusively using static land-cover data to study the effects of LULC change on watershed hydrologic modeling. Watershed processes represented by static land-use data inadequately estimate the temporal and spatial hydrological variation (Wagner *et al.*, 2016). Perhaps, the use of dynamic land use (DLU) data may improve the spatial and temporal model simulation performance by capturing better LULC evolution. Moreover, the DLU approach help to disaggregate the effects of land-use change, climate variability and land management practices on the hydrological response (Chiang *et al.*, 2010; Fang *et al.*, 2013). Pai and Saraswat (2011) highlighted that stationarity in hydrological responses could occur in a single LULC application since such an approach simplifies the land-use changes with time. The stationarity of hydrological responses can be resolved by integrating land-use change modules into hydrological modeling approaches (Chiang *et al.*, 2010; Saraswat *et al.*, 2010). For example, Wagner *et al.* (2016) integrated land use-change and SWAT model, and they found sound seasonal and gradual changes in the water balance estimates. Similarly, Pai and Saraswat (2011) used SWAT model through integration of land-use change module and they found substantial improvement in the estimation of the spatial and temporal hydrological fluxes such as surface runoff, groundwater, and evapotranspiration. However, several of these integrated land-use change studies have the limitation of relying solely on model parameters derived from the calibration period that applied static land-use data. This approach overlooks the effects of land-use changes on certain model parameters. For example, the study conducted by Gebremicael *et al.* (2013) showed there was a clear high discrepancy of calibrated model parameters between the 1973 and 2000 land-use data for the 1971–1973 and 2000–2002 simulation periods, respectively. Since Gebremicael *et al.* (2013) used different land-use and climate data, the source of model parameter variation was not clear. Unlike previous studies, this research applied the SWAT model using

dynamic and static land use data to assess the effect of land-use change on the SWAT model performance and hydrological processes.

2.2 Materials and Methods

2.2.1 Study area

This study was conducted in Gumara watershed, in the eastern part of the Lake Tana basin (Figure 2.1). The watershed has an area of 1269 km^2, and is located in the Amhara region, Ethiopia, between 37.63^o to 38.18^o longitude and 11.57^o to 11.90^o latitude. The topography of the study area is generally flat to a moderate slope where 60% of the area has an average slope of less than 15%. The elevation in the basin ranges from 1794 to 3704 meters above sea level, with a mean elevation of 2272 meters.

The majority of the watershed area is covered by cultivated land (92%), and the remaining area is covered by shrubs (3%), grassland (4%), and forest (1%). The most dominant soil type is Haplic Luvisols (64%) which is found in the midstream parts of the watershed. The second dominant soil is Eutric Vertisols which is found in the downstream parts. Chromic Luvisols mainly extends to downstream and upstream parts of the watershed. Eutric Fluvisols is the least common soil type (< 1%) in the watershed. The climate of the watershed is humid with a long-term average annual rainfall is 1387 mm. The long-term average daily minimum and maximum temperatures are 9 ^{o}C and 28.5 ^{o}C, respectively. The average daily streamflow ranges between 0.2 m^3/s and 397.5 m^3/s.

2.2.2 Land use land cover analysis

Remote sensing satellite data used for this study were obtained from the United States Geological Survey (USGS) Earth Resources Observation and Science (EROS) data center (http://espa.cr.usgs.gov). Satellite data included in the study were Landsat 5 TM, Landsat 7 ETM+, and Landsat 8 OLI images (Table 2.1). The images of February and March were used because of the minimum cloud cover and surface features changes during the dry months in the study watershed. The image pre-processing was made using QGIS and ArcGIS 10.1 software packages. The satellite data were projected to Universal Transverse Mercator (UTM) projection system zone 37N and datum of World Geodetic System 1984. The un-scanned gaps in ETM+ were filled using a standardized ordinary co-kriging method (Zhang *et al.*, 2007).

Table 2.1 Sensor, Acquisition dates, Path/Row, and Resolution of the study area image.

Sensor	Date of acquisition	Path and row	Spatial resolution (m)
Landsat 5 TM	26/02/1985	169/52	30*30
Landsat 5 TM	06/02/1995	169/52	30*30
Landsat 7 ETM+	29/03/2005	169/52	30*30
Landsat 8 OLI	13/02/2015	169/52	30*30

Transect field campaigns were conducted to observe land use land cover conditions and record Global Position System (GPS) locations from each land use type during February 2016 and March 2016. The information collected from visual observation, informal discussion with local elders and GPS records were used for supervised land-use classification and accuracy assessment. Observations were made from 268 training locations where 108, 47, 57 and 56 were taken from agriculture, forest, shrub-land, and grassland, respectively. The majority of the field data (192 observation points) were used for classification, and the remaining (76) were used for the accuracy assessment. Of the 192 training locations, 77, 34, 42, and 39 were in the agriculture, forest, shrub-land, and grassland, respectively. The maximum likelihood classifier (Lillesand *et al.*, 2015) algorithm was used for image classification based on data from training locations and visual interpretation of the images. The distribution and spectral homogeneity of the training location pixels were checked using a histogram, scatterplots, and spectral statistics. The pixels in the training location had a normal distribution, and it represented well the entire area. LULC types were classified into four major classes such as agricultural land, grassland, shrub-land, and forest since these are the dominant land-use types in the highland parts of Ethiopia (Teferi *et al.*, 2013). The accuracy of the classification was overall satisfactory with an accuracy of 84% and a Kappa coefficient of 0.81 (Tadele *et al.*, 2017). The classified land-use types were used as LULC data in the SWAT model. LULC data (1985, 1995, 2005, and 2015) were used to represent different land-use regimes over the watershed during four periods: 1985–1989, 1990–1999, 2000–2009, and 2010–2015.

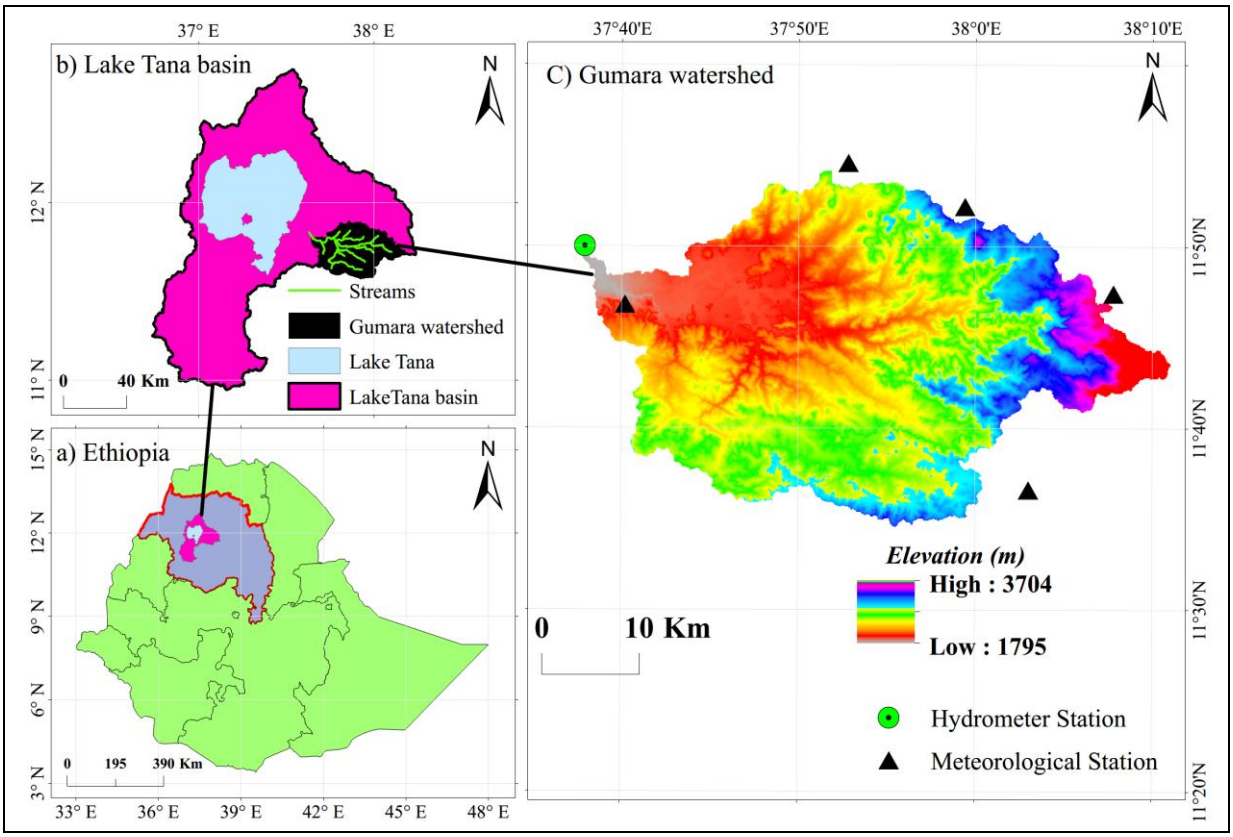

Figure 2.1 Study watershed in the Lake Tana basin and Ethiopia. a) The location of the study watershed in the Amhara region (red border) and Ethiopia. b) Lake Tana basin showing the Gumara watershed in a black border, and c) Gumara watershed zoomed with the elevation data as background, hydrometer station (green circle) and meteorological stations (black triangles).

2.2.3 SWAT model inputs

The SWAT model requires a Digital Elevation Model (DEM), land-use, soil, and climate data to simulate different hydrological processes. The DEM data with a spatial resolution of 90 m was obtained from the Shuttle Radar Topographic Mission (SRTM) (http://srtm.csi.cgiar.org/SELECTION/inputCoord.asp). The land-use maps for the years 1985, 1995, 2005, and 2015 were prepared as presented in section 3.2.2. The soil map was obtained from the Ministry of Water, Irrigation, and Electricity of Ethiopia (MoWIE). The physical and chemical soil properties that required by the SWAT model were extracted from the International Soil Reference and Information Center (http://www.isric.org). Observed streamflow data for model calibration and validation for the period 1985-2015 was obtained from the MoWIE. Daily rainfall, minimum/maximum temperature, solar radiation, wind speed, and average humidity data for the period 1982–2015 were collected from the National Meteorological Agency (NMA) of Ethiopia. These climate data were collected from five meteorological stations (Amedber, Debretabor,

Gassay, Mekaneysus, and Wanzaye). The Tuckey fence was used to screen the outliers of climate and streamflow which greater than a threshold value that can affect the detection of inhomogeneity (Ngongondo et al., 2011).

2.2.4 SWAT model setup

This study applied the ArcSWAT-2012 model to assess the effect of Static Land Use (SLU) and Dynamic Land Use (DLU) data on the performance of SWAT model simulations. The two model setups (SLU and DLU) used similar input data except for land-use. The SLU setup used only the 1985 land-use data for the entire simulation period, whereas the DLU setup used 1985, 1995, 2005, and 2015 land-use data to simulate the hydrologic process for the four periods (i.e., 1982-1989, 1990-1999, 2000-2009, and 2010-2015). These land-use data were applied using the land use update (LUU) tool of the SWAT DLU model setup. The general workflow of the model setup is presented in Figure 2.2. Both model setups followed similar SWAT modeling procedures except the integration of the LUU tool (the dotted background in Figure 2.2) in the DLU setup. The 1985 land-use data was used to define the hydrological response units (HRUs) in both model setups since it represents the beginning phase of the model simulation period. Both model setups were calibrated and validated using observed streamflow. The calibrated model was used to study the impacts of land-use change on the hydrological response in Gumara watershed. The model setup produced 22 sub-basins and 651 HRUs. The HRU definition considers every parcel of land-use, soil, and slope to account for the full representation of watershed (Arnold *et al.*, 2012). The SWAT model has several options to simulate biophysical processes. The surface runoff was estimated using the soil conservation service curve number (SCS CN) method (Fentaw *et al.*, 2018; Bekele *et al.*, 2019). Flow within the channels was routed using variable storage method. The evapotranspiration was estimated using the Penman-Monteith method (Gebre and Ludwig, 2015).

2.2.5 SWAT model calibration and validation

The SWAT model parameters were calibrated using the Sequential Uncertainty Fitting version 2 (SUFI-2) in the SWAT-CUP (SWAT Calibration and Uncertainty Program) (Abbaspour *et al.*, 2004). The SWAT SLU and DLU models were calibrated and validated using observed daily streamflow data at the Gumara river gauging station (Figure 2.1). The models were calibrated for the period from 1985 to 2005 with three years (1982-1984) of model warm-up (Daggupati *et al.*, 2015). The models were validated for the period from 2006 to 2015. The calibration and validation

considered 18 hydrological parameters (Table 2.3) based on literatures recommendation in the watershed (Setegn *et al.*, 2008; Dile *et al.*, 2016; Melke and Abegaz, 2017).

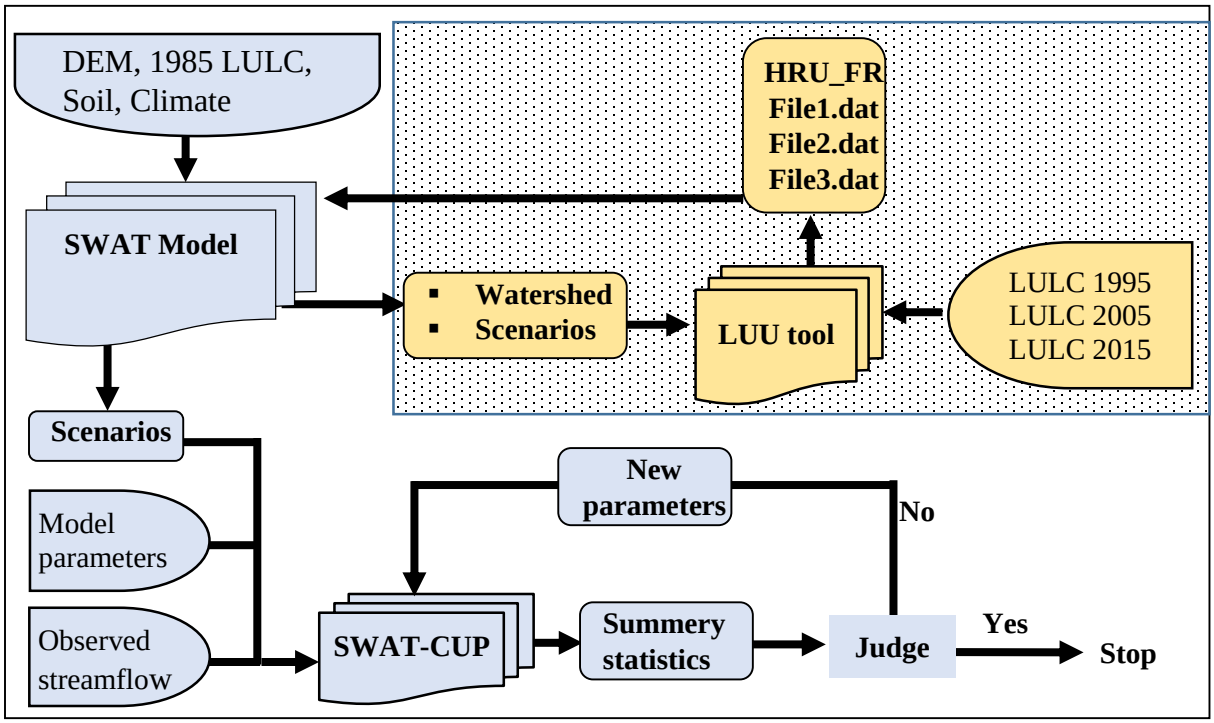

Figure 2.2 Flow chart of general methodology for evaluation of SWAT model with and without LUU tools.

2.2.6 SWAT model performance evaluation

Model performance evaluation is necessary to examine the representation of the modeling process to the actual biophysical conditions. The Nash-Sutcliffe Efficiency (NSE) and Percent Bias (PBIAS) were used to evaluate the performance of the model simulations. The NSE indicates how well the observed versus simulated data fit the 1:1 line (Equation 2.1). The NSE value theoretically ranges from $-\infty$ to 1. The NSE of 1 corresponds to a perfect match between observed and simulated values. Moriasi *et al.* (2007) suggested that a model simulation that provides the NSE value of 0.75-1, 0.65-0.75, 0.5-0.65, and < 0.5 are considered as a very good, good, satisfactory, and unsatisfactory model performance, respectively.

$$NS = 1 - \left(\sum_{i=1}^{n} (O_i - S_i)^2 / \sum_{i=1}^{n} (O_i - \overline{O})^2 \right) \quad (2.1)$$

where O_i is the observed streamflow data, S_i is the simulated streamflow data, $\overline{O}$ is the mean of the observed streamflow data, and n is the total number of streamflow data.

The PBIAS (Equation 2.2) is commonly used to measure the average tendency that the simulated data is higher or lower than the observed data. PBIAS value can be positive or negative, where the value of zero represents the best model simulation performance. Positive values indicate model underestimation bias, and negative values indicate model overestimation bias. PBIAS value of $< \pm 10\%, \pm 10\% - \pm 15\%, \pm 15\% - \pm 25\%, \text{and} \geq 25\%$ indicates that the model performs very well, good, satisfactory, and unsatisfactory, respectively (Moriasi *et al.*, 2007).

$$PBIAS = \left(\sum_{i=1}^{n} (O_i - S_i) / \sum_{i=1}^{n} O_i \right) * 100 \quad (2.2)$$

where O_i is the observed streamflow data, S_i is the simulated streamflow data, and n is the total number of streamflow data.

2.3 Results and Discussion

2.3.1 Land use land cover change

The spatial distribution of major LULC classes for 1985, 1995, 2005, and 2015 were presented in Figure 2.3. It can be observed that the agriculture land-use coverage was dominant in the upstream, midstream, and downstream parts of the watershed. However, the forest and shrub coverage were found dispersedly in the upstream and midstream parts. In a visual examination of land-use maps, it was evident that from 1985 to 2015, the area under forest and shrub diminished significantly in the midstream region. The area under different LULC categories in Gumara watershed for different periods is presented in Table 2.2.

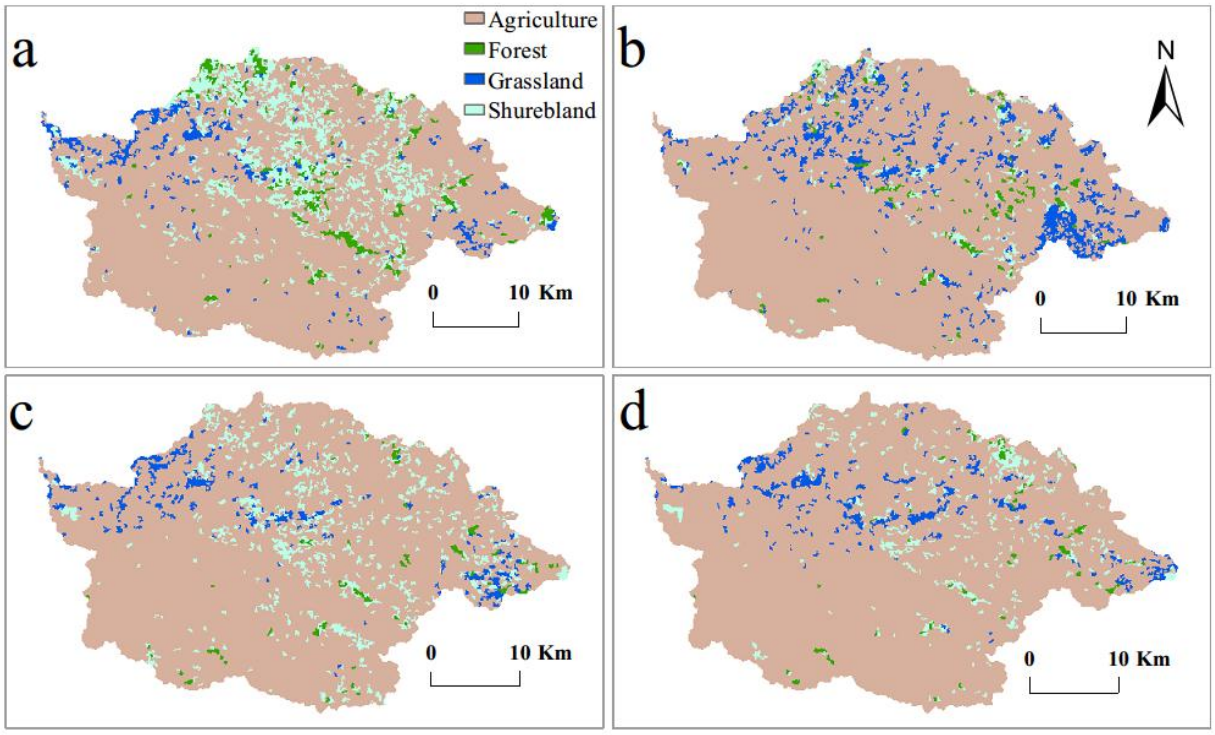

Figure 2.3 Land use land cover maps of the Gumara watershed: land-uses for a) 1985, b) 1995, c) 2005, and d) 2015.

Agriculture was the predominant land-use type in Gumara watershed, and it covered 80% in 1985 and 91% in 2015 (Table 2.2). The forest coverage of the area was very small which accounted for only 0.8% in 2015 and 3.1% in 1985 (Table 2.2). The time-series analysis of the LULC maps in the years between 1985 and 2015 indicated the expansion of agriculture land-use and a reduction of forest and shrub-land use.

A significant expansion of agricultural land-use (~8%) occurred between 1985 and 1995, and a slight reduction (~0.2%) occurred between 1995 and 2005. On the other hand, the forest coverage diminished between 1985 and 2015, which accounted for 73% of the 1985 forest cover. This was equivalent to a clearing of ~45%, ~22%, and ~6% forest in 1985-1995, 1995-2005, and 2005-2015, respectively. For the period from 1985 to 2015, agricultural land-use increased by 11% and forest cover decreased by 2.3%. This estimate is consistent with the previous findings in the highlands of Ethiopia (Rientjes *et al.*, 2011; Teferi *et al.*, 2013; Biru *et al.*, 2015). The grassland and shrub-land area changed with a wavy pattern.

Table 2.2 Land use land cover area percentage and changes for the 1985-2015 period in Gumara watershed.

Land use type	Land use land cover (%)				Changes in land use land cover (%)		
	1985	1995	2005	2015	1985-1995	1995-2005	2005-2015
Agriculture	80.1	87.8	87.6	91.2	7.7	-0.2	3.6
Forest	3.1	1.7	1.0	0.8	-1.4	-0.7	-0.2
Grassland	3.6	7.8	3.2	3.6	4.2	-4.6	0.4
Shrubs	13.2	2.7	8.2	4.4	-10.5	5.5	-3.8
Total	100	100	100	100	0	0	0

2.3.2 SWAT model calibration and validation

The ranges for the SWAT model parameters and their adjusted values for the SLU and DLU model setups are presented in Table 2.3. The initial minimum and maximum values were based on a recommendation from published literatures in the basin (Setegn *et al.*, 2008; Gebremicael *et al.*, 2013; Dile *et al.*, 2016; Melke and Abegaz, 2017). The calibrated best model parameter values were different for the SLU and DLU model setups (Table 2.3) which was mainly because of the difference in the land-use data between the two model setups. Curve number (CN2), Manning's "n" value for overland flow (OV-N), and maximum canopy storage (CANMX) model parameters highly related to the land-use type (Neitsch *et al.*, 2011). These parameters significantly affect surface runoff and evapotranspiration simulation in the SWAT model. CN2 model parameter decreased from its original value by 9.1% and 9.5% in the DLU and SLU setup, respectively. However, the OV_N and CANMAX model parameters in the SLU setup were large, compared to the DLU setup. The higher value of CN2 and the lower value of OV_N and CANMAX in the DLU setup associated with the expansion of agriculture and reduction of forest and shrub-land use in the study period. These findings agree with Gebremicael *et al.* (2013) study in the Blue Nile basin

and Briones *et al.* (2016) study in the Palico watershed. Groundwater deep percolation fraction (RCHRG_DP) value was higher in the SLU model setup, compared to the DLU model setup; which indicated that SLU setup simulated more groundwater storage. The higher RCHRG_DP value mainly related to the higher forest and shrub coverage in the SLU setup. This result agrees with Nejadhashemi *et al.* (2010) study in the agricultural region of Michigan and Wisconsin. As a whole, the variance among these model parameters of both model setups consistently reflect differences in hydrological processes under different land-use information.

Table 2.3 Ranges for model parameter changes and best parameter values for SLU and DLU model setup for streamflow calibration. The SLU and DLU refer to static land-use and dynamic land-use conditions, respectively.

No.	Parameter Name	Description	Range	Defualt value	DLU	SLU
1	r__CN2.mgt	SCS runoff curve number	± 0.15	84.2	-0.091	-0.095
2	v__ALPHA_BF.gw	Base-flow alpha factor (Days)	0-0.5	0.048	0.40	0.25
3	v__GW_DELAY.gw	Groundwater delay (Days)	15-109	31	29.50	24.87
4	v__GWQMN.gw	Threshold depth of water in the shallow aquifer required for return flow to occur (mm)	0-10	0	5.75	0.45
5	v__ GW_REVAP.gw	Groundwater "revap" coefficient	0.1-0.2	0.02	0.10	0.13
6	v__RCHRG_DP.gw	Deep aquifer percolation fraction	0-0.88	0.05	0.06	0.15
7	v__GWHT.gw	Initial groundwater height (m)	0-10	1	8.90	1.45
8	v__REVAPMN.gw	Threshold depth of water in the shallow aquifer for "revap" to occur (mm)	0-10	1	9.85	8.15
9	r__SOL_AWC.sol	Available water capacity of the soil layer	-0.13-11	0.105	-0.10	-0.09
10	r__SOL_K.sol	Saturated hydraulic conductivity (mm/hr)	0.02-0.2	3.35	0.04	0.08
11	r__ESCO.hru	Soil evaporation compensation factor	± 0.15	0.95	-0.04	0.12
12	r__EPCO.hru	Plant uptake compensation factor	± 0.15	1	0.03	-0.08
13	r__OV_N.hru	Manning's "n" value for overland flow	± 0.15	0.14	-0.02	0.01
14	r__SLSUBBSN.hru	Average slope length	± 0.15	48	-0.12	0.14
15	v__CANMX.hru	Maximum canopy storage	10-50	0	11.80	21.00
16	v__SURLAG.bsn	Surface runoff lag time	0-9	4	0.15	0.02
17	v__CH_N2.rte	Manning's "n" value for the main channel	0.02-0.3	0.014	0.15	0.15
18	v__CH_K2.rte	Effective hydraulic conductivity in main channel alluvium (mm/hr)	6-28	0	17.33	14.03

Note: "r__": Relative change to the existing parameter value, i.e the existing value is multiplied by 1 + a given value, "v__": The existing parameter value is to be replaced by the given value.

The model performance statistics for the calibration and validation periods are presented in Table 2.4. The NSE values of the DLU setup were 0.75 for the calibration period and 0.71 for the validation period, corresponding to model performance ratings (Moriasi *et al.*, 2007) of very good and good, respectively. However, the model performance was good in the case of SLU setup calibration and validation with the NSE values of 0.73 and 0.71, respectively. Likewise, evaluation using the R^2 for the DLU model simulation in the calibration and validation period was 0.75 and 0.80, respectively. The SLU model calibration and validation had similar R^2 values (0.74). The higher R^2 for both model setups indicated a very good linear relationship between simulated and observed streamflow data. Positive values of PBIAS for DLU setup (5.3% for calibration and 29.1% for validation) and SLU setup (7.1 % for calibration and 24.9% for validation) indicated a tendency for underestimation of daily streamflow. However, the low magnitude of PBIAS values corresponded to a performance rating of "very good" during the calibration period, and the high magnitude of PBIAS values corresponded to a performance rating of "unsatisfactory" during the validation period. The PBIAS result showed a very small accumulation of difference in streamflow volume between the simulated and observed data for the calibration period. But, the model simulation in the DLU and SLU setups had a significant underestimation tendency during the validation period. A more stringent test of model performance was found during the validation period since the parameters range were fixed during this period (Saraswat *et al.*, 2010). Therefore, according to the model evaluation criteria recommended by Moriasi *et al.* (2007), the performance of SLU and DLU SWAT model was satisfactory during the calibration period. This result agrees well with the previous studies in Gumara watershed (Setegn *et al.*, 2008; Dile *et al.*, 2016).

The DLU model setup showed satisfactory model uncertainty during the calibration (validation) period with P-factor of 0.87 (0.77) and R-factor of 0.65 (0.54). Comparable uncertainty level was found in the SLU model setup with P-factor of 0.87 (0.78) and R-factor of 0.64 (0.57) for calibration (validation) periods. The uncertainty factors showed acceptable model uncertainty estimates. According to Abbaspour *et al.* (2007) recommendation, P-factor ≥ 0.75 and R-factor ≤ 1.5 would be desirable for streamflow.

Table 2.4 Goodness-of-fit evaluation statistical for the calibration and validation periods in SLU and DLU model setups.

Model Setup		NSE	R^2	PBIAS	P-Factor	R-Factor
Dynamic Land Use (DLU)	Calibration	0.75	0.75	5.3	0.87	0.65
	Validation	0.71	0.80	29.1	0.77	0.54
Static Land Use (SLU)	Calibration	0.73	0.74	7.1	0.87	0.64
	Validation	0.71	0.74	24.9	0.78	0.57

Simulated daily streamflow from SLU and DLU model setup were compared with observed values during the calibration and validation period (Figure 2.4). Generally, there was a good agreement between the observed and simulated flows in both model setups, but a few peak flow events were not adequately captured during the rainy period. DLU and SLU simulated peak flow values were higher than observed values on July 29/1988, August 28/1999, August 22/2005 and August 04/2010 (Figure 2.4a and 2.4b), which mainly caused by the higher rainfall input during these periods. Both model setups had underestimation (61%) and overestimation (39%) tendency for the peak event simulation. The SLU and DLU simulated streamflow were consistently underestimated compared to observed values, in particular from 1990 to 1992, 1995 to 1997 and 2008 to 2009.

Comparable goodness-of-fit and P-factor and R-factor values indicated that the model performance between DLU and SLU setup did not show a significant difference. Although the DLU setup did not show pronounced improvement, the calibration period DLU model setup performed slightly better than the SLU model setup. The higher NSE and R^2, and lower PBIAS values revealed the slightly better performance of the DLU model setup, which was mainly due to the better representation of the temporal land-use changes in the DLU setup. During the validation period, both model setups were noticeably worse (lower NSE and higher PBIAS) than during the calibration period. Based on the similar values of NSE, both model setups were equally able to predict daily streamflow during the validation period. The PBIAS for both model setups did not agree with other criteria, and the values of DLU were higher than the SLU during the validation period. Wagner *et al.* (2016) and Pai and Saraswat (2011) also found improvement in model simulation by applying dynamic land-use data.

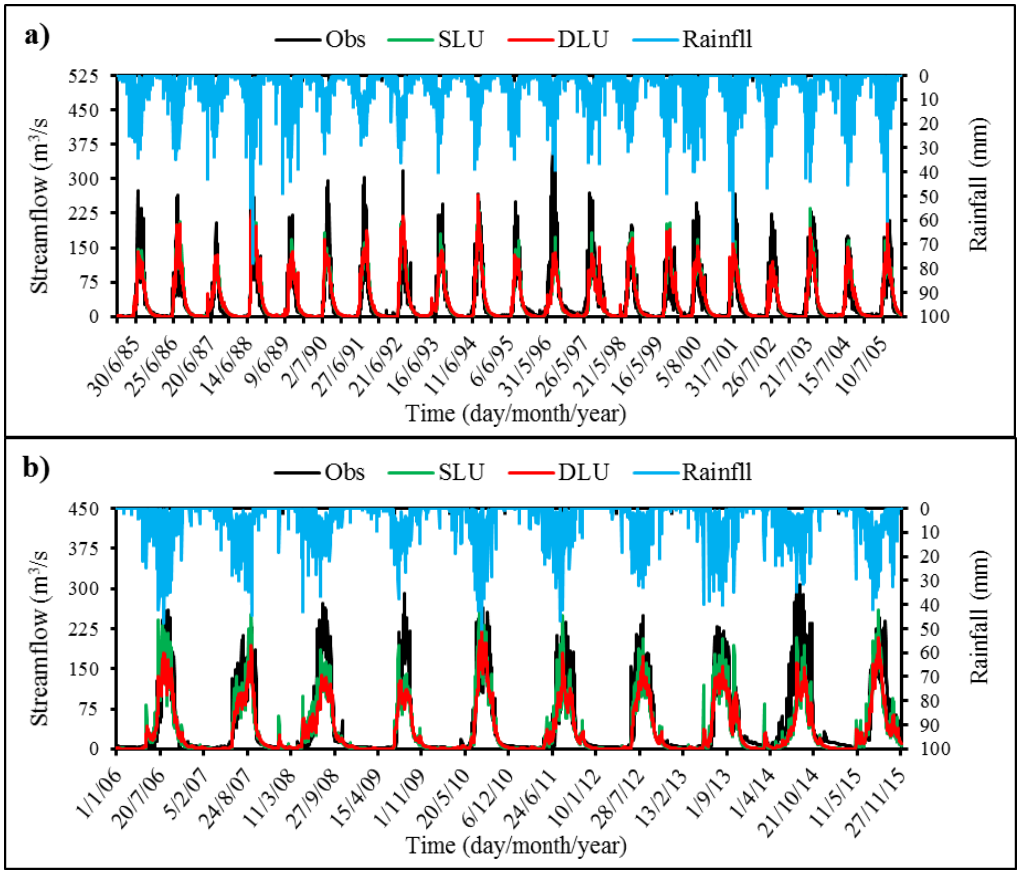

Figure 2.4 The observed and simulated (DLU and SLU) daily streamflow in Gumara watershed during: a) calibration period (1985-2005), and b) validation period (2006-2015).

2.3.3 Temporal variation of the hydrological response

The temporal land-use effects on surface runoff, evapotranspiration, and peak flow were studied in the four periods where dynamic land-use change was implemented. The hydrological responses with agricultural and forest land-use percentages are summarized and presented in Table 2.5. The simulated hydrological processes from the SLU model setup were different between the four periods (1985-1999, 1990-1999, 2000-2009, and 2010-2015), which mainly associated with climate (rainfall) variations (Table 2.5). However, the hydrological responses difference in the DLU model setup related to climate variability and land-use change. Therefore, the difference in the hydrological components between the SLU and DLU model setups provided the isolated impact of land-use change.

Table 2.5 The average hydrological response in the agricultural and forest land-use types in the periods where static and dynamic land use was implemented.

Simulation Period	Agricultural land-use (%)		Forest land-use (%)		PRECIP (mm)		SR (mm)		ET (mm)		Peak flow (m^3/s)	
	SLU	DLU	SLU	DLU	SLU	DLU	SLU	DLU	SLU	DLU	SLU	DLU
1985-1989	80.1	80.1	3.1	3.1	1443	1443	363.7	363.7	523.0	523.0	219.3	219.3
1990-1999	80.1	87.7	3.1	1.7	1387	1387	348.7	358.1	491.5	487.3	175.7	176.8
2000-2009	80.1	87.6	3.1	1.0	1332	1332	313.1	321.1	479.3	473.5	184.6	187.5
2010-2015	80.1	91.2	3.1	0.8	1435	1435	397.2	408.8	445.0	439.7	220.6	223.0

Note: PRECIP = average annual precipitation, SR = average annual surface runoff, ET = average annual evapotranspiration, SLU = Static land use, and DLU = Dynamic land use.

The simulated surface runoff, evapotranspiration, and peak flow in the SLU and DLU model setups were similar in the 1985-1989 period, which used 1985 land-use data. The estimated hydrological responses in DLU and SLU setup were different in 1990-1999, 2000-2009, and 2010-2015 period, since the DLU model setup dynamically replaced the 1985 land-use by 1995, 2005, and 2015 land-use data during respective periods. In these periods, the DLU model setup simulated lower evapotranspiration and higher surface runoff and peak flow. The maximum and minimum variation of these hydrologic responses occurred in the 2010-2015 and 2000-2009 period, respectively. The maximum difference in surface runoff and peak flow between the two model setups was 11.6 mm and 2.4 m^3/s, respectively. This variation directly related to the agricultural land-use expansion by 11.1% and forested area reduction by 2.3% in the DLU model setup. Andualem and Gebremariam (2015) showed similar findings in Gilgel Abay watershed, Lake Tana basin. Likewise, Yin *et al.* (2017) found a similar experience in a semi-humid and semi-arid transition zone in northwest China. The simulated evapotranspiration values were lower in the DLU model setup mainly because of the consideration of low forest coverage, compared to the SLU model setup. Higher evapotranspiration occurred in forested and vegetated watersheds (Alemu *et al.*, 2014) due to higher transpiration and evaporation from the canopy (Getahun and Haj, 2015). This result agrees well with the study conducted by Fang *et al.* (2013) in the Laohahe River basin, China. Their study showed that the expansion of vegetation cover areas decreased surface runoff and increased actual evapotranspiration.

Since the SLU model setup considered static land-use data for the entire simulation period and ignored the temporal land-use dynamics, but it can help to study the temporal climate variability. On the contrast, the DLU model setup captured both the land-use and climatic dynamics.

Therefore, the DLU model explained very well the effects of land-use change on the temporal variation of the surface runoff, evapotranspiration and peak flow. The DLU setup used realistic past land-use change conditions. As also stated by Wagner *et al.* (2016) and Chiang *et al.* (2010), the temporal components of land-use change were assessed well in the dynamic land-use setup. Thus, surface runoff, peak flow, and evapotranspiration were assumed to be more realistically estimated in the DLU setup. The comparison between DLU and SLU surface runoff, peak flow and evapotranspiration in the four simulation periods is shown in Figure 2.5. The variations of hydrological responses (surface runoff, peak flow, and evapotranspiration) were directly proportional to the magnitude of land-use change (Figure 2.5). The contrast between the DLU and SLU setup indicated the influence of land-use change between the two simulation periods. DLU surface runoff simulation increased by 45.1 mm between 1985-1989 and 2010-2015 period while the SLU setup increased the surface runoff simulation by 33.5 mm. The isolated land-use change increased surface runoff by 11.6 mm, which accounted for 25.7% of the total surface runoff change (45.1 mm). The contrast between 1985-1989 and 2010-2015 simulation in the SLU setup indicated the influence of climate variation. The climate variation increased surface runoff by 33.5 mm, which accounted for about 74.3% of the total surface runoff increment. The above results showed that land-use change and climate variation during 1985-1989 and 2010-2015 increased surface runoff, but the contribution of land-use change was smaller than that of climate variation. Between this simulation period, combined land-use change and climate variation increased peak flow by 3.7 m^3/s, and the percent contributions were 64.9% (2.4 m^3/s) from land-use change and 35.1% (1.3 m^3/s) from climate variability. The integrated effect of land-use change and climate variability (DLU) decreased evapotranspiration by 83.3 mm. From this evapotranspiration change, 93.6% (78 mm) and 6.4% (5.3 mm) decrease resulted from climate variability and land-use change, respectively. From the three hydrological responses considered in this research, peak flow variation was highly sensitive to land-use change in Gumara watershed.

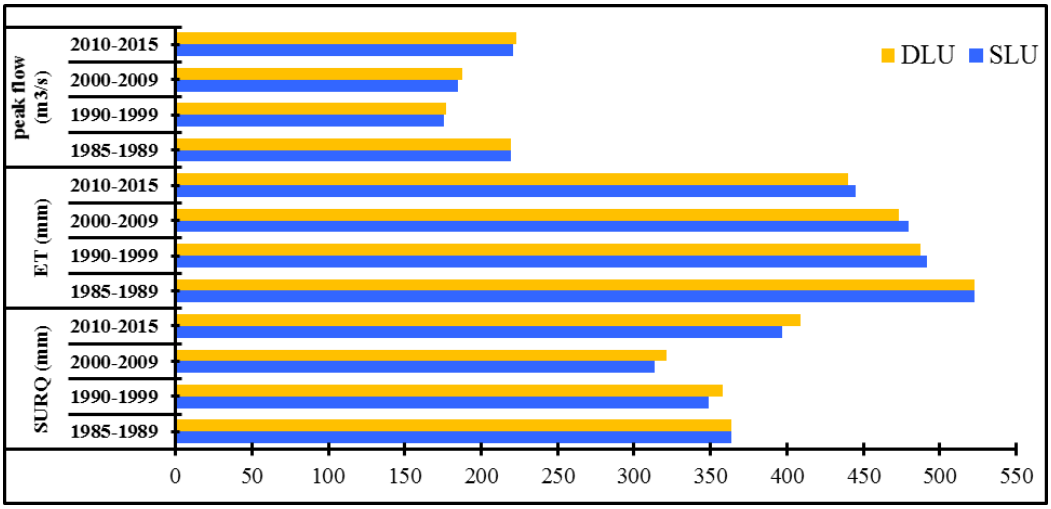

Figure 2.5 Temporal comparison of SLU and DLU setup surface runoff, peak flow and evapotranspiration.

2.3.4 Spatial variation of the hydrological response

The effect of sub-basin level land-use change on the hydrological components was studied using simulations based on the 1985 and 2015 land-use data. Sub-basin level land-use changes between 1985 and 2015 are presented in Figure 2.6. During this period, the agricultural land-use area increased in all sub-basins except in sub-basin 6, 9, 15, and 21 (Figure 2.6), with the maximum expansion of 47.1% in sub-basin 1. The forest coverage slightly increased in sub-basin 21, whereas insignificant land-use change was noticed in sub-basin 6.

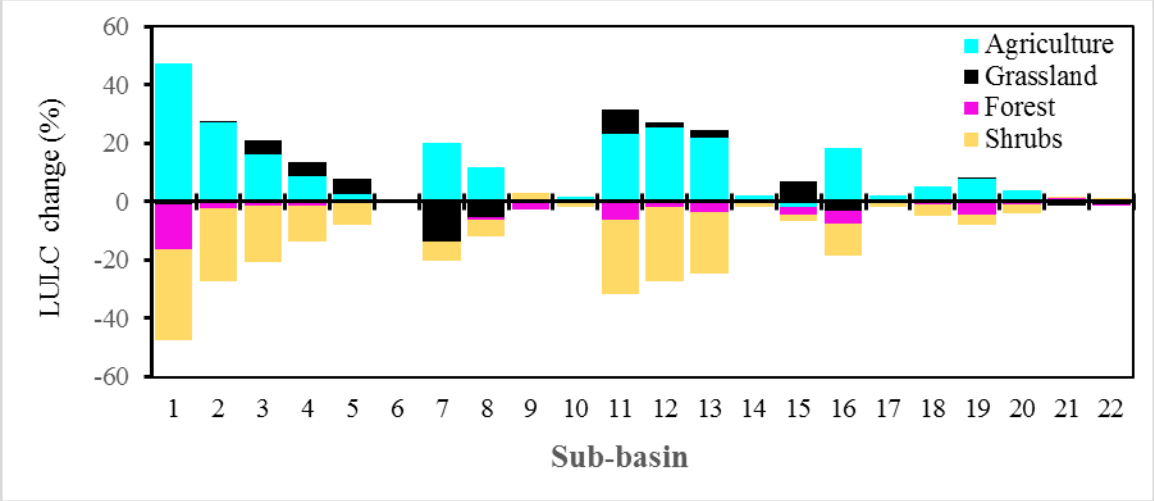

Figure 2.6 Percentage of LULC change over each sub-basin between 1985 and 2015.

The spatial impacts of land-use change on the hydrological response were investigated using the average of SLU and DLU simulation in the 2010-2015 period. Sub-basin surface runoff, peak flow

and evapotranspiration change between DLU and SLU setup are presented in Figure 2.7. The magnitude and direction of the sub-basin level hydrological response change were assessed with 1985 and 2015 land-use data. Due to the expansion of agricultural land-use and reduction of forest coverage in most of the sub-basins, higher surface runoff and peak flow were found in the DLU model setup. Sub-basin 1, 12, and 13, had the largest change in surface runoff, with a maximum increase of 50.1 mm (Figure 2.7a). These maximum changes in surface runoff associated with the maximum expansion of agricultural land-use by 47.5% in sub-basin 1. The expansion of shrubs and forest lands in sub-basin 9 and 21 resulted in surface runoff decrease. Shrub-land expansion (2.5%) in sub-basin 9 decreased surface runoff (0.5 mm). Likewise, 1.1% expansion of forest coverage in sub-basin 21 decreased surface runoff by 1.2 mm. Similar results about surface runoff increment due to the expansion of agricultural land-use and the reduction of forest were reported in another region (Huang and Lo, 2015). As shown in Figure 2.7b, the largest peak flow variation between DLU and SLU occurred in the downstream parts of the watershed (sub-basin 1, 5, 7, and 8) which may be due to the higher expansion of agricultural land-use over these sub-basins. The highest agricultural land-use expansion (47.5%) caused a higher peak flow (2.2 m^3/s) variation in sub-basin 1. During the simulation period 2010-2015, the SLU setup considered higher forest and shrub coverage, which caused higher evapotranspiration compared to the DLU model setup. The largest change in evapotranspiration occurred in sub-basins 1, 2, 7, and 13, with a maximum decrease of 39.7 mm (Figure 2.7c). A slightly higher forest coverage (1.1%) in the DLU model setup over sub-basin 21 caused 1.1 mm more evapotranspiration simulation when compared to the SLU model setup. This result is consistent with Dias *et al.* (2015) study where watersheds with an increase in forest cover tend to have higher evapotranspiration, and lower surface runoff and peak flow. As a result of static land-use in sub-basin 6, there was an insignificant change in surface runoff, peak flow, and evapotranspiration.

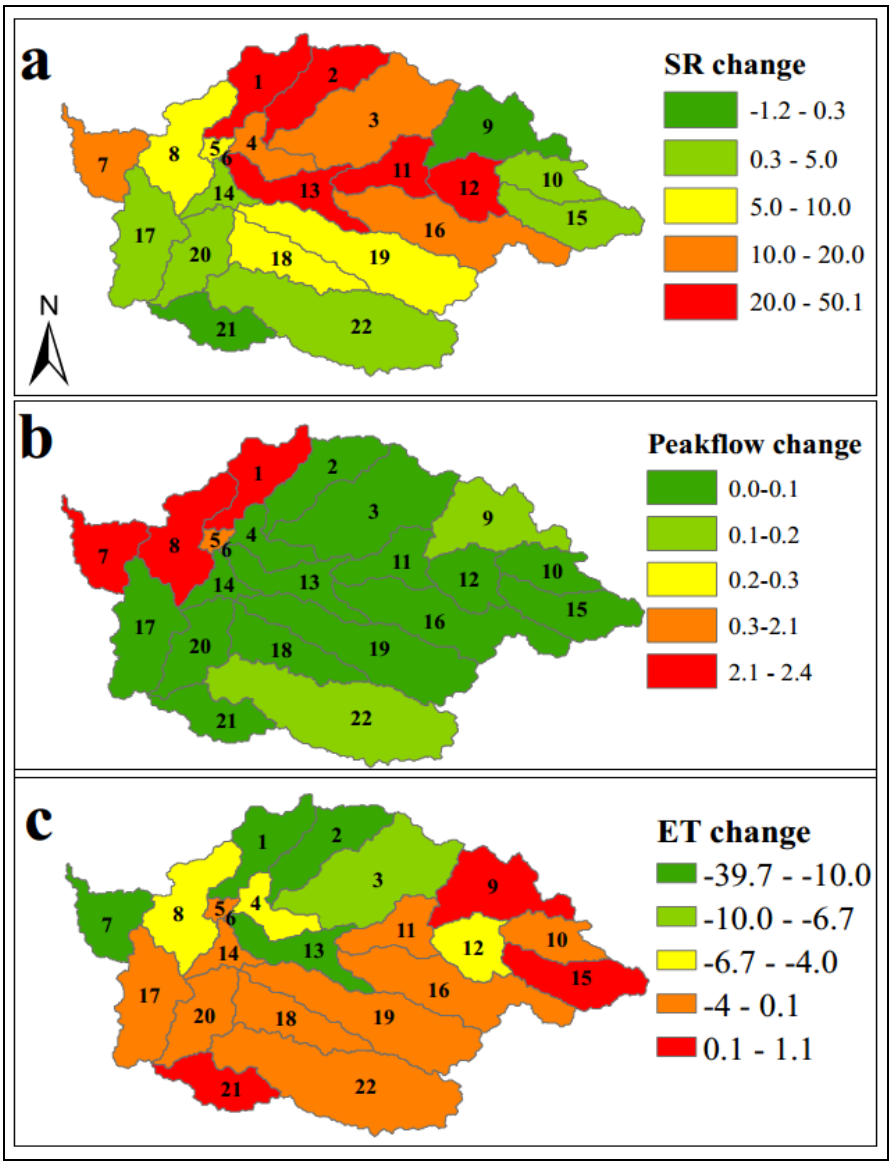

Figure 2.7 Sub-basin level change in hydrological response: change in a) surface runoff (SR, mm), b) peak flow (m^3/s) and c) Evapotranspiration (ET, mm) between DLU and SLU model setups for the simulation period 2010-2015.

The dynamic changes in land-use and their spatial distribution were analyzed to assess the effects of land-use change on surface runoff, peak flow, and evapotranspiration simulation in the selected sub-basins (Table 2.6). The DLU and SLU model setups were compared in the 2010-2015 simulation period. In this period, the DLU setup used 2015 land-use data, while the SLU setup used 1985 land-use. Thus, the DLU setup considered the realistic representation of spatial land-use coverage and their effects on hydrologic response. The curve number (CN2) is the most sensitive parameter in determining the fraction of precipitation converted to surface runoff (Briones *et al.*, 2016). The alteration of land-use between 1985 and 2015 affected the sub-basins

CN2. The consideration of the actual expansion of agricultural land-use in the DLU setup caused a higher CN2 (sub-basin 1, 7, 10, 12, and 13), whereas the expansion of forest and shrubs resulted in a lower CN2 (sub-basin 21). The expansion of agricultural land-use in sub-basin 1 caused the CN2 to rise from 76.2 to 79.6. Because of this change, the simulated surface runoff increased from 285 mm to 335 mm and peak flow increased from 10.8 m^3/s to 13 m^3/s (Table 2.6). The result agrees with the findings of Dang and Kumar (2017) who reported that the magnitude of surface runoff and peak flow simulation positively correlated with CN2 change. The increase in surface runoff can be attributed to reduce evapotranspiration. Higher surface runoff and lower evapotranspiration are expected in agricultural land-use than forest and shrubs area (Anaba *et al.*, 2017). The static land-use coverage in sub-basin 6 resulted in invariant CN2 and hydrological responses. Expansion of forest and shrubs coverage would result in an increase in the interception and infiltration opportunity time and thereby result in more water being infiltrated into the soil and decline surface runoff. In the afforested sub-basin 21, high evapotranspiration was found mainly because of the higher transpiration and interception. Overall, the consideration of the real land-use change in the DLU setup reproduced the non-stationary hydrologic response. This finding agrees with the previous research result which indicated that land-use dynamics causes of non-stationary hydrologic response (Guse *et al.*, 2015; Ajami *et al.*, 2017).

Table 2.6 Impact of LULC changes on surface runoff, peak flow and evapotranspiration in the selected sub-basins.

Sub-basin	Hydrological responses						Curve number (CN2)		LULC change between 1985 and 2015			
	SR (mm)		ET (mm)		Peak flow (m^3/s)				Agriculture	Forest	Grassland	Shrubland
	SLU	DLU	SLU	DLU	SLU	DLU	SLU	DLU				
1	285	335	563	523	10.8	13.0	76.2	79.6	48	-16	-1	-31
6	347	347	544	544	116	116	80.3	80.3	0	0	0	0
7	558	569	482	471	220	223	80.7	81.1	20	0	-14	-6
10	408	411	303	302	9	9	79.6	79.7	2	-1	0	-1
12	380	406	305	300	33	33	77.9	79.6	26	-2	2	-26
13	314	339	540	526	83	83	78.1	79.8	22	-4	3	-21
21	527	526	477	479	12	12	79.5	79.4	-0.5	1	-0.8	0.3

2.4 Conclusions

This study evaluated the impacts of Static Land Use (SLU) and Dynamic Land Use (DLU) on the representative hydrological processes using the SWAT hydrological model. The SWAT model evaluation showed that the SLU and DLU setups affected the model parameters and the SWAT model performance. The SWAT model calibration under SLU and DLU setup provided satisfactory results during the calibration period. The DLU setup, which represented the 31 years' land-use dynamics, had a higher curve number, and a lower canopy storage and groundwater recharge parameters due to the conversion of forest and shrub-land into agricultural land. Statistical comparison between simulated and observed streamflow showed a slight model performance improvement in the case of dynamic land-use setup.

The temporal and spatial analysis showed that implementing dynamic land-use data affected the hydrological responses of Gumara watershed in terms of surface runoff, peak flow, and evapotranspiration. The average annual surface runoff and peak flow increased while the evapotranspiration decreased when the forest and shrub coverage converted into agricultural land. However, the effects of land-use change on the hydrological response were non-uniform over space and time. The DLU model setup can better represent the spatial and temporal variability of hydrologic processes caused by the temporal land-use change. Sub-basins with an increase of agricultural land-cover tend to increase surface runoff and peak flow, and a decrease in evapotranspiration. On the other hand, sub-basins with an increase in shrubs and forest land resulted in a decrease in surface runoff and an increase in evapotranspiration. The increase in surface runoff may have positive implications for irrigation activities since it can be harvested using water harvesting structures and used for crop production. On the other hand, an increase in surface runoff may also cause flooding problems for the surrounding area.

The findings from this study have shown that applying dynamic land-use in the hydrological simulation slightly improved model performance and thereby improved water resource estimations in watersheds. It can also help in implementing sustainable land and water management practices. However, SLU model setup can be applied in land use data scare condition for water resources planning.

3. IMPACTS OF LAND SURFACE MODEL AND LAND USE DATA ON WRF MODEL SIMULATIONS OF RAINFALL AND TEMPERATURE OVER LAKE TANA BASIN, ETHIOPIA

Abstract

The Weather Research and Forecasting (WRF) model is one of the regional climate models for dynamically downscaling climate variables at finer spatial and temporal scales. The objective of this study was to evaluate the performance of the WRF model for simulating temperature and rainfall over the Lake Tana basin in Ethiopia. The WRF model was configured for six experimental setups using three land surface models (LSMs): Noah, Thermal Diffusion (TD), and Rapid Update Cycle (RUC); and two land-use datasets: USGS and updated New Land Use (NLU). The performances of WRF configurations were assessed by comparing simulated and observed data from March to August 2015. The result showed that temperature and rainfall simulations were sensitive to LSM and land-use data choice. The combination of NLU with RUC and TD produced very small cold bias (0.27 °C) and warm bias (0.20 °C) for 2m maximum temperature (Tmax) and 2m minimum temperature (Tmin), respectively. WRF model with RUC and NLU captured well the observed spatial and temporal variability of Tmax, while TD and NLU represented temporal variability in Tmin. Moreover, rainfall simulation was better with NLU; especially NLU and Noah configuration produced the smallest mean bias (2.39 mm/day) and root mean square error (6.6 mm/day). All the WRF model configuration poorly detected the occurrence of heavy rainfall. Overall, findings showed that the application of updated land-use data substantially improved the WRF model performance in simulating temperature and rainfall. The study would provide valuable support for identifying suitable LSM and land-use data that can accurately predict the climate variables in the Blue Nile basin.

Keywords: Dynamical downscaling, Updated land-use, LSM, WRF, Lake Tana basin

3.1 Introduction

Rainfall and temperature affect various components of the hydrological cycle including, river flow, evapotranspiration, groundwater recharge, and soil moisture. Reliable rainfall and temperature data at reasonable spatial and temporal resolutions are essential for quantifying the seasonal hydrological cycle (Dile *et al.*, 2013; Tabari *et al.*, 2016). However, attaining good quality climate data is challenging in developing countries like Ethiopia. In such cases, numerical models can be used to produce climate data at a fine resolution (Sisay *et al.*, 2017). For example, such data can be used to predict future climate that can inform policy-maker on climate change adaptation and mitigation (Gashaw *et al.*, 2014).

In this regard, Regional Climate Models (RCMs) could be useful tools to downscale climate variables at a fine spatial and temporal resolutions at a regional scale (Yhang *et al.*, 2017). Moreover, RCMs realistically simulate climate information by incorporating land surface properties and detailed descriptions of physical processes (He *et al.*, 2017). Recently, Weather Research and Forecasting (WRF) model has been applied as an RCM for research and operational purposes in many parts of the world, for example in Africa (Diaz *et al.*, 2015), Europe (Banks and Baldasano, 2016), North America (Burakowski *et al.*, 2016), and Asia (Cannon *et al.*, 2017). Previous studies showed that the performance of WRF model was influenced by the selection of physical parameter schemes including, microphysics (Gao *et al.*, 2017), radiation (Mooney *et al.*, 2016), planetary boundary layer (Kim *et al.*, 2015), cumulus (Mugume *et al.*, 2017), and land surface model (Jain *et al.*, 2017). Other model inputs such as initial boundary condition (Yang and Duan, 2016), land-use data (Cheng *et al.*, 2013), and domain size and resolution (Zeyaeyan *et al.*, 2017) also affect the performance of WRF model.

Many studies in recent years have focused on the selection of suitable Land Surface Models (LSMs) for climate simulation at the mesoscale level. For example, Zu-Heng *et al.* (2014) evaluated Noah, Pleim-Xiu, and Noah-MP LSMs for simulating extreme rainfall events over Southwest China. They found that WRF simulations with Noah-MP reproduced well the spatial and temporal variations of rainfall. Lee *et al.* (2016) reported that Noah LSM resulted in better simulations of observed climate variables compared to Thermal Diffusion (TD), Rapid Update Cycle (RUC) and Pleim-Xiu LSMs in a case study in South Korea. On the other hand, the Pleim-Xiu LSM simulated better temperature and wind speed over the Delhi-Mumbai Industrial Corridor

region in India (Jain *et al.*, 2017), while RUC LSM was better for rainfall simulation in the Western Disturbances of India (Thomas *et al.*, 2014). The discrepancy of LSM recommendation in the above studies indicates that the performance of LSM is highly dependent on the simulation region, studied climate variable, seasonality, and considerations of other physical parameters. Therefore, site-specific studies are important to identify suitable LSM to simulate climate variables accurately.

Besides, the accuracy of the land surface datasets significantly affects the performance of the WRF model (Göndöcs *et al.*, 2015). The advancement of Remote Sensing (RS) and Geographic Information System (GIS) enable land surface datasets for the WRF model at finer spatial and temporal resolutions (Cannon *et al.*, 2017; Cao *et al.*, 2017), which help to improve WRF simulations. However, the WRF model takes most land surface properties from the default 1993 U.S. Geological Survey (USGS) land-use data (Yang and Duan, 2016). This dataset has a certain degree of land-use misrepresentations (Cheng *et al.*, 2013; Puliafito *et al.*, 2015). To circumvent this problem, updated and fine resolution land-use data has been employed in the WRF model (Cao *et al.*, 2015; He *et al.*, 2017) which improves regional climate simulations. For example, the application of CORINE land-use improved the WRF model performance compared to the USGS dataset (De Meij and Vinuesa, 2014). Also, Lai *et al.* (2016) showed that Global Land Cover 2009 data performed better than the default 1993 USGS dataset. Sertel *et al.* (2009) found evidence that inaccurate specification of land-cover in the default configuration of the WRF model, and in particular, poor representation of the extent of urban areas, impaired the simulation of surface temperature. The above reviews demonstrate that there have been numerous individual studies on the sensitivity of the WRF model to either LSM or land-use data. However, few studies have focused on the influence of LSM and land-use data combination on mesoscale climate simulations. This study contributes to filling this gap.

Although the climate of Lake Tana basin has a strong association with the topography and land-use dynamics (Haile *et al.*, 2009), most of the previous studies have applied statistical downscaling method (Ayele *et al.*, 2016; Roth *et al.*, 2018); which overlooked the local landscape conditions mainly complex topography and accelerated land-use change. Besides, RCM has rarely studied in this region, and suitable LSM and land-use data configuration were not identified yet. Therefore, a focused study comparing climate variables on different LSMs along with and without updated

land-use information promises to provide valuable insight for WRF modelers and regional climate simulation.

In this study, six WRF experiments using three LSMs (Noah, RUC, and TD) and two land-use data (USGS and NLU) were considered to investigate the sensitivity of the WRF model to updated land-use and identify the best performing LSM. This study is novel in the sense that it evaluates the combined effect of LSMs and land-use data on the WRF model simulation performance. The WRF model was configured at fine grid spacing in order to include the complex topography and land-use change dynamics. The fine grid spacing (<6 km) is adequate to depict mesoscale topography (Goswami *et al.*, 2012), which resolve areas of high and low elevation. The result will provide useful insights into the advantages of using updated land-use information in the WRF regional climate modeling applications. Moreover, the study will provide valuable information about the relative performance of land-use data and LSMs for the regional climate simulation and inputs for the WRF model improvement program. This study tested the hypotheses that updated land-use improves the RCM at basin scale that strong spatial and temporal climate heterogeneity. Besides, the study addressed two major research questions: a) is there any difference among the land surface models for climate simulation at finer spatial resolution? and b) does the choice of land-use data result in substantial biases in rainfall and temperature? Model prediction performances were verified using observed rainfall and temperature data using different statistical and categorical verification methodologies. Thus, a thorough evaluation of the model performance and the best-identified parameters contributing to mesoscale climate simulation in this particular area results of general relevance.

3.2 Materials and Methods

3.2.1 Study area

Lake Tana basin is located in the Amhara region in Ethiopia and covers a catchment area of ~15,140 km^2. Lake Tana, which accounts for 20% of the basin area, is the largest freshwater body in Ethiopia and considered as the source of the Upper Blue Nile River. The basin is located at 10.95°N to 12.78°N and 36.89°E to 38.25°E (Figure 3.1), and its elevation ranges from 1780 to 4100 meter above sea level.

The majority of the basin (75%) is located in temperate to cool semi-humid zone and the remaining 25% is found in cool to cold humid zone. In general, the climate in the basin is divided into rainy and dry seasons. The rainy season mainly spans from June to September (Tigabu *et al.*, 2018), which account for 70–90% of the rainfall amount (Enyew *et al.*, 2014). The dry season occurs from October to March. However, in the southern parts of the basin less intense sporadic rainfall occurs in April and May (Enyew *et al.*, 2014). There is high temporal and spatial rainfall variability in the Lake Tana basin because of extreme topographic variation and the presence of the lake water body (Haile *et al.*, 2009). The long-term basin mean annual rainfall over the period of 1982-2015 is about 1394 mm. The rainfall ranges between 964 and 2000 mm in the northern and southern parts of the basin, respectively. The temperature is warmer around Lake Tana and becomes cooler moving away from Lake Tana. The mean annual minimum and maximum temperature over the period of 1982-2015 is about 15 °C and 27 °C, respectively.

3.2.2 WRF model configuration

In this study, Weather Research and Forecasting (WRF) model version 3.8 was used for climate simulation. The WRF model is developed by the National Center for Atmospheric Research (NCAR). This model is a flexible and state-of-the-art atmospheric numerical simulation which is implementable parallel computing platforms (Skamarock *et al.*, 2008) to predict weather on a mesoscale level for operational and research needs. The model was configured for a fine spatial resolution with three domains (Figure 3.1a). The outer domain (D1) covers a total distance of 2775 km in the East and 1998 km in the North direction at 36 km grid spacing. This domain size was chosen to cover the Indian Ocean, red sea and East Africa region which influence rainfall patterns in Ethiopia (Conway, 2000). The intermediate domain (D2) covers a distance of 1225 km in the

East and 1332 km in the North direction at 12 km resolution. The inner domain (D3) centered at Lake Tana and covers an area of 280 km in the East and 333 km in the North directions. This domain had a 4 km resolution. This fine grid spacing was selected to resolve the mesoscale forcing associated with complex topography, lake and vegetation characteristics that influence local climate (Goswami *et al.*, 2012). The three domains were run in one-way nesting mode with 35 vertical layers from near the surface to the model top at 50 hPa.

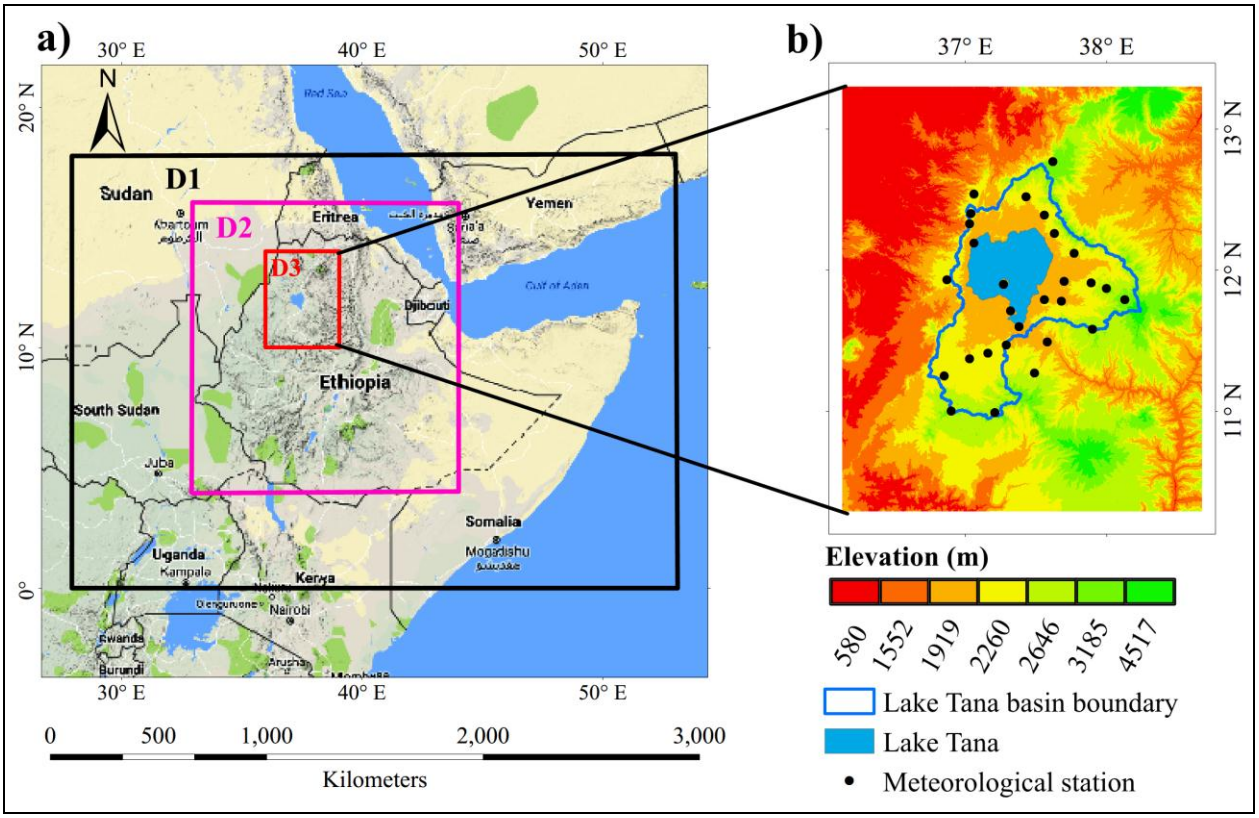

Figure 3.1 Study area; a) three nested domains: the black rectangle represents the outer domain (D1) representing Eastern Africa, South Asia, and the Indian Ocean, the purple rectangle shows the intermediate domain (D2) covering most part of Ethiopia, and the red rectangle is the inner domain (D1) covering north western Amhara Region where the Lake Tana basin is located. b) Topographic features of the inner domain with the Lake Tana basin boundary, Lake Tana, and meteorological stations that were used for model evaluation.

The WRF physical parameterizations were selected based on preliminary test and previous findings for the Africa region (e.g., Pohl *et al.*, 2011; Hagos *et al.*, 2014; Abdallah *et al.*, 2015; Kerandi *et al.*, 2017; Mugume *et al.*, 2017). The parameterization schemes used in this study were Thompson microphysics (Thompson *et al.*, 2008), Rapid Radiative Transfer Model for GCMs (RRTMG) for long-wave and shortwave radiation (Iacono *et al.*, 2008), revised meso-scale model (MM5) Monin-Obukhov surface layer (Jiménez *et al.*, 2012), Yonsei University planetary

boundary layer (Hong *et al.*, 2006), and Kain-Fritsch cumulus (Kain, 2004). However, the cumulus scheme was not activated for the inner domain because cumulus parameterizations are valid for coarse grid sizes, which is greater than 10 km (Skamarock *et al.*, 2008).

The WRF model was initialized using boundary conditions obtained from the National Centers for Environmental Prediction (NCEP) dataset. These datasets are available at a spatial resolution of 1° × 1°. The lateral boundary conditions in the WRF model were updated at 6 h intervals. The WRF model was forced to read-in the time-varying data and to update the sea surface temperature field. Due to the shortage of computational resources, the simulation period was six months (March–August 2015). These months were selected purposively to represent the dry and wet season in the Lake Tana basin. The WRF simulation period was split into 6 days with 1 day of overlap between consecutive runs to allow for spin-up time. These short-run were considered to minimize the accumulation of errors as the forecast day's increases (Skamarock *et al.*, 2008).

3.2.3 Experimental setup

Six WRF model experiments were configured using a factorial combination of two land-use data and three LSMs. All the experimental configurations used the same physical parameters except LSM and land-use data. The effect of updated land-use information on the performance of the WRF model was studied using the United States Geological Survey (USGS) land-use and new land-use (hereafter NLU) data. The USGS land-use data was generated in 1993 from Advanced Very High-Resolution Radiometer data (Eidenshink and Faundeen, 1994). This data has 24 land-use classes at ~900 m resolution. The inner domain USGS land-use data is presented in Figure 3.2a, where the larger part is covered by savanna and which failed to capture agriculture expansion in 2015 (Rientjes *et al.*, 2011; Biru *et al.*, 2015; Teklay *et al.*, 2018). Moreover, the USGS land-use data did not show Alemsaga and Tara Gedam forest coverage in the Lake Tana basin, which covers ~19 km^2. The NLU data was obtained from the Regional Centre for Mapping of Resources for Development (RCMRD) (http://geoportal.rcmrd.org). This data was produced from 30 m Landsat thematic mapper using a supervised classification method for the 2016 Ethiopia land-cover scheme II. The classification was satisfactory with an overall accuracy of 87.9% and a Kappa coefficient of 0.79 (Tadele *et al.*, 2017). The NLU data represented well land-use categories compared to USGS data. For example, the NLU captured agriculture expansion and notable land-use features such as Alemsaga and Tara Gedam forest coverage (Figure 3.2b).

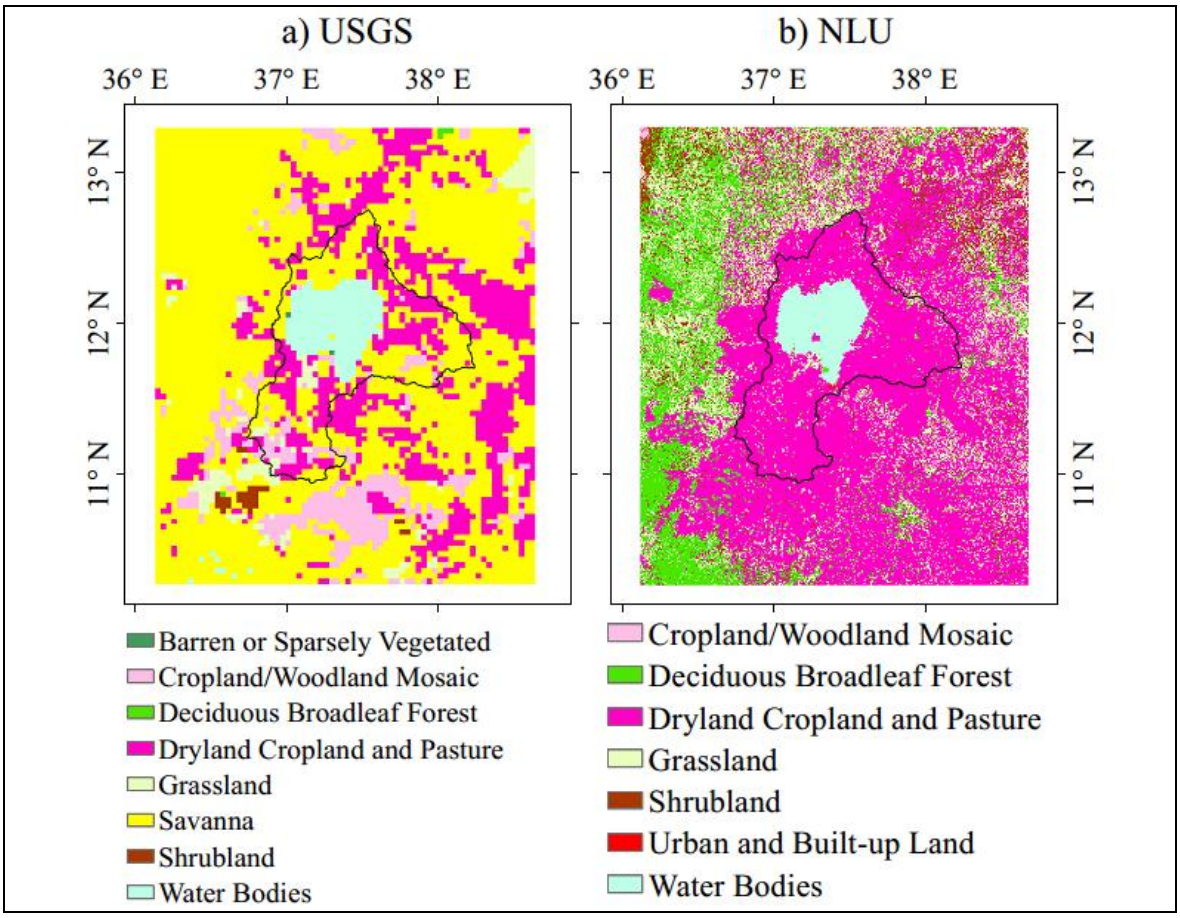

Figure 3.2 Land use coverage for the inner domain; a) U.S. Geological Survey (USGS) land-use, and b) new land-use (NLU).

Major differences in land-use distributions between USGS and NLU data were reflected in the forestland, cropland, grassland, and savanna (Table 3.1). The USGS data underestimated cropland coverage compared to previous research findings in the Ethiopian highlands (e.g., Teferi *et al.*, 2013; Biru *et al.*, 2015; Teklay *et al.*, 2018), while the NLU data was consistent with previous studies in capturing the urban, forest and cropland coverage.

Table 3.1 Summary of land-use coverage for USGS and NLU data in the inner domain.

Land use type	USGS (%)	NLU (%)
Barren or Sparsely Vegetated	0.03	0
Cropland/Woodland Mosaic	7.99	0.03
Dryland Cropland and Pasture	20.97	65.65
Deciduous Broadleaf Forest	0.09	14.00
Grassland	3.35	14.71
Savannas	63.13	0
Shrub-land	0.51	2.02
Urban and Built-up Land	0	0.02
Water Bodies	3.93	3.57

Three land surface models (LSMs) namely; Noah, RUC, and TD were also considered in the WRF experiments. The Noah LSM uses soil temperature and moisture at four layers with a total depth of 2 m. This scheme calculates the soil temperature, water-equivalent snow depth, soil ice and soil and canopy moisture (Skamarock *et al.*, 2008). The RUC LSM estimates heat and moisture transfer for the nine layers from 0 to 3 m, and the model realistically represents soil moisture, soil temperature and snow (Smirnova *et al.*, 2016). The RUC scheme accounts for the different phases of soil surface water, vegetation effects, and canopy water. The RUC LSM has a thin layer feature that covers the ground surface including half of the first atmospheric layer and half of the topsoil layer to properly solve the energy budgets. The model accounts for vegetation impact on evaporation capturing the role of canopy moisture and soil texture. The TD LSM calculates the energy budget from a 1-D equation assuming a linear temperature profile across 5 layers of soil. The TD LSM does not predict soil moisture (Skamarock *et al.*, 2008). In the TD model, initial soil moisture is fixed with the land-use type and a season-dependent constant value. The bottom layer can be at a deep of 16 cm, where the average temperature is applied. The TD LSM does not explicitly account for vegetation processes. Table 3.2 presents WRF experimental setup that combines LSMs and land-use data.

Table 3.2 The WRF experimental configurations based on land surface models (LSMs) and land-use data.

Simulation Number	Land surface model	Land use data	WRF Experiment
1	Noah	USGS	Noah-U
2	Noah	NLU	Noah-N
3	RUC	USGS	RUC-U
4	RUC	NLU	RUC-N
5	TD	USGS	TD-U
6	TD	NLU	TD-N

3.2.4 Observation data

Observed climate data were used to validate the performance of the WRF model. The observed daily temperature and rainfall data in the Lake Tana basin and nearby weather stations were obtained from the National Meteorological Agency (NMA) of Ethiopia. Meteorological stations that have data more than 95% of the period from March to August 2015 were considered for model evaluation. Based on the availability and quality of the data, temperature and rainfall data were

collected from 24 meteorological stations (Figure 3.1b). Missing values in climate data were filled using an arithmetic average method (Sattari *et al.*, 2017).

3.2.5 Model evaluation

The WRF model performance was evaluated by examining the temporal and spatial agreement between simulated and observed values. The evaluation was done using the correlation coefficient (r), mean bias (MB) and root mean square error (RMSE). A correlation coefficient is widely used to quantify the linear relation between simulated and observed values (Equation 3.1). The r values near one indicate a strong positive correlation while values near zero indicate no correlation. The MB is a measure of the difference between simulated and observed mean (Equation 3.2); a positive value of MB indicates an overestimation and a negative value indicates an underestimation. The RMSE describes the amount of error in terms of the difference between simulated and observed values (Equation 3.3), the lower the RMSE values the smaller the errors. A Student's t-test was applied to assess the significance of the difference between simulated and observed values. The two-tail test was computed based on the two-sample assuming equal variance method at a 95% confidence level.

$$r = \frac{\sum_{i=1}^{n}\left(S_i - \overline{S}\right)\left(O_i - \overline{O}\right)}{\sqrt{\sum_{i=1}^{n}(S_i - \overline{S})^2 \sum_{i=1}^{n}(O_i - \overline{O})^2}} \tag{3.1}$$

$$MB = \frac{1}{n}\sum_{i=1}^{n}\left(S_i - O_i\right) \tag{3.2}$$

$$RMSE = \sqrt{\frac{1}{n}\sum_{i=1}^{n}(S_i - O_i)^2} \tag{3.3}$$

where S_i is the simulated climate variable, O_i is the observed climate variable, $\overline{S}$ is the mean of simulated climate variable, $\overline{O}$ is the mean of observed climate variable, and n is the total number of climate data.

Categorical statistics, which comprise Bias Score (BS), Probability of Detection (POD), False Alarm Ratio (FAR) and Critical Success Index (CSI), were also used to verify the WRF model's

performance in simulating rain/no rain events at different thresholds. In this study, rainfall amount below 0.2 mm was considered as no rain (Schirmer and Jamieson, 2015). The simulated and observed pairs of a given threshold were classified into four categories and assigned in a 2 x 2 contingency table (Table 3.3).

Table 3.3 Contingency table between observed and simulated rainfall events for a given threshold level.

		Observed		
		Yes	No	Total
Simulated	Yes	a	b	a + b
	No	c	d	c + d
	Total	a + c	b + d	n = a + b + c + d

Note: a = hits, if both the simulated and observed values are above threshold; b = false alarms, if the simulated value is above the threshold and observed value is below the threshold; c = misses, if the simulated value is below the threshold and observed value is above the threshold; d = correct non-events, if both the simulated and observed values are below the threshold, and n = total number of events.

The BS is a ratio between the frequency of simulated to the frequency of observed events (Equation 3.4). BS provides an evaluation of the model's tendency to overestimates (BS > 1) or underestimates (BS < 1) observed events. BS value of one indicates that the number of simulated events is the same as the observed events.

$$BS = \frac{a+b}{a+c} \tag{3.4}$$

where a is hits, b is false alarm and c is misses.

The POD estimates the proportion of rainfall events successfully simulated by the model (Equation 3.5). A POD value of one means a perfect rainfall event simulation.

$$POD = \frac{a}{a+c} \tag{3.5}$$

The FAR measures the number of simulated rainfall events when in fact there were no observed rainfall events (Equation 3.6). The best FAR score corresponds to zero.

$$FAR = \frac{b}{a+b} \tag{3.6}$$

The CSI is the fraction of observed rainfall that was correctly detected by the model (Equation 3.7).

$$CSI = \frac{a}{a+b+c} \tag{3.7}$$

The monthly and seasonal simulation performance of the WRF model was evaluated by aggregating daily rainfall values. The model results were interpolated bi-linearly to the station location. The spatial patterns of WRF model simulation were also assessed through a comparison of the observed and simulated map and Taylor diagram (Taylor, 2001). The station average temperature and rainfall values were interpolated to 4 km spatial resolution using the ordinary Kriging method. This method was selected because of its simplicity and reliability for spatial evaluation purposes (e.g., Pennelly *et al.*, 2014; Sahlu *et al.*, 2016; Zeyaeyan *et al.*, 2017).

3.3 Results

The WRF model was used to simulate temperature and rainfall at daily time steps spatially across the Lake Tana basin. The temporal and spatial simulation performance of the model was evaluated using the observed temperature and rainfall data.

3.3.1 WRF model for daily temperature simulation

Temporal variation of daily 2 m maximum temperature (Tmax) averaged for all meteorological observations and WRF simulations for the period March to August 2015 is shown in Figure 3.3a. The comparison result indicated that Tmax simulation using RUC-U and RUC-N experiments showed generally good representation of the observed temporal variation in the Lake Tana basin. However, in some points, Tmax simulation values were not still high accurate (Figure 3.3a). Both Noah and TD LSMs tended to underestimate the Tmax events from March to mid-May. During this period, Noah-N and Noah-U experiments slightly underestimated for Tmax. However, TD-U and TD-N experiment severely underestimated all the Tmax values. The comparison indicated that TD-N and TD-U experminet simulated 2 m minimum temperature (Tmin) fairly well in general; the simulated and observed values were coincident in most time profiles. However, Tmin simulated by TD experiments slightly underestimated during the initial simulation periods and overestimated in sometimes profile in August. Both Noah and RUC LSMs experiments well captured Tmin temporal fluctuation but they had an extreme overestimation tendency in most time profile (Figure 3.3b). Overall, the TD-N and TD-U experiments agreed well with the observed magnitude in most events in Tmin.

Comparisons between observed and simulated Tmax and Tmin from six WRF experiments are presented in Table 3.4. The correlation coefficient values in Tmax were considerably high for all Noah and RUC experiments with values in the range from 0.91 to 0.94. The highest correlation was found at RUC-N and Noah-U experiments, and the lowest at TD-N experiment. The LSM comparison showed that RUC experiments slightly underestimated the observed Tmax, while the simulated Tmax under Noah and TD experiment was considerably lower than the observed Tmax. The MB value for Tmax from RUC-N and RUC-U experiment was significantly different from other experiments ($p < 0.05$). The RUC-N experiment resulted in the smallest cold bias (0.27 °C) for Tmax. On the other hand, considerable cold biases in Tmax were observed from the Noah and TD simulations with the worst performance from the Noah-U (MB = 1.78 °C) experiment. The

root mean square error (RMSE) values for Tmax ranged from 1.21 to 2.48 °C, with the lowest value occurring from RUC-N and the highest value from TD-U experiment. This result showed that the simulated Tmax in the RUC-N experiment was very close to the observed Tmax. Although the difference between USGS and NLU data for Tmax simulation was insignificant ($p > 0.05$), the NLU data along with Noah and RUC slightly improved the Tmax simulation. In RUC LSM, replacing USGS by NLU data reduced the Tmax RMSE value by 0.02 °C and slightly improved the WRF model performance. Overall, the RUC-N experiment was the best in simulating Tmax compared to the other five experiments.

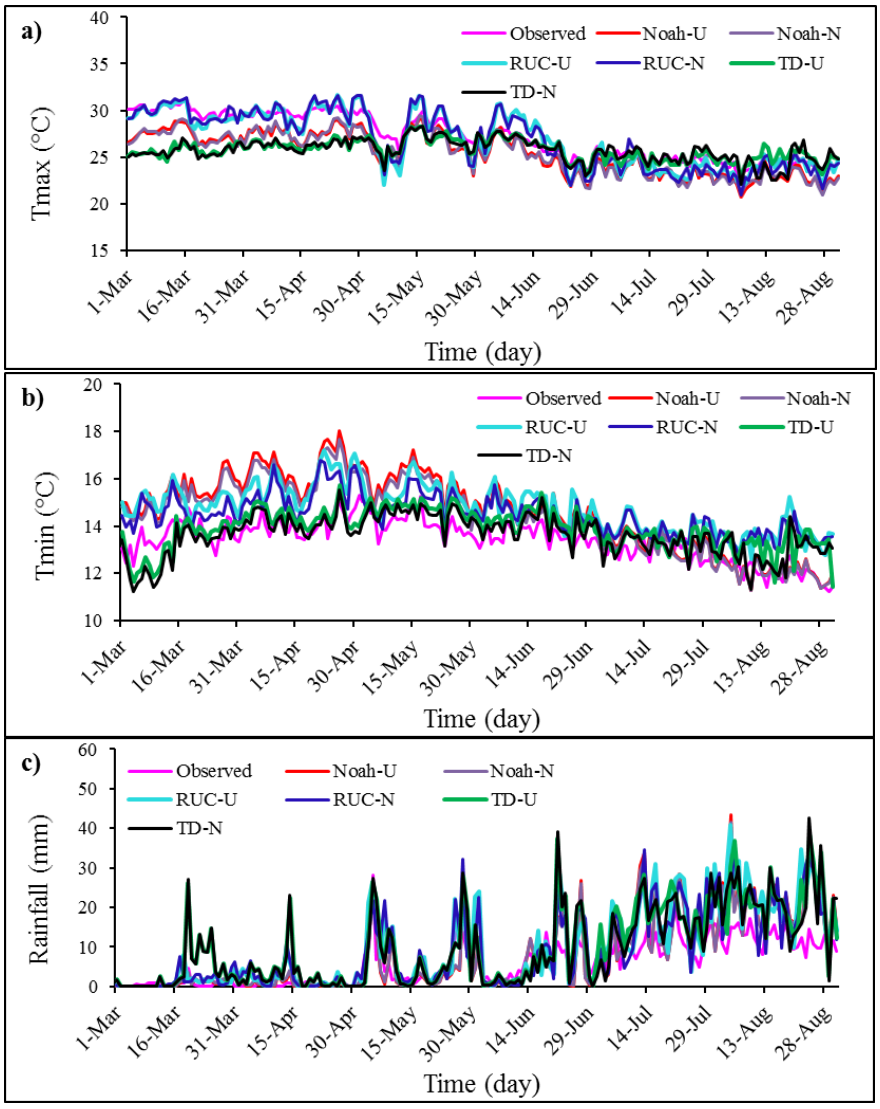

Figure 3.3 The six WRF experimental simulation and observation; a) 2 m maximum temperature (Tmax), and b) 2 m minimum temperature (Tmin), and c) rainfall based stations average over the Lake Tana basin for the period March to August 2015.

LSM selection had greater influence in simulating Tmin when compared to land-use data selection (Table 3.4). The correlation coefficients for Tmin were good but slightly lower than Tmax except for TD experiments. The highest agreement was found from the Noah-N and Noah-U experiments, and the lowest from the TD-U experiment. In general, all the WRF experiments overestimated Tmin with a range from 0.20 to 1.35 °C. Although the warm biases were high in most experiments, TD-N simulation was very close to the observed Tmin (MB = 0.20 °C). Tmin RMSE values in NLU experiments were considerably lower than USGS. Similar to the Tmax simulation, updated land-use information improved Tmin simulation and TD-N experiment was the most consistent to replicate the observed Tmin.

Table 3.4 Performance of WRF experiments in simulating daily 2 m maximum temperature (Tmax) and 2 m minimum temperature (Tmin) for the period March to August 2015.

WRF	Tmax			Tmin		
Experiment	r	MB (°C)	RMSE (°C)	r	MB (°C)	RMSE (°C)
Noah-U	0.94	-1.78	1.96	0.85	1.21	1.58
Noah-N	0.93	-1.76	1.94	0.85	1.02	1.39
RUC-U	0.91	-0.28	1.23	0.76	1.35	1.49
RUC-N	0.94	-0.27	1.21	0.75	1.07	1.22
TD-U	0.61	-1.42	2.42	0.63	0.46	0.84
TD-N	0.57	-1.47	2.48	0.65	0.20	0.77

3.3.2 WRF model for daily rainfall simulation

Amongst all the experiments, relatively Noah-N and Noah-U experiments had the best performance in simulating rainfall (Figure 3.3c). Overall, the Noah and RUC experiment reasonably captured the temporal fluctuations of low and moderate rainfall events. All the WRF experiments consistently overestimated the observed rainfall amounts in most time profiles, especially from June to August. However, TD-N and TD-U experiment severely overestimated the rainfall amount during the simulation period. From these, TD-N experiment simulated considerable rainfall amount as high as 42.4 mm and 42.2 mm on June 21 and August 24, respectively (Figure 3.3c).

Comparisons between observed and simulated rainfall from the six WRF experiments are presented in Table 3.5. All the WRF experiments overestimated the average daily rainfall with a range from 2.39 to 4.53 mm/ day. The lowest overestimation was found in the Noah-N experiment and the highest in TD-U experiment. The impact of LSM and land-use data on average daily rainfall was statistically significant. However, the LSM effect was much higher than the land-use

data. For example, Noah (Noah-U and Noah-N average value) LSM produced 1.91 mm/day lower rainfall than TD (TD-U and TD-N average value), whereas the NLU (Noah-N, RUC-N, and TD-N average value) slightly reduced model bias by 0.31 mm/day compared to USGS (Noah-U, RUC-U, and TD-U average value). The MB values in Noah-N and Noah-U experiment were significantly lower than other experiments. Also, Noah-N and Noah-U experiments produced significantly lower RMSE values than TD-U and TD-U. These results demonstrated that Noah rainfall simulations resulted in better RMSE values than and TD. The application of NLU data instead of USGS improved the WRF model performance by reducing the RMSE by 0.33, 0.59, 0.09 mm/day in Noah, RUC, and TD LSM, respectively. The correlation coefficients between simulated and observed rainfall were significant ($p < 0.05$). Amongst all the LSM, Noah yielded very small mean bias and model error. Overall, the combination of Noah and NLU relatively captured well the observed rainfall compared to other experiments.

Table 3.5 Performance of WRF experiments in simulating daily rainfall for the period March to August 2015.

WRF Experiment	r	MB (mm/day	RMSE (mm/day)	BS	POD	FAR	CSI
Noah-U	0.77	2.44	6.88	0.92	0.86	0.07	0.81
Noah-N	0.77	2.39	6.55	0.97	0.88	0.09	0.81
RUC-U	0.80	4.18	7.98	1.03	0.91	0.11	0.82
RUC-N	0.79	3.71	7.39	1.02	0.92	0.10	0.83
TD-U	0.76	4.53	8.24	1.01	0.91	0.10	0.83
TD-N	0.75	4.12	8.15	1.01	0.90	0.10	0.82

The high values of BS, POD, and CSI showed that the WRF experimental simulations correctly detected most rainfall events (Table 3.5). Amongst all the experiments, Noah-N and Noah-U slightly underestimated the frequency of observed rainfall events. On the contrary, RUC and TD experiment slightly overestimated the frequency of observed rainfall events. As can be seen in Table 3.5, the WRF model detected most rainfall events as high as 0.92 in the RUC-N experiment. Also, all the WRF experiments had very high CSI value ranging from 0.81 to 0.83. This indicated that the WRF model properly detected more than 81% of the observed rainfall events. However, the WRF experimental simulations missed some rain events or reported false alarm. From these; the RUC-U experiment missed 11% of the rainfall events.

The WRF model performance in simulating different rainfall threshold values was assessed using four skill scores (Figure 3.4). Amongst all the experiments, Noah slightly overestimated the

frequency of light rainfall events (<5 mm/day), while RUC and TD slightly underestimated the frequency of light rainfall events (Figure 3.4a). However, almost all the WRF experiments substantially underestimated and overestimated the frequency of moderate (5–15 mm/day) and high (>20 mm/day) rainfall events, respectively. For the rainfall threshold up to 15 mm/day, Noah-N experiment displayed the highest skill scores with BS close to one. The POD in the Noah-N experiment was appreciably high, especially for the low and moderate events (Figure 3.4b). This experiment detected more than 22% of rain occurrences at a threshold of 10 mm/day, but it was incapable of detecting high threshold values. The POD values generally decreased in a wave pattern as the increase in rainfall threshold. This result demonstrated that the capability of the WRF model in detecting heavy rainfall events was low compared to light rainfall events. Unlike POD, FAR was increased with the increasing of threshold values. The WRF experiments had different FAR values in 10 and 15 mm/day threshold values (Figure 3.4c). Both Noah-U and Noah-N experiments produced small FAR in moderate rainfall events. The CSI values were so high for low threshold and extremely low for high threshold (Figure 3.4d), which indicates that the WRF experiments correctly estimated low and moderate threshold events than high threshold events.

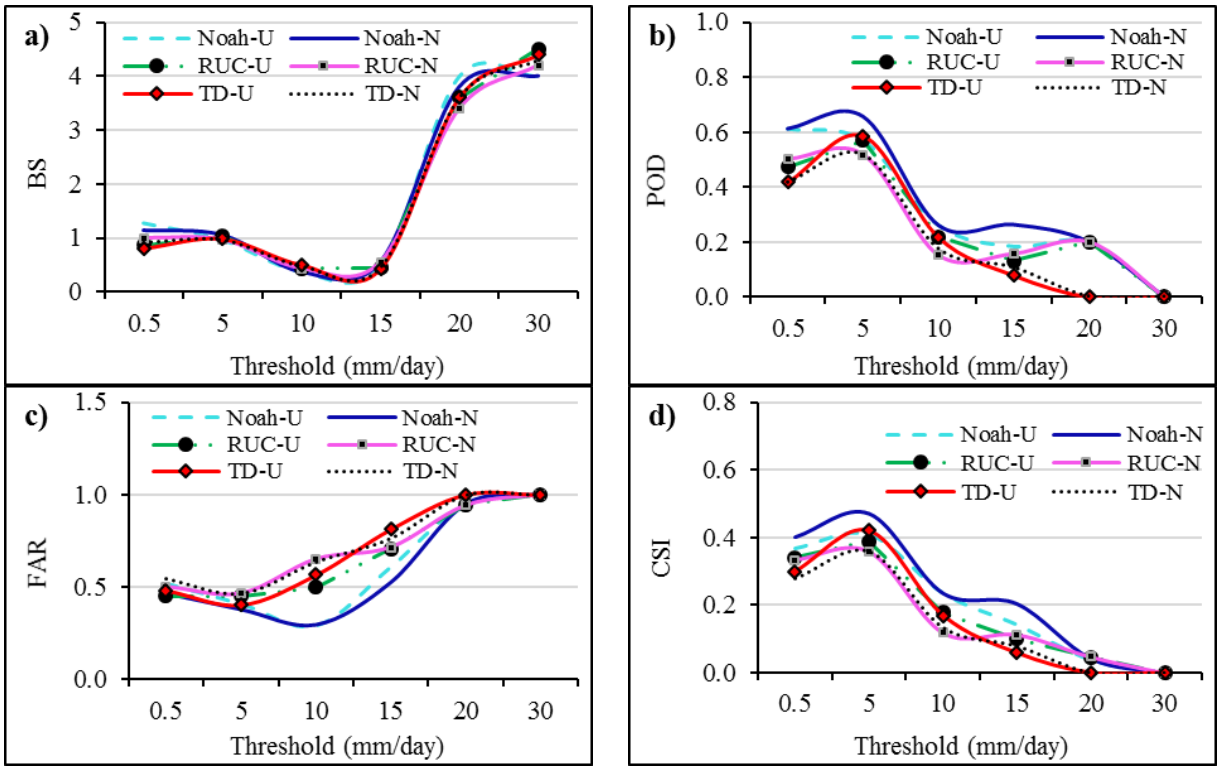

Figure 3.4 Skill scores as a function of rainfall threshold from six WRF experiments for the periods March to August 2015; a) bias score (BS), b) probability of detection (POD), c) false alarm ratio (FAR), and d) critical success index (CSI).

3.3.3 Monthly and seasonal temperature simulation

Figure 3.5 shows a comparison between WRF experimental simulation and observation average monthly temperature and rainfall. RUC-U and RUC-N average monthly Tmax was very close to the observed Tmax in most of the months (Figure 3.5a), which caused lower model biases. Contrarily Noah and TD simulation was considerably lower than the observed Tmax, especially in March and April. During the simulation periods, most of the WRF experiments underestimated the observed Tmax with a range of 0.1–4.4 °C. As can be seen in Figure 3.5b, Noah-U and Noah-N experiment produced the highest (16.5 °C) and lowest (12 °C) average monthly Tmin in April and August, respectively. In general, Noah-N produced the lowest overestimation (0.2 °C) in July, while Noah-U produced the highest overestimation (2.1 °C) in April.

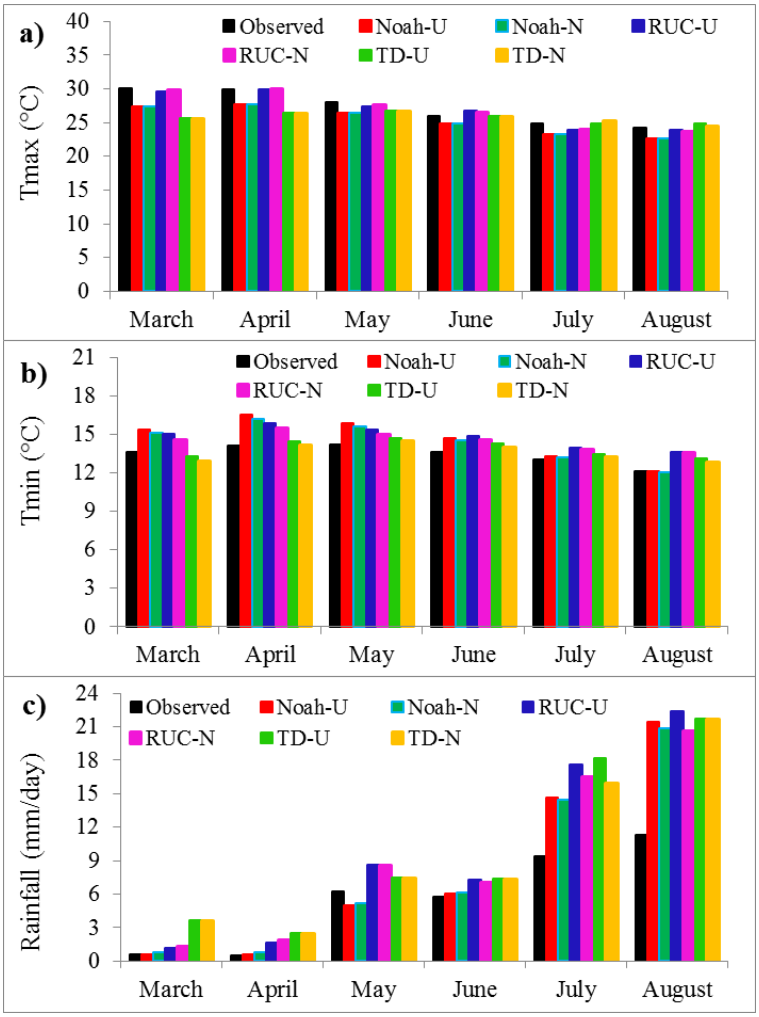

Figure 3.5 Average monthly 2m maximum temperature (a), 2m minimum temperature (b), and rainfall (c) for the simulation period March to August 2015 over the Lake Tana basin.

The rainy season in the study area occurs from June to September (Enyew *et al.*, 2014; Tigabu *et al.*, 2018). Thus, the months from June to August were considered as the wet season, and the months of March to May were considered as the dry season. Table 3.6 presents the comparison between simulated and observed Tmax on a monthly and seasonal basis. The correlation between simulated and observed average monthly Tmax was very strong for the RUC-N experiment. From the seasonal comparison, RUC-N and Noah-N experiment had a very strong correlation during the dry and wet season, respectively. All the six experiments underestimated both dry and wet season Tmax except TD in the wet season. During the dry season, considerably high and low cold biases in Tmax occurred in the TD-N and RUC-N experiments, respectively. Overall, TD-N experiment well captured wet season Tmax. These results showed that dry season biases were significantly higher than the respective wet season biases except for the RUC-N experiment. Based on RMSE values, RUC-N and TD-N experiment provided a better outcome during the dry and wet season, respectively. This result showed that the application of NLU data captured well the seasonal cycle in the study area. Overall, better monthly and dry season WRF simulation performance was obtained from the RUC-N experiment.

Table 3.6 Performance of WRF experiments in simulating monthly and seasonal 2 m maximum temperature (Tmax) for the period March to August 2015.

WRF Experiment	Monthly			Dry season			Wet season		
	r	MB (°C)	RMSE (°C)	r	MB (°C)	RMSE (°C)	r	MB (°C)	RMSE (°C)
Noah-U	0.81	-1.78	2.76	0.73	-2.12	3.04	0.70	-1.42	2.45
Noah-N	0.81	-1.77	2.76	0.73	-2.11	3.03	0.71	-1.41	2.44
RUC-U	0.82	-0.28	2.14	0.74	-0.36	2.14	0.69	-0.20	2.14
RUC-N	0.83	-0.27	2.10	0.75	-0.19	2.09	0.69	-0.34	2.12
TD-U	0.64	-1.42	3.09	0.64	-3.01	3.85	0.68	0.17	2.07
TD-N	0.65	-1.47	3.11	0.63	-3.06	3.91	0.70	0.12	2.01

During monthly time steps, most of the experimental simulations had the best agreement with the observed Tmin (Table 3.7). However, the MB and RMSE in TD-N experiment were significantly different from others. This result showed that the TD-N experiment reproduced the monthly Tmin. The seasonal comparison of Tmin showed that wet season RMSE values were lower than dry season RMSE. This result revealed that the WRF model had a better capability in simulating wet season Tmin compared to the dry season. Amongst all the experiments, TD-N produced significantly lower RMSE in both dry and wet seasons. The correlations between observation and simulation were very strong in both seasons, but the dry season r values were slightly higher

compared to wet season simulation (Table 3.7). Overall, the TD-N experiment adequately captured the monthly and seasonal Tmin cycle.

Table 3.7 Performance of WRF experiments in simulating monthly and seasonal 2 m minimum temperature (Tmin) for the period from March to August 2015.

WRF Experiment	Monthly			Dry season			Wet season		
	r	MB (°C)	RMSE (°C)	r	MB (°C)	RMSE (°C)	r	MB (°C)	RMSE (°C)
Noah-U	0.83	1.21	2.09	0.88	1.96	2.80	0.84	0.46	1.77
Noah-N	0.83	1.02	2.00	0.88	1.70	2.65	0.84	0.35	1.74
RUC-U	0.87	1.35	2.05	0.86	1.45	2.56	0.87	1.23	2.01
RUC-N	0.88	1.07	1.84	0.88	1.05	2.22	0.87	1.06	1.90
TD-U	0.88	0.46	1.73	0.89	0.21	2.04	0.85	0.70	1.83
TD-N	0.88	0.20	1.66	0.89	-0.08	1.99	0.86	0.46	1.73

3.3.4 Monthly and seasonal rainfall simulation

Observed and simulated average monthly rainfall for the period from March to August 2015 is shown in Figure 3.5c. Amongst all the WRF experiments, RUC-U and Noah-U simulated the largest (22.4 mm/day) and the smallest (0.6 mm/day) average monthly rainfall in August and March, respectively. From March to July, rainfall in the Noah (Noah-U and Noah-N) experiment was slightly lower than other experiments. In August, the RUC-N experiment produced the lowest rainfall compared to others. The average monthly rainfall was remarkably overestimated, primarily in July and August, and, to a lesser extent in March and April. The lowest overestimation (0.1 mm/day) occurred in March and April in the Noah-U experiment, while the highest overestimation (11 mm/day) occurred in August in the RUC-U.

The analysis at a monthly level showed that the correlation coefficient values were between 0.71 and 0.79 (Table 3.8). The monthly MB and RMSE value in the Noah-N experiment was significantly lower than others. This result indicated that the Noah-N experiment captured well the monthly rainfall cycle. Similar to temperature simulations, the use of NLU data produced better rainfall simulation compared to USGS data. Overall, the Noah-N experiment provided the best performance, while TD-U was the worst.

The wet season r values were slightly lower than the dry season values, indicating difficulties of the WRF model to reproduce the wet season rainfall. All the WRF experiments considerably overestimated the wet season rainfall with MB value ranging from 153.8 to 215.1 mm/month.

However, in the dry season, the Noah experiments slightly underestimated the observed rainfall. In the wet season, the MB values in the NLU experiment were significantly different from the MB values in the USGS. The NLU data produced so low MB values with the lowest value in the Noah-N experiment. In all the WRF experiments, the wet season RMSE values were considerably larger than the respective dry season values, which caused by the higher rainfall magnitude in the wet season. This result agrees with Jain *et al.* (2017) study in the Delhi-Mumbai Industrial Corridor. They found that the WRF model error was increased with the rainfall amount increased. In the Noah simulations, the application of NLU data instead of USGS improved the WRF model performance by reducing the RMSE by 0.6 and 9.9 mm/month in the dry and wet season, respectively. However, during the dry season, the updated land-use information with the TD LSM did not show model improvement. As can be seen in Table 3.8, Noah and RUC LSM have better skill in responding to the updated land-use information. Overall, the Noah-N experiment was the most accurate in replicating the monthly and seasonal temporal patterns (Table 3.8).

Table 3.8 Performance of WRF experiments in simulating monthly and seasonal rainfall (mm/month) for the period from March to August 2015.

WRF	Monthly			Dry season			Wet season		
Experiment	r	MB	RMSE	r	MB	RMSE	r	MB	RMSE
Noah-U	0.77	74.1	178.8	0.79	-11.6	61.1	0.58	161.0	229.3
Noah-N	0.77	72.7	171.5	0.79	-7.3	60.5	0.58	153.8	219.4
RUC-U	0.79	127.9	206.8	0.77	42.2	84.3	0.60	214.8	262.1
RUC-N	0.76	113.8	192.7	0.75	46.3	81.2	0.55	182.2	241.3
TD-U	0.75	138.6	217.3	0.61	63.3	101.6	0.59	215.1	269.8
TD-N	0.71	125.8	210.3	0.60	61.9	102.3	0.50	190.6	259.5

3.3.5 Temperature spatial pattern

RUC-N experiment resulted in the highest spatial correlation pattern (r = 0.85) for Tmax (Figure 3.6a), while the Noah-N experiment produced the highest r (0.96) for Tmin (Figure 3.6b). Moreover, RUC-N and Noah-N experiment provided much lower RMSE values in Tmax and Tmin simulation, respectively. From the six experiments, TD-N and TD-U standard deviations were slightly smaller than the observed Tmax standard deviation. In contrast, all the six WRF experiment standard deviations were considerably lower than the observed Tmin standard deviation. Overall, the RUC-N experiment replicated well the observed Tmax spatial patterns with a higher spatial correlation and a lower RMSE value, whereas the Noah-N experiment consistently

simulated the observed Tmin spatial pattern. On the other hand, TD simulations poorly replicated both Tmax and Tmin spatial patterns with lower correlation and higher RMSE value.

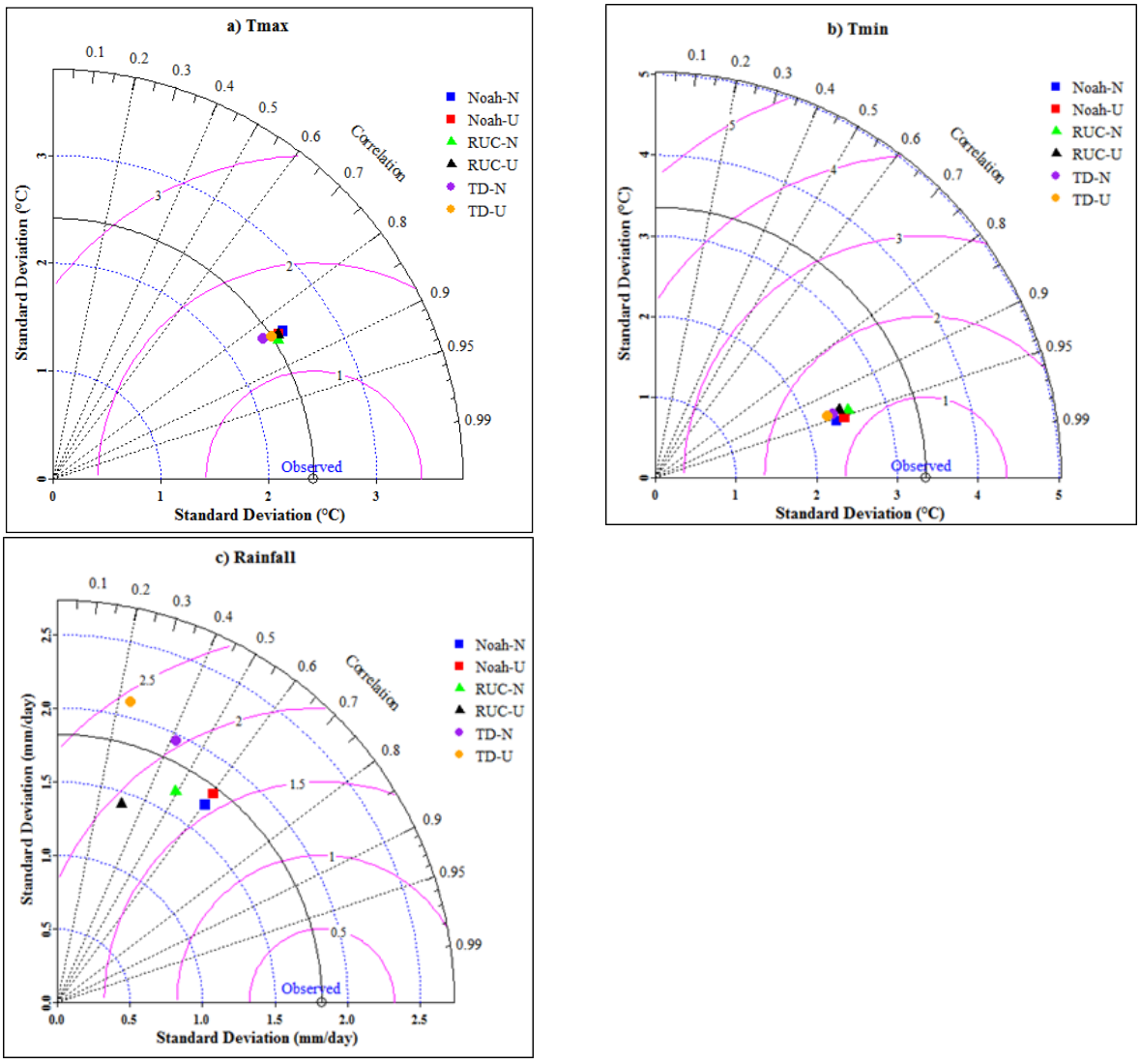

Figure 3.6 Taylor diagram showing a statistical comparison of six WRF experimental simulations; a) 2 m maximum temperature (Tmax), b) 2 m minimum temperature (Tmin), and c) rainfall for the period from March to August 2015.

Tmax spatial pattern over the Lake Tana basin is shown in Figure 3.7, where Figure 3.7a and b are averages for the simulation period from observation and WRF experimental simulations, respectively. Figure 3.7c shows the difference between WRF experimental simulation (Figure 3.7b) and observation (Figure 3.7a). The observed Tmax magnitude and spatial pattern were represented well by RUC-N and RUC-U experiments compared to others. During the simulation period, the highest Tmax was found over the eastern part of the Lake Tana border with an average

daily Tmax above 29 °C in the RUC-N and RUC-U experiments; while the lowest Tmax was observed in the northern and eastern mountainous parts of the basin with an average daily Tmax below 22 °C in the Noah-N and Noah-U experiments. All the WRF experiments substantially underestimated Tmax in most parts of the basin with a cold bias as high as 4 °C in Noah and TD experiments over the northern and southern mountainous part of the basin. From the six experiments, RUC-N produced considerable small cold biases (> -3 °C) and warm biases (<1 °C) over the basin, which indicates that the combination of RUC with NLU data replicated well Tmax spatial patterns in the Lake Tana basin. In general, the comparison between NLU and USGS simulation showed that the consideration of real-time land-use data slightly enhanced the spatial representation performance of the WRF model. This result agrees well with Sertel *et al.* (2009) study in the Marmara Region in Turkey. They found that the updated land-cover data improved the WRF model performance in temperature simulations. In the outlet part of the basin, the NLU data produced higher Tmax than USGS land-use data. This variation may have been related to the urban and cropland representation of the area by NLU and USGS data, respectively. Higher temperature simulation was commonly observed in urban land-use coverage (Li *et al.*, 2018).

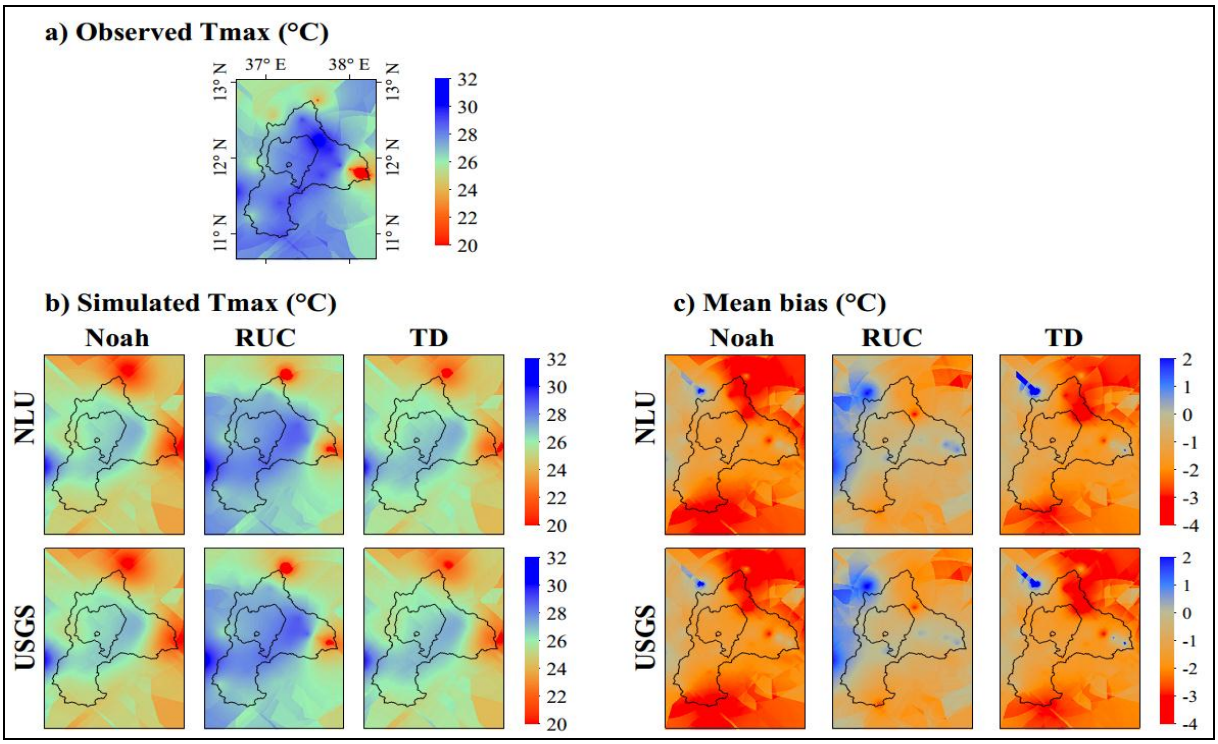

Figure 3.7 Spatial distribution of average 2 m maximum temperature (Tmax) across the Lake Tana basin; a) Observed average, b) Simulated average from WRF experiment, and c) Mean bias, which is simulated minus observed.

All the WRF experiments showed similar spatial patterns with the observed Tmin, especially the Noah-U experiment replicated well the higher Tmin and experiments with RUC and TD LSM captured well the lower Tmin (Figure 3.8). Overall, the six WRF experiments produced reasonable cold biases of Tmin over the northern parts of the Lake Tana basin. The Noah and RUC experiment produced strong warm biases up to 3 °C in the southern part, while TD-N and TD-U experiment yielded strong cold biases as high as 4 °C in the northern part. In most parts of the basin, the TD-N experiment produced slight warm biases. Overall, Tmin simulation with TD-N experiment was the best to replicate the spatial distribution of the observed data.

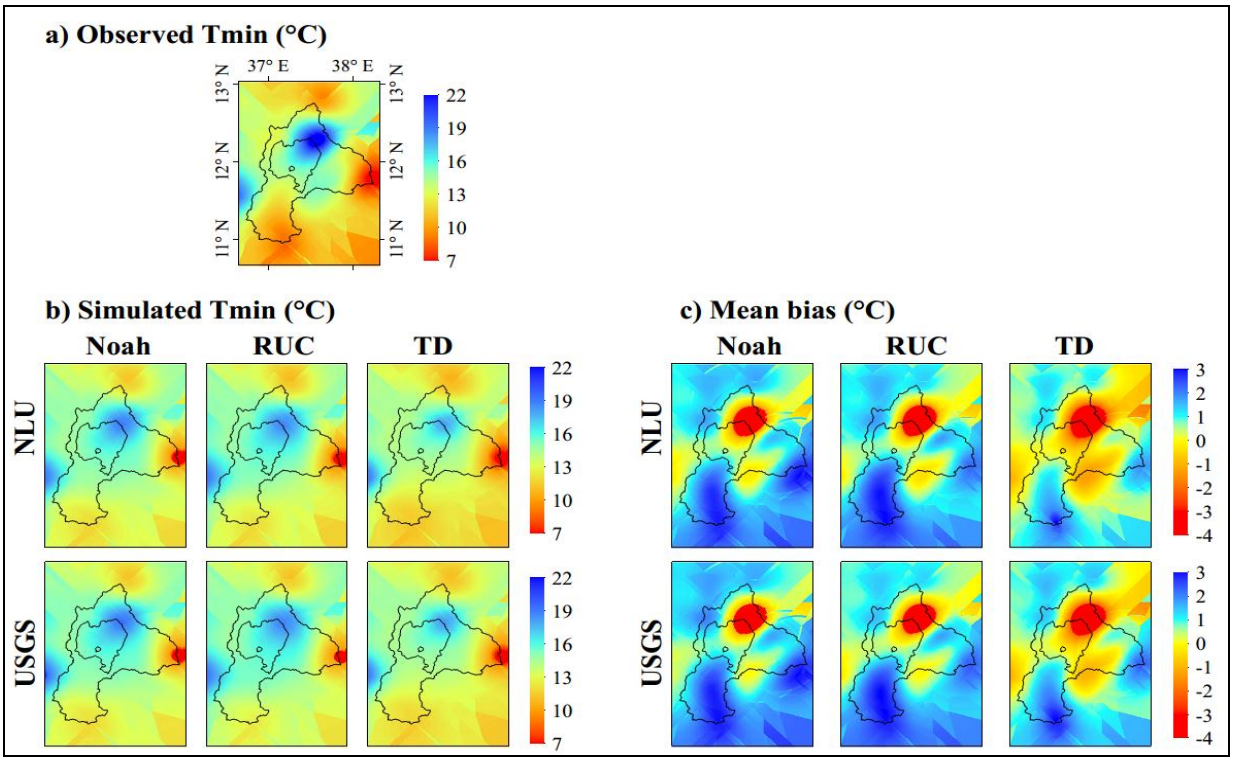

Figure 3.8 Spatial distribution of average 2 m minimum temperature (Tmin) across the Lake Tana basin; a) Observed average, b) Simulated average from WRF experiment, and c) Mean bias, which is simulated minus observed.

3.3.6 Rainfall spatial pattern

The spatial rainfall pattern was extremely sensitive to LSM selection compared to land-use data (Figure 3.6c). The standard deviations in Noah and RUC experiments were slightly lower than the observed standard deviation (1.8 mm/day). The simulated pattern of average rainfall using NLU data agreed well with the observed rainfall compared to USGS data; especially the Noah-N

experiment provided the best spatial agreement with observations. The worst performance of spatial rainfall distribution was found from the TD-U experiment.

As can be seen in Figure 3.9, the spatial pattern showed large discrepancies between observed and simulated rainfall in some parts of the basin. This may be due to the insufficient number of rainfall stations for the spatial model comparison (Osuri *et al.*, 2015). The simulated spatial rainfall under Noah-N and Noah-U experiments represented the spatial patterns and magnitude well, perhaps more strongly in the mountainous parts of the Lake Tana basin. However, there were pockets of large overestimations by the Noah experiment over the central and southwestern part of the basin. This result demonstrated that Noah-N and Noah-U experiment was the best in capturing the spatial rainfall distribution with slight underestimation in the northern and eastern parts and slight overestimation in the southern part of the basin. However, TD and RUC LSM considerably overestimated the average rainfall in most parts of the basin. Overall, the Noah-N experiment was the most accurate configuration to reproduce the spatial pattern over the basin except around Lake Tana.

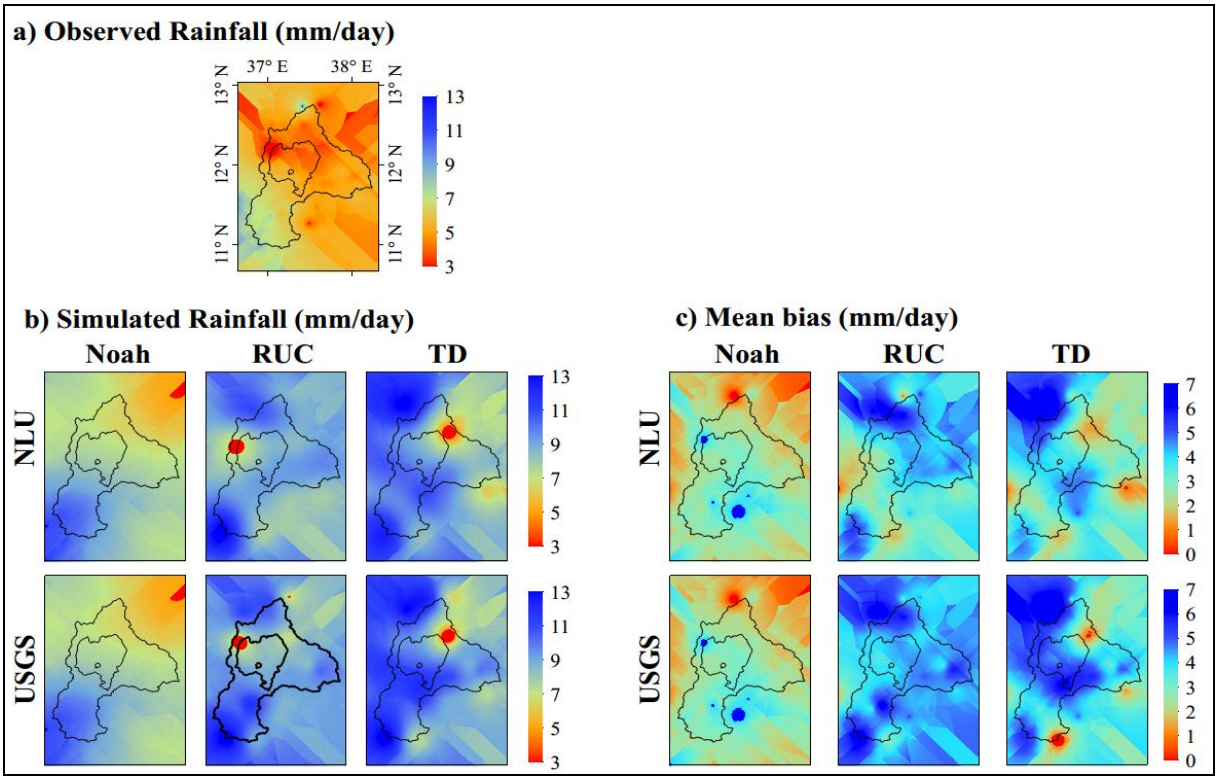

Figure 3.9 Spatial distribution of average rainfall across the Lake Tana basin; a) Observed average, b) Simulated average from WRF experiment, and c) Mean bias, which is simulated minus observed rainfall.

3.4 Discussion

Although WRF is a widely used RCM, the choice of parameterization schemes is site-specific (Mooney *et al.*, 2016; Jain *et al.*, 2017; Mugume *et al.*, 2017). The LSMs and land-use data affect the local climate simulations, especially in areas where land surface characteristics dynamically changed (Deng *et al.*, 2013). Because of this, the sensitivity of LSMs and land-use data on the WRF simulation over the Lake Tana basin was investigated in this study. In general, rainfall and temperature simulation were sensitive to the choice of LSM and land-use data. The NLU with Noah and RUC simulated higher Tmax than USGS land-use since the NLU represented more cropland area than the USGS data (Table 3.1 and Figure 3.2). The temperature increase may result from a lower vegetation greenness. This is in agreement with the findings of Müller *et al*. (2014). The comparison results demonstrated that there was no single best WRF model configuration exists for simulations of dry and wet season climate in the Lake Tana basin. The combination of updated NLU with RUC and TD well reproduce Tmax and Tmin, respectively. This performance variation of LSM may arise from the consideration of soil layers and land-use information, which was consistent with the previous finding (Chen *et al.*, 2014; Burakowski *et al.*, 2016). The RUC LSM has a better capability in resolving the soil moisture and temperature at tiny layers (Smirnova *et al.*, 2016), which results in lower model biases in Tmax simulation. As a result of fine spatial resolution and the real-time representation of land-use categories, the NLU data provided reasonably better simulation than USGS. The WRF improvements resulted from updated land-use data agree with Cheng *et al.* (2013), Cao *et al.* (2015) and He *et al.* (2017). However, during Tmax simulation, the combination of TD and NLU had slightly lower performance than TD and USGS combination. This may be related to the application of fixed soil moisture with land-use type in TD LSM (Lee *et al.*, 2016).

The simulated rainfall in the WRF experiments was much higher than the observed rainfall, which may have been caused by the excessive convection in the Indian Ocean (Diaz *et al.*, 2015) and Kain-Fritsch cumulus scheme application (Ramarohetra *et al.*, 2015; Chawla *et al.*, 2018). Moreover, the presence of the Lake Tana water body may influence the rainfall simulation in the WRF model (Haile *et al.*, 2009). Although the WRF experiments poorly captured the average rainfall magnitude, the relative performance of Noah LSM and NLU data were significantly higher compared to others. The high performance of Noah LSM and NLU is consistent with Ramarohetra

et al. (2015) and Göndöcs *et al.* (2015). In general, the deficiency of rainfall simulation using RCM is a common phenomenon (Chotamonsak *et al.*, 2012; Chawla *et al.*, 2018), which result from the incapability of the models to handle complex biogeochemical and bio-geophysical processes (Pongratz *et al.*, 2010), and the non-linear interactivity of model parameters including microphysics, cumulus, and planetary boundary layer.

Although the hypotheses were supported statistically, the WRF model had considerable limitations to reproduce the temporal and spatial variations of rainfall over the Lake Tana basin. Future research should, therefore, include other physical parameterization such as microphysics, cumulus, and pantry boundary layers to evaluate in greater detail whether the rainfall magnitude and spatial coverage improved in the WRF model.

3.5 Conclusions

This study evaluated the Weather Research and Forecasting (WRF) model for regional climate simulations in the Lake Tana basin in Ethiopia. Six WRF experiments were configured to assess the performance of three LSM (Noah, RUC and TD) and two land-uses (USGS and NLU) to simulate temperature and rainfall. The new land-use data captured well the land-use dynamics in the basin such as cropland and urban expansions, and reduction of Lake Tana water body. However, the USGS land-use data extremely underestimated the cropland and forest coverage in the basin.

The temporal and spatial comparison showed that the impact of LSM choice was slightly higher than land-use data. Differences in land-use data provide a slight difference for both temperature and rainfall simulations across space. On the other hand, the simulated average temperature and rainfall by the different LSMs were substantially different. The RUC-N and TD-N simulations yielded small cold bias for Tmax (0.27 °C) and small warm bias (0.20 °C) for Tmin, respectively. For rainfall simulations, the Noah-N and Noah-U experiment provided similar results; with slightly better spatial and temporal representation in favor of Noah-N. On average, TD produced 1.91 mm/day more rainfall when compared to Noah. The application of updated and accurate land-use information improved the spatial and temporal representation of the WRF model in simulating temperature and rainfall. During rainfall simulation under Noah, updated land-use improved model performance by reducing the RMSE by 0.33 mm/day when compared to USGS data. However,

the effect of land-use data on rainfall magnitude and distribution was complex due to the presence of Lake Tana water and the extreme topographic variability in the Lake Tana basin.

This study was able to show modeling approaches that can provide temperature and rainfall data in data-scarce environments and would provide valuable supports in identifying suitable land-use data and LSM on climate and hydrological process modeling. The findings suggested that the combination of new land-use data with RUC, TD, and Noah LSM in the WRF model can be used to simulate Tmax, Tmin, and rainfall, respectively. Such data will be vital for climate change impact research for sustainable water resources management in the Lake Tana basin.

4. MODELING THE IMPACT OF CLIMATE CHANGE ON HYDROLOGICAL RESPONSES IN THE LAKE TANA BASIN, ETHIOPIA

Abstract

Hydrologic systems have been changing due to the impact of climate change and variability. The impacts of climate change are set to increase in the future due to the rise of global warming. Quantifying the impact of climate change on the spatial and temporal hydrological processes is important for integrated water resource management. The Lake Tana basin, which is the source of the Upper Blue Nile River, is vulnerable to climate change and variability. This study was conducted in the four major tributary watersheds of the Lake Tana basin: Gilgel Abay, Gumara, Ribb, and Megech. Climate and hydrological model were used to (i) assess the future rainfall and temperature variability with respect to baseline scenario, and (ii) examine the impact of climate change on watershed hydrology. The study used dynamically downscaled climate data for the baseline (2005–2015) and the future period (2045–2055) under two Representative Concentration Pathway (RCP) scenarios (RCP4.5 and RCP8.5). The climate scenarios were simulated using the Weather Research and Forecasting (WRF) model, with a 4-km horizontal resolution. The model biases were corrected using power transformation and variance scaling method. The SWAT model was used to estimate the baseline and future hydrology using the bias-corrected climate data. The performance of the SWAT model was 'good' to 'very good' for both the calibration and validation periods, with the Nash–Sutcliffe efficiency values between 0.72 and 0.93. The projected changes in rainfall vary with seasons under both scenarios. On average, mean annual rainfall may increase by 7.9% and 21.2% under RCP4.5 and RCP8.5 scenarios, respectively. Minimum temperature may increase by 1.4 °C and 1.9 °C while maximum temperature may increase by 1.4 °C and 2.4 °C, respectively, under RCP4.5 and RCP8.5 scenarios. Climate change under RCP4.5 and RCP8.5 scenarios may cause streamflow increase by 7.2% and 33% and evapotranspiration increase by 11.2% and 15.2%, respectively. The findings provide valuable insights to implement appropriate water management strategies to mitigate and adapt to the negative impacts of climate change and variability on the Lake Tana basin, and other regions which have similar agro-ecology.

Keywords: climate change, streamflow, evapotranspiration, WRF, SWAT, Lake Tana basin

4.1 Introduction

Climate change is expected to occur as a result of anthropogenic changes in atmospheric composition by burning fossil fuels such as oil and coal which emit greenhouse gasses into the atmosphere (IPCC, 2014). Several studies have shown that climate change is one of the global environmental challenges to humanity and affecting social and ecological systems (Ngongondo *et al.*, 2013; Clifton *et al.*, 2018). The hydrological cycle will be directly altered by the impacts of climate change, subsequently affect local water resource availability in most regions in the world (Faramarzi *et al.*, 2013; Mechal *et al.*, 2015; Li *et al.*, 2016; Awal *et al.*, 2018; Jin *et al.*, 2018). However, the magnitude and direction of the impact vary from region to region; for the impact severe to Ethiopia as its economy is rain-fed agriculture, which is highly vulnerable to climate change and variability (Conway and Schipper, 2011). Understanding the impacts of climate change is vital especially in regions where the social and ecological systems are highly dependent on climate and water resources such as in Africa.

The potential impacts of climate change and variability on water resources have been studied in different regions in Africa. For example, Faramarzi *et al.* (2013) analyzed the impact of climate change on freshwater availability in Africa at a coarser resolution for the period of 2020–2040. The results showed that the available water in Africa may increase for entire Africa. Aich *et al.* (2014) assessed the impact of climate change on streamflow in four large representative river basins (Niger, Upper Blue Nile, Oubangui and Limpopo basin) and found a statistically significant increase in streamflow for the period 2070 to 2099 compared to the baseline period 1970 to 1999. Liersch *et al.* (2018) also showed that climate change may decrease streamflow in the Upper Blue Nile River for the months June and July, but an increase for the period August to November. Local-scale climate change studies have also been conducted to assess the impacts of climate change and variability on the hydrology of the Upper Blue Nile basin (Abdo *et al.*, 2009; Setegn *et al.*, 2011; Dile *et al.*, 2013; Gebre and Ludwig, 2015; Nigatu *et al.*, 2016). For example, Dile *et al.* (2013) estimated the impact of climate change on streamflow in Gilgel Abay watershed using the SWAT model and downscaled climate data from HadCM3A2 and HadCM3B2 scenarios with a statistical downscaling tool. They found that the mean monthly flow may decrease during 2010-2040 period and increase during 2070-2100. Recently, Ayele *et al.* (2016) used a stochastic weather generation approach to downscale climate data from six General Circulation Models (GCMs) for the high

(A2) and low (B1) emission scenarios in Gilgel Abay and Gumara watersheds. The climate data was used as input for the General Water Loading Function (GWLF) hydrological model to simulate runoffs. The results showed that the future (2020-2039) runoff may increase in both watersheds under all the six GCM outputs. Besides, Melke and Abegaz (2017) estimated the impact of climate change on streamflow in Gumara watershed using statistical downscaled HadCM3A2a and HadCM3B2a climate outputs and they found different trends of streamflow between GCMs. Although the above studies used different emission scenarios, GCMs, downscaling techniques, and hydrological models, the findings attest that climate change may unequivocally affect the water availability in Africa.

Although there is a consensus that climate change may affect the water resources in the Lake Tana basin, most of the previous studies in the basin assumed empirical-statistical relationships between large-scale predictors (i.e., GCM-derived atmospheric parameters) and local predictands (e.g. rainfall or temperature) (Abdo *et al.*, 2009; Setegn *et al.*, 2011; Dile *et al.*, 2013; Enyew *et al.*, 2014; Ayele *et al.*, 2016). However, the climate simulation has a strong association with local soil condition, topography, and land-use dynamics (Haile *et al.*, 2009; Collow *et al.*, 2014; Cao *et al.*, 2015), which is not properly considered in statistical downscaling procedure. Although most of these concerns were better addressed in the IPCC Fifth Assessment Report (IPCC-AR5) Representative Concentration Pathways (RCPs) (Van Vuuren *et al.*, 2011; Knutti *et al.*, 2013), the climate change studies in the Lake Tana basin used GCM based on Special Report on Emissions Scenarios (SRES). Therefore, estimates from these studies are less reliable since they do not account for local details such as land-use, topography, and soil due to the coarse spatial resolution of the GCMs. Although climate change studies in other regions showed that Regional Climate Models (RCMs) provide more reliable results in assessing climate change impacts than GCM-based estimates (Fang *et al.*, 2015; Yhang *et al.*, 2017; Wulong *et al.*, 2018), such studies are lacking in the Lake Tana basin.

This study, therefore, applied a high-resolution RCM with RCP scenarios to study the impact of climate change on the hydrology of the Gilgel Abay, Gumara, Ribb, and Megech of the Lake Tana basin. These watersheds contribute more than 93% of the inflow to Lake Tana (Kebede *et al.*, 2006). This study is the first of its kind to assess the impact of climate change on the seasonal and annual water resources at finer spatial resolution. The findings of this study will have paramount

importance for the policymakers in Ethiopia since the Lake Tana basin is one of the main growth corridors in the country because of its significance for hydropower generation and irrigation. Besides, the employed methodology can be replicated to investigate the impact of climate change on other basins.

4.2 Materials and Methods

4.2.1 Study area

The study is conducted in the Lake Tana basin, which is located in the Amhara region of Ethiopia (Figure 4.1). The Lake Tana basin is the headwater of the Upper Blue Nile basin having a catchment area of ~15,140 km^2. The elevation of the basin ranges between 1780 and 4100 meter above sea level (masl). The Lake Tana, which is the largest freshwater body in Ethiopia, covers 20% of the basin area. Although more than 40 tributary rivers flow into Lake Tana, the major tributaries are Gilgel Abay, Gumara, Ribb, and Megech, which account for more than 93% of the flow to Lake Tana (Kebede *et al.*, 2006). The Gilgel Abay river is the largest tributary that originates from the southern part of the basin and has a catchment area of 4553 km^2 having its outlet at the Lake. The Ribb river is the second largest tributary with a catchment area of 1970 km^2 joining the Lake from east. The Gumara river flows from the eastern part of the basin with a drainage area of 1780 km^2. The Megech watershed is the smallest of the four major tributaries of the Lake Tana basin with a catchment area of 860 km^2. The Megech river joins the Lake Tana from the north.

The climate in the Lake Tana basin is monsoon tropical highland with a rainy season from June to September and a dry season from October to March. The long-term basin mean annual rainfall over the period of 1982-2015 is about 1394 mm. The rainfall in the basin differs widely between mean annual rainfall of 964 mm in the northeastern part of the basin and 2000 mm in the southern. The temperature is warmer around Lake Tana and gets cooler moving away from Lake Tana. The mean annual temperature over the period of 1982-2015 is between 18.6°C and 21.2°C.

4.2.2 Modeling approach

This study considered climate and hydrological modeling to estimate the impact of climate change in the Lake Tana basin. Initially, the quality of observed climate and streamflow data were checked using basic statistical error checking approaches. Thereafter, the baseline and two future climate scenarios (RCP4.5 and RCP8.5) were dynamically downscaled using the Weather Research and Forecasting (WRF) model. The downscaled climate datasets were corrected from model biases using the power transformation and variance scaling method. The Soil and Water Assessment Tool (SWAT) model was calibrated and validated using observed climate and streamflow data. Finally,

the calibrated and validated SWAT model was used to estimate the baseline and future hydrology using bias-corrected climate data. The detailed procedures for the climate and hydrologic modeling are presented as follows.

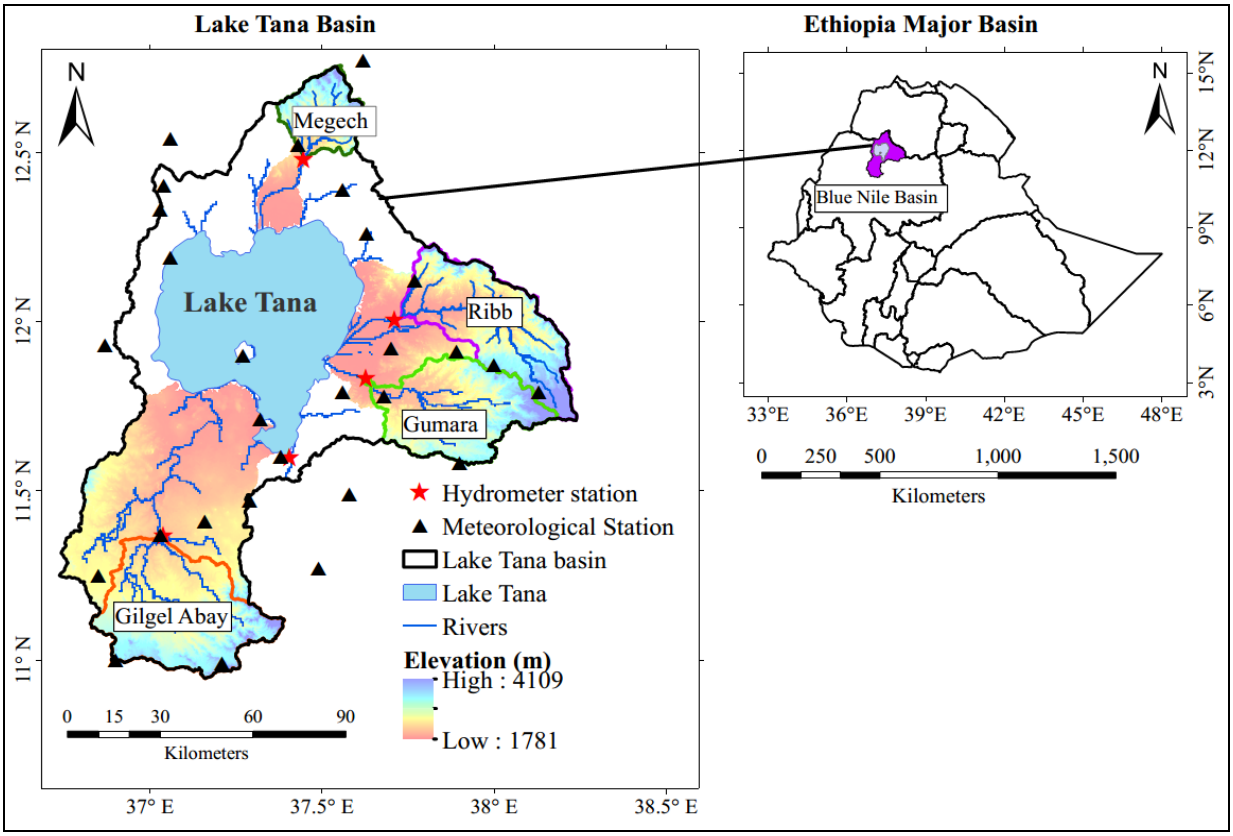

Figure 4.1 The Lake Tana basin showing its four major watersheds (Gilgel Abay, Gumara, Ribb, and Megech river), streamflow and climate gauging stations with Digital Elevation Model (DEM) as a background. The map on the left shows the major river basins (12) in Ethiopia.

4.2.3 Climate simulation

Daily rainfall and temperature datasets for this study were estimated using WRF (version 3.8) regional climate model. The WRF model assumes a fully compressible and a terrain-following hydrostatic pressure coordinate (Skamarock *et al.*, 2008). Initial and boundary forcing data for dynamic downscaling were obtained from the Community Earth System Model version 1 (CESM), produced by the National Center for Atmospheric Research (NCAR). The NCAR is jointly participating in the coupled model intercomparison project phase 5 (CMIP5) experiments and supported the intergovernmental Panel on Climate Change Fifth Assessment Report (Bruyere *et al.*, 2015). CESM is a coupled GCM comprised of four component models that simulate the atmosphere, ocean, land surface and sea-ice. Knutti *et al.* (2013) showed that CESM ranks at the

top of all CMIP5 GCMs in its ability to simulate global patterns of observed temperature and rainfall. The spatial and temporal resolutions of the CESM data are 1° × 1° and 6 h, respectively. A detailed description of the model is provided in Bruyere *et al.* (2015). The future scenarios were based on Representative Concentration Pathways (RCPs) from the IPCC fifth assessment report (AR5). This study used RCP4.5 and RCP8.5 emission scenarios. The RCPs are the latest developed climate scenarios, which covers a wider range of futures than those from the SRES (Van Vuuren *et al.*, 2011). The RCP4.5 is an intermediate stabilization scenario with an equivalent concentration of carbon dioxide ranging from 580 to 720 part per million (ppm) in 2100, while the RCP8.5 is a very high emission scenario representing an equivalent concentration of carbon dioxide larger than 1000 ppm in 2100 (IPCC, 2014).

This study used the WRF model physical parameterization schemes and model configurations by Teklay *et al.* (2019). The WRF simulation was configured in three nested domains (Figure 3.1). The WRF simulation in the inner domain covering the Lake Tana basin and has a 4 km horizontal resolution. The physical processes used in this study consist of the Thompson microphysics (Thompson *et al.*, 2008), the Kain-Fritsch cumulus parameterization (Kain, 2004), the Rapid Radiative Transfer Model for GCMs (RRTMG) for long-wave and shortwave radiation (Iacono *et al.*, 2008), the revised MM5 Monin-Obukhov surface layer physics (Jiménez *et al.*, 2012), the Yonsei University planetary boundary layer physics (Hong *et al.*, 2006), and the Noah land surface model (Teklay *et al.*, 2019).

Due to the shortage of computational resources, the WRF simulations were conducted for eleven years from 31 December 2004 to 31 December 2015 for the baseline run, and from 31 December 2044 to 31 December 2055 for the RCP4.5 and RCP8.5 runs. The simulation outputs were daily rainfall, and daily maximum and minimum temperature at 2 meter above the ground over the respective simulation periods.

Direct application of the RCM outputs for assessing the impact of climate change on hydrological response is not recommended due to biases resulting from limitations in the global forcing fields and RCMs (Hurkmans *et al.*, 2010; Smitha *et al.*, 2018). There are different methods to correct the model biases. For example, Wulong *et al.* (2018) used the local intensity scaling (LOCI) method for precipitation correction and the linear scaling (LS) method for temperature correction. Both LOCI and LS approach were applied to correct biases in the mean climate dataset by assuming a

static coefficient of variation (CV) for the dataset distribution. However, the temporal variability of the dataset is important for estimating hydrological responses accurately (Hurkmans *et al.*, 2010). In this study, the power transformation (PT) and variance scaling (VS) method were used to correct model biases. The PT method specifically considers changes in both the mean and variance in rainfall dataset (Fang *et al.*, 2015). This method corrected the downscaled rainfall using a non-linear empirical relationship (Equation 4.1).

$$R_c = aR^b \tag{4.1}$$

where R_c is the corrected rainfall, R is the uncorrected rainfall, and a and b are estimated from changes in the mean and CV from observed and simulated rainfall. First, b is fitted to minimize the difference between the CV of the observed rainfall and the CV of the simulated rainfall. After finding optimal b in the first step, a is determined such that the mean of the simulated rainfall corresponds to the observed mean rainfall.

The VS method was developed to correct both the mean and variance of temperature time series (Terink *et al.*, 2010). Temperature was corrected using the VS method with Equation 4.2.

$$T_c = \left[T - \mu(T)\right] \times \frac{\sigma(T_o)}{\sigma(T)} + \mu(T_o) \tag{4.2}$$

where T_c is the corrected temperature; T is the uncorrected temperature; $\sigma(T_o)$ is the standard deviation of the observed temperature; $\sigma(T)$ is the standard deviation of the uncorrected temperature; $\mu(T)$ is the simulated mean temperature; and $\mu(T_o)$ is the observed mean temperature.

To verify the bias correction method, the average daily observation and WRF simulation (before and after bias correction) were compared using statistical measures such as mean bias (MB), correlation coefficient (r) and root mean square error (RMSE).

4.2.4 Hydrological model

The Soil and Water Assessment Tool (SWAT) model was used to assess the impact of climate change on hydrological response in Gilgel Abay, Gumara, Ribb, and Megech watersheds. The

SWAT model has been widely applied in the Upper Blue Nile basin and showed satisfactory results (Gebremicael *et al.*, 2013; Dile *et al.*, 2016; Fentaw *et al.*, 2018). The SWAT model is developed to predict the impact of land-use, land management practices, and climate change on water balance, nutrient cycling, and sediment transport at a watershed to a river basin and regional scale. It is a physically-based semi-distributed model that functions on a continuous-time step. In the SWAT model, a watershed is divided into sub-basins where each sub-basin will have one or more Hydrologic Response Units (HRUs). HRU is a unique combination of land-use, soil, and slope classes. Most of the biophysical processes are calculated at the HRU level and aggregated at the sub-basin level (Neitsch *et al.*, 2011). The hydrological cycle simulated by SWAT is based on following equation:

$$SW_t = SW_o + \sum_{t=1}^{t} (R_{day} - Q_{surf} - E_a - w_{seep} - Q_{gw}) \quad (4.3)$$

where SW_t is the final soil water content (mm), SW_o is the initial soil water content on day *i* (mm), *t* is the time (days), R_{day} is the amount of precipitation on day *i* (mm), Q_{surf} is the amount of surface runoff on day *i* (mm), E_a is the amount of evapotranspiration on day *i* (mm), w_{seep} is the amount of water entering the vadose zone from the soil profile on day *i* (mm), and Q_{gw} is the amount of return flow on day *i* (mm).

Runoff is predicted separately for each HRU and routed to obtain the total runoff for the watershed. Surface runoff will commence whenever the rate of water application to the ground surface exceeds the rate of infiltration. SWAT provides two methods for estimating surface runoff: the soil conservation service curve number (SCS CN) and the Green and Ampt (Green-Ampt) infiltration method (Neitsch *et al.*, 2011). In the curve number method, the curve number varies non-linearly with moisture content of the soil. The curve number drops as the soil approaches the wilting point and increase to near 100 as the soil approaches to saturation. The Green-Ampt infiltration method requires sub-daily precipitation data and calculates the infiltration as a function of the wetting front matric potential and effective hydraulic conductivity. The advantages of SCS curve number method over the Green-Ampt method clearly mentioned in King *et al.* (1999). SCS curve number

method is widely used in the data-scarce region (Arnold *et al.*, 1998). In this method, the accumulated runoff is estimated with Equation 4.4:

$$Q_{surf} = \frac{\left(R_{day} - 0.2S\right)^2}{\left(R_{day} + 0.8S\right)} \tag{4.4}$$

where Q_{surf} is the amount of surface runoff on day i (mm), R_{day} is the amount of precipitation on day *i* (mm), and *S* is the retention parameter (mm). The retention parameter is a function of curve number (CN) and defined by Equation 4.5:

$$S = 25.4 * \left(\frac{1000}{CN} - 10\right) \tag{4.5}$$

4.2.5 SWAT Input data

The SWAT model requires spatio-temporal data such as topography, land-use, soil, weather, and land-management interventions to simulate different processes in the watershed. The model also requires hydrological data (e.g., streamflow) to calibrate and validate the performance of the model. Digital Elevation Model (DEM) is used to delineate the watershed and generate other topographic characteristics. This study used DEM data from the Shuttle Radar Topographic Mission (SRTM), which has a spatial resolution of 90 m. Land-use data is required in the SWAT model to define the HRUs and link the landscape with the crop database. Land-use data was produced from a 30 m Landsat image using a supervised classification method for the 2016 Ethiopia land-cover (Figure 4.2a). This data was obtained from the Regional Centre for Mapping of Resources for Development (RCMRD) (http://geoportal.rcmrd.org). The soil data was used to create HRUs and provide physiochemical information about the soils in the landscape (Figure 4.2b). The soil map was obtained from the Ministry of Water, Irrigation, and Electricity (MoWIE) of Ethiopia. The physical and chemical soil properties that required by the SWAT model were extracted from the International Soil Reference and Information Center (http://www.isric.org). Climate data within and around the Lake Tana basin were collected from the National Meteorology Agency (NMA) of Ethiopian. Rainfall and temperature data were collected from 24 meteorological stations (Figure 4.1) for the period 1982 to 2015. Missing values in climate data were filled using an arithmetic average method (Sattari *et al.*, 2017). Streamflow data was used to calibrate and

validate the performance of the SWAT model. This study used monthly streamflow data of Gilgel Abay, Gumara, Ribb, and Megech for model calibration and validation. Observed streamflow data for the period 1990-2015 was obtained from the MoWIE.

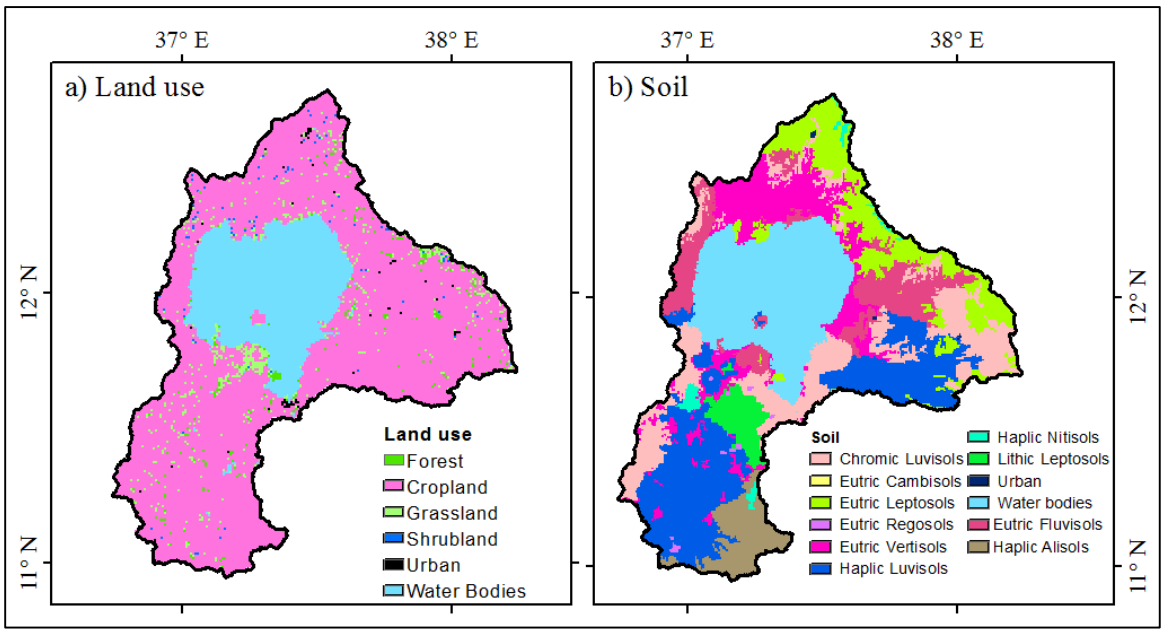

Figure 4.2 Lake Tana basin land-use and soil map subjected to hydrological model simulation.

4.2.6 SWAT model setup, calibration and validation

The watershed boundary was delineated by considering the hydrometer station as an outlet (Figure 4.1). The HRUs were defined using accounting all the slope, land-use, and soil features in the sub-basins. Angereb reservoir is located in the Megech watershed, which was included in the SWAT model setup. Angereb dam was constructed in 1997 to supply potable water to Gondar town (Haregeweyn *et al.*, 2012). The reservoir has a total area of 50 ha and 60 ha at its principal spillway and emergency spillway, respectively. The volume of the reservoir at the principal and emergency spillway is 3,530,000 m^3 and 5,160,000 m^3, respectively. SWAT has several options to simulate biophysical processes. The surface runoff was estimated using the Soil Conservation Service Curve Number (SCS CN) method (Fentaw *et al.*, 2018; Bekele *et al.*, 2019). Flow within the channels was routed using variable storage method. The evapotranspiration was estimated using the Penman-Monteith method (Gebre and Ludwig, 2015).

The model parameters were calibrated using the Sequential Uncertainty Fitting version 2 (SUFI-2) in the SWAT-CUP (SWAT Calibration and Uncertainty Program) (Abbaspour *et al.*, 2004).

The model was calibrated and validated using observed monthly streamflow data at the Gilgel Abay, Gumara, Ribb, and Megech river gauging stations (Figure 4.1). The calibration and validation were conducted for the periods 1990–2004 and 2005–2015, respectively. The model was warm-up for three years (1987-1989) to properly initiate the biophysical processes. The model calibration considered 18 hydrological parameters (Appendix 4), which were selected based on the literature (Setegn *et al.*, 2008; Gebremicael *et al.*, 2013; Dile *et al.*, 2016).

4.2.7 Model evaluation

Model performance was evaluated by comparing the observed and simulated streamflow using the Nash-Sutcliffe Efficiency (NSE) and percent bias (PBIAS). The NSE is a normalized statistic that estimates the relative magnitude of the residual variance compared to the observed data variance (Nash and Sutcliffe, 1970). PBIAS compares the average tendency of the simulated data to the corresponding observed data (Gupta *et al.*, 1999). The NSE value theoretically ranges from negative infinity to 1; a value of 1 corresponds to a perfect match between observed and simulated values (Nash and Sutcliffe, 1970). While the PBIAS value can be positive or negative, in which a value of zero represents the best model simulation performance (Moriasi *et al.*, 2007). A positive PBIAS value indicates model underestimations, and a negative value indicates model overestimations. The NSE and PBIAS are computed using Equation 4.6 and 4.7, respectively. Moriasi *et al.* (2007) suggested that a model simulation that provides a NSE value of >0.5 and PBIAS value is considered as satisfactory.

$$NS = 1 - \left(\sum_{i=1}^{n} (O_i - S_i)^2 / \sum_{i=1}^{n} (O_i - \overline{O})^2 \right) \tag{4.6}$$

$$PBIAS = \left(\sum_{i=1}^{n} (O_i - S_i) / \sum_{i=1}^{n} O_i \right) * 100 \tag{4.7}$$

where, O_i is the observed streamflow data, S_i is the simulated streamflow data, $\overline{O}$ is the mean of the observed streamflow data, and n is the total number of streamflow data.

The uncertainty of the simulations was estimated using a P-factor and R-factor (Abbaspour *et al.*, 2007). The P-factor measures percent of observed data bracketed by the 95% prediction uncertainty (95PPU). While the R-factor measures the thickness of the uncertainty band. It is estimated by dividing the average thickness of the 95PPU band by the standard deviation of the observed data. The P-factor value ranges between 0 and 1, while the R-factor ranges between 0

and infinity. A P-factor of 1 and R-factor of 0 represent a simulation that exactly matches the observed data. According to Abbaspour *et al.* (2007), a model providing a P-factor ≥ 0.75 and R-factor ≤ 1.5 is considered robust for streamflow simulation.

4.3 Results

4.3.1 Climate variable before and after bias correction

Daily rainfall and temperature data were extracted from the grid-based WRF simulations using coordinates of meteorological stations. Figure 4.3 shows observed and simulated rainfall and temperature data, averaged over the Lake Tana basin, for the baseline period (2005 – 2015). The WRF model performed well in simulating rainfall during the dry season (January to May); while it considerably overestimated rainfall during the rainy season (June to August) (Figure 4.3a). Besides, the model consistently underestimated maximum temperature (Tmax) (Figure 4.3b), while the WRF model overestimated minimum temperature (Tmin) (Figure 4.3c) in all months. These results highlighted the need for bias correction, and it improved the WRF model's outputs considerably. Cold and warm biases of maximum and minimum temperatures, respectively were substantially reduced. Similarly, the bias-corrected WRF model (WRF-BC) reproduced monthly rainfall very well except for slight overestimations during the rainy months of July and August.

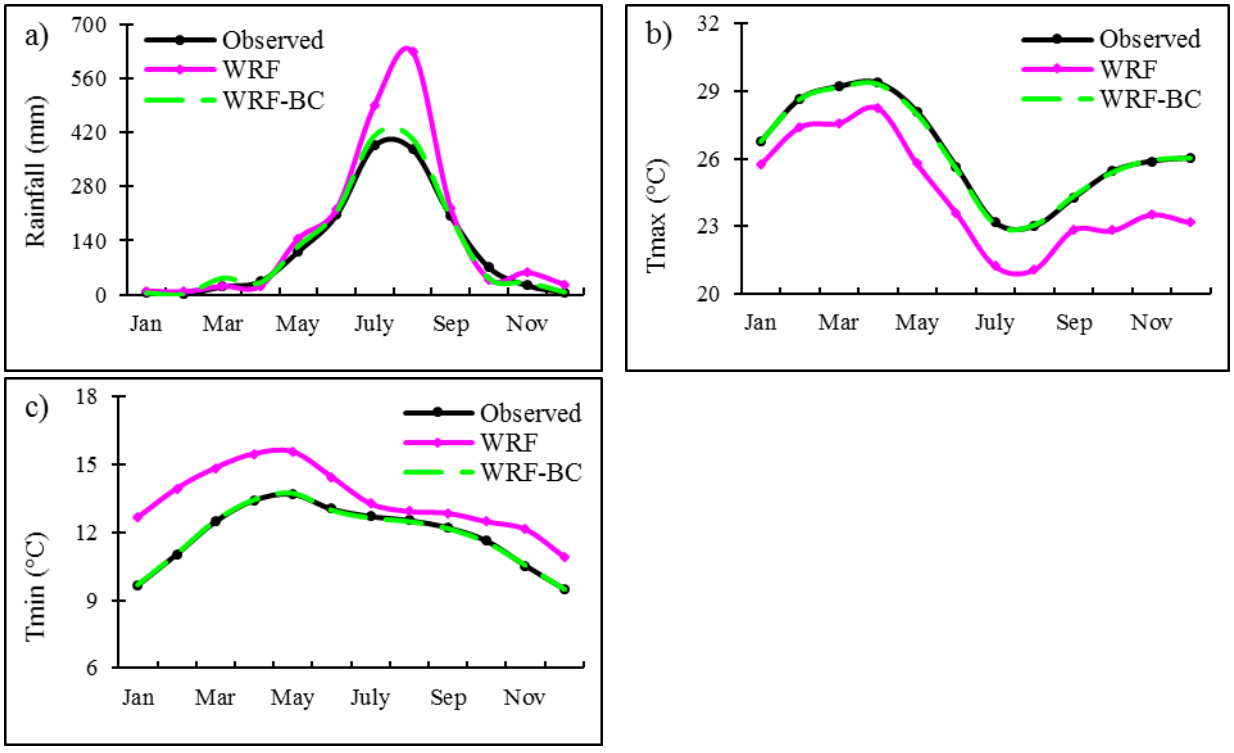

Figure 4.3 Monthly mean observed and WRF simulated (before and after bias correction) rainfall (a), maximum temperature (b), and minimum temperature (c) from the Lake Tana basin during 2005-2015. WRF and WRF-BC represent model simulations before and after bias correction, respectively.

While bias correction improved overall performances of the WRF model in simulating rainfall and temperature; there were differences in the model evaluation statistics (Table 4.1). For temperature, bias-corrected values were very close to the observed. After bias correction, the average cold bias was substantially reduced from 1.87 ºC to 0.02 ºC for maximum temperature and the warm bias decreased from 1.46 ºC to 0.03 ºC for minimum temperature (Table 4.1). Moreover, the RMSE was considerably reduced by 1.36 ºC and 1.19 ºC for maximum and minimum temperatures, respectively. However, RMSE for rainfall was decreased from 5.85 to 4.77 mm/day. Besides, bias-corrected simulations showed good agreement with the observed data. Correlations between observed and simulated data were improved from 0.78 and 0.61 to 0.88 and 0.82 for maximum and minimum temperatures, respectively. However, the correlation between observed and simulated rainfall did not show significant improvement after bias correction. These results suggested that bias correction output was acceptable and consistent with the previous studies (Gebre and Ludwig, 2015; Sisay *et al.*, 2017).

Table 4.1 The statistical measures of climate variables before bias correction (WRF) and after bias correction (WRF-BC) for the Lake Tana basin from 2005 to 2015.

Variables	Statistics	Observed	WRF	WRF-BC
Rainfall	Mean (mm/day)	3.97	5.19	4.13
	Bias (mm/day)	-	1.22	0.16
	Correlation	-	0.70	0.71
	RMSE (mm/day)	-	5.85	4.77
Maximum temperature (Tmax)	Mean (ºC)	26.27	24.40	26.25
	Bias (ºC)	-	-1.87	-0.02
	Correlation	-	0.78	0.88
	RMSE (ºC)	-	2.55	1.20
Minimum temperature (Tmin)	Mean (ºC)	11.88	13.46	12.01
	Bias (ºC)	-	1.45	0.03
	Correlation	-	0.61	0.82
	RMSE (ºC)	-	2.17	0.98

Note: WRF=Weather Research Forecasting (WRF) simulation before bias correction, and WRF-BC=Weather Research Forecasting (WRF) simulation after bias correction.

4.3.2 Projected temperature

Temperature projections using the WRF model were averaged by season to investigate overall trends of future climate in Gilgel Abay, Gumara, Ribb, and Megech watersheds. The baseline (2005 – 2015) and projected (2045 - 2055) seasonal temperature distributions in the four study

watersheds are presented in Figure 4.4. The baseline and projected minimum and maximum temperatures flowed a similar seasonal pattern. The simulated maximum temperature is high in spring, whereas minimum temperature is high in summer in most watersheds. Compared to the baseline period, both RCP4.5 and RCP8.5 seasonal maximum and minimum temperatures are predicted to increase in all the watersheds. In the Gilgel Abay watershed, the mean annual maximum temperature is projected to increase by 1.4 °C and 2.4 °C under RCP4.5 and RCP8.5 scenarios, respectively, while minimum temperature is expected to increase by 1.2 °C under RCP4.5 and 1.7 °C under RCP8.5. The seasonal increase in maximum temperature shows a large variation with a range from 0.2 °C to 2.5 °C under RCP4.5 and 1.9 °C to 2.8 °C under RCP8.5 (Figure 4.4a). Under both scenarios, the summer and autumn season maximum temperature change is higher than other seasons (Figure 4.4a). However, minimum temperature change in spring is projected to be as high as 1.5 °C and 2.5 °C under RCP4.5 and RCP8.5 scenarios, respectively (Figure 4.4b). In the Gumara watershed, the mean annual maximum temperature is projected to increase by 1.7 °C and 2.6 °C and minimum temperature by 1.5 °C and 2.0 °C under RCP4.5 and RCP8.5, respectively. The seasonal increase in maximum temperature display a large variation with a range from 0.6 °C to 2.6 °C for RCP4.5 and 2.2 °C to 3.2 °C for RCP8.5 (Figure 4.4c). The highest minimum temperature increase is projected to occur in winter (1.9 °C) and spring (2.5 °C) under RCP4.5 and RCP8.5 scenarios, respectively (Figure 4.4d). In the Ribb watershed, the mean annual maximum temperature may increase by 1.2 °C and 2.3 °C and minimum temperature by 1.4 °C and 2.0 °C under RCP4.5 and RCP8.5, respectively. Compared to the baseline period, the seasonal maximum temperature increase under RCP4.5 vary between 0.1 °C and 2.3 °C, while the increase under RCP8.5 is expected to vary between 1.8 °C and 3.0 °C (Figure 4.4e). However, the minimum temperature changes under RCP4.5 did not show considerable variation among seasons (Figure 4.4f). In the Megech watershed, the mean annual maximum temperature is projected to increase by 1.3 °C and 2.2 °C while the minimum temperature is projected to increase by 1.4 °C and 2.0 °C under RCP4.5 and RCP8.5, respectively. The seasonal maximum temperature increase is expected to vary between 0.1 °C to 2.3 °C and 1.9 °C to 2.6 °C under RCP4.5 and RCP8.5, respectively (Figure 4.4g).

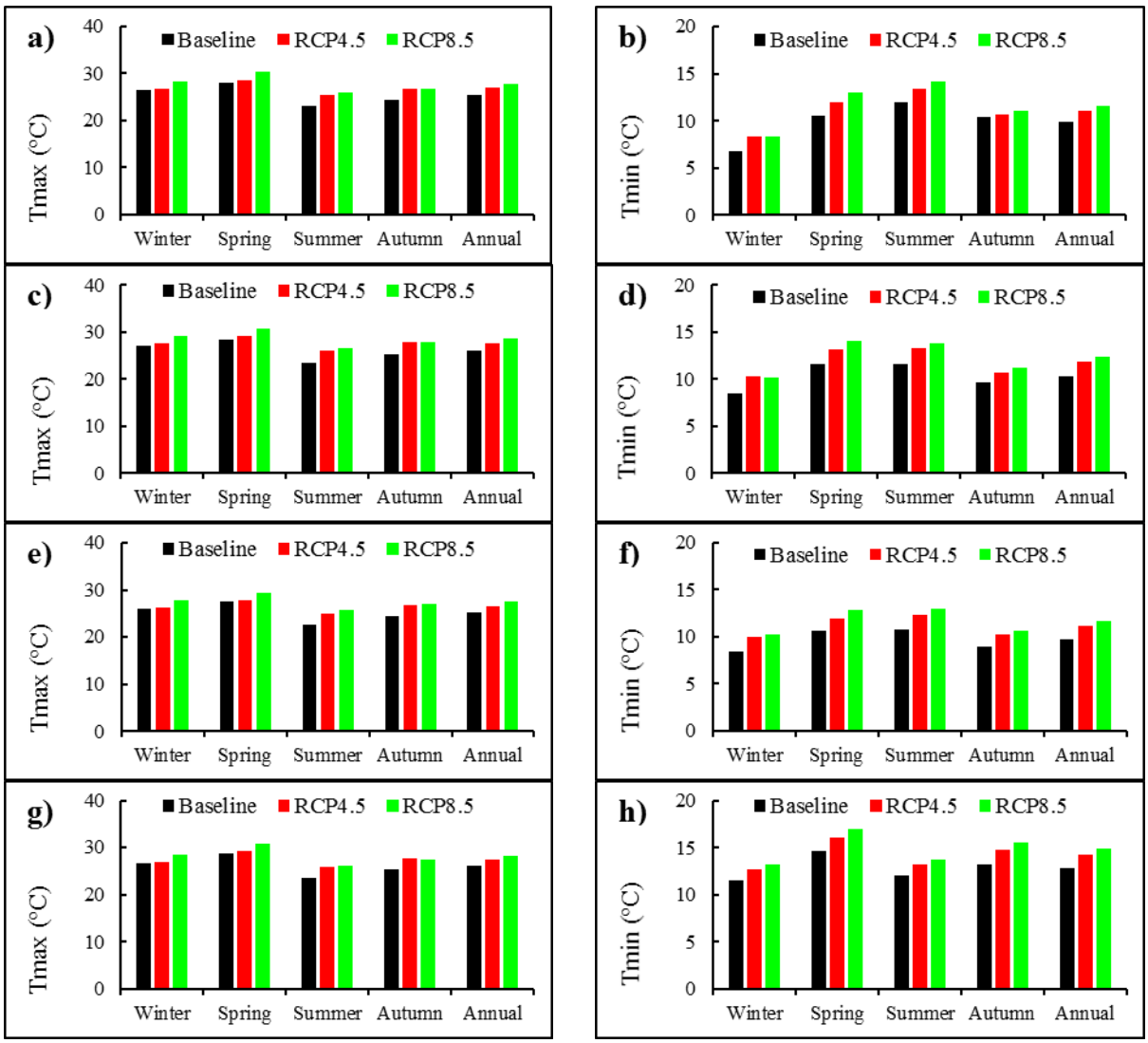

Figure 4.4 Seasonal and annual maximum temperature (a, c, e, and g) and minimum temperature (b, d, f, and h) in Gilgel Abay watershed (a and b); Gumara watershed (c and d); Ribb watershed (e and f); and Megech watershed (g and h) in the Lake Tana basin.

4.3.3 Projected rainfall

The seasonal rainfall distribution under RCP4.5 and RCP8.5 scenarios were similar to the baseline period (Figure 4.5). The highest rainfall occurred in summer (781 – 1713 mm) while the smallest rainfall (6 – 51 mm) was simulated in winter. However, the mean annual rainfall under RCP4.5 and RCP8.5 scenarios are larger than the baseline period in all the four watersheds. Similar to temperature, rainfall simulations under RCP8.5 is substantially greater than that of under RCP4.5 in all watersheds except for Megech. Under RCP8.5, the mean annual rainfall is projected to increase by 578 mm, 377 mm, 313 mm, and 47 mm in Gilgel Abay, Gumara, Ribb, and Megech

watersheds, respectively. The greatest increase (28%) is expected to occur under RCP8.5 scenario in Gilgel Abay watershed, while Megech watershed could experience the smallest increase (2.8 %) under RCP4.5 scenario. As shown in Figure 4.5, Megech watershed may receive the smallest mean annual rainfall in the future.

In the Gilgel Abay watershed, rainfall under both scenarios is projected to increase in all four seasons except for autumn under RCP4.5 (Figure 4.5a). The largest increase in rainfall is expected to occur in spring (56%) and Summer (30%) under RCP4.5 and RCP8.5, respectively. In the Gumara watershed, rainfall under RCP8.5 is larger than the baseline values in all seasons with a maximum increase of 23% in summer (Figure 4.5b). However, rainfall under RCP4.5 may decrease by 17.4% and 34.6% in summer and autumn, respectively. In spring, rainfall under RCP4.5 is projected to increase by 172%. In the Ribb watershed, the seasonal rainfall is projected to increase by up to 220% and 75.6% under RCP4.5 and RCP8.5 scenarios, respectively (Figure 4.5c). The rainfall under RCP4.5 may decrease by 16.2% and 47.6% in summer and autumn, respectively. On the contrary, rainfall under RCP8.5 may increase by 7.8% mm and 33.8% in summer and autumn, respectively. In the Megech watershed, rainfall under both scenarios may increase in spring (Figure 4.5d). However, rainfall in autumn may decrease by 59.8% and 33.5% under RCP4.5 and RCP8.5 scenarios, respectively.

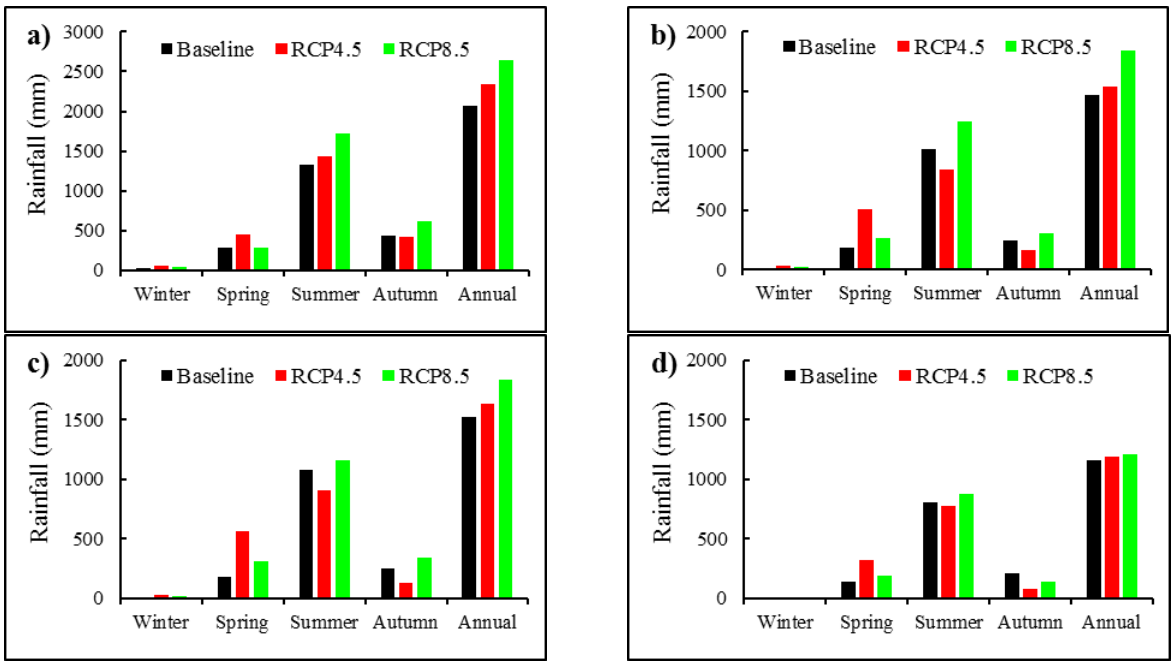

Figure 4.5 The seasonal and mean annual rainfall distribution in the Gilgel Abay watershed (a); Gumara watershed (b); Ribb watershed (c); and Megech watershed (d).

4.3.4 SWAT model calibration and validation

Statistical analysis of the SWAT model indicates that the monthly streamflow was well simulated for the calibration period, with NSE > 0.72 (Table 4.2). Besides, the SWAT model simulated the mean streamflow well, with PBIAS < ±15% in all the four watersheds. The model evaluation during the calibration period revealed that the SWAT model slightly underestimated the mean streamflow in Gilgel Abay (4.6%), Gumara (10.7%) and Ribb (0.6%) watershed. However, the SWAT model overestimated the mean streamflow in Megech watershed (14.1%). The agreement between observed and simulated flow was slightly better for Gilgel Abay, Gumara, and Ribb watershed, compared to Megech watershed. Validation results also showed overall very good model performances in all watersheds, with NSE values > 0.77 and PBIAS < ±9 (Moriasi *et al.*, 2007). During the validation period, the SWAT model slightly overestimated the mean streamflow by about 5.3% in the Ribb watersheds, whereas it slightly underestimated the mean streamflow by about 7.2%, 8.7% and 8.4% in Gilgel Abay, Gumara and Megech watershed, respectively.

The uncertainty bands of the model captured most of the observed streamflow with P-factor > 0.82 in both calibration and validation period in Gilgel Abay and Gumara watershed. However, the 95PPU relative width was slightly small in Megech (0.75) and Ribb (0.78) watershed, but it was under the acceptable model estimates (Abbaspour *et al.*, 2007). Overall, the model simulation results demonstrated that the SWAT model replicated the observed streamflow very well during the calibration and validation period in all study watersheds. These findings are in agreement with previous studies in the region (Setegn *et al.*, 2008; Dile *et al.*, 2016). Therefore, it is safe to conclude that the SWAT model is reliable to simulate the watershed hydrological processes in the Ethiopian highlands.

Table 4.2 Goodness-of-fit statistics of streamflow simulation results during both calibration and validation periods at the four watersheds.

Watersheds	Calibration				Validation			
	NSE	PBIAS	P-factor	R-factor	NSE	PBIAS	P-factor	R-factor
Gilgel Abay	0.93	4.6	0.97	0.76	0.81	7.2	0.85	0.79
Gumara	0.89	10.7	0.83	0.53	0.85	8.7	0.82	0.42
Ribb	0.84	0.6	0.78	0.74	0.82	-5.3	0.75	0.74
Megech	0.72	-14.1	0.74	0.89	0.77	8.4	0.76	0.80

Moreover, the graphical comparison results showed that the simulated streamflow was in a very good agreement with observations at the four watersheds (Figure 4.6). However, the model tends to underestimate the peak flows in most times while overestimating low flows. The majority of the peak events were not captured adequately over the study watersheds owing to the poor performance of the SWAT model for peak flow simulations (Polanco *et al.*, 2017; Lee *et al.*, 2018).

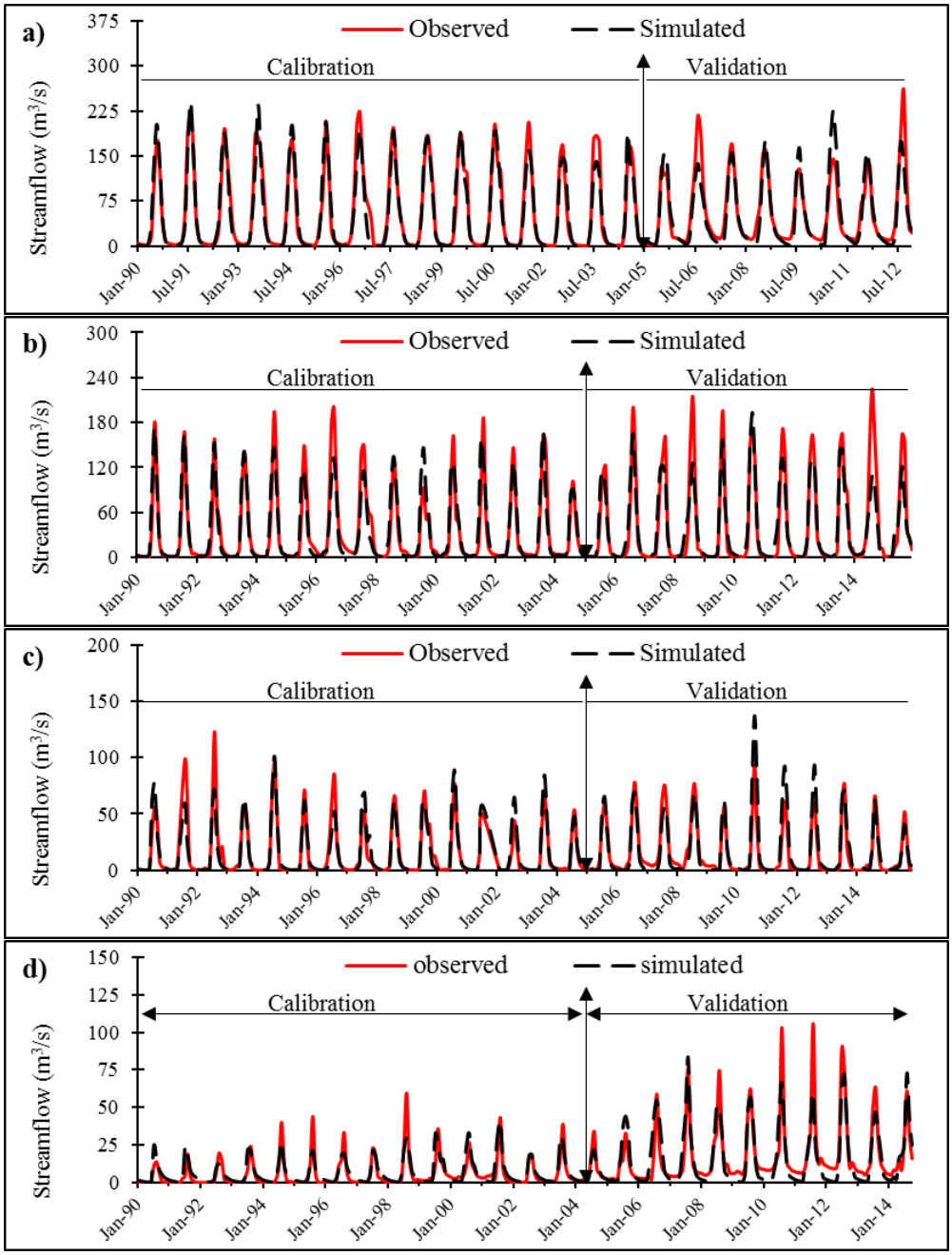

Figure 4.6 Observed and simulated monthly streamflow for the calibration period (1990-2004) and validation period (2005-2015) at; a) Gilgel Abay, b) Gumara, c) Ribb, and d) Megech watershed.

4.3.5 The impacts of climate change on hydrological responses

The hydrological components were simulated using the calibrated SWAT model and bias-corrected climate date. The simulated hydrological components for the projected period (2045-2055) under RCP4.5 and RCP8.5 scenarios were compared to the corresponding values in the baseline period (2005–2015). Overall, the mean annual rainfall, temperature, streamflow, and evapotranspiration are projected to increase compared to the baseline period in all the four study watersheds (Table 4.3). However, the direction of seasonal streamflow and evapotranspiration changes were different among watersheds except for Gumara and Ribb (Figure 4.7).

In the Gilgel Abay watershed, the mean annual streamflow may increase by 15% and 40%, which corresponds to 13.4% and 28% rainfall increase under RCP4.5 and RCP8.5 scenarios, respectively (Table 4.3). On a seasonal scale, the streamflow under RCP4.5 and RCP8.5 is projected to increase in all seasons except for winter (Figure 4.7a). The streamflow changes are mostly related to rainfall change over the watershed. Under RCP8.5, the changes in summer rainfall clearly show the largest increase (390.5 mm) in comparison to other seasons (Figure 4.5a), which may yield the largest streamflow increase (296 mm). Similarly, rainfall in spring may increase by 159.1 mm under RCP4.5, thereby considerably increasing streamflow by 51 mm. However, the winter season streamflow is projected to decrease slightly by 2.4 mm under RCP4.5, despite projected rainfall increase (9.8 mm) during the same time, since rainfall increase substantially contributes to evapotranspiration increase. The mean annual evapotranspiration under RCP8.5 is expected to increase by 17.5% due to the average temperature increase of 2.1 °C and rainfall increase of 28%. At the seasonal scale, evapotranspiration under RCP4.5 may increase in all seasons except for autumn. The increase in rainfall and temperature in winter, spring, and summer causes evapotranspiration increase. Although the average temperature under RCP4.5 may increase in autumn (1.4 °C), evapotranspiration may decrease by 35 mm. In this season, potential evapotranspiration may increase by 14.5% (Appendix 5), whereas the rainfall amount may decrease by 3% (Figure 4.5a). These results indicate that all the temperature increase may not contribute to evapotranspiration increase

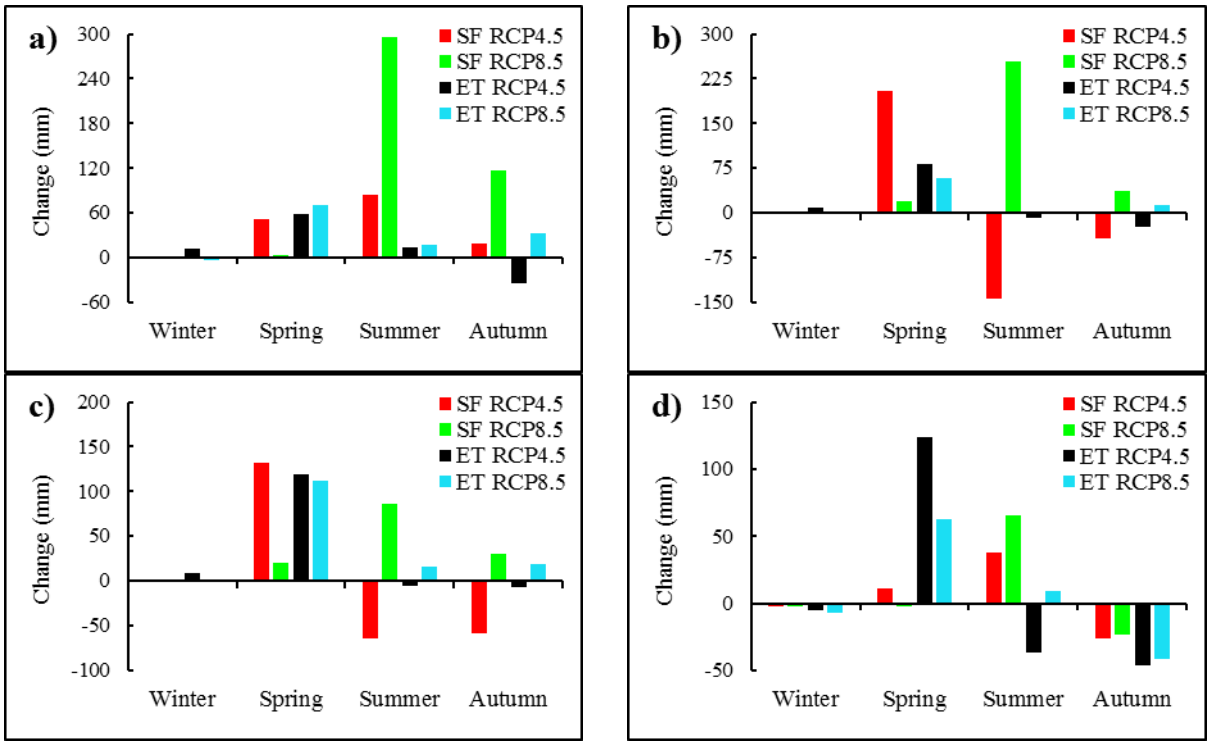

Figure 4.7 Projected (2045-2055) seasonal streamflow (SF) and evapotranspiration (ET) changes relative to the baseline period (2005-2015) at: (a) Gilgel Abay, (b) Gumara, (c) Ribb, and (d) Megech watershed.

As can be seen in Figure 4.7, the direction of hydrologic response changes in Gumara and Ribb watersheds were similar in most time, since the hydrologic model in both watersheds used almost the same meteorological stations that are located in the eastern part of the Lake Tana basin (Figure 4.1). Therefore, the results of the Gumara watershed are presented here for clarity purposes. The mean annual streamflow increase under RCP4.5 is very small (1.6%), while the mean annual streamflow increase under RCP8.5 is considerably large (34.3%). This may relate to a larger increase in mean annual rainfall under RCP8.5 than RCP4.5. Under RCP4.5, the streamflow is projected to decrease in most season, with the largest decrease of 144 mm (22.5%) in summer. However, the streamflow increase during spring is extremely large (203.4 mm), which may cause flooding. The RCP8.5 streamflow may increase in all seasons with a range between 19.4 mm (45.3%) in spring and 254.1 mm (39.7%) in summer. The mean annual evapotranspiration is projected to increase by 10.7% and 12.1% under RCP4.5 and RCP8.5 scenarios, respectively, which corresponds with the projected increases in average annual temperature by 1.6 °C and 2.4 °C and rainfall by 5% and 25.7%, under RCP4.5 and RCP8.5, respectively (Table 4.3). The

RCP4.5 projection shows a decrease of evapotranspiration in summer and autumn, while the RCP8.5 shows an increase of evapotranspiration in all four seasons except for winter.

In the Megech watershed, the mean annual streamflow may increase in the future period under both scenarios. The increase in streamflow under RCP8.5 is slightly greater than under RCP4.5. The streamflow projection under both scenarios may increase in summer with a maximum increase of 66 mm under RCP8.5, while it may decrease considerably in autumn (Figure 4.7d) with a maximum decrease of 25.8 mm under RCP4.5. Unlike to other watersheds, the increase in evapotranspiration under RCP4.5 (6.7%) is slightly greater than that of under RCP8.5 (4.3%). This may relate to the simulation of extremely large evapotranspiration in spring (Appendix 8). Compared to the baseline, evapotranspiration in spring may increase by 124 mm and 62.9 mm under RCP4.5 and RCP8.5 scenarios, respectively. Evapotranspiration, however, is expected to decrease during winter and autumn under both scenarios.

Table 4.3 Mean annual climate variables and hydrologic components for the baseline and projected period in the four study watersheds.

Variable	Statistics	Gilgel Abay			Gumara			Ribb			Megech		
		Base	RCP4.5	RCP8.5	Base	RCP4.5	RCP8.5	Base	RCP4.5	RCP8.5	Base	RCP4.5	RCP8.5
AT	Mean (°C)	17.6	19.0	19.7	18.1	19.7	20.5	17.4	18.7	19.6	19.4	20.8	21.6
	Change (°C)	-	1.4	2.1	-	1.6	2.4	-	1.3	2.2	-	1.4	2.2
Rainfall	Mean (mm)	2066	2342	2644	1465	1539	1842	1526	1636	1839	1163	1196	1210
	Change (%)	-	13.4	28	-	5	25.7	-	7.2	20.5	-	2.8	4
SF	Mean (mm)	1016	1169	1423	898	912	1206	521	527	655	254	275	292
	Change (%)	-	15.0	40.0	-	1.6	34.3	-	1.1	25.8	-	8.3	15
ET	Mean (mm)	670	719	787	547	605	613	567	683	714	542	578	565
	Change (%)	-	7.3	17.5	-	10.7	12.1	-	20.4	25.9	-	6.7	4.3

Note: Base = Baseline period; AT = Average Temperature; SF = Streamflow; and ET = Evapotranspiration.

4.4 Discussion

The Lake Tana basin is one of the growth corridors in Ethiopia where large and small scale irrigation and hydropower projects are under construction. Many studies indicate that climate change has a substantial impact on streamflow in the major tributaries of the Lake Tana basin, and they found that the streamflow variability of tributary rivers is the result of rainfall and temperature change. These studies used rainfall and temperature output from coarse spatial resolution. However, few studies have evaluated the impact of climate change on streamflow response in the major tributaries rivers of the Lake Tana basin using dynamically downscaled climate data.

The projected mean annual maximum and minimum temperatures under RCP4.5 and RCP8.5 scenarios are higher than the baseline period. The mean annual temperature increase under RCP8.5 is considerably larger than that under RCP4.5 because the RCP8.5 scenario represents a higher radiative force (Wulong *et al.*, 2018). The climate projections show that overall warming over the Lake Tana basin, with an average temperature increase of 1.4 ℃ and 2.2 ℃ under RCP4.5 and RCP8.5 scenarios, respectively. These results are comparable with the previous studies in the Upper Blue Nile basin (e.g., Dile *et al.*, 2013; Nigatu *et al.*, 2016; Liersch *et al.*, 2018; Mekonnen and Disse, 2018). Besides, the results agree with the study by Ayele *et al.* (2016) in Gilgel Abay and Gumara watersheds. They reported that the projected (2020-2039) temperature in the A2/B2 scenarios increased by 1.2/1.1°C and 0.8/0.7°C in Gilgel Abay and Gumara watershed, respectively. The simulated mean annual rainfall under RCP4.5 and RCP8.5 is larger than the baseline period. The result shows that the RCP4.5 rainfall increase rate is greater in spring than other seasons, which is in agreement with Worqlul *et al.* (2018) findings in the Upper Blue Nile basin. Moreover, rainfall under RCP8.5 is expected to increase in all seasons in all the watersheds except for Megech. These results are in agreement with results from previous studies in the Lake Tana basin (Gebre and Ludwig, 2015; Ayele *et al.*, 2016; Nigatu *et al.*, 2016; Melke and Abegaz, 2017), though variations exist in the magnitude of change. This could be due to differences in GCM, emission scenarios, and downscaling methods used between studies. However, this result contradicted the study by Setegn *et al.* (2011) in the Lake Tana basin who reported decreasing trends in future rainfall. A decrease in seasonal rainfall in Gumara, Ribb, and Megech watershed resemble the results by Beyene *et al.* (2010), who found a decrease in the mean monthly rainfall in 2040-2069 in Nile river basin, where these study watersheds are located.

Several researchers (Dile *et al.*, 2013; Gebre and Ludwig, 2015; Ayele *et al.*, 2016) showed that the streamflow and evapotranspiration were projected to increase in the major tributary rivers in the Lake Tana basin, and this was very similar to the results of this study. The seasonal streamflow variation mainly associated with seasonal rainfall variation. However, streamflow increase rate is larger than the rainfall increases rate, which is consistent with the findings of Aich *et al.* (2014) from four African River basins. They reported that a 25% increase in rainfall leads to a 50% increase in the river discharge over the Upper Blue Nile basin. The decrease in streamflow during the rainy season (summer) associate with rainfall reduction. This result corresponds with the findings of Worqlul *et al.* (2018) in the Upper Blue Nile Basin, Ethiopia. This highlights climate variation during the rainy season could have a profound effect on the annual hydrological responses. Although the rainfall under RCP4.5 shows a slight decrease in autumn in Gilgel Abay watershed, streamflow does not show a reduction trend in this season. This could be due to the excess soil moisture in the previous season (Appendix 5). Similar findings were reported in the Upper Blue Nile basin (Roth *et al.*, 2018) and Northern Lake Erie basin in Canada (Zhang *et al.*, 2018). Evapotranspiration is expected to increase at rates similar to those of the temperature and rainfall dynamics, which is in agreement with findings (Gebre and Ludwig, 2015; Teklesadik *et al.*, 2017; Lemann *et al.*, 2018) in the Upper Blue Nile basin. Evapotranspiration, however, is expected to decrease during winter under RCP8.5, contrary to most of the studies conducted in the surrounding watersheds (Enyew *et al.*, 2014; Ayele *et al.*, 2016).

Although the climate variables were simulated using the RCM and updated emission scenarios, there are several uncertainties associated with the climate and hydrological models. Both hydrological and climate model simulations have not considered land-use dynamics; but land-use has a significant role in the partitioning of the hydrologic components into infiltration, interception, and evapotranspiration (Wagner *et al.*, 2016; Marhaento *et al.*, 2018; Sunde *et al.*, 2018; Woldesenbet *et al.*, 2018). Besides, land-use dynamics will directly influence the land surface-atmosphere interaction and consequently alter the climate processes and patterns (Deng *et al.*, 2013). Therefore, future studies should consider the combined impact of climate and land-use change on hydrological responses. Moreover, climate simulation should incorporate a very fine spatial resolution to resolve the complex topography.

4.5 Conclusions

This study assessed the hydrological responses in four major tributaries of Lake Tana basin (Gilgel Abay, Gumara, Ribb, and Megech watershed) to a possible future climate change scenarios using the WRF model and a physical based hydrological model (SWAT). Overall, WRF simulations reproduced the average monthly observation but large biases were found in some cases. The power transformation and variance scaling bias correction method were capable in correcting most biases in the WRF model rainfall and temperature simulation, respectively. Climate projections show that rainfall and temperature may increase in the mid-21st century (2045-2055) in all the four study watersheds. Compared to the baseline period (2005-2015), the average temperature is likely to increase by 1.4 °C and 2.2 °C under RCP4.5 and RCP8.5 scenarios, respectively. Similarly, the mean annual rainfall is likely to increase by 7.9% and 21.1% under RCP4.5 and RCP8.5 scenarios, respectively.

In all the watersheds, the mean annual streamflow is predicted to increase by 1.1 – 15% and 15 - 40% under RCP4.5 and RCP8.5 scenarios, respectively, which implies that the overall amount of the water resources may not decrease in the future period over the Lake Tana basin. However, there is considerably high spatial and temporal variation in streamflow. The simulated annual evapotranspiration in the watersheds will vary on average from 6.7 to 20.4% under RCP4.5 and 4.3 to 25.9% under RCP8.5. While the magnitude and direction of the changes of streamflow and evapotranspiration can vary, impacts of climate change on water resources in the Lake Tana basin need to be taken in to account for future water resources planning. Moreover, the results obtained from this modeling study provide critical insights, potentially helping resource managers, and policymakers to develop effective water resource management strategies in the face of climate change. Based on the results, flood controlling practices should be considered in Gilgel Abay watershed because streamflow may increase by 296 mm (41%) during the main rainy season (summer). In the Gumara and Ribb watersheds, a considerable amount of streamflow is expected to occur in spring which may support irrigation practices. However, the projected climate and hydrologic components in Megech watershed highlight the need to put in place appropriate adaptation measures to meet the future water demand for domestic and agricultural production.

5. THE IMPACT OF CLIMATE AND LAND USE LAND COVER CHANGE ON HYDROLOGICAL RESPONSE IN GUMARA WATERSHED, ETHIOPIA

Abstract

The Lake Tana basin has experienced both land-use and climate change over the past 40 years, and this change can continue in the future. Several studies have addressed the separate impacts of either land-use or climate change on the watershed's hydrology, but few have explored the combined impact of land-use and climate change. In this study, the SWAT model was applied to evaluate the combined impacts of land-use and climate change on hydrological responses in Gumara watershed. This study examined four land-use scenarios that include the present (2015) and projected (2050) land-use based on the business-as-usual trend (BAU), expansion of irrigation crop (EIC), and expansion of forestland (EFL). The climate variables were simulated using Weather Research and Forecasting (WRF) model for the baseline (2005-2015) and projected period (2045-2055) under RCP4.5 and RCP8.5 scenarios. The result showed that sutface runoff (SR) increase by 5.1% under BAU scenario while base-flow (BF) decrease by 6.5% without altering streamflow (SF) and evapotranspiration (ET) noticeably. On the contrary, SF decrease by 12.5% and 5.2% respectively under EIC and EFL scenarios, while ET increase by 4.8% and 8.9% respectively under EIC and EFL scenarios. The simulated SF, SR, and ET under RCP8.5 may increase significantly by 34.3%, 51.8%, and 12.2%, respectively, due to the substantial rainfall increase (377 mm) and the warmer temperature (+2.4 °C more than baseline period). Similarly, the simulated SF, SR and ET may increase significantly under the combination of all three land-use and RCP8.5 scenarios. The findings suggested that climate change may have a greater effect on hydrologic responses than land-use change. The expansion of agriculture *(BAU) and the wetter climate (RCP8.5) would exacerbate flooding, while the expansion of irrigation and forest offset SF increases. The results of this study can be useful to decision-makers and planners in the design of adaptive measures to LULC and climate changes*.

Keywords: hydrological response, land-use change, climate change, SWAT, WRF.

5.1 Introduction

Both land use land cover (LULC) and climate change affect the spatial and temporal variability of the watershed hydrology through modifying streamflow, surface runoff, base-flow and evapotranspiration (Rahman *et al.*, 2015; Liu *et al.*, 2017). According to the Intergovernmental Panel on Climate Change report (IPCC, 2014), global average temperatures and frequency of heavy precipitation events are expected to increase in the mid-21st century. These changes will affect the hydrologic cycle through enhanced evaporation, peak flow, and flooding. Furthermore, land-use change seriously affects water resources mainly through partitioning of the rainfall amount into interception, evapotranspiration, infiltration, and soil moisture storage, thereby affecting the availability of watershed hydrology (Mishra *et al.*, 2010; Mango *et al.*, 2011). Human activities especially agricultural land expansion at the expense of forest cover have been the primary reason for the land-use change (Mottet *et al.*, 2006). The impact assessment study showed that interactions between land-use and climate could create serious challenges for water quantity and quality. Therefore, understanding the combined effects of land-use and climate change can be a basis for improved water resources management.

In recent years, many studies examined the combined impact of land-use and climate change on hydrologic processes (Koch *et al.*, 2015; Hyandye *et al.*, 2018; Aboelnour *et al.*, 2019; Chimdessa *et al.*, 2019). The findings from these studies consistently highlight the water balance components including streamflow, surface runoff, groundwater, and evapotranspiration are likely to be impacted by future land-use and climatic changes. However, the relative impacts of land-use and climate change may vary from place to place due to the rate and extent of changes in climate and land-use. For example, some studies have found that the hydrological processes are impacted more by climate change than land-use change (Mekonnen *et al.*, 2018; Aboelnour *et al.*, 2019), and other studies have indicated that the impacts of land-use change are more significant as compared to the impacts of climate change (Mwangi *et al.*, 2016; Yin *et al.*, 2017). The interaction between climate change and land-use change is non-linear (Jung *et al.*, 2011), and their impact on the water resources either magnify (Hein *et al.*, 2018; Woldesenbet *et al.*, 2018) or offset each other (Sunde *et al.*, 2018; Berihun *et al.*, 2019). For example, some studies reported that the increase in streamflow due to land-use change was amplified by wetting climate scenarios (Marhaento *et al.*, 2018), and other studies found that climate change could substantially offset runoff increment due

to urbanization (Sunde *et al.*, 2018). This highlights the importance of considering the combination of scenarios to understand the impact of environmental changes in the future availability of water resources. Therefore, investigating the effects of changes in climate and land-use on watershed hydrology has a great practical significance; especially in the tropical region like Ethiopia, where climate and land-use change rapidly (Legesse *et al.*, 2010; Berihun *et al.*, 2019; Chimdessa *et al.*, 2019).

In Ethiopia, during the past four decades, there has been extensive land-use changes and intensification of climate change. The land-use studies across different parts of Ethiopia have shown that the coverage of cropland has been expanded extensively (Teferi *et al.*, 2013; Biru *et al.*, 2015; Getahun and Haj, 2015; Jemberie *et al.*, 2016; Gebremicael *et al.*, 2019). This land-use dynamic has resulted in a change in the fluxes of the hydrological cycle (Teklay *et al.*, 2018), which caused an increase in surface runoff and a decrease in soil moisture and evapotranspiration (Woldesenbet *et al.*, 2017; Gebremicael *et al.*, 2019). Climate change may further intensify this process through alteration of the hydrological cycle (Bekele *et al.*, 2019). According to World Bank (2019), climate projections for Ethiopia indicate an overall increase in temperature and precipitation for all months, especially during the wet season. The changes in both temperature and precipitation exhibit remarkable regional variability as evident from the Lake Tana basin predict to experience a warmer and wetter climate in the future (Ayele *et al.*, 2016; Nigatu *et al.*, 2016).

Although the water resources in the Lake Tana basin is highly vulnerable to both land-use and climate change (Woldesenbet *et al.*, 2018; Berihun *et al.*, 2019), several studies have investigated the impact of either land-use change (Andualem and Gebremariam, 2015; Gumindoga *et al.*, 2015; Woldesenbet *et al.*, 2017; Gashaw *et al.*, 2018) or climate change (Abdo *et al.*, 2009; Dile *et al.*, 2013; Enyew *et al.*, 2014; Taye *et al.*, 2015; Ayele *et al.*, 2016) on the hydrological responses. Very few studies investigated the combined effect of land-use and climate change on water resources in the basin (McCartney and Girma, 2012; Woldesenbet *et al.*, 2018). Moreover, most of the studies which examined the impact of climate change on water resources have assumed that land-use remains static. On the other hand, studies that investigated the impact of land-use change rarely considered climate dynamics. However, land-use and climate in the future will change intensively due to urbanization, population growth, economic development, and global warming

(McCartney and Girma, 2012). The expansion of cropland and deforestation accompanied by climate change may impose an unprecedented impact on watershed hydrology, whereas afforestation and water harvesting structure may modify the negative impact of climate change (McCartney and Girma, 2012). Gumara river is one of the tributaries in Lake Tana basin where small and large scale irrigation projects are planned to improve the livelihood of the community. However, there is inadequate information about land management practices in modifying the impact of climate change on water resources in the watershed level.

Therefore, this research is designed to investigate the combined and individual impact of land-use and climate change on the hydrological responses in Gumara watershed, Ethiopia. In this study, four land-use and three climate change scenarios were used for hydrological simulations using the SWAT model for the projected period (2045–2055) and the reference period (2005-2015).

5.2 Materials and Methods

5.2.1 Study area

Gumara watershed is located in the northwestern part of Ethiopia between 37.63°-38.18° longitude and 11.57°-11.90° latitude. Gumara river originates from a small spring located near Guna Mountain and drains to the eastern part of Lake Tana (Figure 5.1). The catchment area of the Gumara river is 1269 km^2. Gumara river is one of the main streams on the east side, flowing into Lake Tana. Elevation of Gumara watershed varies from 1794 and 3704 meter above sea level, with a mean elevation of 2272 m. From the slope map, around 60% of the catchment area falls in the slope range from 0 to 15% and 32% of the area falls in the slope range of 15–30%. The remaining 8% of the area has slopes steeper than 30%.

The watershed has a tropical humid climate with distinct dry and wet seasons. The mean annual rainfall is 1387 mm, of which about 70–90% falls from June to September rainy season while less than 10% during April and May. The long term average daily minimum and maximum temperatures are 9 °C and 28.5 °C, respectively. The majority of the watershed area is covered by cultivated land (92%), and the remaining area is covered by shrubs (3%), grassland (4%), and forest (1%). The most dominant soil type is Haplic Luvisols (64%) which is found in the midstream parts of the watershed. The second dominant soil is Eutric Vertisols which is found in the downstream parts. Chromic Luvisols mainly extends to downstream and upstream parts of the watershed. Eutric Fluvisols is the least common soil type (< 1%) in the watershed.

5.2.2 Data availability

Spatial and non-spatial data were collected for the hydrological model evaluation and future land-use modeling. Land-use maps of 30-m spatial resolution for the years 1985, 1995 and 2015 were available for Gumara watershed from Teklay *et al.* (2018). The soil map, streamflow and Gumara Irrigation Project (GIP) plan were collected from the Ministry of Water, Irrigation and Electricity of Ethiopia (MoWIE, 1998, 2008). DEM data with a spatial resolution of 90 m was obtained from the Shuttle Radar Topographic Mission (SRTM). The meteorological dataset was collected from the National Meteorological Agency (NMA) of Ethiopia from five stations (Figure 5.1). The spatial road network and town map were available from Ethiopia Mapping Agency. The population size and agricultural management practices such as major crops, planting, harvesting and killing,

tillage, and fertilize application data for the watershed were obtained from the Central Statistical Agency of Ethiopia and South Gondar Zone Agriculture Office (CSA, 2007; SGZOA, 2016).

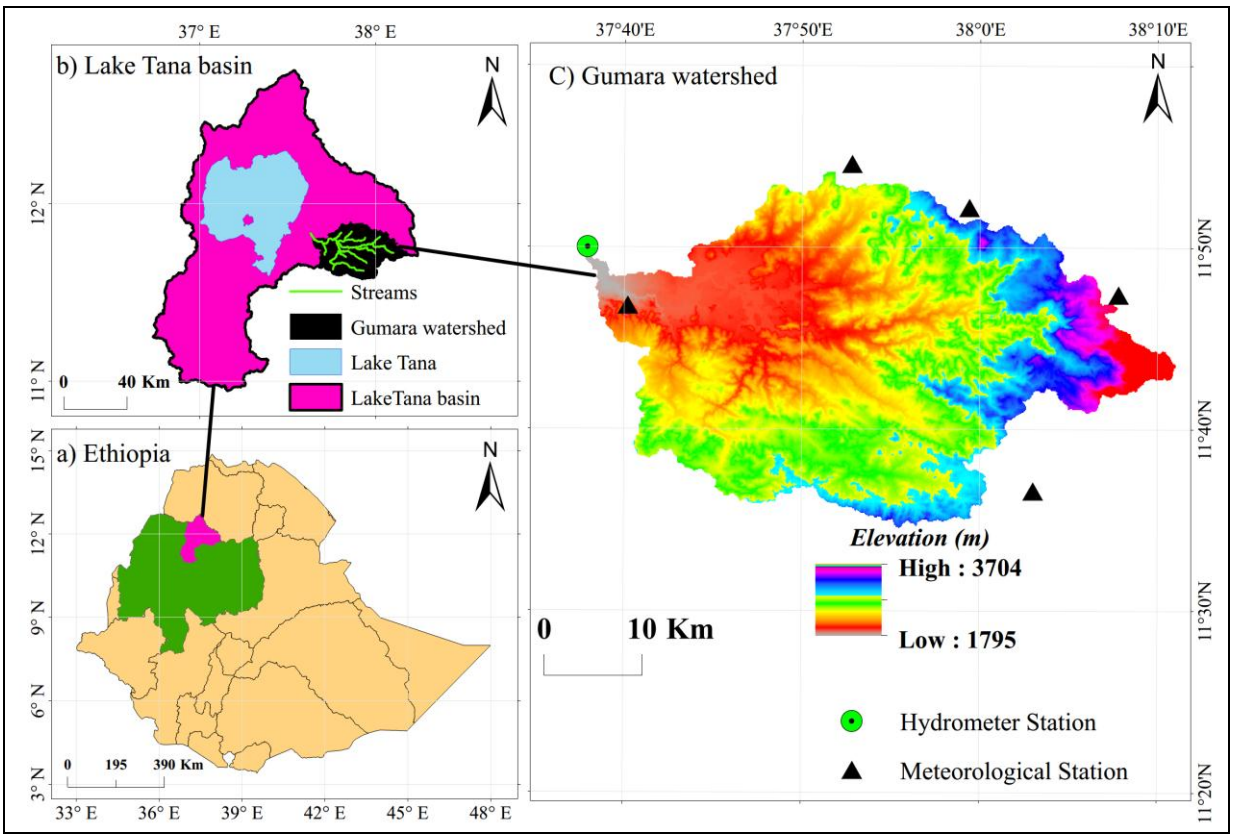

Figure 5.1 Location of the study area: a) major river basin (12) in Ethiopia (the green color is Upper Blue Nile Basin), b) Lake Tana basin (purple color), and c) Gumara watershed zoomed with the elevation data as background.

5.2.3 Hydrological model

The Soil and Water Assessment Tool (SWAT) is a physically-based, computationally efficient, semi-distributed model to simulate and predict the impacts of land management practices on water, sediment and agricultural chemical yields in large complex watersheds with varying soils, land-use, and management conditions over long periods (Neitsch *et al.*, 2011). The model has been widely used in different watersheds across the world and proved to be an effective tool to examine hydrological responses to land-use and climate changes (e.g., Abbaspour *et al.*, 2010; Kumar *et al.*, 2017; Pandey *et al.*, 2017; Polanco *et al.*, 2017; Lee *et al.*, 2018). In the SWAT model, the target watershed is divided into sub-basins linked by the channel network, each sub-basin is further subdivided into several hydrological response units (HRUs) of homogeneous land-use, slope and soil characteristics. Hydrological components, nutrients and sediment yield are simulated at the

HRU level and then aggregated for each sub-basin. The detailed model description is found in Neitsch *et al.* (2011).

The suitability of the SWAT model to estimate hydrologic processes to land-use change in Gumara watershed was assessed by Teklay *et al.* (2018). In this study, the SWAT model set-up followed the same settings as in the previous chapter. Therefore, this study presented only a summary of the model set-up and evaluation results. The watershed area was discretized into 22 sub-basins. These sub-basins were further discretized into HRUs by setting zero percent threshold level for land-use, slope, and soil. The Penman-Monteith method was chosen to calculate reference evapotranspiration (Gebre and Ludwig, 2015). The Soil Conservation Service Curve Number and the variable storage method were used to calculate surface runoff and flow routing, respectively.

Based on the previous studies in the region and literature survey (Setegn *et al.*, 2008; Gebremicael *et al.*, 2013; Dile *et al.*, 2016), eighteen SWAT parameters were calibrated using the Sequential Uncertainty Fitting version 2 (SUFI-2) in the SWAT-Calibration and Uncertainty Procedure (SWAT-CUP) package (Arnold *et al.*, 2012). The model was calibrated using monthly streamflow data for a period of fifteen years from 1990 to 2004. The calibration was performed through a "trial and error" process by manually adjusting the parameter ranges based on published literature (Van Griensven *et al.*, 2012; Dile *et al.*, 2016; Fentaw *et al.*, 2018). After calibration, the model was validated using streamflow data from 2005 to 2015. The performance of the SWAT model was assessed using two qualitative statistics recommended by Moriasi *et al.* (2007): Nash-Sutcliffe Efficiency (NSE) value and Percent Bias (PBIAS). The results of the model calibration show that the simulated mean monthly streamflow in the calibration period agrees well with the observed records, with NSE and PBIAS values of 0.89 and 10.7%, respectively. For the validation period, the NSE and PBIAS model performance of the SWAT model was 0.85 and 8.7%, respectively. These findings are in agreement with previous studies in the region (Setegn *et al.*, 2008; Dile *et al.*, 2016; Teklay *et al.*, 2018).

5.2.4 Land-use scenario

A scenario-based land-use change simulation can help to assess the potential impacts of land-use change on water resources in an uncertain future (Cao *et al.*, 2019). To examine the impact of land-use changes on the hydrological response in Gumara watershed, three future land-use scenarios for the year 2050 were developed. These scenarios were made to include the ongoing trends of

land-use change within the study area, the future water resource development plan, and the idealized afforestation program. The land-use scenarios included:

i. Business-as-usual (BAU) scenario

In this scenario, the past land-use change trends were extrapolated into the future by assuming the past trends of land-use change will continue in the future. The BAU land-use scenario was simulated using a Module for Land-use Change Evaluation (MOLUSCE) component of QGIS. The module simulated land use land cover map based on a Monte Carlo Cellular-automata modeling approach. In recent years, this module has been widely used to simulate land-use changes (Rahman *et al.,* 2017; Ashaolu *et al.,* 2019). MOLUSCE is designed to analyze land-use changes and predict the future direction of change by using spatial change variables. The spatial variables including elevation, slope, and population density, as well as the distance to town and roads, were considered. These biophysical and socio-economic variables are widely used to analyze the change patterns and to extract effective information about the effects of human activities on land-use change (Doğan and Buğday, 2018). ArcGIS 10.1 software was used to prepare a raster spatial map. In this study, Artificial Neural Networks was used to model LULC transition potential between 1985 and 1995. The land-use map for 2015 was predicted based on the change transition area matrix. Then, both the present and predicted images of the year 2015 were compared for validation of the model. The classified land-use map of 2015 had a high overall accuracy of 86.4% and a kappa coefficient of 0.82. Finally, the land-use for 2050 was predicted using a fitted model and transition matrix generated between 1995 and 2015 land-use maps.

ii. Expansion of Irrigation Crop (EIC) scenario

The future water resource development plan was considered in the EIC scenario. Gumara Irrigation Project (GIP) map was scanned from the feasibility study document from the Ministry of Water, Irrigation and Electricity of Ethiopia (MoWIE, 2008). A dam is planned on the Gumara River at the midstream part of the watershed which covers a 3.51 km^2 area at the full reservoir level. The stored water will then irrigate about 14.0 km^2 land at the downstream side of the watershed. The EIC scenario was developed by replacing the present land-use pixels with irrigated cropland and reservoir pixels. Tomato, onion, and maize are the most widely cultivated crop types in the watershed (SGZAO, 2016). In the SWAT modeling, the whole irrigation farm was seeded to grain

the three crops with equal proportion. The planting data started on January 1 of every simulation year.

iii. Expansion of Forestland (EFL) scenario

Expansion of forestland (EFL) scenario is an idealized land-use condition for the 2050 period. The EFL scenario was developed by assuming that the forest area will expand in the future especially on sloppy areas. The agriculture and shrub-land area on a slope greater than 15% are replaced by forest land-use. In this scenario, only the grassland and urban area were preserved.

5.2.5 Climate scenario

The baseline and future climate variables used in this study were simulation output from the Weather Research and Forecasting (WRF) model as presented in the previous chapter. GCMs data has too low spatial resolution for hydrological applications (Hurkmans *et al.*, 2010). Thus they were dynamically downscaled using the WRF model in three steps. First, the WRF output with a resolution of 36 km was obtained from the outer domain, which was reduced to 12 km (intermediate domain) and 4 km (inner domain) (Teklay *et al.*, 2019). In this study climatic data (rainfall and temperature) from the simulation of the internal domain were considered in the hydrological modeling processes.

The future scenarios were based on Representative Concentration Pathways (RCPs) radiative forcing as defined by the IPCC (2014). This study used RCP4.5 and RCP8.5 emission scenarios. The RCPs are named according to radiative forcing target level for 2100. The radiative forcing estimates are based on the forcing of greenhouse gases and other forcing agents. The RCP4.5 is a stabilization scenario without an overshoot pathway to 4.5 W/m^2 after 2100. The total radiative forcing under RCP4.5 is stabilized before 2100 by the employment of a range of technologies and strategies for reducing GHG emissions. The RCP8.5 refers to high GHGs concentration levels and characterized by increasing GHG emissions over time, leading to a radiative forcing of 8.5 W/m^2 at the end of the century.

Compared to observations, the baseline climate dataset had some errors. This model bias need to be corrected by using observation climate data. For this purpose, five observation stations within and around Gumara watershed were used. The biases in rainfall simulation were corrected by power transformation (PT) method, whereas biases in temperature were corrected by variance

scaling (VS). These bias correction methods are discussed in detail in section 5.2.3. The bias correction was employed separately at each meteorological station. To evaluate the bias correction performance, the average daily observation and WRF simulation (before and after bias correction) were compared using statistical measures such as correlation coefficient (r) and root mean square error (RMSE). While bias correction improved overall performances of the WRF model in simulating rainfall and temperature; there were differences in model evaluation statistics (Appendix 13 and 14). For temperature, bias-corrected mean values were very close to the observed. After bias correction, the RMSE was significantly reduced from 2.99 ºC to 1.53 ºC and 2.69 ºC to 1.37 ºC for maximum and minimum temperature, respectively, whereas RMSE was slightly decreased from 7.86 to 7.05 mm/day for rainfall. The bias-corrected data also showed a good agreement with observed data, especially for temperature. The correlation coefficients between observed and simulated data were significantly improved from 0.72 to 0.85 for maximum temperature and from 0.68 to 0.82 for minimum temperature, while it did not show significant improvement for precipitation correction. These results suggested that bias-corrected output was acceptable and consistent with previous studies (Elshamy *et al.*, 2009; Sisay *et al.*, 2017; Goshime *et al.*, 2019).

5.2.6 Combined land-use and climate change scenario

The combination of four land-use scenarios (present, BAU, EIC, and EFL) and three climate scenarios (baseline, RCP4.5, and RCP8.5) leads to 12 (1 reference + 11 future) scenarios, for which hydrologic responses were simulated using the calibrated SWAT model. For the reference period (2005-2015), the SWAT model used bias-corrected baseline climate data and present land-use of 2015. Table 5.1 shows the 12 scenarios that implemented in the study by categorizing the impacts of land use land cover change alone (LULCC), climate change alone (CC), and combined land use land cover and climate change (LULCC_CC) scenarios on hydrological responses. For each scenario, four water balance components, namely streamflow (SF), surface runoff (SR), base-flow (BF) and evapotranspiration (ET) were analyzed and compared to the reference conditions. A Student's t-test at a 95% confidence level was employed to assess the significance of the difference between the reference and scenario simulations.

Table 5.1 The combination of land use land cover and climate scenarios subjected to the SWAT model. Reference simulation represents the combination of the present land-use of 2015 (PRE) and the baseline climate (2005-2015).

No.	Land use land cover Change (LUC)	Climate change (CC)	Combined (LULC_CC)	Remark
1	PRE	Baseline	REF	Reference
2	BAU	Baseline	BAUB	LULCC (BAUB – REF)
3	EIC	Baseline	EICB	LULCC (EICB – REF)
4	EFL	Baseline	EFLB	LULCC (EFLB – REF)
5	PRE	RCP4.5	PRE4.5	CC (PRE4.5 – REF)
6	BAU	RCP4.5	BAU4.5	LULCC_CC (BAU4.5 – REF)
7	EIC	RCP4.5	EIC4.5	LULCC_CC (EIC4.5 – REF)
8	EFL	RCP4.5	EFL4.5	LULCC_CC (EFL4.5 – REF)
9	PRE	RCP8.5	PRE8.5	CC (PRE8.5 – REF)
10	BAU	RCP8.5	BAU8.5	LULCC_CC (BAU8.5 – REF)
11	EIC	RCP8.5	EIC8.5	LULCC_CC (EIC8.5 – REF)
12	EFL	RCP8.5	EFL8.5	LULCC_CC (EFL8.5 – REF)

5.3 Results

5.3.1 Land-use change

The most commonly distributed land-use type in 2050 under BAU is agriculture (Table 5.2). Compared to the present land-use (2015), BAU scenario grassland, shrub-land and forestland decreased by 1.6%, 2.6% and 0.3%, respectively, while agriculture and urban increased by 4.3% and 0.2%, respectively (Table 5.2). In the downstream and upstream parts of the watershed, grassland and shrub-land areas were mainly converted into agriculture (Figure 5.2). The results of agriculture and urban land expansion in the BAU scenario agrees with Gashaw *et al.* (2018) study in the Upper Blue Nile basin.

Under EIC, land-use in 2050 is predominantly agriculture, followed by irrigation crops, shrub-land, grassland, water, forestland, and urban. Compared to the present land-use, agriculture, grassland and shrub-land decreased by 9.2%, 1.0% and 0.2%, respectively, while the new land-use, such as irrigation crop and water, covered the watershed area by 9.3% and 0.9%, respectively. However, forestland and urban land coverage remain static in the future. Figure 5.2 shows that, under EIC, the irrigation command area was located in the downstream part and the reservoir was found in the midstream part of the watershed.

Table 5.2 Land use land cover distribution percentage under the four scenarios and relative change between the present land-use of 2015 (PRE) and future land-use of 2050 (BAU, EIC and EFL) scenarios.

Land-use type	PRE (%)	BAU (%)		EIC (%)		EFL (%)	
	2015	2050	Change	2050	Change	2050	Change
Agriculture	91.1	95.4	4.3	81.9	-9.2	55.0	-36.1
Irrigation crop	-	-	-	9.3	9.3	-	-
Grassland	3.6	2.0	-1.6	2.8	-0.8	3.6	0.0
Shrub-land	4.4	1.8	-2.6	4.2	-0.2	1.3	-3.1
Forest	0.8	0.5	-0.3	0.8	0.0	40	39.2
Water	-	-	-	0.9	0.9	-	-
Urban	0.1	0.3	0.2	0.1	0.0	0.1	0.0
Total	100.0	100.0	0.0	100.0	0.0	100.0	0.0

Under EFL, land-use in 2050 is mainly agriculture, followed by forestland, grassland, shrub-land, and urban. Compared to the present land-use, agriculture and shrub-land decreased by 36.1% and 3.1%, respectively, while forestland coverage significantly increased by 39.2%. Figure 5.2 shows

that, under EFL, reduction of shrub-land found in the midstream part of the watershed, while the expansion of forest and reduction of agriculture occurred in the entire watershed.

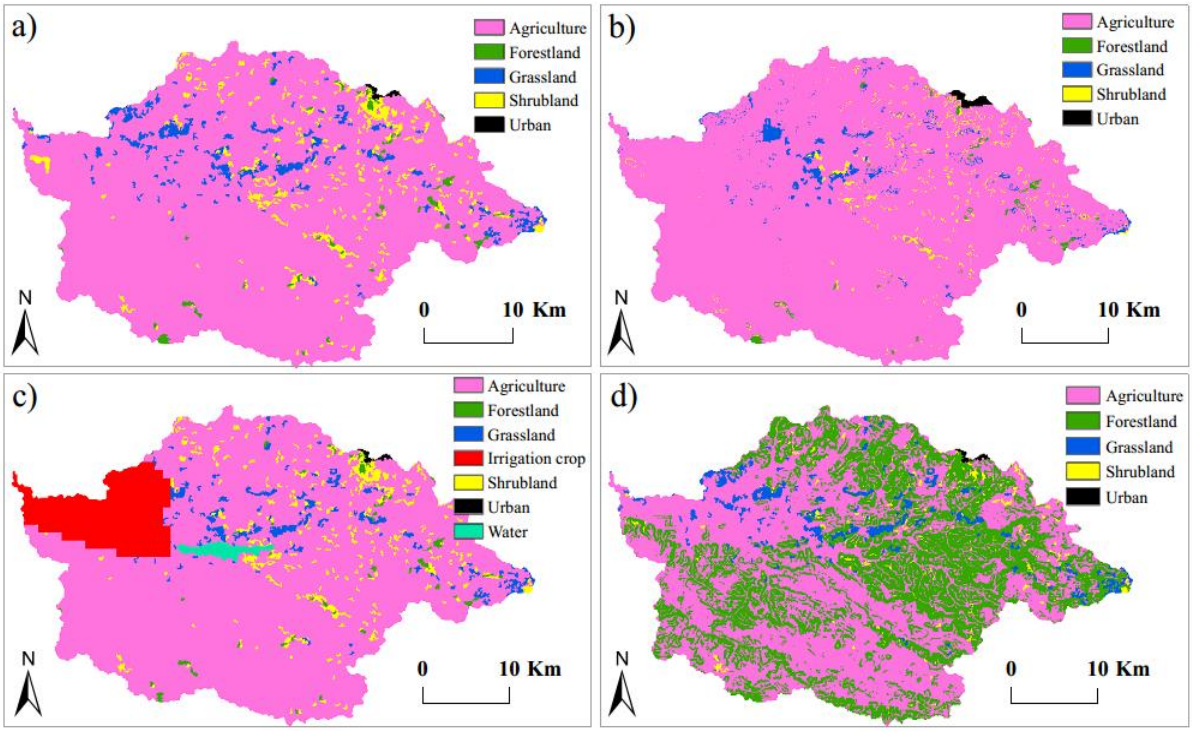

Figure 5.2 Land use land cover of the Gumara watershed in 2015 present (PRE) land-use (a), 2050 business-as-usual (BAU) scenario (b), 2050 expansion of irrigation crop (EIC) scenario (c), and 2050 expansion of forest land (EFL) scenario (d).

5.3.2 Climate change

The projected monthly rainfall shows inconsistent directions and magnitude of change between RCP4.5 and RCP8.5 scenarios. However, as shown in Figure 5.3a, the mean monthly rainfall may increase during the dry season (February and April) while it may decrease in August and November under RCP4.5 and RCP8.5 scenarios. The mean annual rainfall in the study watershed is projected to increase by 73.7 mm (5%) under RCP4.5 and 376.5 mm (25.7%) under RCP8.5 (Figure 5.3a). Under RCP8.5, rainfall increase may occur in most months of the year. In RCP4.5, rainfall may decrease during the rainy months (June to September) and the dry months (October and November). On the contrary, rainfall increase under RCP8.5 mainly concentrated in the rainy months (June and July). In spring, rainfall is projected to increase by 320.6 mm (172.5%) and 84.5 mm (45.5%) under RCP4.5 and RCP8.5 scenarios, respectively. However, rainfall under RCP4.5 may decrease by 176.2 mm (17.4%) and 86.3 mm (34.6%) in summer and autumn season, respectively.

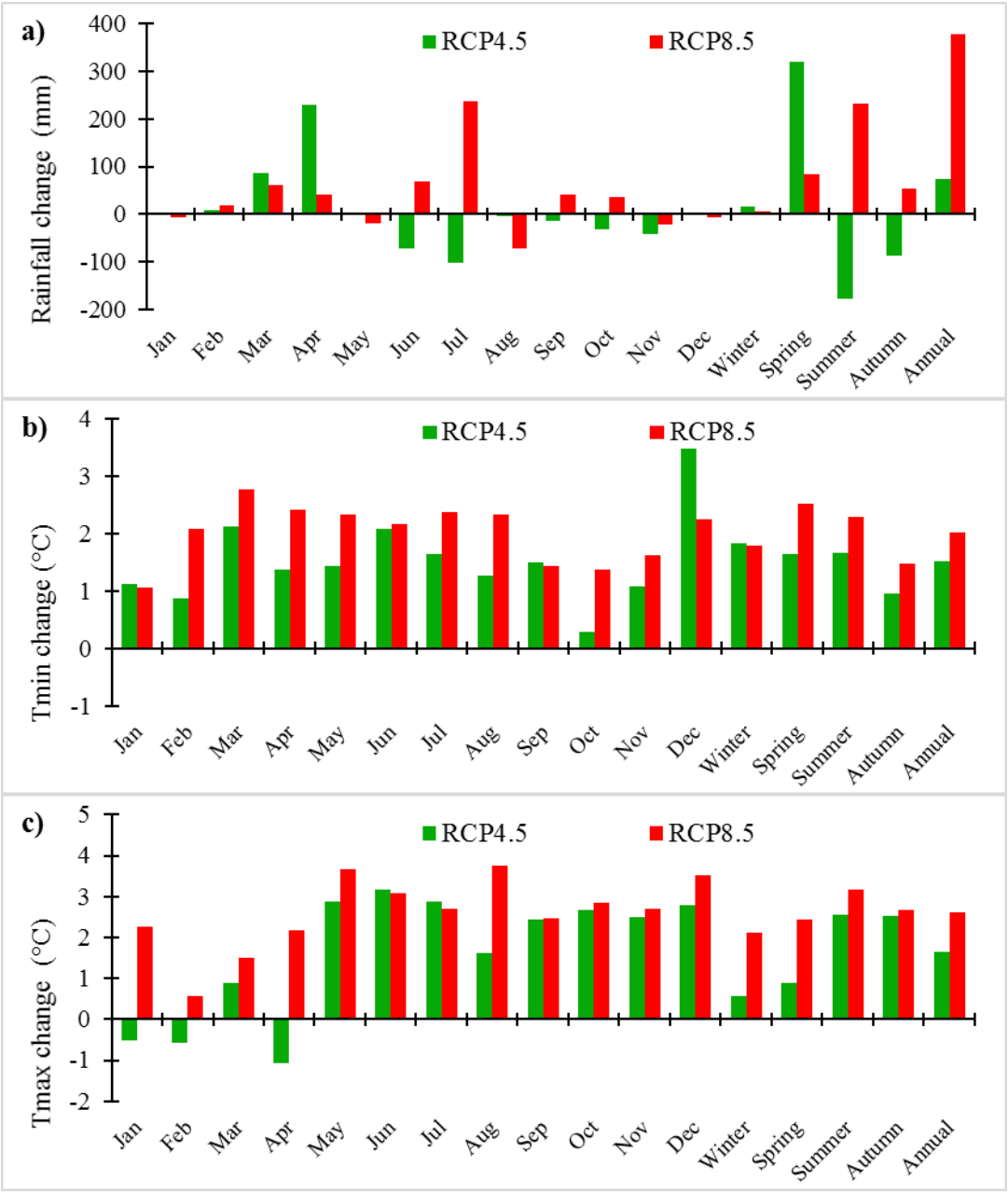

Figure 5.3 Changes in monthly, seasonal and annual rainfall (a), minimum b) and maximum temperature (c) in Gumara watershed in the future period (2045–2055) relative to the baseline period (2005–2015) under RCP4.5 and RCP8.5 scenarios.

The simulated minimum temperature shows a consistent increase in all months under both RCP4.5 and RCP8.5 scenarios (Figure 5.3b). The mean annual minimum temperature is projected to increase by 1.5 °C and 2.0 °C under RCP4.5 and RCP8.5, respectively. The monthly minimum temperature increases under RCP4.5 is between 0.3 °C and 3.5 °C with the maximum increase in

December, while minimum temperature increases under RCP8.5 ranged from 1.1 °C to 2.8 °C with the maximum increase in March. Unlike minimum temperature, the simulated maximum temperature shows a distinct direction of changes between RCP4.5 and RCP8.5 scenarios in some months. Figure 5.3c shows an increase of the simulated maximum temperature in all months under RCP8.5, whereas maximum temperature under RCP4.5 may decrease in January, February and April. Under RCP4.5, the monthly maximum temperature may increase by 0.9 °C to 3.2 °C, and decrease by 0.5 °C to 1.1 °C. Under RCP8.5, the magnitude of increase in maximum temperature varies between 0.6 °C and 3.7 °C. The mean annual maximum temperature is expected to increase by 1.7 °C and 2.6 °C under RCP4.5 and RCP8.5 scenarios, respectively. It is noted that the increase in maximum temperature is higher than the increase in minimum temperature. The increase in mean annual minimum/maximum temperature under RCP8.5 is larger than that under RCP4.5 because the RCP8.5 scenario represents a higher radiative force (Wulong *et al.*, 2018). These results are in agreement with results from previous studies in the Gumara watershed (Gebre and Ludwig, 2015; Ayele *et al.*, 2016; Melke and Abegaz, 2017).

5.3.3 The impact of land-use change on hydrologic response

To evaluate the impacts of land-use change, hydrological processes were simulated using the calibrated SWAT model under four land-use (PER in 2015 and BAU, EFL, and EIC in 2050) scenarios with baseline climate. The relative change between the present and future land-use in streamflow (SF), surface runoff (SR), base-flow (BF), and evapotranspiration (ET) are shown in Table 5.3 and Figure 5.4. Compared to the REF simulation, BAU scenario show marginal increase in mean annual SF (0.4%), while a decrease in SF is predicted under EFL (5.2%) and EIC (12.5%). Similarly, the mean annual SR under EFL and EIC scenario is predicted to decrease by 10% and 7.9%, respectively, whereas SR under BAU is expected to increase by 5.1%. The mean annual BF under EFL is slightly higher than that of under present land-use. However, agriculture practices in both rain-fed and irrigation under EIC scenario can significantly decrease the mean annual BF as high as 19%. In BAU and EIC scenarios, BF contribution to SF is 38%, which is lower than BF contribution under present land-use. The mean annual ET under EFL and EIC is likely to increase by 8.9% and 4.9%, respectively, while BAU scenario yields a marginal decrease (0.5%) in ET. The mean annual ET account for 37%, 41% and 39% of the mean annual rainfall, respectively, under BAU, EFL and EIC scenarios. Both EFL and EIC scenarios have a slightly higher tendency

on the rainfall partitioned into ET, whereas BAU scenario has a slightly lower tendency compared to the present land-use.

Table 5.3 The simulated mean annual streamflow (SF), surface runoff (SR), base-flow (BF), and evapotranspiration (ET) under the reference (2005-2015) and future land-use scenarios (2045-2055).

Hydrological processes	Statistics	REF	BAU	EFL	EIC
Rainfall (R)	Mean (mm)	1465	1465	1465	1465
	Change (%)	-	0	0	0
SF	Mean (mm)	897	900	850	785
	Change (%)	-	0.4	-5.2	-12.5
	SF/R	0.61	0.61	0.58	0.54
SR	Mean (mm)	529	556	476	487
	Change (%)	-	5.1	-10.0	-7.9
	SR/SF	0.59	0.62	0.56	0.62
BF	Mean (mm)	368	344	374	298*
	Change (%)	-	-6.5	1.6	-19.0
	BF/SF	0.41	0.38	0.44	0.38
ET	Mean (mm)	548	545	597	575
	Change (%)	-	-0.5	8.9	4.9
	ET/R	0.38	0.37	0.41	0.39

Note: the asterisk (*) represents a statistically significant change ($p<0.05$) between the reference and future land-use scenarios.

On monthly scale, the simulated SF under BAU scenario is slightly higher (up to 3 mm) than the REF simulation during the main rainy season (June to August) and similar to the REF simulation during the dry season (Figure 5.4a). SF under EFL may decrease from May to September, with the largest decrease of 15.8 mm in July. Under EIC scenario, SF is projected to decrease significantly from July to October. Regarding other hydrological processes, the increase of agriculture by the expense of shrub and grassland under BAU depict a trend of increasing SR and decreasing BF and ET from May to September. Under EFL, BF is projected to increase during the end of summer (August) and late-autumn (September). However, ET under EFL may increase consistently in most months, with the largest increase of 10.6 mm in September (Figure 5.4d). Under EIC, BF may decrease by up to 56.6 mm during the rainy months (July to September) and late-rainy month (October), while ET may increase in most months. However, ET increases in January and February are significantly higher than that in other months, which may relate to the crop growth stage.

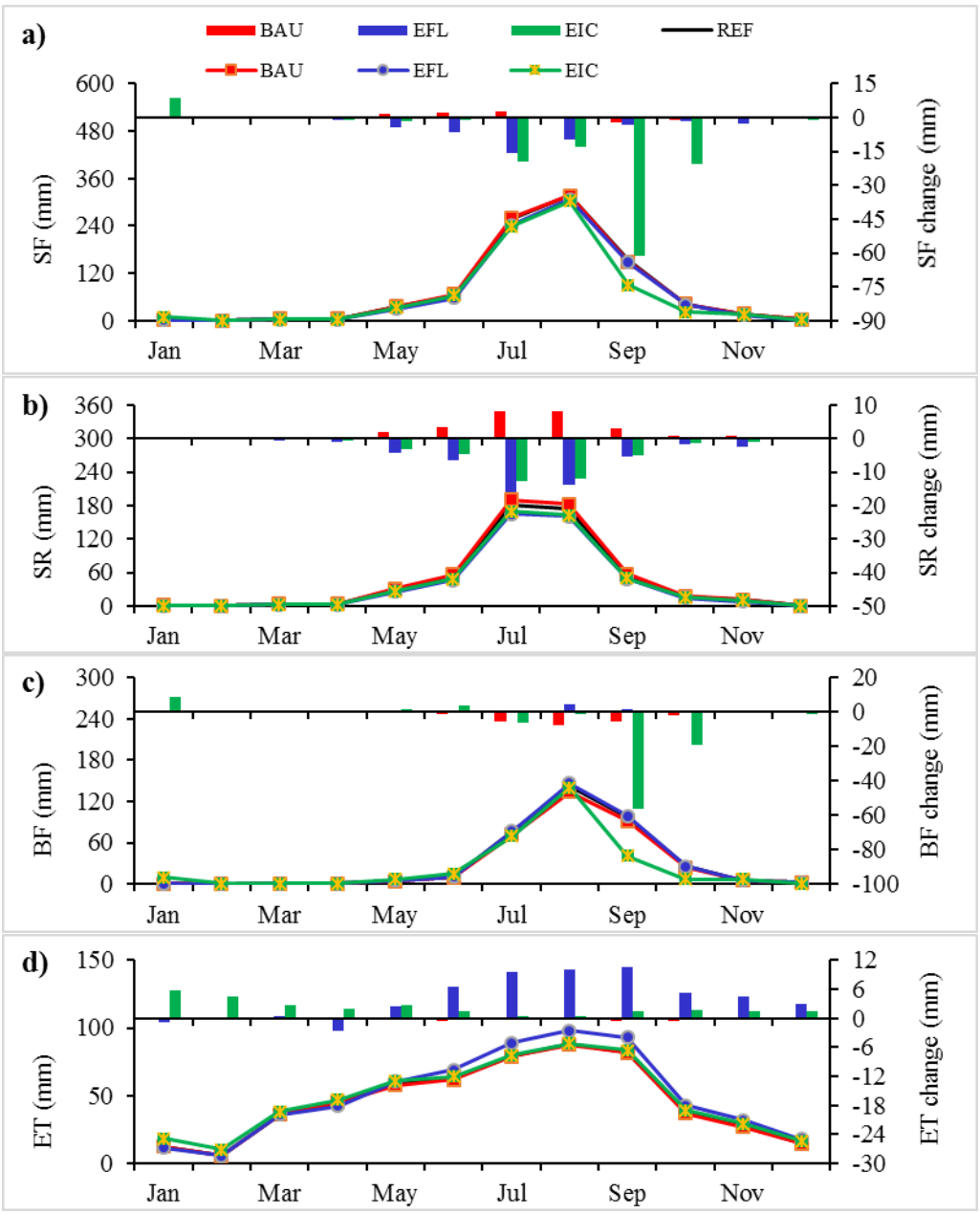

Figure 5.4 The simulated mean monthly streamflow (a), surface runoff (b), base-flow (c), and evapotranspiration (d). The solid line represents the monthly water balance component for the reference (REF) and the future land-use (BAU, EFL, and EIC) scenarios. The bar graph represents the monthly changes between the reference and future scenario (future scenario – REF).

5.3.4 The impact of climate change on hydrologic response

To assess the impacts of climate change, hydrological processes were simulated using the calibrated SWAT model under three climate scenarios (Baseline, RCP4.5 and RCP8.5) with the PRE land-use. The simulated hydrological components for the projected period under RCP4.5 and RCP8.5 scenarios were compared to the corresponding values in the baseline period. Overall, an

average of about 74 mm and 377 mm more rainfall per year was estimated to fall in the watershed in the future under RCP4.5 and RCP8.5 scenarios, respectively (Table 5.4). From the total annual rainfall, 99% contributed to SF and ET in both the reference (REF) and future simulation (RCP4.5 and RCP8.5). The remaining 1% contributed to groundwater recharge. Under RCP4.5, about 81% of the rainfall increase contribute to ET increase (60 mm). The remaining 19% contributed to SF (13 mm) and groundwater recharge (1 mm). On the contrary, 81% of the rainfall increase under RCP8.5 contribute to SF increase (308 mm) and 18% of the rainfall increase contribute to ET increase (67 mm). The remaining 1% contribute to groundwater recharge increase (2 mm). The simulated SR under RCP4.5 and RCP8.5 scenarios is greater than the reference simulation. However, SR under RCP8.5 (51.8%) is significantly higher than the reference simulation. The mean annual BF under RCP4.5 may decrease by 6.8%, whereas BF under RCP8.5 may increase by 9.2%. In RCP4.5 and RCP8.5 simulations, BF contribution to the watershed SF is 38% and 33%, respectively.

Table 5.4 The simulated mean annual streamflow (SF), surface runoff (SR), base-flow (BF), and evapotranspiration (ET) under the reference (2005-2015) and climate change scenarios (2045-2055).

Hydrological processes	Statistics	REF	RCP4.5	RCP8.5
Rainfall (R)	Mean (mm)	1465	1539	1842*
	Change (%)	-	5	25.7
SF	Mean (mm)	897	910	1205*
	Change (%)	-	1.4	34.3
	SF/R	0.61	0.59	0.65
SR	Mean (mm)	529	567	803*
	Change (%)	-	7.2	51.8
	SR/SF	0.59	0.62	0.67
BF	Mean (mm)	368	343	402
	Change (%)	-	-6.8	9.2
	BF/SF	0.41	0.38	0.33
ET	Mean (mm)	548	608	615*
	Change (%)	-	10.9	12.2
	ET/R	0.38	0.40	0.34

Note: the asterisk (*) represents a statistically significant change ($p<0.05$) between the reference and climate change scenarios.

As can be seen in Figure 5.5, the peak flow under RCP4.5 is projected to decrease, while a higher and earlier peak flow (shifting from August to July in the future) is simulated under RCP8.5. This may be due to the future rainfall decreases under RCP4.5 and increases under RCP8.5 during the main rain months (June and July). The simulated SF under RCP4.5 is likely to increase from February to May with the largest increase of 85.9 mm in April (Figure 5.5a). However, SF may decrease by up to 81.5 mm during the rainy months (July to September) and up to 14.9 mm during the dry period (October to January). Under RCP8.5, SF is expected to increase from February to July with the largest increase of 265 mm in July, while SF decreases are projected to occur during the dry period (November to January) and rainy month (August). With the exception of magnitude, the direction of monthly changes in SR is closely mirrored the changes simulated for SF (Figure 5.5b). Under RCP4.5, BF contribution to SF may increase during the dry months (March to May), while the contribution may decrease from July to September (Figure 5.5c). However, under RCP8.5, the highest BF increase and decrease may occur during the rainy months (July and August), which corresponds to the rainfall changes during rainy months. The simulated ET under both scenarios is larger than the reference simulation in most months (Figure 5.5d). Under RCP4.5, the largest increase in ET is projected to occur in April (48.1 mm) while the largest decrease may occur in November (18.2 mm). Under RCP8.5, a maximum increase in ET is predicted in March (33.4 mm), whereas the highest decrease in ET will occur in December (6.1 mm).

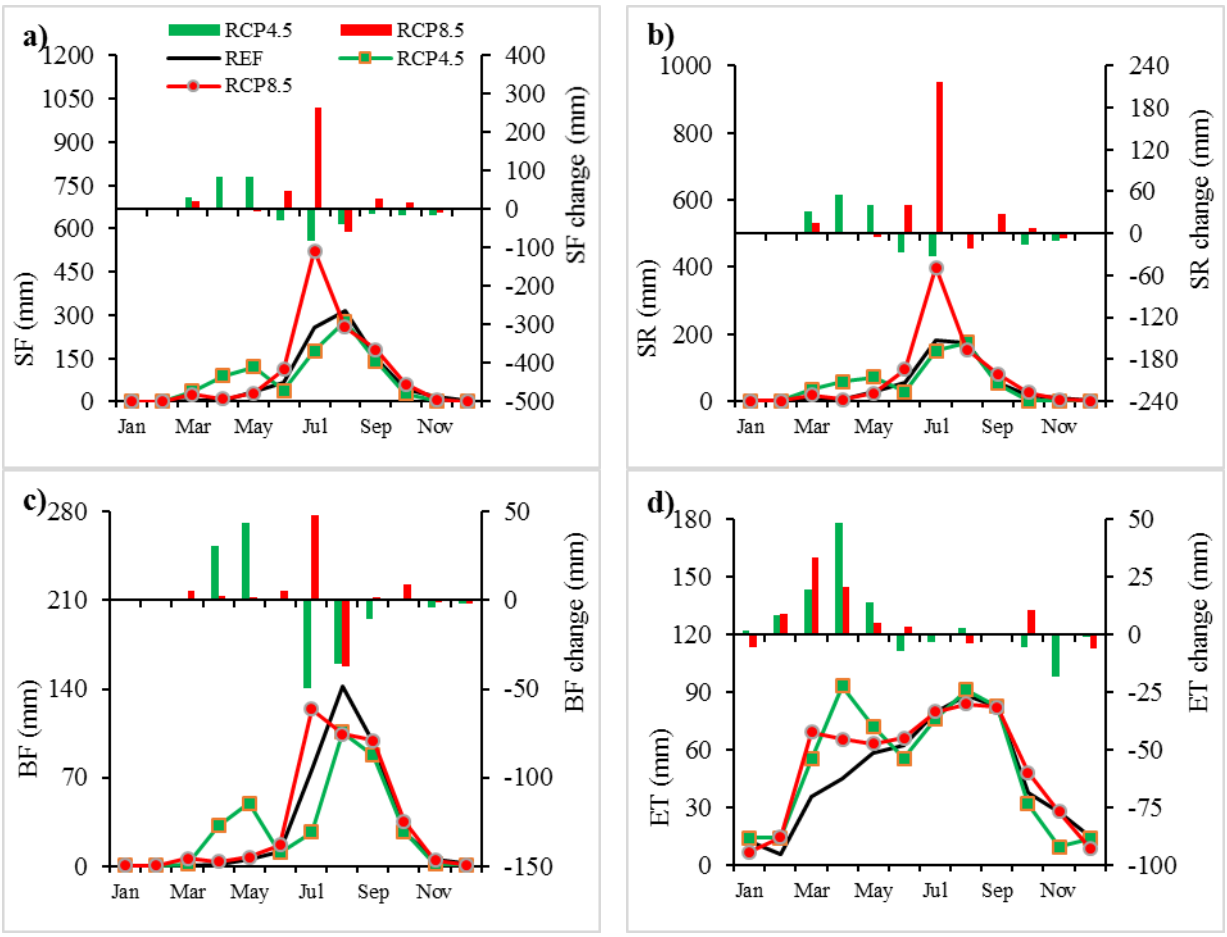

Figure 5.5 The simulated mean monthly streamflow (a), surface runoff (b), base-flow (c), and evapotranspiration (d). The solid line represents the monthly water balance components for the reference (REF) and future climate change (RCP4.5 and RCP8.5) scenarios. The bar graph represents the monthly changes between the reference and future scenario (future scenario – REF).

5.3.5 The combined impact of land-use and climate change on hydrologic response

To assess the combined impacts of land-use and climate change on hydrological processes, six simulations were carried out by using a combination of three land-use and two climate change scenarios. The changes in hydrological processes were profound in the combined land-use and climate scenarios (Table 5.5 and Figure 5.6). The mean annual SF is projected to increase under BAU4.5, BAU8.5, EFL8.5 and EIC8.5 scenarios. The largest increase in SF may occur under BAU8.5 (34.9%). Conversely, SF is projected to decrease under EFL4.5 and EIC4.5 scenarios, with the largest decrease of 11.9% under EIC4.5. The combination of land-use and climate scenario will have an additive effect on SF simulation. For example, SF increase under BAU8.5 (34.9%) is the simple addition of SF increase under BAU land-use scenario alone (0.4%, Table 5.3) and RCP8.5 climate scenario alone (34.3%, Table 5.4). The RCP8.5 climate scenario in

combination with land-use scenarios has a considerable influence on SR. Overall, SR under BAU8.5, EFL8.5 and EIC8.5 are significantly larger than the reference simulation. Such increases in SR are mainly derived by RCP8.5 rainfall increases. The expansion of irrigated cropland (EIC) combined with climate change scenarios may substantially decrease BF. Similarly, the combination of BAU and RCP4.5 will yield significantly lower BF compared to the reference simulation. The EFL8.5 scenario produce the largest increase in BF (12.2%), while the EIC4.5 scenario yield the largest decreases in BF (26.8%).

Table 5.5 The simulated mean annual streamflow (SF), surface runoff (SR), base-flow (BF) and evapotranspiration (ET) under the reference (2005-2015) and the combined future scenarios (2045-2055).

Hydrological processes	Statistics	REF	BAU4.5	BAU8.5	EFL4.5	EFL8.5	EIC4.5	EIC8.5
Rainfall (R)	Mean (mm)	1465	1539	1842*	1539	1842*	1539	1842*
	Change (%)	-	5.0	25.7	5.0	25.7	5.0	25.7
SF	Mean (mm)	897	914	1209*	856	1157*	790	1069
	Change (%)	-	2.0	34.9	-4.5	29.0	-11.9	19.3
	SF/R	0.61	0.59	0.66	0.56	0.63	0.51	0.58
SR	Mean (mm)	529	597	834*	509	744*	521	758*
	Change (%)	-	12.9	57.8	-3.7	40.7	-1.5	43.4
	SR/SF	0.59	0.65	0.69	0.59	0.64	0.66	0.71
BF	Mean (mm)	368	317*	375	347	413	269*	311*
	Change (%)	-	-13.7	1.9	-5.6	12.2	-26.8	-15.3
	BF/SF	0.41	0.35	0.31	0.41	0.36	0.34	0.29
ET	Mean (mm)	548	604	612*	664*	665*	638*	632*
	Change (%)	-	10.1	11.5	21.0	21.1	16.4	15.3
	ET/R	0.38	0.39	0.33	0.43	0.36	0.41	0.34

Note: the asterisk (*) represents a statistically significant change ($p<0.05$) between the reference and the combined scenario simulation.

The result shows that all the combined scenarios increase mean annual ET, with the largest increase of 21.1% under EFL8.5 and the smallest increase of 10.1% under BAU4.5. The increases in mean annual ET under the combined land-use and climate change scenarios is more pronounced than that under land-use and climate scenario alone. For example, the increases in ET under EFL (49 mm) alone (Table 5.3) and RCP4.5 (60 mm) alone (Table 5.4) are not significant, but the combination of the two scenarios (EFL4.5) may produce a significantly larger mean change (116 mm). The result also shows that the combined impacts of land-use and climate change are additive

to the separate impacts. For example, ET decrease of 3 mm under BAU alone (Table 5.3) and ET increase of 67 mm under RCP8.5 alone (Table 5.4) result in an increase of 64 mm under BAU8.5 (Table 5.5). However, the combined land-use and climate change impacts is slightly greater than the sum of the separate changes under EFL4.5 and EIC4.5 scenarios.

The changes in SF show increases in most months under the combined land-use and RCP8.5 scenarios (Figure 5.6a). The greatest increase will occur in July (267 mm) under BAU8.5. However, in July, SF under the combination of RCP4.5 and land-use scenarios may decrease due to rainfall decrease under RCP4.5 (Figure 5.3a). Moreover, in August, SF under all the combined scenarios are substantially lower than the reference simulation, which corresponds to monthly rainfall distribution under both climate scenarios. This indicate that the direction of monthly SF changes is mainly driven by climate change scenarios. In most months, SF change between land-use scenarios are very small compared to changes between emission scenario. (Figure 5.6a) The change in monthly SR follow similar pattern as for SF; the mean increase of up to 227 mm and decrease of up to 46 mm may occur in July under BAU8.5 and EFL4.5 scenarios, respectively (Figure 5.6b). BF under all the combined scenarios are projected to increase during the dry months from March to May, whereas it may decrease substantially during August (Figure 5.6c). The directions of change in the monthly BF under different scenarios are similar to those under the climate change scenario alone. ET under all the combined scenarios show increases in most months. However, the increases in March and April are substantially higher than other months. From February to May, ET under all the combined scenarios is larger than that under the reference simulation. This is similar to what is found with the climate simulations alone. The direction and magnitude of changes in ET are mainly driven by the climate change scenarios. However, during June to September, the direction of change in ET follows similar patterns to those under EFL land-use scenario. For example, ET under EFL4.5 is slightly larger (1.2 mm) than the reference simulation in June, which result from the counterbalance between ET increase under EFL alone (6.6 mm) and a decrease under RCP4.5 alone (7.2 mm).

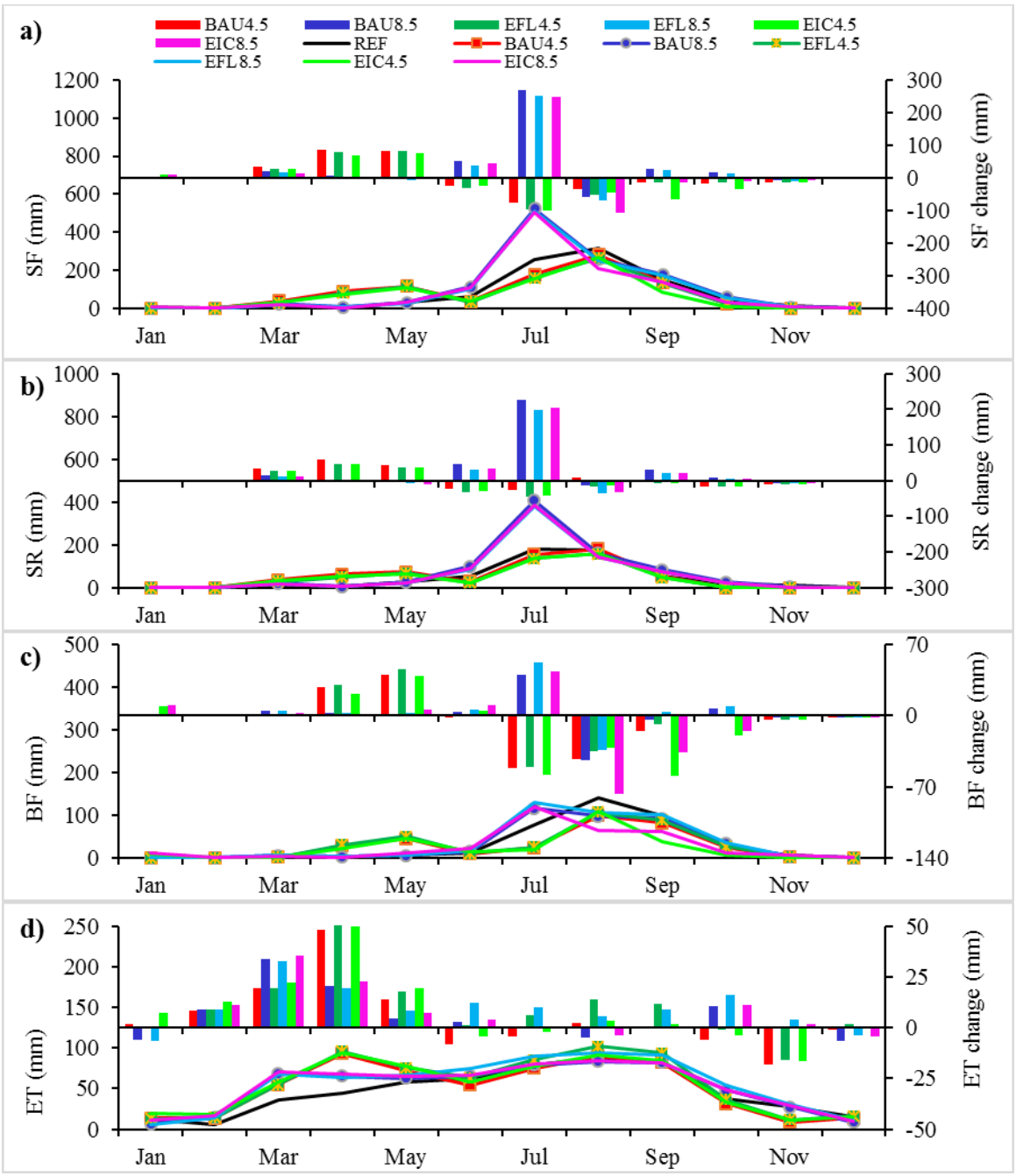

Figure 5.6 The simulated mean monthly streamflow (a), surface runoff (b), base-flow (c), and evapotranspiration (d). The solid line represents the monthly water balance components for the reference (REF) and the combined future scenarios. The bar graph represents the monthly changes between the reference and future scenario (future scenario – REF).

5.4 Discussion

Gumara watershed is one of the major tributaries of Lake Tana basin where large and small scale irrigation projects are under construction. Previous studies have indicated that the watershed hydrology is substantially influenced by either land-use change (Woldesenbet *et al.*, 2017) or climate change (Ayele *et al.*, 2016). However, few studies have evaluated the combined impact of land-use and climate change on water balance components in Gumara watershed. Therefore, this study is designed to investigate the combined and separate impacts of land-use and climate change on water balance components in Gumara watershed.

5.4.1 The impact of land-use change on hydrological response

The BAU scenario had less forest and shrub-land area than the PRE land-use, and its total agriculture area increase by 4.4%. As a result of this, the simulated SR may increase and BF may decrease in the future under BAU scenario. Agriculture areas have been positively correlated to SR. For example, in the Upper Blue Nile basin, Woldesenbet *et al.* (2017) found a strong positive correlation between the area of agriculture and mean annual runoff. This result is consistent with previous studies where the increase of agriculture coverage resulted in SR increase owing to reduced percolation and evaporation (Gashaw *et al.*, 2018; Mekonnen *et al.*, 2018; Teklay *et al.*, 2018; Berihun *et al.*, 2019; Gebremicael *et al.*, 2019). The expansion of agriculture (BAU) increase the contribution of SR to SF (Table 5.3). The cultivation practices could form soil crusting, which result in low infiltration and BF (Nakayama, 2011; Rahbeh *et al.*, 2013).

The SF decrease under EFL can be attributed to lower SR due to increasing forestland which improve the water holding capacity of the soil, infiltration and recharge. This result is in agreement with findings that show forestland expansion reduce SF and SR (Guzha *et al.*, 2018; Gebremicael *et al.*, 2019). A decrease in SF and SR are also attributed to the increase of water retained in the watershed and increase of ET as forest cover increase. These results are comparable with those from Woldesenbet *et al.* (2018) in the Upper Blue Nile basin, Ethiopia and Bossa *et al.* (2014) in the West Africa region. The increase in ET due to forest expansion has been reported by Hyandye *et al.* (2018), wherein they found that forest expansion (+7%) in Ndembera watershed located in Tanzania increased ET by approximately 8%.

The introduction of irrigated cropland and water reservoir under EIC may decrease SF during the main rainy season (Figure 5.4a). This is due to the diversion of SF into the reservoir to stores water for the dry season irrigation demand. Evaporation from the reservoir may contribute to ET increase. Besides, ET increase under the expansion of irrigation crops may result from the high leaf area index and transpiration demand for irrigation crops. This result agrees well with the study by Hyandye *et al.* (2018) and who reported that ET would increase by 30 mm due to the expansion of irrigated onion and rice farms by 10%.

Overall, most of the water balance component changes between the present and future land-use scenarios were insignificant ($p>0.05$, Table 5.3), since the converted land-use areas were smaller than the threshold level which cause significant change on hydrological processes. These results agree with Li *et al.* (2007) study in the West African basins. They simulated the hydrological impact of land-use change and found that deforestation below 50% has no significant impact on streamflow and water yield; however, the water yield was dramatically increased when land-cover change exceeds this threshold. In other regions, Eckhardt *et al.* (2003) also quantified the minimum proportion of a watershed that has to undergo a land-use change to detect apparent water balance differences. They found that the mean surface runoff amount was changed when approximately 20% of the watershed area was changed.

5.4.2 The impact of climate change on hydrological response

The future climate simulations show increases in mean annual rainfall by about 74 mm under RCP4.5 and 377 mm under RCP8.5, yet some simulation may decrease from June to November under RCP4.5 and from November to January, and in May and August under RCP8.5. The mean annual SF is simulated to increase mainly due to the increase of mean annual rainfall. However, the relationship between rainfall and SF is complicated and non-linear. The projected rainfall change can be amplified in the SF hydrograph (Figure 5.5a). This amplification may occur when the projected rainfall increases concentrate on rainy months of June and July (Figure 5.3a) when soil moisture is relatively high in the study watersheds. The increase in streamflow due to rainfall increment was also discussed by Pandey *et al.* (2017); they revealed that a 28% increase in annual rainfall resulted in streamflow increase by approximately 49% from their study in the Armor watershed in Godavari river basin, India. Besides, the temporal distribution of rainfall also affects peak flow and SF change. SF change under RCP4.5 is very small, owing to the rainfall decline in

the main rainy months (June to September). However, rainfall increase under RCP4.5 concentrate in the dry season (March and April), which leads to an increase in rainfall partitions to percolation. As a consequence, ET is projected to increase mainly attributed to the soil moisture evaporation (Figure 5.5d). This indicate that warmer temperature shifted rainfall increase into ET increase, which is consistent with the findings of Mango *et al.* (2011a) in the East African watershed. They found that the modest increases in precipitation are partitioned largely to increase ET. The monthly ET changes are almost similar pattern with monthly rainfall changes. This result agrees with Marhaento *et al.* (2018) study in Indonesia, who found that ET simulation highly influenced by rainfall change compared to temperature change. However, Hyandye *et al.* (2018) found different results from this study. They found that changes in ET mainly associated with changes in temperature.

5.4.3 The combined impact of land-use and climate change on hydrological response

The results show that the combined land-use and climate change have a more noticeable effect on SF and SR. The significant increase in rainfall and expansion of agriculture will have an additive impact on SF and SR (Legesse *et al.*, 2010; Mango *et al.*, 2011). Moreover, the highest SF increase during the main rainy months may cause flooding in the future. Afforestation in the steep slope area is recommended to reduce SR which is the major cause of flooding and soil erosion (Nyssen *et al.*, 2004). The forest expansion in the sloppy areas improve rainfall partitioned into infiltration, subsequently reduce SR (Table 5.5). The results related to forest expansion effect on water balance components are consistent with the findings of Woldesenbet *et al.* (2018) in the Upper Blue Nile basin and Marhaento *et al.* (2018) in the Samin catchment. Besides, conserving the rainy season excess water for the dry season irrigation play a substantial role in reducing SF (Table 5.5). However, irrigation practice may increase SR during the dry season (Figure 5.6b) and will cause soil erosion. Therefore, different water management practices must be implemented to reduce SR.

The expansion of forest and irrigation along with climate change may increase ET significantly (Table 5.5). The slight increase of rainfall alone (RCP4.5) does not show significant ET change, whereas both climate and land-use change have a significant impact on ET (Table 5.5). The combination of climate change and land-use (BAU) have additive impacts on ET. However, ET increase under forest and irrigation expansion (EFL and EIC) is amplified by projected future climate (RCP4.5), which result from plant transpiration and evaporation from soil moisture and

canopy interception. This result is consistent with the findings of Marhaento *et al.* (2018). However, the climate change signal had a dominant effect on simulated water balance components. Similar conclusions have been reported in the Upper Blue Nile basin (Mekonnen *et al.*, 2018) and other regions (Yan *et al.*, 2019). The combined impacts of climate and land-use change show a non-linear effect on water balance components, which is consistent with results found for climate and land-use change impacts on hydrological responses in Hinkson Creek Watershed in central Missouri (Sunde *et al.*, 2018).

5.5 Conclusions

This study presented an integrated modeling approach for assessing the separate and combined effects of land-use and climatic changes on hydrologic processes in Gumara watershed. The study used Weather Research Forecasting (WRF) model to downscale GCM output from the latest generation of climate models (CMIP5), Land-use Change Evaluation (MOLUSCE) module to generate future land-use scenarios, and a process-based watershed hydrologic model (SWAT). In this study, four land-use and three climate scenarios were developed and used as input for the SWAT model to determine the relative and the interaction impacts of the two changes.

The results suggest that most of the combined scenarios have a pronounced effect on streamflow and surface runoff. However, climatic changes could have a larger impact than land-use change on streamflow and surface runoff. When the expansion of agriculture scenario (BAU) is replaced by the expansion of forest scenario (EFL), the mean annual surface runoff may decrease by 14.7% and 10.8% under RCP4.5 and RCP8.5 scenarios, respectively, while the mean annual base-flow may increase by about 9.3% and 10.1% under RCP4.5 and RCP8.5, respectively. The monthly changes in streamflow are mainly driven by climate change scenarios. Moreover, the influence of the combined effect on streamflow does not vary directionally in most months. The largest uncertainty in streamflow simulation (-99.3 mm to 267 mm) may occur in July which can be attributed to the uncertainty of rainfall prediction (-102.3 mm to 235.5 mm). The result also indicates that the effect of climate change on the mean annual evapotranspiration is extremely larger than the effect of land-use change. The increases of evapotranspiration under climate change scenarios are augmented by increases under the expansion of forest and irrigation scenarios, while the marginal decrease in evapotranspiration under the expansion of agriculture scenario is offset by increases under climate change scenarios. Similarly, the magnitude and direction of monthly

changes in evapotranspiration are mainly driven by climate change scenarios, but the forest expansion effect is most influential from June to September.

In general, the results were not conclusive but provide insight into the future hydrologic scenario of Gumara watershed. Projections of future availability of water resources contain a large number of uncertainties, and this work demonstrates that the relative and the combined effect of land-use and climate change on water balance components. Moreover, the model output can provide useful information about the contribution of each land-use to water balance components as well as to water balance dynamics due to climate change. The results suggest that water resources in the Gumara watershed may increase or decrease in the mid-21st century as a consequence of climate and land-use changes, it is a great difficulty to ascertain an accurate magnitude of change.

6. GENERAL CONCLUSIONS AND RECOMMENDATION FOR FURTHER RESEARCH

6.1 General Conclusions

The potential effects of land use land cover (LULC) and climate change on the water resources of the Lake Tana basin have been investigated by considering the past and future LULC and climate variables. Emphasis was given to evaluate a modeling methodology for water resource impact assessment of the basin. Several activities were conducted to achieve the overall objective: (1) analysis of LULC change for 31 years (1985–2015), (2) calibration and validation of the SWAT hydrological model, (3) evaluation of Weather Research and Forecasting (WRF) model, (4) simulation of baseline and future climate data using a dynamical downscaling model, (5) correction of climate model biases, (6) prediction of future LULC using land-use change model, and (7) simulation of hydrological processes with different scenarios for an impact assessment on water resources of the basin. Based on the results the following main conclusions can be drawn:

- This research tried to examine the long-term dynamics in LULC in the case study site (Gumara watershed). It revealed that there were substantial land-use changes in the area during the past 31 years (1985–2015). The dominant changes were a decrease in forest and shrubs coverage and an increase in cultivated land.
- The performance of static and dynamic land-use model setups was approximately equivalent, with dynamic setup showing marginally improved comparison statistics. However, the results of the dynamic LULC hydrological simulation were more accurate than those of the static LULC.
- The changes in LULC affected surface runoff, peak flow, and evapotranspiration considerably, however, the negative and positive impacts offset each other in the long term average on the watershed level. An analysis on the sub-basin level revealed that agriculture expansion led to an increase in runoff and peak flow, and a decrease in evapotranspiration whereas an increase in forest coverage resulted in more evapotranspiration due to the increase in transpiration and canopy evaporation.
- The WRF model with updated land-use information slightly improved climate simulation (temperature and rainfall) when compared to the default USGS land-use data. Among the three land surface models (LSMs), Noah showed the best accuracy of the dry and wet

season rainfall estimate. The simulated pattern of average rainfall using NLU data agreed well with the observed rainfall compared to USGS data; notably the combination of Noah and updated land-use (NLU) provided the best spatial agreement with observations. The worst performance in spatial rainfall distribution was found from the combination of TD LSM and USGS land-use.

- The WRF model detected more than 80% of the observed rainfall events. However, the WRF model falsely detected nearly 11% of rainfall events. The WRF model performed well in simulating light and moderate rainfall events, while none of the WRF configurations captured high-threshold events correctly. Overall, rainfall simulations under WRF model need to improve further to predict well the wet season rainfall and to detect the occurrence of high rainfall events.
- The WRF model with RUC and TD well captured temporal variability of maximum and minimum temperature, respectively. RUC outperformed TD LSM for the spatial pattern estimation.
- Bias correction reduced cold and warm biases significantly for maximum and minimum temperature simulation, respectively. Similarly, the bias-corrected WRF model reproduced monthly rainfall very well except for a slight overestimation during the wet season (July and August).
- The results of the WRF simulation showed that mean annual rainfall, maximum and minimum temperature are projected to increase in the mid-21st century (2045-2055) under both RCP4.5 and RCP8.5 scenarios. However, temperature and rainfall increases under RCP8.5 are considerably higher than under RCP4.5. Rainfall under RCP4.5 may increase substantially in spring in all four major tributary watersheds (Gilgel Abay, Gumara, Ribb, and Megech), while rainfall may decrease in summer and autumn in all watersheds except Gilgel Abay.
- The findings also showed that mean annual streamflow increase can vary from 1.1% to 40%, the highest increase may occur in Gilgel Abay watershed, and the increase in evapotranspiration may vary from 4.3% to 25.9%, the highest increase can occur in Ribb watershed.
- Projection of land-use change in the business-as-usual (BAU) scenario showed expansion of agriculture at Gumara Watershed in 2050. As a result of this change, surface runoff is

projected to increase while base-flow is projected to decrease in the future. On the contrary, forest land expansion (EFL) scenario can reduce streamflow and surface runoff, and raise base-flow and evapotranspiration. Similar to EFL, expansion of irrigated cropland (EIC) can reduce streamflow and surface runoff, and increase evapotranspiration.

- Based on the WRF simulation, Gumara watershed may experience higher rainfall (5% - 25.7%) and temperature (1.6 °C - 2.4 °C) under both emission scenarios compared to the baseline condition (2005-2015). The results also show that all the mean annual water balance components (except for RCP 4.5 base-flow) can increase in the future.
- The combination of agriculture expansion (BAU) and climate change results in a significant increase in streamflow, surface runoff and evapotranspiration. The expansion of forest and irrigation offset surface runoff rise because of climate change. The results show that the combined impact of climate and LULC is more pronounced than the isolated climate and LULC change effect. However, climate change plays a dominant role in impacting hydrology when compared to land-use change.

6.2 Recommendation for Further Research

Although the four research questions proposed in the first chapter were addressed in chapter 3-6, there remain important uncertainties related to them that need to be addressed in the future study. This thesis can be seen as a starting point to enhance the knowledge about the coupling of climate, LULC, and hydrological models. However, the modeling about the potential impact of LULC and climate change on hydrological response also needs some improvement.

- The SWAT model was calibrated and validated using only streamflow data. Therefore, the interpretation for the other water balance components including surface runoff, base-flow, and evapotranspiration should be considered with the uncertainty involved. In addition, sediment and nutrient modeling, which were left out from this study due to a lack of quality data, are nevertheless of great importance in the Lake Tana basin and require careful modeling effort.
- Both biological and physical soil and water conservation measure have been constructed in the Lake Tana basin. Such intervention measures influence hydrological processes significantly (Hyandye *et al.*, 2018). However, the constructed soil and water conservation

measures were not fully considered in this research. Therefore, it should be addressed in future research.

- This study identified the best land-use and LSM configuration in the WRF model simulation. However, the selection of microphysics, cumulus, and planetary boundary layer scheme also affects the WRF climate simulation. Therefore, such WRF parametrization should be considered in the future study for accurate climate simulation.
- Climate modeling has been subjected to various uncertainties, such as climate system natural variability, climate model algorithms (model structure), coarse GCMs resolution, and greenhouse gas emissions (Fronzek *et al.*, 2012). The uncertainties emerge from the natural variability of the climate system and climate model algorithms can be addressed by using a multi GCMs and RCMs analysis (Wulong *et al.*, 2018). However, this study used a single RCM and GCM to project the climate variables. Further studies should be carried out with the inclusion of diverse GCMs and RCMs for better quantification of uncertainties in climate projection.
- Even though climate change analysis required a minimum of 30 years of data, this study's prediction was based on short time series (11 years) due to a shortage of computational resources. Therefore, a long period of simulation should be considered in future studies to support the regional climate change adaptation project.
- Coupling of the SWAT hydrological model and WRF atmospheric model should be considered to capture important feedback and interaction between the land surface and climatic variables (rainfall and temperature) and improve model simulation performance for water resources analysis.

REFERENCES

Abbaspour, K. C., Faramarzi, M., Ghasemi, S. S., & Yang, H. (2010). Assessing the impact of climate change on water resources in Iran. *Water Resources Research*, *45*, 1–16. https://doi.org/10.1029/2008WR007615

Abbaspour, K. C., Yang, J., Maximov, I., Siber, R., Bogner, K., Mieleitner, J., Zobrist, J., & Srinivasan, R. (2007). Modelling hydrology and water quality in the pre-alpine/alpine Thur watershed using SWAT. *Journal of Hydrology*, *333*, 413–430. https://doi.org/10.1016/j.jhydrol.2006.09.014

Abbaspour, K., Johnson, C., & van Genuchten, M. (2004). Estimating Uncertain Flow and Transport Parameters Using a Sequential Uncertainty Fitting Procedure. *Vadose Zone Journal*, *3*(4), 1340–1352.

Abdallah, A. ., Eid, M. M., Wahab, M. A., & El-Hussainy, F. (2015). Regional Climate Simulation of WRF Model over North Africa : Temperature and Precipitation. *World Environment*, *5*(4), 160–173. https://doi.org/10.5923/j.env.20150504.04

Abdo, K. S., Fiseha, B. M., Rientjes, T. H., Gieske, A. S., & Haile, A. T. (2009). Assessment of climate change impacts on the hydrology of Gilgel Abay catchment in Lake Tana basin, Ethiopia. *Hydrological Processes*, *23*(26), 3661–3669. https://doi.org/10.1002/hyp.7363

Aboelnour, M., Gitau, M. W., & Engel, B. A. (2019). Hydrologic response in an urban watershed as affected by climate and land-use change. *Water*, *11*(8), 1–23. https://doi.org/10.3390/w11081603

Ahn, G., Gordon, S. I., & Merry, C. J. (2014). Impacts of Remotely Sensed Land Use Data on Watershed Hydrologic Change Assessment. *International Journal of Geospatial and Environmental Research*, *1*(1), 1–17. Available at: http://dc.uwm.edu/ijger/vol1/iss1/9

Aich, V., Liersch, S., Vetter, T., Huang, S., Tecklenburg, J., Hoffmann, P., Koch, H., Fournet, S., Krysanova, V., Müller, E. N., & Hattermann, F. F. (2014). Comparing impacts of climate change on streamflow in four large African river basins. *Hydrology and Earth System Sciences*, *18*(4), 1305–1321. https://doi.org/10.5194/hess-18-1305-2014

Ajami, H., Sharma, A., Band, L. E., Evans, J. P., Tuteja, N. K., Amirthanathan, G. E., & Bari, M. A. (2017). On the non-stationarity of hydrological response in anthropogenically unaffected catchments: An Australian perspective. *Hydrology and Earth System Sciences*, *21*(1), 281–294. https://doi.org/10.5194/hess-21-281-2017

Alam, A., Rashid, S. M., Bhat, M. S., & Sheikh, A. H. (2011). Impact of land use/land cover dynamics on himalayan wetland ecosystem. *Journal of Experimental Science*, *2*(3), 60–64.

Alemu, H., Senay, G. B., Kaptue, A. T., & Kovalskyy, V. (2014). Evapotranspiration variability and its association with vegetation dynamics in the Nile Basin, 2002-2011. *Remote Sensing*, *6*(7), 5885–5908. https://doi.org/10.3390/rs6075885

Alexakis, D. D., Grillakis, M. G., Koutroulis, A. G., Agapiou, A., Themistocleous, K., Tsanis, I. K., Michaelides, S., Pashiardis, S., Demetriou, C., Aristeidou, K., & Hadjimitsis, D. G. (2014). GIS and remote sensing techniques for the assessment of land use change impact on

flood hydrology: The case study of Yialias basin in Cyprus. *Natural Hazards and Earth System Sciences*, *14*(2), 413–426. https://doi.org/10.5194/nhess-14-413-2014

Anaba, L. A., Banadda, N., Kiggundu, N., Wanyama, J., Engel, B., & Moriasi, D. (2017). Application of SWAT to Assess the Effects of Land Use Change in the Murchison Bay Catchment in Uganda. *Computational Water, Energy, and Environmental Engineering*, *6*(1), 24–40. https://doi.org/10.4236/cweee.2017.61003

Andualem, T. G., & Gebremariam, B. (2015). Impact of Land Use Land Cover Change on Stream Flow and Sediment Yield : A Case Study of Gilgel Abay Watershed, Lake Tana Sub-basin, Ethiopia. *International Journal of Technology Enhancement and Emerging Engineering Research*, *3*, 28–42.

Arnold, J. G., Moriasi, D. N., Gassman, P. W., Abbaspour, K. C., White, M. J., Srinivasan, R., Santhi, C., Harmel, R. D., van Griensven, A., van Liew, M. W., & Jha, M. K. (2012). SWAT: Model Use, Calibration, and Validation. *Transactions of the ASABE*, *55*(4), 1491–1508.

Arnold, J. G., Srinivasan, R., Muttiah, R. S., & Williams, J. R. (1998). Large Area Hydrologic Modeling and Assessment Part I: Model development. *Journal of the American Water Resources Association*, *34*(1), 73–89.

Ashaolu, E. D., Olorunfemi, J. F., & Ifabiyi, I. P. (2019). Assessing the Spatio-Temporal Pattern of Land Use and Land Cover Changes in Osun Drainage Basin, Nigeria. *Journal of Environmental Geography*, *12*(1–2), 41–50. https://doi.org/10.2478/jengeo-2019-0005

Awal, R., Fares, A., & Bayabil, H. (2018). Assessing potential climate change impacts on irrigation requirements of major crops in the brazos headwaters Basin, Texas. *Water*, *10*(11), 1–15. https://doi.org/10.3390/w10111610

Ayele, H. S., Li, M. H., Tung, C. P., & Liu, T. M. (2016). Assessing Climate Change Impact on Gilgel Abbay and Gumara Watershed Hydrology, the Upper Blue Nile Basin, Ethiopia. *Terrestrial, Atmospheric and Oceanic Sciences*, *27*(6), 1005–1018. https://doi.org/10.3319/tao.2016.07.30.01

Baldassarre, G. D., Elshamy, M., van Griensven, A., Soliman, E., Kigobe, M., Ndomba, P., Mutemi, J., Mutua, F., Moges, S., Xuan, Y., Solomatine, D. & Uhlenbrook, S. (2011). Future Hydrology and Climate in the River Nile Basin: a review. *Hydrological Sciences Journal*, *56*, 199-211. https://doi.org/10.1080/02626667.2011.557378

Banks, R. F., & Baldasano, J. M. (2016). Impact of WRF model PBL schemes on air quality simulations over Catalonia, Spain. *Science of the Total Environment*, *572*, 98–113. https://doi.org/10.1016/j.scitotenv.2016.07.167

Bekele, D., Alamirew, T., Kebede, A., Zeleke, G., & Melesse, A. M. (2019). Modeling Climate Change Impact on the Hydrology of Keleta Watershed in the Awash River Basin, Ethiopia. *Environmental Modeling and Assessment*, *24*, 95–107. https://doi.org/10.1007/s10666-018-619-1

Berihun, M. L., Tsunekawa, A., Haregeweyn, N., Meshesha, D. T., Adgo, E., Tsubo, M., Masunaga, T., Fenta, A. A., Sultan, D., Yibeltal, M., & Ebabu, K. (2019). Hydrological responses to land use/land cover change and climate variability in contrasting agro-ecological

environments of the Upper Blue Nile basin, Ethiopia. *Science of the Total Environment*, *689*, 347–365. https://doi.org/10.1016/j.scitotenv.2019.06.338

Bewket, W., & Sterk, G. (2005). Dynamics in land cover and its effect on stream fl ow in the Chemoga watershed, Blue Nile basin, Ethiopia. *Hydrological Processes*, *19*, 445–458. https://doi.org/10.1002/hyp.5542

Beyene, T., Lettenmaier, D. P., & Kabat, P. (2010). Hydrologic impacts of climate change on the Nile River Basin: Implications of the 2007 IPCC scenarios. *Climatic Change*, *100*(3), 433–461. https://doi.org/10.1007/s10584-009-9693-0

Biru, M. K., Minale, A. S., & Debay, A. B. (2015). Multitemporal Land Use Land Cover Change and Dynamics of Blue Nile Basin by Using GIS and Remote Sensing Techniques, North-Western Ethiopia. *International Journal of Environmental Sciences*, *4*, 81–88.

Bossa, A. Y., Diekkrüger, B., & Agbossou, E. K. (2014). Scenario-based impacts of land use and climate change on land and water degradation from the meso to regional scale. *Water*, *6*(10), 3152–3181. https://doi.org/10.3390/w6103152

Boysen, L. R., Brovkin, V., Arora, V. K., Cadule, P., De Noblet-Ducoudré, N., Kato, E., Pongratz, J., & Gayler, V. (2014). Global and regional effects of land-use change on climate in 21st century simulations with interactive carbon cycle. *Earth System Dynamics*, *5*(2), 309–319. https://doi.org/10.5194/esd-5-309-2014

Briones, R. U., Ella, V. B., & Bantayan, N. C. (2016). Hydrologic impact evaluation of land use and land cover change in Palico Watershed, Batangas, Philippines Using the SWAT model. *Journal of Environmental Science and Management*, *19*(1), 96–107.

Bruyere, C. L., Monaghan, A. J., Steinhoff, D. F., Yates, D., Bruyère, C. L., Monaghan, A. J., & Steinhoff, D. F. (2015). Bias-Corrected CMIP5 CESM Data in WRF/MPAS Intermediate File Format. *NCAR Technical Note NCAR/TN-515+STR*, 27. https://doi.org/10.5065/D6445JJ7

Budiyanto, S., Tarigan, S. D., Sinukaban, N., & Murtilaksono, K. (2015). The Impact of Land Use on Hydrological Characteristics in Kaligarang Watershed. *International Journal of Science and Engineering*, *8*(2), 125–130. https://doi.org/10.12777/ijse.8.2.125-130

Burakowski, E. A., Ollinger, S. V., Bonan, G. B., Wake, C. P., Dibb, J. E., & Hollinger, D. Y. (2016). Evaluating the climate effects of reforestation in new england using a weather research and forecasting (WRF) model multiphysics ensemble. *Journal of Climate*, *29*(14), 5141–5156. https://doi.org/10.1175/JCLI-D-15-0286.1

Cannon, F., Carvalho, M. V., Jones, C., Norris, J., Bookhagen, B., & Kiladis, G. N. (2017). Effects of topographic smoothing on the simulation of winter precipitation in high mountain Asia. *Journal of Geophysical Research*, *122*(3), 1456–1474. https://doi.org/10.1002/2016JD026038

Cao, M., Zhu, Y., Quan, J., Zhou, S., Lü, G., & Chen, M. (2019). Spatial Sequential Modeling and Predication of Global Land Use and Land Cover Changes by Integrating a Global Change Assessment Model and Cellular Automata. *Earth's Future*, *7*, 1102–1116. https://doi.org/10.1029/2019EF001228

Cao, Q., Yu, D., Georgescu, M., Han, Z., & Wu, J. (2015). Impacts of land use and land cover

change on regional climate: a case study in the agro-pastoral transitional zone of China. *Environmental Research Letters*, *10*. https://doi.org/doi:10.1088/1748-9326/10/12/124025

Cao, Y., Cervone, G., Barkley, Z., Lauvaux, T., Deng, A., & Taylor, A. (2017). Analysis of errors introduced by geographic coordinate systems on weather numeric prediction modeling. *Geoscientific Model Development*, *10*(9), 3425–3440. https://doi.org/10.5194/gmd-10-3425-2017

CDKN. (2014). The IPCC's Fifth Assessment Report offers the following key messages for Africa. Climate and Development Knowledge Network (CDKN). London, England.

Chakilu, G. G., & Moges, M. A. (2017). Assessing the Land Use/Cover Dynamics and its Impact on the Low Flow of Gumara Watershed, Upper Blue Nile Basin, Ethiopia. *Hydrology Current Research*, *8*. https://doi.org/10.4172/2157-7587.1000268

Chawla, I. & Mujumdar, P. P. (2015). Isolating the Impacts of Land Use and Climate Change on Stream Flow. *Hydrology and Earth System Science*, *12*, 2201–2242. https://doi.org/10.5194/hessd-12-2201

Chawla, I., Osuri, K. K., Mujumdar, P. P., & Niyogi, D. (2018). Assessment of the Weather Research and Forecasting (WRF) model for simulation of extreme rainfall events in the upper Ganga Basin. *Hydrology and Earth System Sciences*, *22*(2), 1095–1117. https://doi.org/10.5194/hess-22-1095-2018

Chen, Feng, Liu, C., Dudhia, J., & Chen, M. (2014). A sensitivity study of high-resolution regional climate simulations to three land surface models over the western United States. *Journal of Geophysical Research*, *119*(3), 7271–7291. https://doi.org/10.1002/2014JD021827

Cheng, F. Y., Hsu, Y. C., Lin, P. L., & Lin, T. H. (2013). Investigation of the effects of different land use and land cover patterns on mesoscale meteorological simulations in the Taiwan area. *Journal of Applied Meteorology and Climatology*, *52*(3), 570–587. https://doi.org/10.1175/JAMC-D-12-0109.1

Chiang, L., Chaubey, I., Gitau, M. W., & Arnold, J. G. (2010). Differentiating Impacts of Land Use Changes from Pasture Management in A Ceap Watershed using SWAT Model. *Transactions of the ASABE*, *53*(5), 1569–1584.

Chimdessa, K., Quraishi, S., Kebede, A., & Alamirew, T. (2019). Effect of land use land cover and climate change on river flow and soil loss in Didessa River Basin, South West Blue Nile, Ethiopia. *Hydrology*, *6*(1). https://doi.org/10.3390/hydrology6010002

Chotamonsak, C., Salathe, E. P., Kreasuwan, J., & Chantara, S. (2012). Evaluation of precipitation simulations over Thailand using a WRF regional climate model. *Chiang Mai Journal of Science*, *39*(4), 623–628.

Claessens, L., Hopkinson, C., Rastetter, E., & Vallino, J. (2006). Effect of Historical Changes in Land Use and Climate on the Water Budget of an Urbanizing Watershed. *Water Resource Research*, *42*, 1-3. https://doi.org/10.1029/2005WR004131

Clifton, C. F., Day, K. T., Luce, C. H., Grant, G. E., Safeeq, M., Halofsky, J. E., & Staab, B. P. (2018). Effects of climate change on hydrology and water resources in the Blue Mountains, Organ, USA. *Climate Services*, 1–11. https://doi.org/10.1016/j.cliser.2018.03.001

Collow, T. W., Robock, A., & Wu, W. (2014). Influences of soil moisture and vegetation on convective precipitation forecasts over the United States Great Plains. *Journal of Geophysical Research: Atmospheres*, *119*, 9338–9358. https://doi.org/10.1002/2014JD021454

Conway, D. (2000). The Climate and Hydrology of the Upper Blue Nile River. *The Geographical Journal*, *166*(1), 49–62.

Conway, D. (2005). From headwater tributaries to international river: Observing and adapting to climate variability and change in the Nile basin. *Global Environmental Change*, *15*, 99-114. https://doi.org/10.1016/j.gloenvcha.2005.01.003

Conway, D., & Schipper, E. L. F. (2011). Adaptation to climate change in Africa: Challenges and opportunities identified from Ethiopia. *Global Environmental Change*, *21*(1), 227–237. https://doi.org/10.1016/j.gloenvcha.2010.07.013

CSA. (2007). Summary and statistical report of 2007 population and housing census of Ethiopia. Central Statistical Agency, Addis Ababa, Ethiopia.

Daggupati, P., Pai, N., Ale, S., Douglas-Mankin, K. R., Zeckoski, R. W., Jeong, J., Parajuli, P. B., Saraswat, D., & Youssef, M. A. (2015). A recommended calibration and validation strategy for hydrologic and water quality models. *Transactions of the ASABE*, *58*(6), 1705–1719. https://doi.org/10.13031/trans.58.10712

Dang, T. N., & Kumar, L. (2017). Application of remote sensing and GIS-based hydrological modelling for flood risk analysis: a case study of District 8, Ho Chi Minh city, Vietnam. *Geomatics, Natural Hazards and Risk*, *8*(2), 1792–1811. https://doi.org/10.1080/19475705.2017.1388853

Daniels, E., Lenderink, G., Hutjes, R., & Holtslag, A. (2016). Relative impacts of land use and climate change on summer precipitation in the Netherlands. *Hydrology and Earth System Sciences*, *20*(10), 4129–4142. https://doi.org/10.5194/hess-20-4129-2016

De Meij, A., & Vinuesa, J. F. (2014). Impact of SRTM and Corine Land Cover data on meteorological parameters using WRF. *Atmospheric Research*, *143*, 351–370. https://doi.org/10.1016/j.atmosres.2014.03.004

Demmissie, N., Demissie, T., & Tufa, F. (2018). Predicting the Impact of Climate Change on Kulfo River Flow. *Hydrology*, *6*(3), 78–87. https://doi.org/10.11648/j.hyd.20180603.11

Demissie, T. A., Saathoff, F., Sileshi, Y., & Gebissa, A. (2013). Climate change impacts on the streamflow and simulated sediment flux to Gilgel Gibe 1 hydropower reservoir – Ethiopia. *European International Journal of Science and Technology*, 2(2), 63-77.

Dessu, S., & Melesse, A. (2012). Impact and uncertainties of climate change on the hydrology of the Mara River basin, Kenya/Tanzania. *Hydrological Processes*, *13*, 551-565. https://doi.org/10.1002/hyp.9434

Deng, X., Zhao, C., & Yan, H. (2013). Systematic modeling of impacts of land use and land cover changes on regional climate: A review. *Advances in Meteorology*. https://doi.org/10.1155/2013/317678

Dias, C. P., Macedo, M. N., Costa, M. H., Coe, M. T., & Neill, C. (2015). Effects of land cover

change on evapotranspiration and streamflow of small catchments in the Upper Xingu River Basin, Central Brazil. *Journal of Hydrology: Regional Studies*, *4*, 108–122. https://doi.org/10.1016/j.ejrh.2015.05.010

Diaz, J. P., González, a., Expósito, F. J., Pérez, J. C., Fernández, J., García-Díez, M., & Taima, D. (2015). WRF multi-physics simulation of clouds in the African region. *Quarterly Journal of the Royal Meteorological Society*, *141*(692), 2737–2749. https://doi.org/10.1002/qj.2560

Dile, Y. T., Daggupati, P., George, C., Srinivasan, R., & Arnold, J. (2016). Introducing a new open source GIS user interface for the SWAT model. *Environmental Modelling and Software*, *85*, 129–138. https://doi.org/10.1016/j.envsoft.2016.08.004

Dile, Y. T., Berndtsson, R., & Setegn, S. G. (2013). Hydrological Response to Climate Change for Gilgel Abay River, in the Lake Tana Basin - Upper Blue Nile Basin of Ethiopia. *PLoS ONE*, *8*(10), 1–13. https://doi.org/10.1371/journal.pone.0079296

Doğan, S., & Buğday, E. (2018). Modeling of Temporal and Spatial Changes of Land Cover and Land Use by Artificial Neural Networks : Kastamonu Sample. *Journal of Bartin Faculty of Forestry*, *20*(3), 653–663. https://doi.org/10.24011/barofd.467974

Du, J., Qian, L., Rui, H., Zuo, T., Zheng, D., Xu, Y., & Xu, C. Y. (2012). Assessing the effects of urbanization on annual runoff and flood events using an integrated hydrological modeling system for Qinhuai River basin, China. *Journal of Hydrology*, *464–465*, 127–139. https://doi.org/10.1016/j.jhydrol.2012.06.057

Eckhardt, K., Breuer, L., & Frede, H. (2003). Parameter uncertainty and the significance of simulated land use change effects. *Journal of Hydrologic Engineering*, *273*, 164–176.

Eidenshink, J. C., & Faundeen, J. L. (1994). The 1 km AVHRR global land data set: First stages in implementation. *International Journal of Remote Sensing*, *15*(17), 3443–3462. https://doi.org/10.1080/01431169408954339

Elshamy, M. E., Seierstad, I. A., & Sorteberg, A. (2009). Impacts of climate change on Blue Nile flows using bias-corrected GCM scenarios. *Hydrology and Earth System Sciences*, *13*(5), 551–565. https://doi.org/10.5194/hess-13-551-2009

Enyew, B., van Lanen, H., & van Loon, A. (2014). Assessment of the Impact of Climate Change on Hydrological Drought in Lake Tana Catchment, Blue Nile Basin, Ethiopia. *Journal of Geology & Geosciences*, *3*(6), 1–17. https://doi.org/10.4172/2329-6755.1000174

Fang, G. H., Yang, J., Chen, Y. N., & Zammit, C. (2015). Comparing bias correction methods in downscaling meteorological variables for a hydrologic impact study in an arid area in China. *Hydrology and Earth System Sciences*, *19*, 2547–2559. https://doi.org/10.5194/hess-19-2547-2015

Fang, X., Ren, L., Li, Q., Zhu, Q., Shi, P., & Zhu, Y. (2013). Hydrologic Response to Land Use and Land Cover Changes within the Context of Catchment-Scale Spatial Information. *Journal of Hydrologic Engineering*, *18*, 1539–1548. https://doi.org/10.1061/(ASCE)HE.1943-5584.0000482

Faramarzi, M., Abbaspour, K. C., Ashraf Vaghefi, S., Farzaneh, M. R., Zehnder, J. B., Srinivasan, R., & Yang, H. (2013). Modeling impacts of climate change on freshwater availability in

Africa. *Journal of Hydrology*, *480*, 85–101. https://doi.org/10.1016/j.jhydrol.2012.12.016

Fentaw, F., Mekuria, B., & Arega, A. (2018). Impacts of Climate Change on the Water Resources of Guder Catchment, Upper Blue Nile, Ethiopia. *Waters*, *1*(1), 16–29. https://doi.org/10.31058/j.water.2018.11002

Fronzek, S., Carter, T. R., & Jylhä, K. (2012). Representing two centuries of past and future climate for assessing risks to biodiversity in Europe. *Global Ecology and Biogeography*, *21*(1), 19–35. https://doi.org/10.1111/j.1466-8238.2011.00695.x

Gao, J., Hou, W., Xue, Y., & Wu, S. (2017). Validating the dynamic downscaling ability of WRF for East Asian summer climate. *Theoretical and Applied Climatology*, *128*, 241–253. https://doi.org/10.1007/s00704-015-1710-9

Gashaw, T., Mebrat, W., Hagos, D., & Nigussie, A. (2014). Climate Change Adaptation and Mitigation Mechanisms in Ethiopia. *Journal of Biology, Agriculture and Healthcare*, *4*(15), 148–152.

Gashaw, T., Tulu, T., Argaw, M., & Worqlul, A. W. (2018). Modeling the hydrological impacts of land use/land cover changes in the Andassa watershed, Blue Nile Basin, Ethiopia. *Science of the Total Environment*, *619–620*, 1394–1408. https://doi.org/10.1016/j.scitotenv.2017.11.191

Gebre, S. L., & Ludwig, F. (2015). Hydrological Response to Climate Change of the Upper Blue Nile River Basin: Based on IPCC Fifth Assessment Report (AR5). *Journal of Climatology & Weather Forecasting*, *3*. https://doi.org/10.4172/2332-2594.1000121

Gebremicael, T. G., Mohamed, Y. A., Betrie, G. D., van der Zaag, P., & Teferi, E. (2013). Trend analysis of runoff and sediment fluxes in the Upper Blue Nile basin: A combined analysis of statistical tests, physically-based models and landuse maps. *Journal of Hydrology*, *482*, 57–68. https://doi.org/10.1016/j.jhydrol.2012.12.023

Gebremicael, T. G., Mohamed, Y. A., & van der Zaag, P. (2019). Attributing the hydrological impact of different land use types and their long-term dynamics through combining parsimonious hydrological modelling, alteration analysis and PLSR analysis. *Science of the Total Environment*, *660*, 1155–1167. https://doi.org/10.1016/j.scitotenv.2019.01.085

Getachew, H. E., & Melesse, A. M. (2012). The Impact of Land Use Change on the Hydrology of the Angereb Watershed, Ethiopia. *International Journal of Water Sciences*, *1(4)*, 1-7. https://doi.org/10.5772/56266

Getahun, Y. S., & Haj, V. L. (2015). Assessing the Impacts of Land Use-Cover Change on Hydrology of Melka Kuntrie Subbasin in Ethiopia, Using a Conceptual Hydrological Model. *Journal of Waste Water Treatment & Analysis*, *6*(3). https://doi.org/10.4172/2157-7587.1000210

Göndöcs, J., Breuer, H., Horváth, Á., Ács, F., & Rajkai, K. (2015). Numerical study of the effect of soil texture and land use distribution on the convective precipitation. *Hungarian Geographical Bulletin*, *64*(1), 3–15. https://doi.org/10.15201/hungeobull.64.1.1

Goshime, D. W., Absi, R., & Ledésert, B. (2019). Evaluation and Bias Correction of CHIRP Rainfall Estimate for Rainfall-Runoff Simulation over Lake. *Hydrology*, *6*(68), 1–22.

https://doi.org/10.3390/hydrology6030068

Goswami, P., Shivappa, H., & Goud, S. (2012). Comparative analysis of the role of domain size, horizontal resolution and initial conditions in the simulation of tropical heavy rainfall events. *Meteorological Applications*, *19*(2), 170–178. https://doi.org/10.1002/met.253

Gumindoga, W., Rientjes, T. H., Haile, A. T., & Dube, T. (2015). Predicting streamflow for land cover changes in the Upper Gilgel Abay River Basin , Ethiopia : A TOPMODEL based approach. *Physics and Chemistry of the Earth*, *76–78*, 3–15. https://doi.org/10.1016/j.pce.2014.11.012

Guo, H., Hu, Q., & Jiang, T. (2008). Annual and Seasonal Stream Flow Responses to Climate and Land-Cover Changes in the Poyang Lake Basin, China. *Journal of Hydrology*, *355*, 106–122.

Gupta, H., Sorooshian, S., & Yapo, P. (1999). Status of Automatic Calibration for Hydrological Models: Comparsion with Multilevel Expert Calibration. *Journal of Hydrologic Engineering*, *4*(2), 135–143.

Guse, B., Pfannerstill, M., & Fohrer, N. (2015). Dynamic Modelling of Land Use Change Impacts on Nitrate Loads in Rivers. *Environmental Processes*, *2*(4), 575–592. https://doi.org/10.1007/s40710-015-0099-x

Guzha, A. C., Rufino, M. C., Okoth, S., Jacobs, S., & Nóbrega, L. B. (2018). Impacts of land use and land cover change on surface runoff, discharge and low flows: Evidence from East Africa. *Journal of Hydrology: Regional Studies*, *15*, 49–67. https://doi.org/10.1016/j.ejrh.2017.11.005

Hagos, S., Leung, L. R., Xue, Y., Boone, A., de Sales, F., Neupane, N., Huang, M., & Yoon, J. H. (2014). Assessment of uncertainties in the response of the African monsoon precipitation to land use change simulated by a regional model. *Climate Dynamics*, *43*(9–10), 2765–2775. https://doi.org/10.1007/s00382-014-2092-x

Haile, A. T., Rientjes, T. H., Gieske, A., & Gebremichael, M. (2009). Rainfall variability over mountainous and adjacent lake areas: The case of Lake Tana basin at the source of the Blue Nile River. *Journal of Applied Meteorology and Climatology*, *48*(8), 1696–1717. https://doi.org/10.1175/2009JAMC2092.1

Haregeweyn, N., Melesse, B., Tsunekawa, A., Tsubo, M., Meshesha, D., & Balana, B. B. (2012). Reservoir sedimentation and its mitigating strategies : a case study of Angereb reservoir (NW Ethiopia). *Journal of Soils and Sediments*, *12*(2), 291–305. https://doi.org/10.1007/s11368-011-0447-z

Haregeweyn, N., Tsunekawa, A., Poesen, J., Tsubo, M., Meshesha, D. T., Fenta, A. A., Nyssen, J., & Adgo, E. (2017). Comprehensive assessment of soil erosion risk for better land use planning in river basins: Case study of the Upper Blue Nile River. *Science of the Total Environment*, *574*, 95–108. https://doi.org/10.1016/j.scitotenv.2016.09.019

Hayhoe, K., Edmonds, J., Kopp, R. E., LeGrande, A. N., Sanderson, B. M., Wehner, M. F., & Wuebbles, D. J. (2017). Climate models, scenarios, and projections. In: Climate Science Special Report: Fourth National Climate Assessment, Volume I. U.S. Global Change Research Program. *Washington, DC, USA*, 133–160. https://doi.org/10.7930/J0WH2N54

He, J. J., Yu, Y., Yu, L. J., Liu, N., & Zhao, S. P. (2017). Impacts of uncertainty in land surface information on simulated surface temperature and precipitation over China. *International Journal of Climatology*, *37*, 829–847. https://doi.org/10.1002/joc.5041

Hein, A., Condon, L., & Maxwell, R. (2018). Evaluating the relative importance of precipitation, temperature and land-cover change in the hydrologic response to extreme meteorological drought conditions over the North American High Plains. *Hydrology and Earth System Sciences*, 23, 1931-1950. https://doi.org/10.5194/hess-23-1931-2019

Homdee, T., Pongput, K., & Kanae, S. (2011). Impacts of Land Cover Changes on Hydrologic Responses: A Case Study of Chi River Basin, Thailand. *Annual Journal of Hydraulic Engineering*, *55*, 31-36

Hong, S. Y., Noh, Y., & Dudhia, J. (2006). A new vertical diffusion package with an explicit treatment of entrainment processes. *Monthly Weather Review*, *134*(9), 2318–2341. https://doi.org/10.1175/MWR3199.1

Huang, C., & Lo, F. (2015). Effects of Land Use Change on Sediment and Water Yields in Yang Ming Shan National Park, Taiwan. *Environments*, *2*, 32–42. https://doi.org/10.3390/environments2010032

Huang, J., Zhou, P., Zhou, Z., & Huang, Y. (2013). Assessing the Influence of Land Use and Land Cover Datasets with Different Points in Time and Levels of Detail on Watershed Modeling in the North River Watershed, China. *International Journal of Environmental Research and Public Health*, *10*, 144-157. https://doi.org/10.3390/ijerph10010144

Hurkmans, R., Terink, W., Uijlenhoet, R., Torfs, P., Jacob, D., & Troch, P. A. (2010). Changes in streamflow dynamics in the Rhine basin under three high-resolution regional climate scenarios. *Journal of Climate*, *23*(3), 679–699. https://doi.org/10.1175/2009JCLI3066.1

Hurni, H., Abate, S., Bantider, A., & Debele, B. (2010). Land degradation and sustainable land management in the Highlands of Ethiopia. *Bern, Switzerland: Geographica Bernensia*, *5*, 187–207.

Hwang, S., Hwang, S., Park, S., & Lee, S. (2016). Examining the Relationships between Watershed Urban Land Use and Stream Water Quality Using Linear and Generalized Additive Models. *Water*, *8*(155), 1–15. https://doi.org/10.3390/w8040155

Hyandye, C. B., Worqul, A., Martz, L. W., & Muzuka, N. N. (2018). The impact of future climate and land use/cover change on water resources in the Ndembera watershed and their mitigation and adaptation strategies. *Environmental Systems Research*, *7*(1). https://doi.org/10.1186/s40068-018-0110-4

Iacono, M. J., Delamere, J. S., Mlawer, E. J., Shephard, M. W., Clough, S. A., & Collins, W. D. (2008). Radiative forcing by long-lived greenhouse gases: Calculations with the AER radiative transfer models. *Journal of Geophysical Research Atmospheres*, *113*(13), 2–9. https://doi.org/10.1029/2008JD009944

IPCC. (2007). Climate Change 2007: Synthesis Report. Contribution of Working Groups I, II and III to the Fourth Assessment Report of the Intergovernmental Panel on Climate Change. IPCC, Geneva, Switzerland. 1–112.

IPCC. (2014). Climate Change 2014: Synthesis Report. Contribution of Working Groups I, II and III to the Fifth Assessment Report of the Intergovernmental Panel on Climate Change. IPCC, Geneva, Switzerland. 1–151.

IPCC. (2019). Climate Change and Land: IPCC Special Report on Climate Change, Desertification, Land Degradation, Sustainable Land Management, Food Security, and Greenhouse gas fluxes in Terrestrial Ecosystems. 1–1542.

Jain, S., Panda, J., Rath, S. S., & Devara, C. S. (2017). Evaluating Land Surface Models in WRF Simulations over DMIC Region. *Indian Journal of Science and Technology*, *10*(18), 1–24. https://doi.org/10.17485/ijst/2017/v10i18/103522

Jemberie, M., Gebrie, T., & Gebremariam, B. (2016). Evaluation of Land Use Land Cover Change on Stream Flow: a Case Study Ofdedissa Sub Basin, Abay Basin, South Western Ethiopia. *International Journal of Innovations in Engineering Research and Technology*, *3*(8), 2394–3696

Jiménez, P. A., Dudhia, J., González-Rouco, J. F., Navarro, J., Montávez, J. P., & García-Bustamante, E. (2012). A Revised Scheme for the WRF Surface Layer Formulation. *Monthly Weather Review*, *140*(3), 898–918. https://doi.org/10.1175/MWR-D-11-00056.1

Jin, J., Wang, G., Zhang, J., Yang, Q., Liu, C., Liu, Y., Bao, Z., & He, R. (2018). Impacts of climate chnage on hydrology in the Yellow River Source region,china. *Journal of Water and Climate Change*, 1–15. https://doi.org/10.2166/wcc.2018.085

Jung, I. W., Chang, H., & Moradkhani, H. (2011). Quantifying uncertainty in urban flooding analysis considering hydro-climatic projection and urban development effects. *Hydrology and Earth System Sciences*, *15*(2), 617–633. https://doi.org/10.5194/hess-15-617-2011

Kain, J. S. (2004). The Kain - Fritsch convective parameterization: An update. *Journal of Applied Meteorology*, *43*(1), 170–181.

Kebede, S., Travi, Y., Alemayehu, T., & Marc, V. (2006). Water balance of Lake Tana and its sensitivity to fluctuations in rainfall, Blue Nile basin, Ethiopia. *Journal of Hydrology*, *316*(1–4), 233–247. https://doi.org/10.1016/j.jhydrol.2005.05.011

Kerandi, N. M., Laux, P., Arnault, J., & Kunstmann, H. (2017). Performance of the WRF model to simulate the seasonal and interannual variability of hydrometeorological variables in East Africa: a case study for the Tana River basin in Kenya. *Theoretical and Applied Climatology*, *130*(1–2), 401–418. https://doi.org/10.1007/s00704-016-1890-y

Kidane, M., Tolessa, T., Bezie, A., Kessete, N., & Endrias, M. (2019). Evaluating the impacts of climate and land use/land cover (LU/LC) dynamics on the Hydrological Responses of the Upper Blue Nile in the Central Highlands of Ethiopia. *Spatial Information Research*, *27*(2), 151–167. https://doi.org/10.1007/s41324-018-0222-y

Kim, Y., Sartelet, K., Raut, J. C., & Chazette, P. (2015). Influence of an urban canopy model and PBL schemes on vertical mixing for air quality modeling over Greater Paris. *Atmospheric Environment*, *107*, 289–306. https://doi.org/10.1016/j.atmosenv.2015.02.011

King, K. W., Arnold, J. G., & Bingner, R. L. (1999). Comparison of Green-Ampt and curve number methods on Goodwin Creek Watershed using SWAT. *Transactions of the American*

Society of Agricultural Engineers, *42*(4), 919–925

Kitoh, A., Ose, T. & Takayabu, I. (2015). Dynamical Downscaling for Climate Projection with High Resolution MRI AGCM-RCM. Journal of the Meteorological Society of Japan. https://doi.org/10.2151/jmsj.2015-022

Knutti, R., Masson, D., & Gettelman, A. (2013). Climate model genealogy: Generation CMIP5 and how we got there. *Geophysical Research Letters*, *40*(6), 1194–1199. https://doi.org/10.1002/grl.50256

Koch, F.L., van Griensven, A., Uhlenbrook, S., Tekleab, S., & Teferi, E. (2012). The Effects of Land use Change on Hydrological Responses in the Choke Mountain Range (Ethiopia) - A new Approach Addressing Land Use Dynamics in the Model SWAT. *International Environmental Modeling and Software Society, International Congress on Environmental Modelling and Software, Managing Resources of a Limited Planet,* Sixth Biennial Meeting, Leipzig, Germany

Koch, H., Biewald, A., Liersch, S., Azevedo, J., Silva, G. N., Kölling, K., Fischer, P., Koch, R., & Hattermann, F. F. (2015). Scenarios of climate and land-use change,water demand and water availability for the São Francisco River basin. *Revista Brasileira de Ciências Ambientais*, (36), 96–114. https://doi.org/10.5327/z2176-947820151007

Kumar, N., Tischbein, B., Kusche, J., Laux, P., Beg, M. K., & Bogardi, J. J. (2017). Impact of climate change on water resources of upper Kharun catchment in Chhattisgarh , India. *Journal of Hydrology: Regional Studies*, *13*, 189–207. https://doi.org/10.1016/j.ejrh.2017.07.008

Lai, A., Liu, Y., Chen, X., Chang, M., Fan, Q., Chan, P., Wang, X., & Dai, J. (2016). Impact of land-use change on atmospheric environment using refined land surface properties in the Pearl River Delta, China. *Advances in Meteorology*, *2016*, 1–15. https://doi.org/10.1155/2016/3830592

Laprise, R. (1992). The Euler equations of motion with hydrostatic pressure as an independent variable. *Monthly Weather Review*, 120, 197–207.

Lawler, J. J., Lewis, D. J., Nelson, E., Plantinga, A. J., Polasky, S., & Withey, J. C. (2014). Projected land-use change impacts on ecosystem services in the United States. *Sustainability Science*, *111*(20). https://doi.org/10.1073/pnas.1405557111

Lee, C. B., Kim, J. C., Belorid, M., & Zhao, P. (2016). Performance evaluation of four different land surface models in WRF. *Asian Journal of Atmospheric Environment*, *10(1),* 42–50. https://doi.org/10.5572/ajae.2016.10.1.042

Lee, S., Yeo, I., Sadeghi, A. M., Mccarty, G. W., Hively, W. D., & Lang, M. W. (2018). Comparative analyses of hydrological responses of two adjacent watersheds to climate variability and change using the SWAT model. *Hydrology and Earth System Sciences*, *22*, 689–708. https://doi.org/doi.org/10.5194/hess-22-689-2018

Legesse, D., Abiye, T. A., Vallet-Coulomb, C., & Abate, H. (2010). Streamflow sensitivity to climate and land cover changes: Meki River, Ethiopia. *Hydrology and Earth System Sciences*, *14*(11), 2277–2287. https://doi.org/10.5194/hess-14-2277-2010

Lemann, T., Roth, V., Zeleke, G., Subhatu, A., Kassawmar, T., & Hurni, H. (2018). Spatial and

temporal variability in hydrological responses of the upper Blue Nile basin, Ethiopia. *Water*, *11*(1). https://doi.org/10.3390/w11010021

Li, F., Zhang, G., & Xu, Y. J. (2016). Assessing Climate Change Impacts on Water Resources in the Songhua River Basin. *Water*, *8*(420), 1–17. https://doi.org/10.3390/w8100420

Li, J., Zheng, X., Zhang, C., & Chen, Y. (2018). Impact of land-use and land-cover change on meteorology in the Beijing-Tianjin-Hebei region from 1990 to 2010. *Sustainability*, *10*(1). https://doi.org/10.3390/su10010176

Li, K. Y., Coe, M. T., Ramankutty, N., & De Jong, R. (2007). Modeling the hydrological impact of land-use change in West Africa. *Journal of Hydrology*, *337*, 258–268. https://doi.org/10.1016/j.jhydrol.2007.01.038

Li, Y., Fan, J., Hu, Z., Shao, Q., Zhang, L., & Yu, H. (2015). Influence of Land Use Patterns on Evapotranspiration and Its Components in a Temperate Grassland Ecosystem. *Advances in Meteorology*, *2015*, 1–12. https://doi.org/10.1155/2015/452603

Li, Z., Deng, X., Wu, F., & Hasan, S. S. (2015). Scenario Analysis for Water Resources in Response to Land Use Change in the Middle and Upper Reaches of the Heihe River Basin. *Sustainability*, *7*, 3086-3108. https://doi.org/10.3390/su7033086

Li, Z., Liu, W. Z., Zhang, X. C., & Zheng, F. (2010). Assessing and Regulating the Impacts of Climate Change on Water Resources in the Heihe Watershed on the Loess Plateau of China. *Science China Earth Sciences*, *53*, 710–720. https://doi.org/10.1007/s114

Liersch, S., Tecklenburg, J., Rust, H., Dobler, A., Fischer, M., Kruschke, T., Koch, H., & Hattermann, F. F. (2018). Are we using the right fuel to drive hydrological models? A climate impact study in the Upper Blue Nile. *Hydrology and Earth System Sciences*, *22*(4), 2163–2185. https://doi.org/10.5194/hess-22-2163-2018b

Lillesand, T. M., Kiefer, R. W., & Chipman, J. W. (2015). Remote Sensing and Image Interpretation. 7th ed. John Wiley & Sons, Inc. USA.

Liu, J., Zhang, C., Kou, L., & Zhou, Q. (2017). Effects of Climate and Land Use Changes on Water Resources in the Taoer River. *Advances in Meteorology*, *2017*, 1-14. https://doi.org/10.1155/2017/1031854

Malhi, Y., Roberts, J. T., Betts, R. A., Killeen, T. J., Li, W., & Nobre, C. A. (2008). Climate change, deforestation, and the fate of the Amazon. *Science*, *319*, 169–172. https://doi.org/10.1126/science.1146961

Mango, L. M., Melesse, A. M., McClain, M. E., Gann, D., & Setegn, S. G. (2011). Land use and climate change impacts on the hydrology of the upper Mara River Basin, Kenya: Results of a modeling study to support better resource management. *Hydrology and Earth System Sciences*, *15*(7), 2245–2258. https://doi.org/10.5194/hess-15-2245-2011

Marhaento, H., Booij, M. J., & Hoekstra, A. Y. (2018). Hydrological response to future land-use change and climate change in a tropical catchment. *Hydrological Sciences Journal*, *63*(9), 1368–1385. https://doi.org/10.1080/02626667.2018.1511054

McCartney, M. P., & Girma, M. M. (2012). Evaluating the downstream implications of planned

water resource development in the Ethiopian portion of the Blue Nile River. *Water International*, *37*(4), 362–379. https://doi.org/10.1080/02508060.2012.706384

Mechal, A., Wagner, T., & Birk, S. (2015). Recharge variability and sensitivity to climate: The example of Gidabo River Basin, Main Ethiopian Rift. *Journal of Hydrology: Regional Studies*, *4*, 644–660. https://doi.org/10.1016/j.ejrh.2015.09.001

McNider, R. T., Handyside, C., Doty, K., Ellenburg, W. L., Cruise, J. F., Christy, J. R., Moss, D., Shard, V., Hoogenboom, G., & Caldwell, P. (2015). An integrated crop and hydrologic modeling system to estimate hydrologic impacts of crop irrigation deman. *Environmental Modelling & Software*, *72*, 341-355.

Mekonnen, D., & Disse, M. (2018). Analyzing the future climate change of Upper Blue Nile River basin using statistical downscaling techniques. *Hydrology and Earth System Sciences*, *22*(4), 2391–2408. https://doi.org/10.5194/hess-22-2391-2018

Mekonnen, D., Duan, Z., Rientjes, T. H., & Disse, M. (2018). Analysis of combined and isolated effects of land-use and land-cover changes and climate change on the upper Blue Nile River basin's streamflow. *Hydrology and Earth System Sciences*, *22*(12), 6187–6207. https://doi.org/10.5194/hess-22-6187-2018

Melke, A., & Abegaz, F. (2017). Impact of climate change on hydrological responses of Gumara catchment, in the Lake Tana Basin - Upper Blue Nile Basin of Ethiopia. *International Journal of Water Resources and Environmental Engineering*, *9*, 8–21. https://doi.org/10.5897/ijwree2016.0658

Mishra, V., Cherkauer, K., Niyogi, D., Lei, M., Pijanowski, B., Ray, D., Bowling, L., & Yang, G. (2010). A regional scale assessment of land use/land cover and climatic changes on water and energy cycle in the upper Midwest United States. *International Journal of Climatology*, 2011–2029. https://doi.org/10.1002/joc.2095

Mooney, P. a., Mulligan, F. J., & Broderick, C. (2016). Diurnal cycle of precipitation over the British Isles in a 0.44° WRF multiphysics regional climate ensemble over the period 1990–1995. *Climate Dynamics*, *47*(9–10), 3281–3300. https://doi.org/10.1007/s00382-016-3026-6

Morán-Tejeda, E., Zabalza, J., Rahman, K., Gago-Silva, A., López-Moreno, J. I., Vicente-Serrano, S., Lehmann, A., Tague, C. L., & Beniston, M. (2014). Hydrological Impacts of Climate and Land-Use Changes in a Mountain Watershed: Uncertainty Estimation Based On Model Comparison. *Ecohydrology*, 1-21. https://doi.org/10.1002/eco.1590

Moriasi, D. N., Arnold, J. G., Liew, M. W. van Bingner, R. L., Harmel, R. D., & Veith, T. L. (2007). Model Evaluation Guidelines for Systematic Quantification of Accuracy in Watershed Simulations. *Transactions of the ASABE*, *50*(3), 885–900.

Moss, R. H., Edmonds, J. A., Hibbard, K. A., Manning, M. R., Rose, S. K., van Vuuren, D. P., Carter, T. R., Emori, S., Kainuma, M., Kram, T., & Wilbanks, T. J. (2010). The next generation of scenarios for climate change research and assessment. *Nature*, *463*(7282), 747–756. https://doi.org/10.1038/nature08823

Mottet, A., Ladet, S., Coqué, N., & Gibon, A. (2006). Agricultural land-use change and its drivers in mountain landscapes: A case study in the Pyrenees. *Agriculture, Ecosystems and*

Environment, *114*(2–4), 296–310. https://doi.org/10.1016/j.agee.2005.11.017

MoWIE. (1998). Abbay River Basin Integrated Development Mater Plan Project: Phase 2, vol. VI, Water Resources Development, Part 2, Large Irrigation and Hydropower Dams. Ministry of Water, Irrigation, and Electricity, Addis Ababa, Ethiopia.

MoWIE. (2008). Gumara Irrigation Project Feasibility Study Report. Ministry of Water, Irrigation, and Electricity, Addis Ababa, Ethiopia.

Mugume, I., Waiswa, D., Mesquita, M., Reuder, J., Basalirwa, C., Bamutaze, Y., Twinomuhangi, R., Tumwine, F., Sansa, O., Jacob, N., & Ayesiga, G. (2017). Assessing the Performance of WRF Model in Simulating Rainfall over Western Uganda. *Journal of Climatology & Weather Forecasting*, *5*(1), 1–9. https://doi.org/10.4172/2332-2594.1000197

Müller, O. V., Berbery, E., Alcaraz-Segura, D., & Ek, M. B. (2014). Regional model simulations of the 2008 drought in southern South America using a consistent set of land surface properties. *Journal of Climate*, *27*, 6754–6778. https://doi.org/10.1175/JCLI-D-13-00463.1

Mwangi, H. M., Julich, S., Patil, S. D., McDonald, M. A., & Feger, K. H. (2016). Relative contribution of land use change and climate variability on discharge of upper Mara River, Kenya. *Journal of Hydrology: Regional Studies*, *5*, 244–260. https://doi.org/10.1016/j.ejrh.2015.12.059

Nakayama, T. (2011). Simulation of the effect of irrigation on the hydrologic cycle in the highly cultivated Yellow River Basin. *Agricultural and Forest Meteorology*, *151*(3), 314–327. https://doi.org/10.1016/j.agrformet.2010.11.006

Nakićenović, N., & Swart, R. (2000). Special Report on Emissions Scenarios. Cambridge University Press, Cambridge.

Nash, J., & Sutcliffe, J. (1970). River Flow Forecasting Through Conceptual Models Part 1 - A Discussion of principles. *Journal of Hydrology*, *10*, 282–290.

Neitsch, S., Arnold, J., Kiniry, J., & Williams, J. (2011). Soil & Water Assessment Tool: Theoretical Documentation Version 2009. Texas A & M University, USA.

Nejadhashemi, A. P., Shen, C., Wardynski, B. J., & Mantha, P. S. (2010). Evaluating the impacts of land use changes on hydrologic responses in the agricultural regions of Michigan and Wisconsin. *American Society of Agricultural and Biological Engineers Annual International Meeting 2010, ASABE 2010*, *3*, 2091–2119. https://doi.org/10.5194/hessd-8-3421-2011

Ngongondo, C., Li, L., Gong, L., Xu, C. Y., & Alemaw, B. F. (2013). Flood frequency under changing climate in the upper Kafue River basin, southern Africa: A large scale hydrological model application. *Stochastic Environmental Research and Risk Assessment*, *27*(8), 1883–1898. https://doi.org/10.1007/s00477-013-0724-z

Nigatu, Z. M., Rientjes, T. H., & Haile, A. T. (2016). Hydrological Impact Assessment of Climate Change on Lake Tana's Water Balance, Ethiopia. *American Journal of Climate Change*, *5*(1), 27–37. https://doi.org/10.4236/ajcc.2016.51005

Nyssen, J., Poesen, J., Moeyersons, J., Deckers, J., Haile, M., & Lang, A. (2004). Human impact on the environment in the Ethiopian and Eritrean highlands - A state of the art. *Earth-Science*

Reviews, *64*(3–4), 273–320. https://doi.org/10.1016/S0012-8252(03)00078-3

Olson, J. M., Alagarswamy, G., Andresen, J. A., Campbell, D. J., Davis, A. Y., Ge, J. J., Huebner, M., Lofgren, B. M., Lusch, D. P., Moore, N. J., Pijanowski, B. C., Qi, J. G., Thornton, P. K., Torbick, N. M., & Wang, J. (2008). Integrating Diverse Methods to Understand Climate–Land Interactions in East Africa. *Geo forum*, *9*, 898-911.

Osuri, K. K., Mohanty, U. C., Routray, A., & Niyogi, D. (2015). Improved prediction of bay of bengal tropical cyclones through assimilation of doppler weather radar observations. *Monthly Weather Review*, *143*(11), 4533–4560. https://doi.org/10.1175/MWR-D-13-00381.1

Pai, N., & Saraswat, D. (2011). SWAT2009_LUC: A Tool to Activate the Land Use Change Module in SWAT 2009. *Transactions of the ASABE*, *54*(5), 1649–1658.

Pandey, B. K., Gosain, A. K., Paul, G., & Khare, D. (2017). Climate change impact assessment on hydrology of a small watershed using semi-distributed model. *Applied Water Science*, *7*(4), 2029–2041. https://doi.org/10.1007/s13201-016-0383-6

Pennelly, C., Reuter, G., & Flesch, T. (2014). Verification of the WRF model for simulating heavy precipitation in Alberta. *Atmospheric Research*, *135–136*, 172–192. https://doi.org/10.1016/j.atmosres.2013.09.004

Pohl, B., Crétat, J., & Camberlin, P. (2011). Testing WRF capability in simulating the atmospheric water cycle over Equatorial East Africa. *Climate Dynamics*, *37*(7–8), 1357–1379. https://doi.org/10.1007/s00382-011-1024-2

Polanco, E. I., Fleifle, A., Ludwig, R., & Disse, M. (2017). Improving SWAT model performance in the upper Blue Nile Basin using meteorological data integration and subcatchment discretization. *Hydrology and Earth System Sciences*, *21*(9), 4907–4926. https://doi.org/10.5194/hess-21-4907-2017

Pongratz, J., Reick, C. H., Raddatz, T., & Claussen, M. (2010). Biogeophysical versus biogeochemical climate response to historical anthropogenic land cover change. *Geophysical Research Letters*, *37*(8), 1–5. https://doi.org/10.1029/2010GL043010

Praskievicz, S., & Chang, H. (2009). A Review of Hydrological Modeling of Basin-Scale Climate Change and Urban Development Impacts. *Progress in Physical Geography, 33(5),* 650–671. https://doi.org/10.1177/0309133309348098

Puliafito, S. E., Allende, D. G., Mulena, C. G., Cremades, P., & Lakkis, S. G. (2015). Evaluation of the WRF model configuration for Zonda wind events in a complex terrain. *Atmospheric Research*, *166*, 24–32. https://doi.org/10.1016/j.atmosres.2015.06.011

Quesada, B., Arneth, A., & De Noblet-Ducoudré, N. (2017). Atmospheric, radiative, and hydrologic effects of future land use and land cover changes: A global and multimodel climate picture. *Journal of Geophysical Research*, *122*(10), 5113–5131. https://doi.org/10.1002/2016JD025448

Rahbeh, M., Chanasyk, D., & Miller, J. (2013). Modelling the effect of irrigation on the hydrological output from a small prairie watershed. *Canadian Water Resources Journal*, *38*(4), 280–295. https://doi.org/10.1080/07011784.2013.849856

Rahman, K., da Silva, A. G., Tejeda, E. M., Gobiet, A., Beniston, M., & Lehmann, A. (2015). An independent and combined effect analysis of land use and climate change in the upper Rhone River watershed, Switzerland. *Applied Geography*, *63*, 264–272. https://doi.org/10.1016/j.apgeog.2015.06.021

Rahman, T. U., Tabassum, F., Rasheduzzaman, M., Saba, H., Sarkar, L., Ferdous, J., Uddin S. Z., & Islam, Z. M. (2017). Temporal dynamics of land use/land cover change and its prediction using CA-ANN model for southwestern coastal Bangladesh. *Environmental Monitoring and Assessment*, *189*(11), 1–18. https://doi.org/10.1007/s10661-017-6272-0

Ramarohetra, J., Pohl, B., & Sultan, B. (2015). Errors and uncertainties introduced by a regional climate model in climate impact assessments: Example of crop yield simulations in West Africa. *Environmental Research Letters*, *10*(12). https://doi.org/10.1088/1748-9326/10/12/124014

Rientjes, T. H., Haile, A. T., Kebede, E., Mannaerts, M. M., Habib, E., & Steenhuis, T. S. (2011). Changes in land cover, rainfall and stream flow in Upper Gilgel Abbay catchment, Blue Nile basin-Ethiopia. *Hydrology and Earth System Sciences*, *15*(6), 1979–1989. https://doi.org/10.5194/hess-15-1979-2011

Roth, V., Lemann, T., Zeleke, G., Subhatu, A. T., Nigussie, T. K., & Hurni, H. (2018). Effects of climate change on water resources in the upper Blue Nile Basin of Ethiopia. *Heliyon*, *4*(9), 1–26. https://doi.org/10.1016/j.heliyon.2018.e00771

Sahlu, D., Nukolopoulos, E., Moges, S., Anafnostou, E., & Hailu, D. (2016). First Evaluation of the Day-1 IMERG over the Upper Blue Nile Basin. *American Meteorological Society*, *17*, 2875–2882. https://doi.org/10.1175/JHM-D-15-0230.1

Saraswat, D., Pai, N., & Daniels, M. (2010). Identifying priority subwatersheds using distributed modeling approach. *ASABE - TMDL 2010:* Watershed Management to Improve Water Quality, 158–173. https://doi.org/10.13031/2013.35752

Sattari, M. T., Rezazadeh-Joudi, A., & Kusiak, A. (2017). Assessment of different methods for estimation of missing data in precipitation studies. *Hydrology Research*, *48*(4), 1032–1044. https://doi.org/10.2166/nh.2016.364

Schirmer, M., & Jamieson, B. (2015). Verification of analysed and forecasted winter precipitation in complex terrain. *The Cryosphere*, *9*, 587–601. https://doi.org/10.5194/tc-9-587-2015

Sertel, E., Robock, A., & Ormeci, C. (2009). Impacts of land cover data quality on regional climate simulations. *International Journal of Climatology*, *123*, 162–173. https://doi.org/doi:10.1002/joc.2036

Setegn, S. G., Rayner, D., Melesse, A. M., Dargahi, B., & Srinivasan, R. (2011). Impact of climate change on the hydroclimatology of Lake Tana Basin, Ethiopia. *Water Resources Research*, *47*(4), 1–13. https://doi.org/10.1029/2010WR009248

Setegn, S. G., Srinivasan, R., & Dargahi, B. (2008). Hydrological Modelling in the Lake Tana Basin, Ethiopia Using SWAT Model. *The Open Hydrology Journal*, *2*(1), 49–62. https://doi.org/10.2174/1874378100802010049

SGZOA. (2016). Agriculture production management document of South Gondor Zone

(Unpublished report). South Gondar Zone Office of Agriculture, Debre Tabor, Ethiopia.

Simane, B., Beyene, H., Deressa, W., Kumie, A., Berhane, K., & Samet, J. (2017). Review of Climate Change and Health in Ethiopia: Status and Gap Analysis. *Ethiopia Journal of Health Development, 30*(1), 1–23. https://doi.org/10.1016/j.physbeh.2017.03.040

Sisay, K., Thurnher, C., & Hasenauer, H. (2017). Daily climate data for the Amhara region in Northwestern Ethiopia. *International Journal of Climatology*, *37*(6), 2797–2808. https://doi.org/10.1002/joc.4880

Skamarock, W. C., Klemp, J. B., Gill, D. O., Barker, D. M., Duda, M. G., Wang, W., & Powers, J. G. (2008). A Description of the Advanced Research WRF Version 3. NCAR/TN–475+STR NCAR TECHNICAL NOTE, Colorado, USA.

Smirnova, T. G., Brown, J. M., Benkamin, S. G., & Kenyon, J. S. (2016). Modifications to the Rapid Update Cycle Land Surface Model (RUC LSM) Available in the Weather Research and Forecasting (WRF) Model. *American Meteorological Society*, *144*, 1851–1865. https://doi.org/10.1175/MWR-D-15-0198.1

Smitha, P. S., Narasimhan, B., Sudheer, K. P., & Annamalai, H. (2018). An improved bias correction method of daily rainfall data using a sliding window technique for climate change impact assessment. *Journal of Hydrology*, *556*, 100–118. https://doi.org/10.1016/j.jhydrol.2017.11.010

Stehr, A., Aguayo, A., Link, O., Parra, O., Romero, F., & Alcayaga, H. (2010). Modelling the hydrologic response of a mesoscale Andean watershed to changes in land use patterns for environmental planning. *Hydrology and Earth System Sciences*, *14*, 1963–1977. https://doi.org/10.5194/hesss-14-1963-2010

Su, Z., Linc, C., Ma, R., Luo, J., & Liang, Q. (2015). Effect of Land Use Change on Lake Water Quality in Different Buffer Zones. *Applied Ecology and Environmental Research*, *13*(3), 639–653. https://doi.org/10.15666/aeer/1303_639653

Sunde, M. G., He, H. S., Hubbart, J. A., & Urban, M. A. (2018). An integrated modeling approach for estimating hydrologic responses to future urbanization and climate changes in a mixed-use midwestern watershed. *Journal of Environmental Management*, *220*, 149–162. https://doi.org/10.1016/j.jenvman.2018.05.025

Tabari, H., De Troch, R., Giot, O., Hamdi, R., Termonia, P., Saeed, S., Brisson, E., van Lipzig, N., & Willems, P. (2016). Local impact analysis of climate change on precipitation extremes: Are high-resolution climate models needed for realistic simulations? *Hydrology and Earth System Sciences*, *20*(9), 3843–3857. https://doi.org/10.5194/hess-20-3843-2016

Tadele, H., Mekuriaw, A., Selassie, Y. G., & Tsegaye, L. (2017). Land Use/Land Cover Factor Values and Accuracy Assessment Using a GIS and Remote Sensing in the Case of the Quashay Watershed in Northwestern Ethiopia. *Journal of Natural Resources and Development*, *7*, 38–44. https://doi.org/10.5027/jnrd.v7i0.05

Taye, M. T., Willems, P., & Block, P. (2015). Implications of climate change on hydrological extremes in the Blue Nile basin: A review. *Journal of Hydrology: Regional Studies*, *4*, 280–293. https://doi.org/10.1016/j.ejrh.2015.07.001

Taylor, K. E. (2001). Summarizing multiple aspects of model performance in a single diagram. *Journal of Geophysical Research*, *106*, 7183–7192.

Teferi, E., Bewket, W., Uhlenbrook, S., & Wenninger, J. (2013). Understanding recent land use and land cover dynamics in the source region of the Upper Blue Nile, Ethiopia: Spatially explicit statistical modeling of systematic transitions. *Agriculture, Ecosystems and Environment*, *165*, 98–117. https://doi.org/10.1016/j.agee.2012.11.007

Teklay, A., Dile, Y. T., Asfaw, D. H., Bayabil, H. K., & Sisay, K. (2019). Impacts of land surface model and land use data on WRF model simulations of rainfall and temperature over Lake Tana Basin, Ethiopia. *Heliyon*, *5*(9), 1–14. https://doi.org/10.1016/j.heliyon.2019.e02469

Teklay, A., Dile, Y. T., Setegn, S. G., Demissie, S. S., & Asfaw, D. H. (2018). Evaluation of static and dynamic land use data for watershed hydrologic process simulation : A case study in Gummara watershed, Ethiopia. *Catena*, *172*, 65–75. https://doi.org/10.1016/j.catena.2018.08.013

Tekleab, S., Mohamed, Y., Uhlenbrook, S., & Wenninger, J. (2014). Hydrologic responsees to land cover change: the case of Jedeb mesoscale catchment, Abay/Upper Blue Nile basin, Ethiopia. *Hydrological processes*, *28*, 5149–5162. https://doi.org/10.1002/hyp.9998

Teklesadik, A. D., Alemayehu, T., van Griensven, A., Kumar, R., Liersch, S., Eisner, S., Tecklenburg, J., Ewunte, S., & Wang, X. (2017). Inter-model comparison of hydrological impacts of climate change on the Upper Blue Nile basin using ensemble of hydrological models and global climate models. *Climatic Change*, *141*(3), 517–532. https://doi.org/10.1007/s10584-017-1913-4

Terink, W., Hurkmans, W. L., Torfs, J. F., & Uijlenhoet, R. (2010). Evaluation of a bias correction method applied to downscaled precipitation and temperature reanalysis data for the Rhine basin. *Hydrology and Earth System Sciences*, *14(4)*, 687–703. https://doi.org/10.5194/hess-14-687-2010

Tetsuya, S. (2004). The Earth Simulator: Roles and Impacts. Nuclear Physics, Proceedings Supplements, 129, 102.

Teutschbein, C., & Seibert, J. (2013). Is bias correction of regional climate model (RCM) simulations possible for non-stationary conditions?. *Hydrology and Earth System Sciences*, *17*, 5061–5077. https://doi.org/10.5194/hess-17-5061-2013

Thomas, L., Dash, S. K., & Mohanty, U. C. (2014). Influence of various land surface parameterization schemes on the simulation of western disturbances. *Meteorological Applications*, *21*(3), 635–643. https://doi.org/10.1002/met.1386

Thompson, G., Field, P., Rasmussen, R., & Hall, W. (2008). Explicit Forecasts of Winter Precipitation Using an Improved Bulk Microphysics Scheme. Part II: Implementation of a New Snow Parameterization. *Monthly Weather Review*, *136*, 5095–5115. https://doi.org/10.1175/2008MWR2387.1

Thornton, P. K., Ericksen, P. J., Herrero, M., & Challinor, A. J. (2014). Climate variability and vulnerability to climate change: A review. *Global Change Biology*, *20*(11), 3313–3328. https://doi.org/10.1111/gcb.12581

Tigabu, T. B., Hörmann, G., Wagner, P. D., & Fohrer, N. (2018). Statistical analysis of rainfall and streamflow time series in the Lake Tana Basin, Ethiopia. *Journal of Water and Climate Change*, *2018*, 1–17. https://doi.org/10.2166/wcc.2018.008

Tigabu, T. B., Wagner, P. D., Hörmann, G., & Fohrer, N. (2019). Modeling the impact of agricultural crops on the spatial and seasonal variability of water balance components in the Lake Tana basin, Ethiopia. *Hydrology Research*, *50*, 1376–1396. https://doi.org/10.2166/nh.2019.170

Tramblay,Y., Ruelland, D., Somot, S., Bouaicha, R., & Servat, E. (2013). High-resolution Med-CORDEX regional climate model simulations for hydrological impact studies: a first evaluation of the ALADIN-Climate model in Morocco. *Hydrology and Earth System Sciences*, 17, 3721–3739. https://doi.org/10.5194/hess-17-3721-2013

Van Griensven, A., Ndomba, P., Yalew, S., & Kilonzo, F. (2012). Critical review of SWAT applications in the upper Nile basin countries. *Hydrology and Earth System Sciences*, *16*(9), 3371–3381. https://doi.org/10.5194/hess-16-3371-2012

Van Vuuren, D., Edmonds, J., Kainuma, M., Riahi, K., Thomson, A., Hibbard, K., Hurtt, G., Kram, T., Krey, V., Lamarque, J., & Rose, S. (2011). The representative concentration pathways: An overview. *Climatic Change*, *109*, 5–31. https://doi.org/10.1007/s10584-011-0148-z

Verbeiren, B., Van De Voorde, T., Canters, F, Binard, M., Cornet, Y., van Der Kwast, J., Engelen, G., & Batelaan, O. (2011). Impact Assessment of Urbanisation on Hydrology for the River Tolka in Dublin, Ireland: A Case Study of Remote Sensing Supported Hydrological Modelling. National Hydrology Conference, Belgium

Wangpimool, W., Pongput, K., Supriyasilp, T., Sakolnakhon, K., & Vonnarart, O. (2013). Hydrological Evaluation with SWAT Model and Numerical Weather Prediction for Flash Flood Warning System in Thailand. *Journal of Earth Science and Engineering, 6*, 349-357.

Wagner, P. D., Bhallamudi, S. M., Narasimhan, B., Kantakumar, L. N., Sudheer, K. P., Kumar, S., Schneider, K., & Fiener, P. (2016). Dynamic integration of land use changes in a hydrologic assessment of a rapidly developing Indian catchment. *Science of the Total Environment*, *539*, 153–164. https://doi.org/10.1016/j.scitotenv.2015.08.148

Wilby, R. L., & Harris, I. (2006). A framework for assessing uncertainties in climate change impacts: low-flow scenarios for the River Thames, UK. *Water Resources Research, 42*. https://doi.org/10.1029/2005WR004065

Woldesenbet, T. A., Elagib, N. A., Ribbe, L., & Heinrich, J. (2017). Hydrological responses to land use/cover changes in the source region of the Upper Blue Nile Basin, Ethiopia. *Science of the Total Environment*, *575*, 724–741. https://doi.org/10.1016/j.scitotenv.2016.09.124

Woldesenbet, T., Elagib, N. A., Ribbe, L., & Heinrich, J. (2018). Catchment response to climate and land use changes in the Upper Blue Nile sub-basins, Ethiopia. *Science of the Total Environment*, *644*, 193–206. https://doi.org/10.1016/j.scitotenv.2018.06.198

World Bank. (2006). Ethiopia: Managing Water Resources to Maximize Sustainable Growth. A World Bank Water Resources Assistance Strategy for Ethiopia. Washington. Retrieved from http://siteresources.worldbank.org/INTWRD/Resources/Ethiopia_final_text_and_cover.pdf

World Bank. (2017). World Bank Data: Ethiopia. Retrieved 12/07/2019, from https://data.worldbank.org/indicator/SP.POP.TOTL?locations=ET.

World Bank. (2019). Climate Change Knowledge Portal. Retrieved 12/07/2019, from https://climateknowledgeportal.worldbank.org/country/ethiopia/climate-data-projections. https://doi.org/10.1016/j.jhydrol.2008.05.012

Worqlul, A. W., Dile, Y. T., Ayana, E. K., Jeong, J., Adem, A. A., & Gerik, T. (2018). Impact of climate change on streamflow hydrology in headwater catchments of the upper Blue Nile Basin, Ethiopia. *Water*, *10*(2), 1–18. https://doi.org/10.3390/w10020120

Wulong, B., Pengfei, D., Tie, L., Anming, B., Min, L., Mujtaba, H., & Chengxin, Q. (2018). Simulating hydrological responses to climate change using dynamic and statistical downscaling methods: a case study in the Kaidu River Basin, Xinjiang, China. *Journal of Arid Land*, *10*(6), 905–920. https://doi.org/10.1007/s40333-018-0068-0

Xu, H., Xu, C., Zhou, B., & Singh, V.P. (2013). Modelling runoff response to land-use change using an integrated approach in Xiangjiang River basin, China. *Climate and Land Surface Changes in Hydrology, Proceedings of H01, IAHS-IAPSO-IASPEI Assembly*, Gothenburg, Sweden, July 2013 (IAHS Publ. 359, 2013) 390-396.

Yalew, S., van Griensven, A. Ray, N., Kokoszkiewicz, L., & Betrie, G. D. (2013). Environmental Modelling & Software Distributed computation of large scale SWAT models on the Grid. *Environmental Modelling and Software*, *41*, 223–230. https://doi.org/10.1016/j.envsoft.2012.08.002

Yan, R., Cai, Y., Li, C., Wang, X., & Liu, Q. (2019). Hydrological responses to climate and land use changes in a watershed of the Loess Plateau, China. *Sustainability*, *11*(5), 1–19. https://doi.org/10.3390/su11051443

Yang, J., & Duan, K. (2016). Effects of initial drivers and land use on WRF modeling for near-surface fields and atmospheric boundary layer over the Northeastern Tibetan Plateau. *Advances in Meteorology*, 1–16. https://doi.org/10.1155/2016/7849249

Yhang, Y. Bin, Sohn, S. J., & Jung, I. W. (2017). Application of Dynamical and Statistical Downscaling to East Asian Summer Precipitation for Finely Resolved Datasets. *Advances in Meteorology*, 1–9. https://doi.org/10.1155/2017/2956373

Yin, J., He, F., Xiong, Y., & Qiu, G. (2017). Effects of land use and climate changes on surface runoff in a semi-humid and semi-arid transition zone in northwest China. *Hydrology and Earth System Sciences*, *21*, 183–196. https://doi.org/10.5194/hess-21-183-2017

Zeyaeyan, S., Fattahi, E., Ranjbar, A., Azadi, M., & Vazifedoust, M. (2017). Evaluating the Effect of Physics Schemes in WRF Simulations of Summer Rainfall in North West Iran. *Climate*, *5*(48), 1–17. https://doi.org/10.3390/cli5030048

Zhang, B., Shrestha, N. K., Daggupati, P., Rudra, R., Shukla, R., Kaur, B., & Hou, J. (2018). Quantifying the impacts of climate change on streamflow dynamics of two major rivers of the Northern Lake Erie basin in Canada. *Sustainability*, *10*(8), 1–23. https://doi.org/10.3390/su10082897

Zhang, C., Li, W., & Travis, D. (2007). Gaps-fill of SLC-off Landsat ETM+ satellite image using

a geostatistical approach. *International Journal of Remote Sensing*, *28*(22), 5103–5122. https://doi.org/10.1080/01431160701250416

Zhang, X. P., Zhang, L., & Zhao, J. (2008). Responses of stream flow to changes in climate and land use/cover in the Loess Plateau, China. Water Resource Research, 44

Zhu, Z., Broersma, K., & Mazumder, A. (2012). Impacts of Land Use, Fertilizer and Manure Application on the Stream Nutrient Loadings in the Salmon River Watershed, South-Central British Columbia, Canada. *Journal of Environmental Protection, 3,* 809-822. https://doi.org/10.4236/jep.2012.328096

Zu-Heng, H., Zhong-Feng, X., Ning-Fang, Z., Ma, Z. G., & Guo-Ping, L. (2014). Evaluation of the WRF Model with Different Land Surface Schemes: A Drought Event Simulation in Southwest China during 2009–10. *Atmospheric and Oceanic Science Letters*, *7*(2), 168–173. https://doi.org/10.3878/j.issn.1674-2834.13.0079

APPENDICES

Appendix 1. namelist.wps for WRF preprocessing system.

```
&share
 wrf_core = 'ARW',
 max_dom = 3,
 start_date = '2044-12-31_00:00:00','2044-12-31_00:00:00','2044-12-31_00:00:00',
 end_date   = '2045-01-31_00:00:00','2045-01-31_00:00:00','2045-01-31_00:00:00',
 interval_seconds = 21600
 io_form_geogrid = 2,
/

&geogrid
 parent_id         =   1,   1,    2,
 parent_grid_ratio =   1,   3,    3,
 i_parent_start    =   1,   16,   33,
 j_parent_start    =   1,   13,   61,
 e_we              =   79,  103,  70,
 e_sn              =   57,  112,  85,

  geog_data_res =
'gmted2010_30s+usgs_lakes+30s+nesdis_greenfrac+10m+usgs_lakes_30s','gmted2010_30s+usg
s_lakes+30s+nesdis_greenfrac+2m+usgs_lakes_30s','gmted2010_30s+usgs_lakes+30s+nesdis_g
reenfrac+10m+usgs_lakes_30s',
 dx = 36000,
 dy = 36000,
 map_proj  = 'mercator',
 ref_lat   =  9.0,
 ref_lon   =  40.5,
 truelat1  =  9.0,
 truelat2  =  60.0,
 stand_lon =  40.5,
 geog_data_path = '/home/ashenafi45/WRF_Data/geog/'
/

&ungrib
 out_format = 'WPS',
 prefix = 'CCSM4_CMIP5_MOAR_BC_RCP45',
/

&metgrid
 fg_name = 'CCSM4_CMIP5_MOAR_BC_RCP45',
 io_form_metgrid = 2,
/
```

Appendix 2. namelist.input for WRF Simulation.

```
&time_control
 run_days                  = 06,
 run_hours                 = 0,
 run_minutes               = 0,
 run_seconds               = 0,
 start_year                = 2044, 2044, 2044,
 start_month               = 12,   12,   12,
 start_day                 = 31,   31,   31,
 start_hour                = 00,   00,   00,
 start_minute              = 00,   00,   00,
 start_second              = 00,   00,   00,
 end_year                  = 2045, 2045, 2045,
 end_month                 = 01,   01,   01,
 end_day                   = 06,   06,   06,
 end_hour                  = 00,   00,   00,
 end_minute                = 00,   00,   00,
 end_second                = 00,   00,   00,
 interval_seconds          = 21600
 input_from_file           = .true.,.true.,.true.,
 history_interval          = 1440,  1440,   1440,
 frames_per_outfile        = 1000, 1000, 1000,
 restart                   = .false.,
 restart_interval          = 14320
 io_form_history           = 2
 io_form_restart           = 2
 io_form_input             = 2
 io_form_boundary          = 2
 io_form_auxinput2         = 2
 debug_level               = 0
 output_diagnostics        = 1
 auxinput4_inname          = "wrflowinp_d<domain>"
 auxinput4_interval        = 720, 720, 720,
 io_form_auxinput4         = 2,
 auxhist3_outname          = "wrfxtrm_d<domain>"
 io_form_auxhist3          = 2
 auxhist3_interval         = 1440,    1440,    1440,
 frames_per_auxhist3       = 1000,
 /

 &domains
 time_step                 = 180,
 time_step_fract_num       = 0,
 time_step_fract_den       = 1,
 max_dom                   = 3,
 i_parent_start            = 1,   16,   33,
```

j_parent_start = 1, 13, 61,
e_we = 79, 103, 70,
e_sn = 57, 112, 85,
e_vert = 35, 35, 35,
p_top_requested = 5000,
num_metgrid_levels = 27,
num_metgrid_soil_levels = 4,
eta_levels = 1.0000, 0.9974, 0.9940, 0.9900, 0.9854, 0.9796, 0.9723, 0.9635, 0.9528, 0.9401, 0.9252, 0.9079, 0.8882, 0.8659, 0.8410, 0.8133, 0.7828, 0.7494, 0.7133, 0.6742, 0.6323, 0.5878, 0.5406, 0.4915, 0.4409, 0.3895, 0.3379, 0.2871, 0.2378, 0.1907, 0.1465, 0.1056, 0.0682, 0.0332, 0.0000
dx = 36000, 12000, 4000,
dy = 36000, 12000, 4000,
grid_id = 1, 2, 3,
parent_id = 1, 1, 2,
parent_grid_ratio = 1, 3, 3,
parent_time_step_ratio = 1, 3, 3,
feedback = 0,
smooth_option = 0,
/

&physics
mp_physics = 8, 8, 8,
ra_lw_physics = 4, 4, 4,
ra_sw_physics = 4, 4, 4,
radt = 30, 30, 30,
sf_sfclay_physics = 1, 1, 1,
sf_surface_physics = 2, 2, 2,
bl_pbl_physics = 1, 1, 1,
bldt = 0, 0, 0,
cu_physics = 1, 1, 0,
cudt = 5, 5, 5,
num_soil_layers = 4,
num_land_cat = 28,
sst_update = 1,
isfflx = 1,
icloud = 2,
kfeta_trigger = 2,
ifsnow = 0,
maxiens = 1,
maxens = 3,
maxens2 = 3,
maxens3 = 16,
ensdim = 144,
slope_rad = 1,
topo_shading = 1,

```
shadlen                  = 25000.,
surface_input_source     = 1,
sf_urban_physics         = 0,
shcu_physics             = 1,
prec_acc_dt              = 1440,  1440,   1440,
mp_zero_out              = 2
mp_zero_out_thresh       = 1.0E-8
/

&fdda
/

&dynamics
w_damping                = 1,
diff_opt                 = 1,      1,      1,
km_opt                   = 4,      4,      4,
diff_6th_opt             = 2,      2,      0,
diff_6th_factor          = 0.12,   0.12,   0.12,
base_temp                = 290.
damp_opt                 = 3,
zdamp                    = 5000.,  5000.,  5000.,
dampcoef                 = 0.2,    0.2,    0.2
khdif                    = 0,      0,      0,
kvdif                    = 0,      0,      0,
non_hydrostatic          = .true., .true., .true.,
moist_adv_opt            = 2,      2,      1,
scalar_adv_opt           = 2,      2,      1,
/

&bdy_control
spec_bdy_width           = 5,
spec_zone                = 1,
relax_zone               = 4,
specified                = .true., .false.,.false.,
nested                   = .false., .true., .true.,
/

&grib2
/

&namelist_quilt
nio_tasks_per_group      = 0,
nio_groups               = 1,
/
```

Appendix 3. Meteorological stations with geographic coordinate and class.

No.	Stations	Latitude	Longitude	Class
1	Addis Zemen	12.12	37.77	3
2	Adet	11.27	37.49	1
3	Ambagiorgis	12.77	37.62	3
4	Amed Ber	11.91	37.89	3
5	Aykel	12.54	37.06	1
6	Bahir Dar	11.60	37.38	1
7	Chanchok	12.40	37.04	3
8	Chandiba	12.33	37.03	3
9	Dangila	11.25	36.85	1
10	Debre Tabor	11.87	38.00	1
11	Deke Estifanos	11.90	37.27	3
12	Delgi	12.19	37.06	4
13	Dera Hamusite	11.79	37.56	3
14	Enfranz	12.26	37.63	3
15	Enjibara	11.00	36.89	4
16	Gassay	11.79	38.13	3
17	Gonder	12.52	37.43	1
18	Maksegnit	12.39	37.56	3
19	Mekaneyesus	11.58	37.90	3
20	Merawi	11.41	37.16	3
21	Meshenti	11.47	37.29	4
22	Sekela	10.99	37.21	3
23	Shahura	11.93	36.87	3
24	Tis Abay	11.49	37.58	4
25	Wanzaye	11.78	37.68	3
26	Wetet Abay	11.37	37.03	3
27	Woreta	11.92	37.70	3
28	Zege	11.71	37.32	3

Appendix 4. The SWAT model calibration paramters for Gilgel Abay, Gumara, Ribb and Megech watersheds.

No.	Parameter Name		Gilgel Abay	Gumara	Ribb	Megech
1	r__CN2.mgt	SCS runoff curve number	-0.065	-0.031	-0.11	-0.147
2	v__ALPHA_BF.gw	Base-flow alpha factor (Days)	0.1	0.067	0.22	0.1
3	v__GW_DELAY.gw	Groundwater delay (Days)	36.7	24	21.69	76
4	v__GWQMN.gw	Threshold depth of water in the shallow aquifer required for return flow to occur (mm)	4.75	1.23	4.91	2.57
5	v__ GW_REVAP.gw	Groundwater "revap" coefficient	0.19	0.07	0.13	0.17
8	v__REVAPMN.gw	Threshold depth of water in the shallow aquifer for "revap" to occur (mm)	4.49	3.17	8.79	4.53
6	v__RCHRG_DP.gw	Deep aquifer percolation fraction	0.58	0.04	0.82	0.82
7	v__GWHT.gw	Initial groundwater height (m)	8.71	1.19	6.19	5.75
9	r__SOL_AWC.sol	Available water capacity of the soil layer	-0.027	0.01	-0.04	0.07
10	r__SOL_K.sol	Saturated hydraulic conductivity (mm/hr)	0.034	0.029	0.19	0.13
18	v__CH_K2.rte	Effective hydraulic conductivity in main channel alluvium (mm/hr)	23.9	21.64	19.68	25.96
17	v__CH_N2.rte	Manning's "n" value for the main channel	0.23	0.11	0.19	0.2
16	v__SURLAG.bsn	Surface runoff lag time	6.05	2.43	6.73	2.04
13	r__OV_N.hru	Manning's "n" value for overland flow	0.10	-0.10	0.15	-0.05
12	v__EPCO.hru	Plant uptake compensation factor	0.88	0.303	0.92	0.64
11	v__ESCO.hru	Soil evaporation compensation factor	0.65	0.857	0.64	0.53
14	r__SLSUBBSN.hru	Average slope length	0.10	-0.12	-0.03	0.13
15	v__CANMX.hru	Maximum canopy storage	27.48	12.52	33.80	15.16

Appendix 5. Average seasonal hydrological parameters for Baseline, RCP4.5 and RCP8.5 scenarios in Gilgel Abay watershed.

Baseline scenario (2005 - 2015)									
Season	PRECIP (mm)	PET (mm)	ET (mm)	SW (mm)	PERC (mm)	SURQ (mm)	GW_Q (mm)	WYLD (mm)	LAT_Q (mm)
Winter	30.5	383.8	50.5	262.7	0.0	3.4	0.0	4.6	1.2
Spring	284.0	429.1	188.5	245.5	12.5	55.1	0.1	56.7	1.5
Summer	1323.4	259.0	222.5	536.8	352.3	659.1	53.4	722.6	10.1
Autumn	428.1	394.3	208.6	348.4	111.0	186.3	38.2	232.3	7.8
Annual	2066.0	1466.2	670.1	1393.4	475.9	904.0	91.7	1016.2	20.5
RCP4.5 scenario (2045 - 2055)									
Season	PRECIP (mm)	PET (mm)	ET (mm)	SW (mm)	PERC (mm)	SURQ (mm)	GW_Q (mm)	WYLD (mm)	LAT_Q (mm)
Winter	51.4	361.4	61.9	253.2	0.0	1.0	0.0	2.2	1.2
Spring	443.1	401.9	246.8	358.9	68.7	104.1	0.3	107.4	3.0
Summer	1432.8	290.7	236.6	558.8	340.6	748.0	50.3	807.4	9.1
Autumn	415.2	451.3	173.7	329.2	138.5	206.3	37.1	251.8	8.4
Annual	2342.4	1505.3	719.0	1500.1	547.8	1059.3	87.7	1168.8	21.7
RCP8.5 scenario (2045 - 2055)									
Season	PRECIP (mm)	PET (mm)	ET (mm)	SW (mm)	PERC (mm)	SURQ (mm)	GW_Q (mm)	WYLD (mm)	LAT_Q (mm)
Winter	35.5	383.3	46.7	269.3	0.1	2.4	0.0	3.7	1.3
Spring	286.8	455.7	259.6	201.0	4.1	43.9	0.0	45.3	1.4
Summer	1713.9	281.9	239.4	539.5	386.9	955.4	58.3	1024.2	10.6
Autumn	608.0	412.6	241.5	355.5	154.7	293.0	47.3	349.3	9.0
Annual	2644.2	1533.5	787.1	1365.4	545.8	1294.6	105.6	1422.5	22.3

Note: PRECIP = Precipitation; PET = Potential Evapotranspiration; ET = Actual evapotranspiration; SW = Soil water content; PERC = Percolation; SURQ = Surface runoff; GW_Q = Groundwater flow; WYLD = Total water yield; and LAT_Q = Lateral flow.

Appendix 6. Average seasonal hydrological parameters for Baseline, RCP4.5 and RCP8.5 scenarios in Gumara watershed.

Baseline scenario (2005 - 2015)									
Season	PRECIP (mm)	PET (mm)	ET (mm)	SW (mm)	PERC (mm)	SURQ (mm)	GW_Q (mm)	WYLD (mm)	LAT_Q (mm)
Winter	15.1	407.0	32.7	256.6	0.2	1.2	1.6	4.3	1.5
Spring	185.9	473.3	139.8	209.2	8.5	36.6	5.0	42.8	1.3
Summer	1015.1	312.2	228.4	438.8	285.1	413.0	216.4	639.9	10.6
Autumn	249.2	420.4	145.8	316.7	68.6	82.4	119.7	211.0	8.9
Annual	1465.2	1612.8	546.7	1221.2	362.5	533.2	342.6	898.1	22.4
RCP4.5 scenario (2045 - 2055)									
Season	PRECIP (mm)	PET (mm)	ET (mm)	SW (mm)	PERC (mm)	SURQ (mm)	GW_Q (mm)	WYLD (mm)	LAT_Q (mm)
Winter	30.6	385.6	41.8	244.2	0.0	0.2	0.0	1.4	1.2
Spring	506.5	435.6	220.8	355.7	91.0	165.2	76.2	246.3	4.9

Summer	838.9	384.6	220.1	452.9	193.2	353.3	134.9	496.0	7.7
Autumn	162.9	461.9	122.4	305.7	56.4	53.2	107.8	168.8	7.8
Annual	1538.9	1667.8	605.1	1358.5	340.6	571.9	318.8	912.4	21.6
RCP8.5 scenario (2045 - 2055)									
Season	PRECIP (mm)	PET (mm)	ET (mm)	SW (mm)	PERC (mm)	SURQ (mm)	GW_Q (mm)	WYLD (mm)	LAT_Q (mm)
Winter	21.1	365.9	29.7	248.0	0.0	0.1	0.0	1.5	1.4
Spring	270.4	435.1	198.5	254.8	17.0	46.5	13.1	62.3	2.7
Summer	1247.8	337.7	227.2	443.9	282.1	650.3	232.9	894.0	10.8
Autumn	302.4	398.2	157.6	307.2	98.2	110.4	128.9	248.4	9.1
Annual	1841.7	1536.8	613.1	1253.9	397.4	807.3	374.9	1206.3	24.0

Appendix 7. Average seasonal hydrological parameters for Baseline, RCP4.5 and RCP8.5 scenarios in Ribb watershed.

Baseline scenario (2005 - 2015)									
Season	PRECIP (mm)	PET (mm)	ET (mm)	SW (mm)	PERC (mm)	SURQ (mm)	GW_Q (mm)	WYLD (mm)	LAT_Q (mm)
Winter	12.8	399.0	27.3	156.8	0.3	0.4	1.4	3.3	1.5
Spring	177.5	475.7	134.9	127.6	17.0	18.1	1.3	21.7	2.3
Summer	1079.7	304.3	246.6	345.0	432.8	308.8	50.7	381.0	21.5
Autumn	255.9	413.2	158.2	208.1	80.6	64.4	37.2	114.6	13.1
Annual	1526.0	1592.2	567.1	837.4	530.7	391.7	90.6	520.7	38.4
RCP4.5 scenario (2045 - 2055)									
Season	PRECIP (mm)	PET (mm)	ET (mm)	SW (mm)	PERC (mm)	SURQ (mm)	GW_Q (mm)	WYLD (mm)	LAT_Q (mm)
Winter	29.3	378.6	36.5	151.2	0.0	0.0	0.6	1.7	1.1
Spring	568.1	433.7	254.6	276.5	163.8	120.8	20.8	153.0	11.3
Summer	904.5	363.3	240.7	369.0	306.1	265.3	35.0	316.6	16.2
Autumn	134.2	442.9	151.0	206.1	49.6	10.7	33.0	55.3	11.6
Annual	1636.1	1618.4	682.8	1002.7	519.5	396.9	89.5	526.6	40.2
RCP8.5 scenario (2045 - 2055)									
Season	PRECIP (mm)	PET (mm)	ET (mm)	SW (mm)	PERC (mm)	SURQ (mm)	GW_Q (mm)	WYLD (mm)	LAT_Q (mm)
Winter	20.5	396.3	28.5	159.0	0.0	0.0	1.3	2.7	1.5
Spring	311.7	479.6	246.4	136.0	41.6	29.7	5.8	41.3	5.8
Summer	1164.5	356.1	263.0	341.7	391.3	396.0	49.1	466.3	21.2
Autumn	342.4	425.3	176.2	206.9	136.5	87.4	41.6	144.7	15.7
Annual	1839.0	1657.4	714.2	843.7	569.4	513.2	97.7	655.1	44.2

Appendix 8. Average seasonal hydrological parameters for Baseline, RCP4.5 and RCP8.5 scenarios in Megech watershed.

Baseline scenario (2005 - 2015)									
Season	PRECIP (mm)	PET (mm)	ET (mm)	SW (mm)	PERC (mm)	SURQ (mm)	GW_Q (mm)	WYLD (mm)	LAT_Q (mm)
Winter	9.9	438.0	19.0	51.6	0.0	0.0	12.0	13.5	1.4
Spring	140.7	529.2	109.4	64.6	10.6	5.4	4.2	12.0	2.5
Summer	803.1	307.3	247.5	194.4	378.7	108.9	19.3	149.2	21.0
Autumn	209.3	429.9	166.0	77.8	62.2	24.1	40.2	78.9	14.6
Annual	1163.0	1704.4	541.8	388.5	451.5	138.4	75.7	253.6	39.4
RCP4.5 scenario (2045 - 2055)									
Season	PRECIP (mm)	PET (mm)	ET (mm)	SW (mm)	PERC (mm)	SURQ (mm)	GW_Q (mm)	WYLD (mm)	LAT_Q (mm)
Winter	8.8	428.8	14.3	48.0	0.0	0.0	10.6	11.6	1.0
Spring	321.6	480.6	233.5	132.7	68.1	7.6	7.4	22.7	7.7
Summer	781.4	375.3	210.7	188.9	338.5	154.2	16.3	187.4	16.9
Autumn	84.2	506.6	119.7	68.6	17.2	2.5	36.9	53.0	13.6
Annual	1196.1	1791.3	578.1	438.2	423.7	164.3	71.2	274.7	39.3
RCP8.5 scenario (2045 - 2055)									
Season	PRECIP (mm)	PET (mm)	ET (mm)	SW (mm)	PERC (mm)	SURQ (mm)	GW_Q (mm)	WYLD (mm)	LAT_Q (mm)
Winter	6.4	454.0	11.8	47.7	0.0	0.0	10.2	11.1	1.0
Spring	188.0	560.0	172.3	40.3	11.7	1.8	3.8	9.3	3.8
Summer	876.5	342.6	256.5	181.6	367.5	167.8	24.2	215.2	23.2
Autumn	139.1	475.3	124.7	61.6	57.0	8.5	35.4	56.0	12.1
Annual	1210.0	1832.0	565.3	331.1	436.2	178.1	73.6	291.6	40.0

Appendix 9. Mean monthly hydrological parameters for combined simulation under present land-use (PER) and climate (Baseline, RCP4.5 and RCP8.5) scenarios in Gumara watershed.

PER land-use + Baseline climate = REF simulation (2005 - 2015)									
Month	PRECIP (mm)	PET (mm)	ET (mm)	SW (mm)	PERC (mm)	SURQ (mm)	GW_Q (mm)	WYLD (mm)	LAT_Q (mm)
1	7.2	135.0	12.4	84.8	0.1	0.7	0.1	1.3	0.5
2	0.3	146.4	5.5	79.6	0.0	0.0	0.0	0.3	0.2
3	35.4	158.9	35.7	75.1	0.5	3.3	0.2	3.9	0.3
4	29.8	167.4	44.8	56.0	0.1	3.6	0.3	4.2	0.3
5	120.8	146.9	57.9	80.0	8.1	29.4	4.5	34.7	0.7
6	188.4	120.6	62.5	128.7	21.1	53.4	9.8	64.4	1.2
7	418.9	93.1	79.5	160.1	119.2	181.5	72.6	257.8	3.7
8	407.7	98.4	88.0	150.7	146.9	174.9	135.7	316.4	5.8
9	163.2	145.3	82.3	116.6	58.3	54.1	92.7	151.6	4.8
10	43.6	150.3	37.4	100.2	5.5	16.7	23.4	42.8	2.7
11	42.3	124.9	27.4	98.7	5.0	10.8	4.1	16.4	1.5
12	7.6	125.6	14.9	90.7	0.2	0.4	1.5	2.8	0.9
Annual	1465.1	1612.7	548.4	1221.2	365.0	528.8	345.0	896.6	22.6

PER land-use + RCP4.5 climate = PER4.5 simulation (2045 - 2055)									
Month	PRECIP (mm)	PET (mm)	ET (mm)	SW (mm)	PERC (mm)	SURQ (mm)	GW_Q (mm)	WYLD (mm)	LAT_Q (mm)
1	9.7	129.1	14.0	81.2	0.0	0.0	0.0	0.3	0.3
2	10.1	137.5	14.0	77.1	0.0	0.1	0.0	0.4	0.2
3	121.5	155.7	55.0	103.6	3.2	35.2	0.8	36.5	0.5
4	260.1	102.7	93.1	152.5	54.5	58.5	29.6	90.1	2.0
5	125.0	177.1	71.9	100.0	34.4	70.6	46.8	119.9	2.6
6	117.2	151.4	55.3	129.4	4.5	26.8	9.0	37.3	1.4
7	316.3	122.7	76.2	163.4	52.3	149.5	24.8	176.3	1.9
8	405.1	110.5	90.9	160.0	136.9	173.6	101.3	279.3	4.4
9	150.2	159.6	82.4	120.7	52.7	52.2	83.1	139.6	4.3
10	12.3	158.9	31.8	96.6	3.9	0.5	24.9	27.8	2.4
11	0.2	143.4	9.2	87.6	0.0	0.0	0.4	1.5	1.1
12	10.8	118.9	13.9	84.5	0.0	0.0	0.0	0.6	0.6
Annual	1538.5	1667.7	607.7	1356.5	342.5	567.3	320.7	909.8	21.9
PER land-use + RCP8.5 climate = PER8.5 simulation (2045 - 2055)									
Month	PRECIP (mm)	PET (mm)	ET (mm)	SW (mm)	PERC (mm)	SURQ (mm)	GW_Q (mm)	WYLD (mm)	LAT_Q (mm)
1	1.7	128.8	6.6	80.0	0.0	0.0	0.0	0.4	0.4
2	18.4	112.0	14.4	83.8	0.0	0.1	0.0	0.4	0.2
3	97.3	137.3	69.1	84.1	8.4	17.9	5.2	24.0	0.9
4	71.7	147.9	65.5	83.7	0.8	5.2	2.7	8.7	0.7
5	101.4	150.0	62.9	89.2	8.5	23.3	5.7	30.1	1.1
6	257.9	113.6	65.9	145.1	38.0	94.7	15.2	111.3	1.4
7	654.4	103.3	79.6	138.8	173.8	398.6	119.5	522.8	4.7
8	335.3	120.9	83.8	160.2	71.9	153.3	99.6	257.8	4.8
9	203.9	138.6	82.0	110.6	87.7	81.1	94.5	180.3	4.7
10	78.8	135.7	48.2	104.6	10.6	24.8	32.6	60.3	3.0
11	19.6	123.9	27.8	92.1	0.5	3.7	2.6	7.9	1.6
12	0.9	125.2	8.8	84.2	0.0	0.0	0.0	0.8	0.8
Annual	1841.5	1537.2	614.6	1256.2	400.2	802.7	377.6	1204.7	24.4

Appendix 10. Mean monthly hydrological parameters for combined simulation under Business-as-usual (BAU) and climate (Baseline, RCP4.5 and RCP8.5) scenarios in Gumara watershed.

BAU land-use + Baseline climate = BAUB simulation (2045 - 2055)									
Month	PRECIP (mm)	PET (mm)	ET (mm)	SW (mm)	PERC (mm)	SURQ (mm)	GW_Q (mm)	WYLD (mm)	LAT_Q (mm)
1	7.2	135.0	12.3	84.9	0.1	0.9	0.1	1.3	0.4
2	0.3	146.4	5.5	79.7	0.0	0.0	0.0	0.2	0.2
3	35.4	158.9	35.9	74.7	0.4	3.7	0.2	4.2	0.3
4	29.8	167.4	45.0	55.2	0.1	4.0	0.3	4.6	0.3
5	120.8	146.9	57.7	78.5	7.0	31.4	3.9	36.0	0.7
6	188.4	120.6	61.9	126.9	19.0	56.6	8.6	66.4	1.1
7	418.9	93.1	79.1	158.4	111.6	189.7	67.3	260.5	3.5

8	407.7	98.4	87.6	149.5	139.2	182.8	128.2	316.5	5.5
9	163.2	145.3	81.7	116.4	54.8	57.2	87.6	149.4	4.6
10	43.6	150.3	37.0	100.3	4.9	17.6	21.7	41.9	2.6
11	42.3	124.9	27.1	98.7	4.5	11.7	3.6	16.7	1.4
12	7.6	125.6	14.7	90.9	0.1	0.5	1.3	2.6	0.8
Annual	1465.1	1612.7	545.5	1214.3	341.7	556.2	322.8	900.4	21.4
BAU land-use + RCP4.5 climate = BAU4.5 simulation (2045 - 2055)									
Month	PRECIP (mm)	PET (mm)	ET (mm)	SW (mm)	PERC (mm)	SURQ (mm)	GW_Q (mm)	WYLD (mm)	LAT_Q (mm)
1	9.7	129.1	14.0	81.4	0.0	0.0	0.0	0.3	0.3
2	10.1	137.5	13.9	77.3	0.0	0.2	0.0	0.4	0.2
3	121.5	155.7	55.1	101.9	2.8	37.6	0.7	38.7	0.4
4	260.1	102.7	93.2	151.3	49.7	63.0	26.5	91.3	1.9
5	125.0	177.1	71.7	99.9	31.2	73.1	42.9	118.4	2.4
6	117.2	151.4	54.4	128.3	3.9	29.4	7.9	38.6	1.4
7	316.3	122.7	75.4	161.3	48.2	155.6	22.7	180.2	1.8
8	405.1	110.5	90.4	158.3	128.8	182.2	94.8	281.2	4.2
9	150.2	159.6	81.7	120.1	49.2	55.3	78.0	137.3	4.1
10	12.3	158.9	31.4	96.6	3.6	0.7	23.0	26.1	2.3
11	0.2	143.4	9.1	87.8	0.0	0.0	0.3	1.3	1.0
12	10.8	118.9	13.7	84.7	0.0	0.1	0.0	0.6	0.6
Annual	1538.5	1667.7	604.1	1349.0	317.4	597.2	296.7	914.6	20.6
BAU land-use + RCP8.5 climate = BAU8.5 simulation (2045 - 2055)									
Month	PRECIP (mm)	PET (mm)	ET (mm)	SW (mm)	PERC (mm)	SURQ (mm)	GW_Q (mm)	WYLD (mm)	LAT_Q (mm)
1	1.7	128.8	6.6	79.7	0.0	0.0	0.0	0.4	0.4
2	18.4	112.0	14.4	83.5	0.0	0.2	0.0	0.4	0.2
3	97.3	137.3	69.3	83.2	7.3	19.6	4.5	25.0	0.8
4	71.7	147.9	65.4	82.3	0.6	6.1	2.3	9.0	0.7
5	101.4	150.0	62.5	88.1	6.8	25.1	4.5	30.6	1.0
6	257.9	113.6	65.2	143.2	35.1	99.4	13.7	114.4	1.3
7	654.4	103.3	79.2	138.0	163.8	408.3	112.0	524.7	4.5
8	335.3	120.9	83.4	158.3	66.9	160.1	93.7	258.3	4.6
9	203.9	138.6	81.9	110.4	82.6	84.8	88.8	178.0	4.4
10	78.8	135.7	48.0	104.2	9.3	26.7	30.1	59.6	2.8
11	19.6	123.9	27.4	91.6	0.5	4.2	2.1	7.7	1.5
12	0.9	125.2	8.6	83.9	0.0	0.0	0.0	0.8	0.7
Annual	1841.5	1537.2	611.7	1246.3	372.8	834.4	351.6	1208.9	22.9

Appendix 11. Mean monthly hydrological parameters for combined simulation under the expansion of forestland (EFL) and climate (Baseline, RCP4.5 and RCP8.5) scenarios in Gumara watershed.

EFL land-use + Baseline climate = EFLB simulation (2045 - 2055)									
Month	PRECIP (mm)	PET (mm)	ET (mm)	SW (mm)	PERC (mm)	SURQ (mm)	GW_Q (mm)	WYLD (mm)	LAT_Q (mm)
1	7.2	135.0	11.5	75.7	0.1	0.6	0.1	1.1	0.5
2	0.3	146.4	5.8	70.3	0.0	0.0	0.0	0.3	0.3
3	35.4	158.9	36.1	66.1	0.4	2.6	0.2	3.1	0.3
4	29.8	167.4	42.3	50.6	0.1	2.6	0.3	3.2	0.3
5	120.8	146.9	60.5	76.2	7.9	25.2	4.4	30.5	0.9
6	188.4	120.6	69.1	125.1	20.8	46.8	9.7	57.7	1.3
7	418.9	93.1	89.0	161.0	121.2	165.0	73.1	241.9	3.9
8	407.7	98.4	98.0	150.7	151.4	160.9	139.6	306.8	6.3
9	163.2	145.3	92.9	111.4	58.0	48.8	94.2	148.1	5.1
10	43.6	150.3	42.6	91.8	5.3	14.9	23.3	41.0	2.8
11	42.3	124.9	31.8	88.8	4.5	8.5	3.7	13.8	1.6
12	7.6	125.6	17.8	78.1	0.1	0.3	1.3	2.5	0.9
Annual	1465.1	1612.7	597.2	1145.9	369.9	476.1	349.8	850.0	24.0
EFL land-use + RCP4.5 climate = EFL4.5 simulation (2045 - 2055)									
Month	PRECIP (mm)	PET (mm)	ET (mm)	SW (mm)	PERC (mm)	SURQ (mm)	GW_Q (mm)	WYLD (mm)	LAT_Q (mm)
1	9.7	129.1	13.3	70.1	0.0	0.0	0.0	0.4	0.4
2	10.1	137.5	14.4	65.6	0.0	0.1	0.0	0.3	0.2
3	121.5	155.7	55.3	96.8	3.4	29.7	0.9	31.2	0.5
4	260.1	102.7	95.7	152.3	53.3	50.5	28.6	81.5	2.4
5	125.0	177.1	75.6	97.0	36.4	66.9	48.1	117.9	2.9
6	117.2	151.4	63.6	123.6	4.3	22.2	9.6	33.4	1.6
7	316.3	122.7	85.8	162.4	51.1	136.1	23.8	162.0	2.1
8	405.1	110.5	102.1	161.1	139.9	156.8	102.3	263.8	4.7
9	150.2	159.6	93.7	115.7	52.8	46.8	84.7	136.1	4.6
10	12.3	158.9	36.5	87.4	3.6	0.3	24.7	27.6	2.6
11	0.2	143.4	11.7	76.0	0.0	0.0	0.4	1.6	1.2
12	10.8	118.9	16.5	70.2	0.0	0.0	0.0	0.7	0.6
Annual	1538.5	1667.7	663.6	1278.2	344.9	509.5	323.2	856.4	23.7
EFL land-use + RCP8.5 climate = EFL8.5 simulation (2045 - 2055)									
Month	PRECIP (mm)	PET (mm)	ET (mm)	SW (mm)	PERC (mm)	SURQ (mm)	GW_Q (mm)	WYLD (mm)	LAT_Q (mm)
1	1.7	128.8	6.0	72.8	0.0	0.0	0.0	0.4	0.4
2	18.4	112.0	14.6	76.4	0.0	0.1	0.0	0.3	0.3
3	97.3	137.3	68.2	82.1	7.6	14.1	4.8	19.9	1.0
4	71.7	147.9	64.2	83.9	0.9	4.1	2.5	7.4	0.8
5	101.4	150.0	66.5	87.1	9.3	21.0	6.4	28.7	1.3
6	257.9	113.6	74.7	143.0	38.3	85.5	15.4	102.4	1.5
7	654.4	103.3	89.4	137.6	181.1	380.0	123.6	508.8	5.2

8	335.3	120.9	93.7	160.8	72.4	140.8	102.4	248.5	5.3
9	203.9	138.6	91.1	106.6	88.8	75.0	96.2	176.3	5.1
10	78.8	135.7	53.8	99.8	9.8	20.8	32.1	56.1	3.2
11	19.6	123.9	31.3	84.7	0.5	2.7	2.5	6.9	1.7
12	0.9	125.2	11.0	74.6	0.0	0.0	0.0	0.9	0.9
Annual	1841.5	1537.2	664.4	1209.5	408.7	744.2	385.9	1156.6	26.5

Appendix 12. Mean monthly hydrological parameters for combined simulation under the expansion of irrigation cropland (EIC) and climate (Baseline, RCP4.5 and RCP8.5) scenarios in Gumara watershed.

EIC land-use + Baseline climate = EICB simulation (2045 - 2055)									
Month	PRECIP (mm)	PET (mm)	ET (mm)	SW (mm)	PERC (mm)	SURQ (mm)	GW_Q (mm)	WYLD (mm)	LAT_Q (mm)
1	7.2	135.8	18.1	88.9	20.3	0.6	8.7	9.9	0.6
2	0.3	147.2	10.1	80.0	0.6	0.0	0.2	0.6	0.3
3	35.3	159.9	38.4	74.6	0.6	2.9	0.1	3.3	0.3
4	29.8	168.4	46.8	55.8	0.2	2.8	0.0	3.2	0.3
5	120.8	147.9	60.7	82.3	11.3	26.1	5.9	32.8	0.8
6	188.3	121.5	63.8	131.9	26.5	48.5	13.6	63.5	1.3
7	418.9	93.9	80.0	163.8	130.7	168.9	65.6	238.4	3.9
8	407.8	99.3	88.4	153.8	159.0	162.8	133.9	303.1	6.3
9	163.3	146.6	83.7	118.2	64.2	49.2	35.8	90.1	5.2
10	43.6	151.4	39.2	101.6	6.8	15.2	4.2	22.2	2.9
11	42.3	125.8	29.0	100.2	5.8	9.6	5.0	16.2	1.6
12	7.6	126.4	16.4	92.2	0.2	0.3	0.3	1.5	0.9
Annual	1465.2	1624.0	574.7	1243.3	426.1	486.9	273.3	784.8	24.6
EIC land-use + RCP4.5 climate = EIC4.5 simulation (2045 - 2055)									
Month	PRECIP (mm)	PET (mm)	ET (mm)	SW (mm)	PERC (mm)	SURQ (mm)	GW_Q (mm)	WYLD (mm)	LAT_Q (mm)
1	9.7	130.0	19.7	85.6	22.7	0.0	9.8	10.3	0.5
2	10.1	138.3	18.2	78.1	0.7	0.1	0.3	0.7	0.3
3	121.5	156.6	58.1	105.8	4.0	31.3	0.7	32.6	0.5
4	260.0	103.4	94.5	154.9	60.2	51.1	20.1	73.4	2.2
5	125.0	178.2	77.1	108.9	48.4	66.5	41.7	111.1	2.8
6	117.3	152.4	58.4	133.1	14.1	23.4	13.9	38.9	1.7
7	316.6	123.7	77.4	168.1	59.9	140.2	16.1	158.4	2.2
8	405.0	111.4	91.5	163.7	149.9	160.9	105.1	270.8	4.8
9	150.3	160.9	83.9	122.8	58.8	47.1	33.3	85.1	4.7
10	12.3	160.1	33.7	98.0	4.5	0.3	3.7	6.6	2.7
11	0.2	144.3	10.8	88.9	0.0	0.0	0.1	1.3	1.2
12	10.8	119.7	15.1	85.8	0.0	0.0	0.0	0.7	0.7
Annual	1538.9	1679.1	638.5	1393.7	423.1	520.9	244.9	790.0	24.2
EIC land-use + RCP8.5 climate = EIC8.5 simulation (2045 - 2055)									

Month	PRECIP (mm)	PET (mm)	ET (mm)	SW (mm)	PERC (mm)	SURQ (mm)	GW_Q (mm)	WYLD (mm)	LAT_Q (mm)
1	1.7	129.6	11.9	86.0	23.7	0.0	10.3	10.8	0.5
2	18.4	112.7	16.9	87.7	0.8	0.1	0.3	0.7	0.3
3	97.2	138.2	70.9	87.7	10.0	15.6	2.0	18.6	1.0
4	71.7	148.7	67.5	87.1	1.1	4.0	0.2	5.0	0.8
5	101.5	151.0	64.9	92.3	16.9	20.4	10.3	32.0	1.2
6	258.0	114.3	66.3	149.2	44.3	88.2	20.2	109.9	1.5
7	654.4	104.2	79.9	141.3	189.0	384.9	114.3	504.4	5.1
8	335.4	121.9	83.9	164.2	79.9	143.9	58.8	208.0	5.2
9	204.0	139.9	82.2	112.5	95.5	75.9	56.1	137.1	5.1
10	78.8	136.8	48.6	107.1	13.5	22.1	8.1	33.4	3.2
11	19.6	124.8	29.1	95.0	0.7	3.1	4.0	8.7	1.7
12	0.9	126.1	10.3	87.1	0.0	0.0	0.0	0.9	0.9
Annual	1841.7	1548.2	632.5	1297.3	475.5	758.1	284.6	1069.4	26.8

Appendix 13. The statistical measures of climate variables before bias correction (WRF) and after bias correction (WRF-BC) for Gumara watershed from 2005 to 2015.

Variables	Statistics	Observed	WRF	WRF-BC
Rainfall	Mean (mm/day)	3.90	4.87	4.03
	Bias (mm/day)	-	0.97	0.13
	Correlation	-	0.67	0.69
	RMSE (mm/day)	-	7.86	7.05
Maximum temperature (Tmax)	Mean (ºC)	25.23	23.01	25.19
	Bias (ºC)	-	-1.87	-0.04
	Correlation	-	0.72	0.85
	RMSE (ºC)	-	2.99	1.53
Minimum temperature (Tmin)	Mean (ºC)	9.85	11.90	9.86
	Bias (ºC)	-	1.45	0.01
	Correlation	-	0.68	0.82
	RMSE (ºC)	-	2.69	1.37

Note: WRF=Weather Research Forecasting (WRF) simulation before bias correction, and WRF-BC=Weather Research Forecasting (WRF) simulation after bias correction.

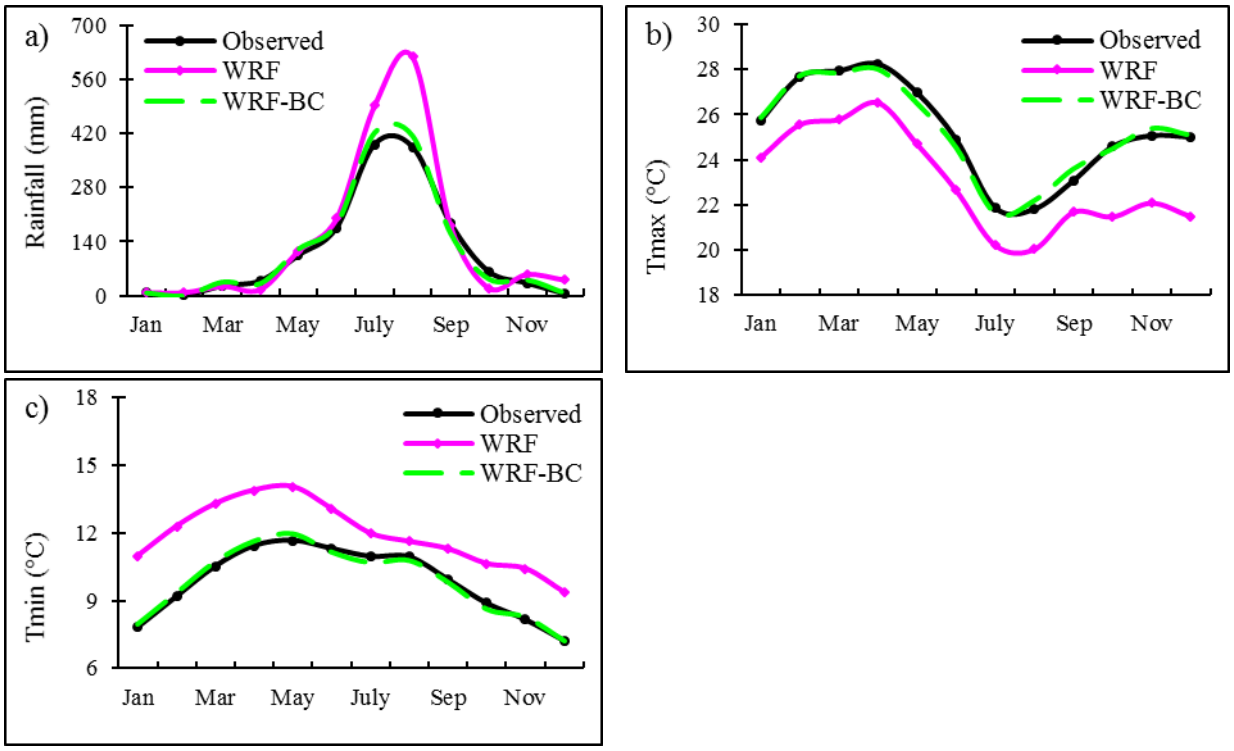

Appendix 14. Monthly mean observed and WRF simulated (before and after bias correction) rainfall (a), maximum temperature (b), and minimum temperature (c) from Gumara watershed during 2005-2015. WRF and WRF-BC represent model simulations before and after bias correction, respectively.

Apendix 15. Land cover class discriptions

Id	Land cover class	Description
1	**Cropland**	Cultivated and fallow land has a characteristic pattern, for example sharp edges between fields. Dark to grey and brown color in the Landsat image (4,3,2 band combination), unless the land lies fallow.
2	**Grassland**	Land under permanent and intensive grazing and bare land (land surface features devoid of vegetation). Homogeneous and have no pattern compared to agricultural land. Bright to white color in the Landsat image (4,3,2 band combination).
3	**Forest**	Refers to those areas covered with trees. There exists variation in vegetation between dense shrub/bush lands with an estimated cover of >50% and open shrub/bush lands with less than 50% cover. Red brown to bright red in the Landsat image (4,3,2 band combination).
4	**shrub land**	Refers to those areas covered with shrub and bushes. In the shrub lands, the vegetation cover is less than 50%, but not bare at all, but being degraded from competing use of grazing, cultivation, and deforestation as some of the degraded shrub/bush lands serve for grazing purposes. Red brown to bright red in the Landsat image (4,3,2 band combination).

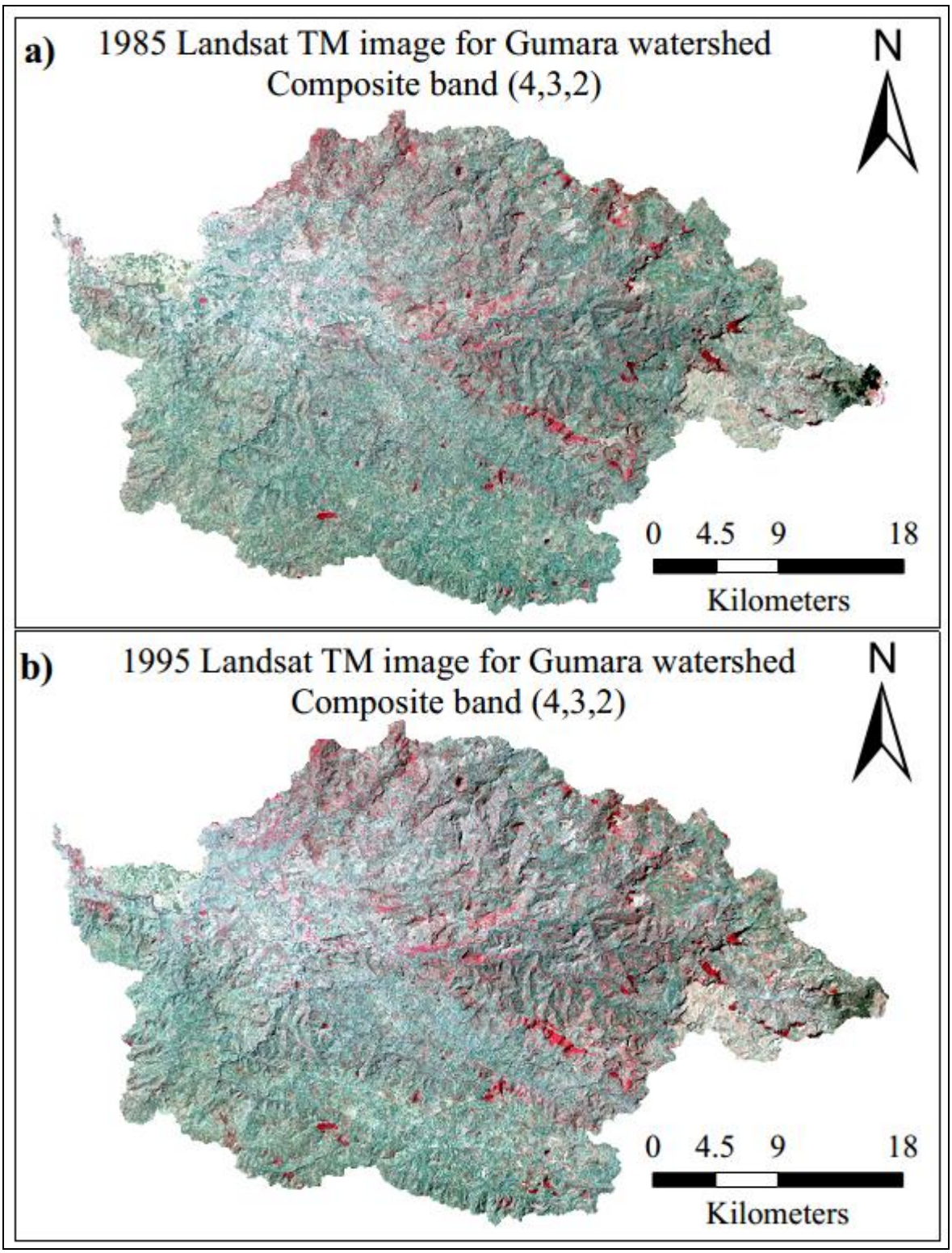

Appendix 16. The standard false color for composite Landsat TM satellite image of the year 1985 (a) and 1995 (b) for Gumara watershed.

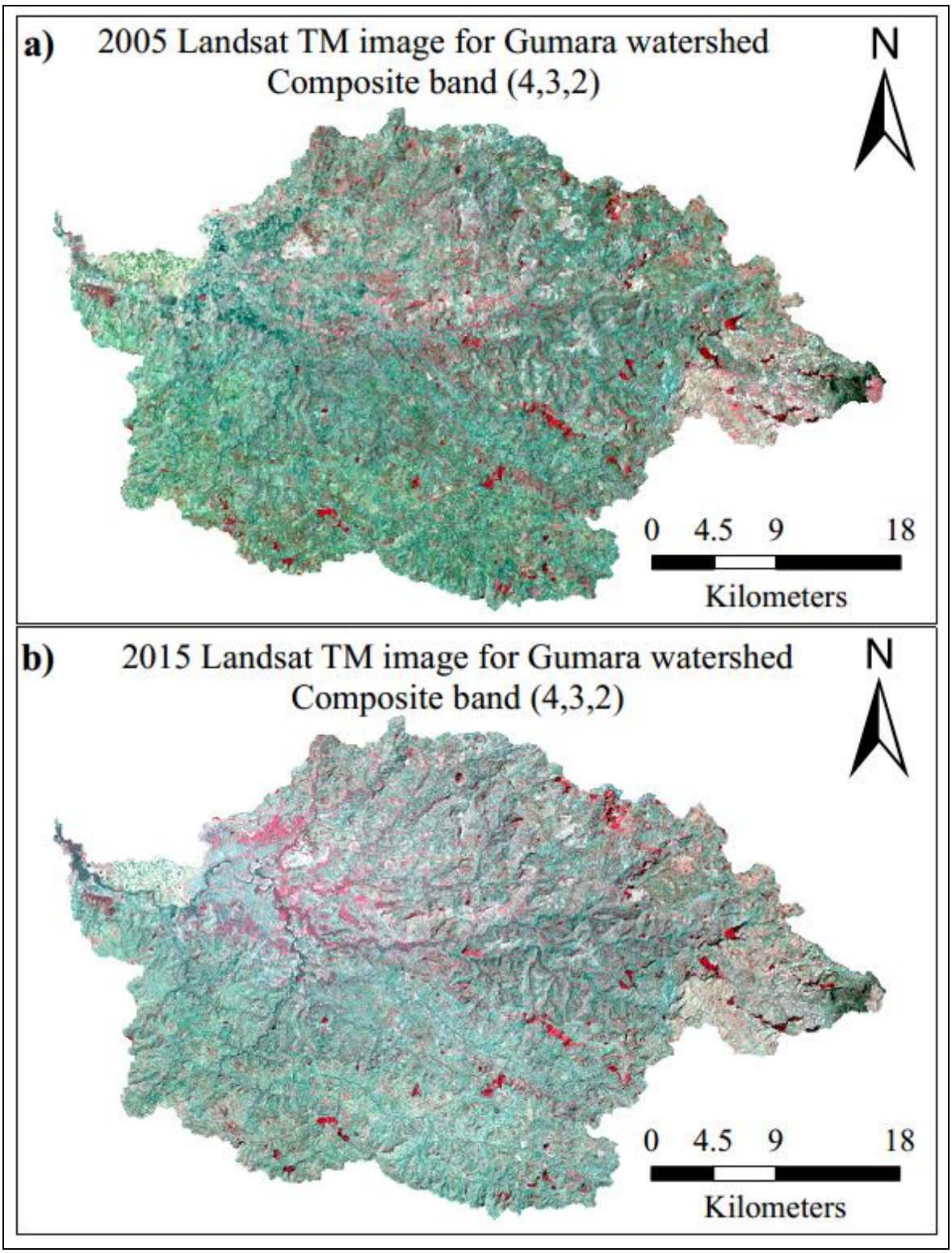

Appendix 17. The standard false color for composite Landsat Enhanced TM and Operational Land Imager (OLI) satellite image of the year 2005 (a) and 2015 (b), respectively for Gumara watershed.

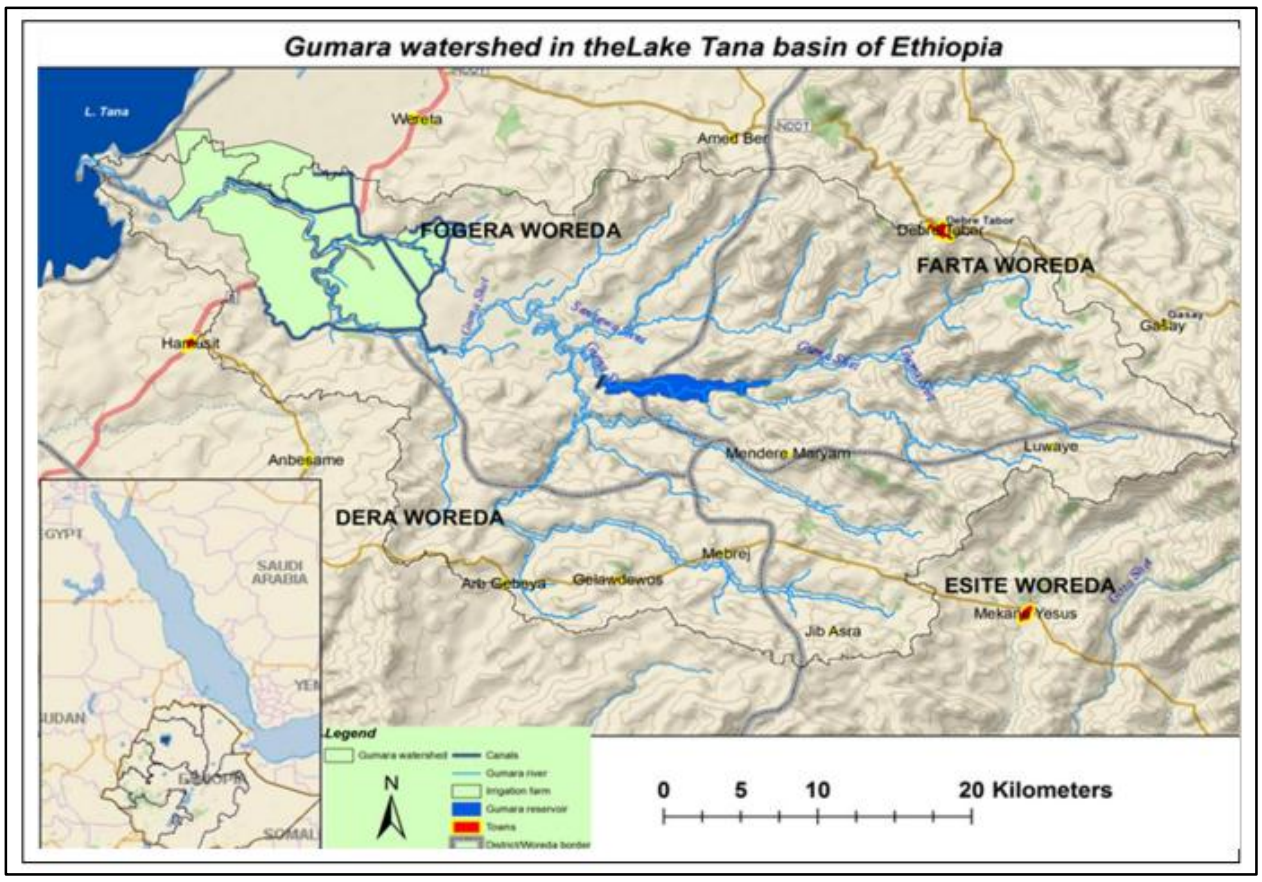

Appendix 18. Gumara Irrigation project (Sources: Ministry of Water, Irrigation and Electricity of Ethiopia).